HEAT PUMP OPERATED HUMIDIFICATION-DEHUMIDIFICATION DESALINATION SYSTEM

BY

DAHIRU UMAR LAWAL

A Dissertation Presented to the

DEANSHIP OF GRADUATE STUDIES

KING FAHD UNIVERSITY OF PETROLEUM & MINERALS

DHAHRAN, SAUDI ARABIA

In Partial Fulfillment of the

Requirements for the Degree of

DOCTOR OF PHILOSOPHY

In

MECHANICAL ENGINEERING

APRIL, 2019

KING FAHD UNIVERSITY OF PETROLEUM & MINERALS

DHAHRAN- 31261, SAUDI ARABIA

DEANSHIP OF GRADUATE STUDIES

This thesis, written by **DAHIRU UMAR LAWAL** under the direction of his thesis advisor and approved by his thesis committee, has been presented and accepted by the Dean of Graduate Studies, in partial fulfillment of the requirements for the degree of **DOCTOR OF PHILOSOPHY IN MECHANICAL ENGINEERING.**

Dr. MOHAMMED A. ANTAR
(Advisor)

Dr. ZUHAIR M. GASEM

Department Chairman

Dr. SYED M. ZUBAIR

(Member)

Dr. Salam A. Zummo
Dean of Graduate Studies

Dr. ATIA E. KHALIFA

(Member)

27/6/2019
Date

Dr. FAHAD AL-SULAIMAN

(Member)

Dr. JAMEL A. ORFI
(Member)

DEDICATION

This work is dedicated to my family

ACKNOWLEDGMENTS

"In the name of Allah, the beneficent, the merciful"

All praise be to Allah for blessing and providing me with good health and knowledge to complete this work

I acknowledge King Fahd University of Petroleum and Minerals (KFUPM) for supporting my work and for creating a conducive environment to accomplish my PhD degree.

I am thankful to my thesis advisor Prof. Mohammed Antar for his exemplary guidance, encouragement and motivation. I really appreciate your kindness towards me and your technical support towards the completion of this work. I'm forever grateful to you.

I would like to express my profound gratitude to my Co-advisor, Distinguished Prof. Syed Zubair for his support and guidance especially in the second law analysis of my task. My immense appreciation goes to Dr Atia Khalifa who have provide me with scientific directions in the experimental part of my thesis. I am grateful to Dr. Fahad Al-Sulaiman for his valuable suggestions and motivation which help me to successfully complete the work. I am thankful to Dr. Jamel Orfi of Mechanical Engineering Department - King Saud University, KSA, for the constructive advice provided during my PhD oral proposal defense.

My gratitude goes to faculty, staffs and graduate students of Mechanical Engineering Department KFUPM. My special thanks goes to my colleagues in Desalination group KFUPM for their support and encouragement.

I would like to express my deepest appreciation to my parents, brothers, sisters, and friends for their moral support and prayers throughout my studies. Lastly, my special thanks to my lovely wife and daughter for their love, patient, endurance, encouragement and prayers. May Allah reward you all.

TABLE OF CONTENTS

LIST OF TABLES

LIST OF FIGURES

LIST OF ABBREVIATIONS

Acronyms

HDH	humidification-dehumidification
HP	heat pump
E	electric heater
GOR	gained output ratio
CAOW	closed air open water
MR	mass flowrate ratio
RR	recovery ratio (%)
SEEC	Specific Electrical Energy Consumption (kWh/m^3)
sW	specific work consumption (kj/kg)
EUF	energy utilization factor
C-F-M	cost flow method
E-E-M	El-Dessouky and Ettouney Method
COE	cost of electricity ($/kWh)

Symbols

h	enthalpy (kJ/kg)
h_{fg}	latent heat of vaporization (kJ/kg)
P	pressure (kpa)
T	temperature (k)
$\dot{m}$	mass flow rate (kg/s)
C_p	specific heat capacity at constant pressure (kJ/kg.K)
$\dot{Q}$	heat transfer rate (kW)
$\dot{W}$	power (kW)
$\dot{V}$	volumetric flowrate (m^3/h)
$\dot{X}$	exergy rate (kW)
Z	capital costs ($)
$\dot{Z}$	rate of fixed charges ($/yr)
n	plant life expectancy
$\dot{A}$	plant availability
$\dot{c}$	cost rate ($/s)

c	product cost ($\$/m^3$)

Greek letters

ε	Effectiveness
ω	humidity ratio
μ	chemical potential
w_s	mass fraction
η	efficiency
β	fuel depletion ratio
χ	relative irreversibility
δ	productivity lack
ξ	exergetic factor
Γ	improvement potential
$\mathcal{L}$	specific cost of operating labor
α	amortization factor
$	US dollars

Subscripts

a	air
b	brine
w, sw	water
fw	fresh water
in	Entering/input
out	outtput/exiting
r	refrigerant
1, 2, 3, …	state points
II	second law
Evap	evaporator
Comp	compressor
cond	condenser
EXV	expansion valve
dest	destroyed
H, hum	humidifier
D, dehum	dehumidifier

FP	feed pump
Elect	electricity
f	fixed charges
L	labor cost
T	total
mt	maintenance
mg	management
p	product
BHX	brine heat exchanger

ABSTRACT

Full Name : Dahiru Umar Lawal

Thesis Title : Heat Pump Operated Humidification-Dehumidification Desalination System

Major Field : Mechanical Engineering

Date of Degree : April, 2019

Humidification Dehumidification (HDH) desalination system is a thermal based desalination technologies that is appropriate for small and medium scale water production. HDH desalination system is especially suitable for decentralized and remote region, because it can be driven by renewable energy and/or waste heat. Most of the thermal energy rejected from the air conditioning/refrigeration systems are discharged into the atmosphere. The present thesis recovers waste heat from heat pump to operate HDH desalination system. The work involves experimental and theoretical investigation of the performance of humidification dehumidification desalination system operated by a heat pump (HP). The proposed integrated system is capable of providing freshwater as the primary objective and cooling load for space conditioning as the secondary benefit. In this work, various layouts and arrangements of HDH system coupled with heat pump system are theoretically analyzed. Energy, Exergy and exergo-economic analysis are performed on various scenarios of the integrated systems. Furthermore, one specific configuration is tested experimentally. The experimental set-up was designed, fabricated, assembled, and tested at KFUPM-ME desalination lab. The general assessment metrics in the form of gained output ratio (GOR), recovery ratio (RR), specific electrical energy consumption (SEEC) and productivity of the integrated system were evaluated based on the influence of water

flowrate, air flowrate, and saline water temperature. Energy utilization Factor (EUF), cooling effect and freshwater cost are the other estimated system performance parameters. Theoretical results show that the integrated system is capable of attaining a GOR > 10 and RR of 6.4%, with a minimum SEEC and freshwater production cost of 90kWh/m^3 (0.09kWh/L) and 2.42\$/m^3 (0.242 Cent/L) respectively. The tested integrated experimental unit has a maximum heat pump coefficient of performance (COP) of 4.86, and it's capable of producing maximum cooling effect of 3.07kW while providing the needed desalinated water of 288 L/day, at a least cost of 10.68\$/m^3 of freshwater. The highest energy utilization factor (EUF) and gained output ratio of the tested experimental unit are 3.04 and 4.07 respectively, while the minimum recorded SEEC of the unit is 160kWh/m^3 of freshwater.

ملخص الرسالة

الاسم الكامل: **داهيرو عمر لاوال**

عنوان الرسالة: **تحلية المياة باستخدام تقنية الترطيب-التكثيف العاملة بالمضخة الحرارية**

التخصص: **هندسه ميكانيكيه**

تاريخ الدرجة العلمية: شعبان ١٤٤٠

تعتبر تقنية الترطيب-التكثيف واحدة من الطرق الحرارية لتحلية المياه والتي تعد مناسبة للتطبيقات الصغيرة والمتوسطة. تعد هذه التقنية خيار ملائماً لتحلية المياه خصوصاً في المناطق البعيدة واللامركزية لإمكانية استخدامها لمصادر الطاقة المتجددة والطاقة الحرارية المهدرة.

معظم الطاقة الحرارية الخارجة من وحدات التكييف والتبريد تذهب هدراً إلى الهواء. هذه الدراسة تستفيد من الطاقة المهدرة من المضخة الحرارية في تشغيل وحدة تحلية المياه باستخدام تقنية الترطيب والتكثيف. يشتمل هذا البحث على تحقيق نظري وعملي لدراسة أداء وحدات تحلية بتقنية الترطيب-التكثيف العاملة بالمضخات الحرارية. بإمكان النظام المبتكر والمقترح في هذا البحث إنتاج مياه عذبة عبر التحلية كناتج أولي بالإضافة لتوليد طاقة لتكييف المساحات كناتج آخر ثانوي. تم في هذا البحث دراسة عدة تصاميم نظريا لأنظمة تعمل بتقنية الترطيب-التكثيف ويتم تشغيلها بمضخات حرارية. تم دراسة الانظمة وتحليلها باستخدام القانون-الثاني للديناميكا الحرارية بالإضافة لدراسة الاقتصاديات المتعلقة بها. بالإضافة لذلك, تم تصميم, تصنيع وتجميع وحدة تجريبية تعمل بهذه التقنية في معامل التحلية التابعة لجامعة الملك فهد للبترول والمعادن. تم تقييم أداء النظام بناءً على عدة وحدات قياس اداء منها: نسبة كسب-الإنتاج, نسبة الاسترداد, الاستهلاك النوعي للطاقة الكهربائية وكمية المياه المنتجة. تم تقييم أثر معدل سريان المياه, معدل سريان الهواء, ودرجة حرارة المياه المالحة على مقاييس الإداء المذكورة اعلاه. بالإضافة لذلك, يشمل تقييم الأداء دراسة مقاييس أخرى مثل عامل استغلال الطاقة, أثر التبريد, وتكلفة إنتاج المياه. أوضحت النتائج النظرية التي توصلنا اليها في هذا البحث أن النظام المقترح يمكنه أن يتحصل على نسبة كسب-انتاج اعلى من ١٠, نسبة استرداد ٦,٤%, استهلاك نوعي للطاقة كهربائية بمقدار ٩٠ كيلو-واط لكل متر مكعب بتكلفة إنتاجية تقدر ب ٤٢. ٢ دولار امريكي لكل متر مكعب. أظهرت

الوحدة العملية في المعمل أن أقصى عامل استغلال للطاقة تم التحصل عليه من النظام هو 4.86 وإمكانية توليد أثر تبريد حراري بمقدار 3.07 كيلو-واط بالإضافة لتوفير الكمية المطلوبة من المياه العذبة بإنتاجيه مقدرة ب ٢٨٨ لتر في اليوم بتكلفة 10.68 دولار للمتر المكعب. أعلى معدل استفادة من الطاقة تم التوصل إليه هو 3.04 وأعلى نسبة كسب الإنتاج هي 4.07, كم أن أقل معدل للاستهلاك النوعي للطاقة الكهربائية هو 160 كيلو-واط لكل متر مكعب من الماء العذب.

.

CHAPTER 1

1.0 INTRODUCTION

It is a known fact that water covers over seventy percent of the earth surface, and more than 96% of all Earth's water is found in ocean. Only 3% of the world's water exist as freshwater and 66.7% of it is found frozen in ice, glaciers, snow and other forms, which are not readily accessible. As such, nearly 20% of the global population (about 2 x 10^9 people) live in areas of scarcity [1]. Currently 66.7% of the human population dwell in region that face scarcity of water for a minimum of a month annually [2].

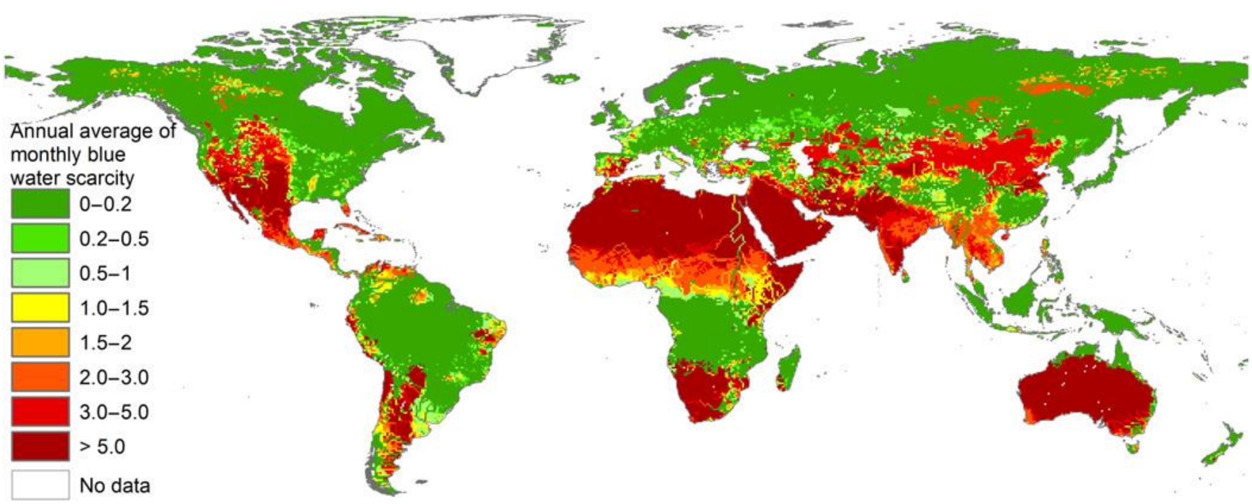

Figure 1.1: Monthly average of blue water scarcity annually for the Period of 1996 to 2005 [2].

The annual average monthly blue water (groundwater and fresh surface water) scarcity is shown in Figure 1.1. Potable-water scarcity is a common challenge faced by large portion of the globe, especially, in the arid, semi-arid, and developing part of the world. The unavailability of clean potable water is contributed by several factors including population growth, urbanization, as well as climate change. Distribution as well as storage water infrastructure is another challenge faced in the developing world.

Brackish water and seawater desalination (unlimited water source) has become a viable and reliable solution to address the lingering problem of fresh water scarcity. However, desalination processes require huge amount of energy especially for large-scale desalination systems (conventional water desalination technologies). The conventional desalination is most appropriate for the developed world which are rich in energy and has the economy to meet the technology demand of such intensive system. They are usually powered by fossil fuel and are characterized by problem of brine disposal, thereby causing environmental hazards [3]. The aforementioned problem have drawn the attention of many researchers toward renewable energy sources which could provide low maintenance, continuous, free source of energy, and reduce environmental pollution [4].

1.1 Desalination Technologies

Several processes for seawater desalination have been developed and can be classified into two major classes, which entails; Thermal (phase change) based and Membrane (single-phase) based desalination technologies. The two main categories are further divided into sub-categories (processes) as identified in Figure 1.2. Energy is needed to operate all desalination technologies for fresh water production. In thermal desalination technologies, saline water is heated to generate vapor and the vapor is condensed to produce clean freshwater (distillate).

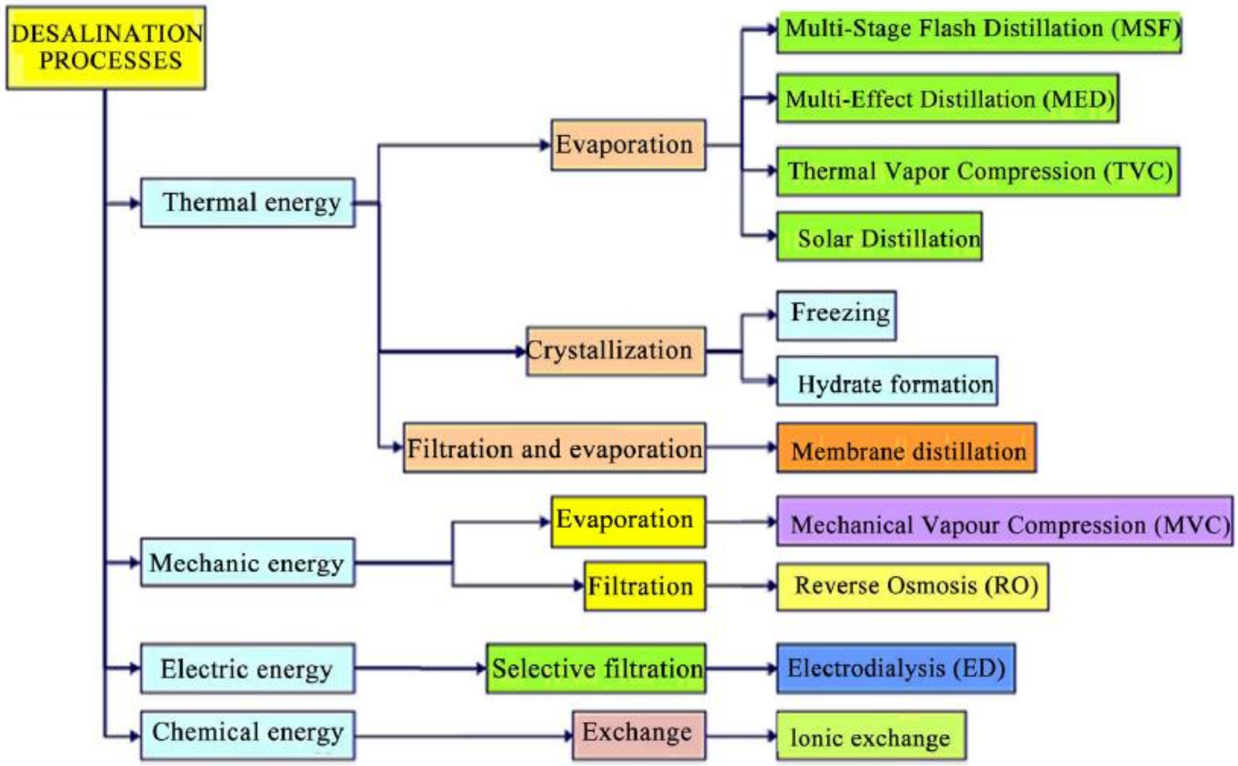

Figure 1.2: Desalination processes [4].

Multiple Effect Distillation (MED), Multi-Stage Flash Distillation (MSF) and Vapor Compression Distillation (VCD) in which compression can be attained mechanically (MVCD) or thermally (TVCD) are the major commercial desalination technologies that is based on thermal energy [5]. The membrane based desalination technologies includes Reverse Osmosis (RO) and Electro-dialysis/Electro-dialysis Reversal (ED/EDR). RO involve the passage of seawater through a semipermeable membrane under pressure to produce fresh water. Usually, electric pumps provide the needed pressure. Neither RO (the most commonly used membrane based desalination process) which demands uninterrupted mechanical or electrical energy supply, nor MED/MSF which are the most widely used thermal based desalination processes, are appropriate for small-scale seawater desalination. Region of the world that are distance away from large scale freshwater production facilities and with neither the economic resources nor the infrastructure to run RO or MSF plants needs the decentralized fresh water production. Therefore, desalination technologies suitable for small to medium scale application and can be powered by renewable energy (example solar energy) in an efficient way, is required. One of such desalination processes is the humidification-dehumidification desalination process.

1.2 Humidification Dehumidification (HDH) desalination system

Humidification Dehumidification desalination system belongs to the thermal based desalination technology that imitates the natural water. In natural water cycle (rain cycle), heat from the sun provides energy to evaporates seawater and the vapor humidifies the carrier gas (air in many case). By rising high, the humidified air form clouds, and subsequently, the vapour in the in the humid air cools and turns back into a liquid 'dehumidify' as rain. Many considered humidification dehumidification system as an improved version of solar still. Solar stills is an integration functions that involve the solar energy absorption, heating of water, evaporation of water, and condensation of vapour, all in single unit (volume). Several works and reviews has been done and reported on solar stills [6–8]. Figure 1.3 shows the basic solar still desalination system. Solar stills results in considerable thermal inefficiency, resulting in a low gain output ratio (GOR < 0.5) because of the latent heat of condensation losses through the solar still glass cover. To produce fresh water, relatively large areas is needed by the solar stills [9]. Separating the solar stills into different components where the various processes in solar stills can takes place in those components may improve the thermal efficiencies and the overall performance of the system [4]. The separation of processes/functions into different components is the characteristic of the HDH system [3]. The HDH system is reported to possess higher GOR over a solar still. This leads to a smaller solar collector area to produce fresh water. Humidification dehumidification system is suitable for decentralized and small-scale water production with huge potential for improvement. HDH system is relatively simple, inexpensive components, and can be powered by waste heat and renewable energy. It required low operational maintenance and technical expertise. As such, HDH system is appropriate for deployment in rural and developing region of the world. The basic drawbacks of HDH systems is the total heat input, which is relatively high as compared to other conventional thermal desalination processes.

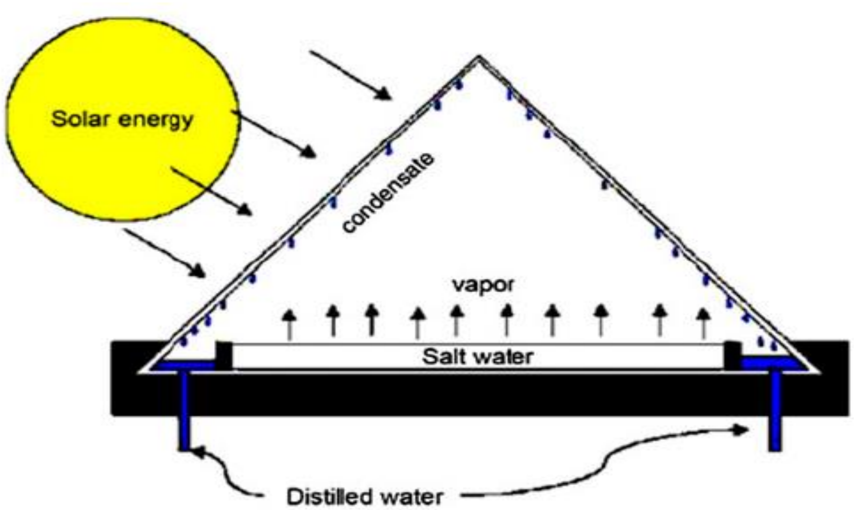

Figure 1.3: Basic design of a solar still desalination [10].

1.3 Principle of the HDH Process

In the humidifier, air come in contact with salt water, it humidified water vapor generated from the seawater. Thereafter, the humid air leaves the humidifier to dehumidifier where the humid air cools down and dehumidified to form clean fresh distilled water. The dehumidification process is achieved with the incoming seawater into the dehumidifier. The seawater is pre-heated by latent heat recovery from the humidified air [3,4,11–14]. The HDH system can be operated as only one cross of saline water (once through) or as brine recirculation, characterized by lower energy consumption and high solution concentration [4,15]. The main components structure of HDH desalination process involves the medium heater, the humidifier, and dehumidifier. The medium heater can be achieved from renewable energy such as solar PV, wind, solar thermal, geothermal, or their combinations [10]. The components of humidification-dehumidification (HDH) process are shown in Figure 1.4.

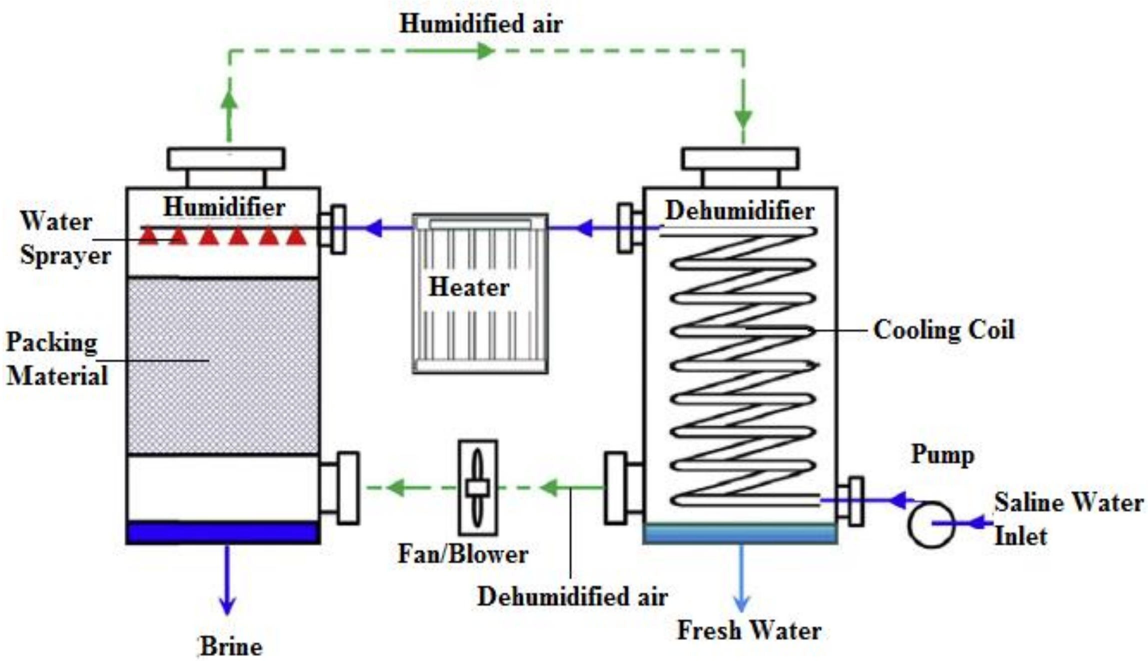

Figure 1.4: A simple humidification-dehumidification (HDH) process

1.4 HDH Classification

Researchers and investigators have proposed and analysed various design configurations of HDH system. These configurations are formed with different components and cycles.

1.4.1 The Basic HDH cycles

Basic HDH cycles can be grouped according to the type of loop (the water or air circuit is open or closed loop), the medium (stream) heated (whether water or air is heated), and type of energy used. Figure 1.5 shows the basic classification of HDH system. HDH systems can be classified according to cycle configuration. In this case, it is classified based on closed-water open-air, closed-air open-water, or open-water open-air systems. HDH system can also be categorized based on the heated stream. This classification includes water or air heated systems, and the heating stream determines the performance of the system. The classification may also be according to the energy source used such as wind, solar, electrical, geothermal, or hybrid systems.

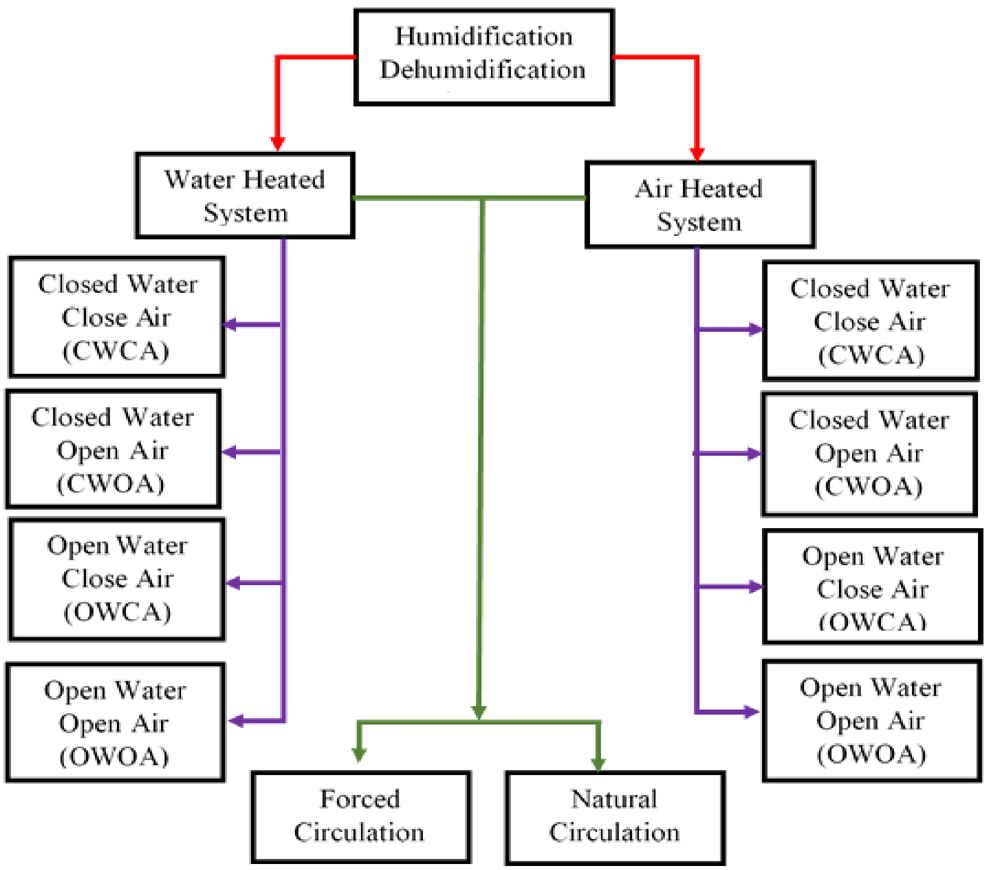

Figure 1.5: Basic HDH systems Classification

This classification portrays the most promising advantage of the HDH concept of utilizing renewable resources. The stream flow can be natural or forced in all these configurations [4].

Examples of basic HDH cycles are water-heated or air-heated cycle with; open-air closed-water cycle (OACW), open-water open-air cycle (OWOA), and closed-air open-water cycle (CAOW) [9].

i. Water Heated, Closed-Air Open-Water (CAOW) System

The line diagram of Closed-Air Open-Water (CAOW) water heated system is shown in Figure 1.6, where saline water flows through the dehumidifier. The seawater passes through the inside tubes of the dehumidifier cools down and dehumidified hot stream of humid air passing over the tubes in the dehumidifier. Seawater is preheated as is passes through the dehumidifier because of heat transferred to it from the hot humid air. After leaving the dehumidifier, the temperature of the preheated saline water is further increased to the desire maximum system temperature by water heater (example, waste heat exchanger, geothermal, or solar collector). The resulting hot saline water from the heater is directed to humidifier where it is sprinkled over a packing-material and part of it evaporates into the air. The packing material increases the surface area for effective evaporation. The unevaporated water is rejected as brine from the humidifier. In the humidifier, air stream flows through the packing material in a counter-flow direction and gets heated and humidified as it come indirect contact with hot evaporated water. The hot humid air is then directed to the dehumidifier where the vapor present in the humid air is condensed (dehumidified) to produce distilled water. The cold dehumidified air stream is directed back to the humidifier for next humidification process, which closed the air stream loop. The issue with this configuration is the energy lost to the environment from the discharged brine. The psychometric chart for this process is shown on line A - B in Figure 1.7.

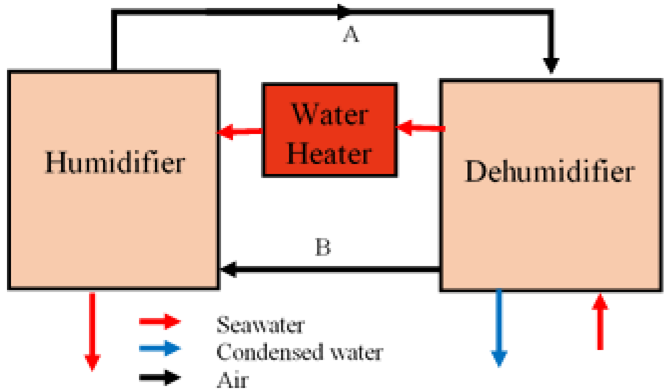

Figure 1.6: Schematic line diagram of Water Heated CAOW System.

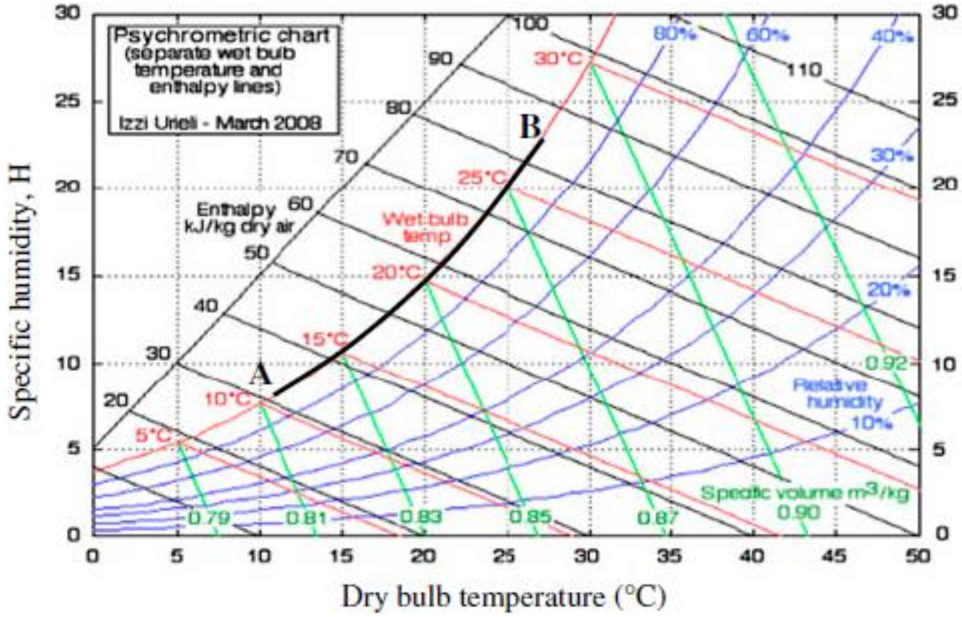

Figure 1.7: Water Heated CAOW System Psychometric Chart [10].

ii. Water Heated, Open-Air Closed-Water (OACW) System

Water Heated OACW configuration is very similar to that of CAOW. The main difference is the saline water path for OACW follow a closed loop, while air follows open path as shown in Figure 1.8. The brine rejected at the humidifier is re-circulated back to the humidifier after passing through other components. In this configuration, a make-up water is needed to make up the evaporated water vapor and to dilute the brine concentration. The major setback of this configuration is the hot brine entering the dehumidifier. The high temperature brine affect the cooling and dehumidification process of the humidified air and consequently lower the productivity of the system in comparison to the open-water cycle. This draw back can be resolved by employing an efficient humidifier, and cycle modifications on the water loop side.

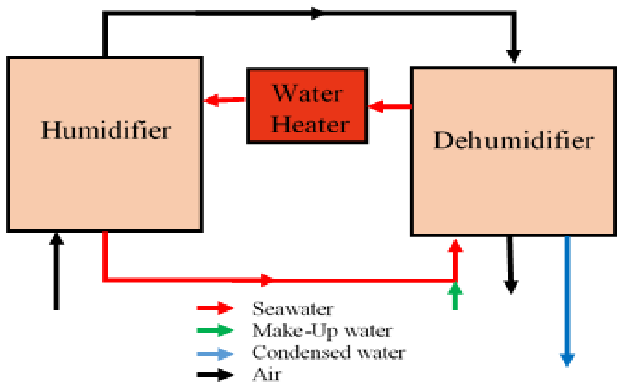

Figure 1.8: Block diagram of Water heated OACW HDH system.

iii. Air Heated, Closed-Air Open-Water (CAOW) System

The HDH configurations presented in Figures 1.6 & 1.8 are both water heated. Air heated system is another category of HDH systems that has drawn the attention of many investigators. Air heated CAOW system belongs to this category of HDH system as shown in Figure 1.9. Air heated CAOW system are of two classes including the multi-stage system and the single stage system. The single stage system is discussed here while the multistage system is discussed under the modifications of basic HDH cycles. In single stage CAOW air heated configuration, an air heater heats air to a desire top system temperature as shown by line A-B of the in the psychometric chart of Figure 1.10. The hot air is directed to humidifier where it is cooled and humidified by the evaporated water vapour. This process is shown in line B-C of the in the psychometric chart. The humid air then enters into the dehumidifier where it further cooled and the moisture content is removed to produce distilled water. This is shown by line C-A of the in the psychometric chart. The dry air leaving the dehumidifier is then recirculated to the air heater to complete the loop. On the other hand, saline water enters the dehumidifier and gets preheated as it condenses the humid air. The preheated saline water is directed into the humidifier where portion of it evaporates and humidified the incoming hot air. The unevaporated water is discharged into the environment as brine.

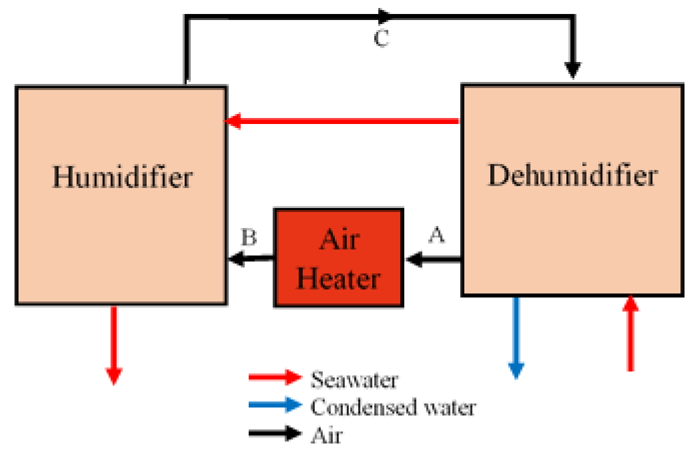

Figure 1.9: Closed-Air Open-Water (CAOW) Air Heated configuration.

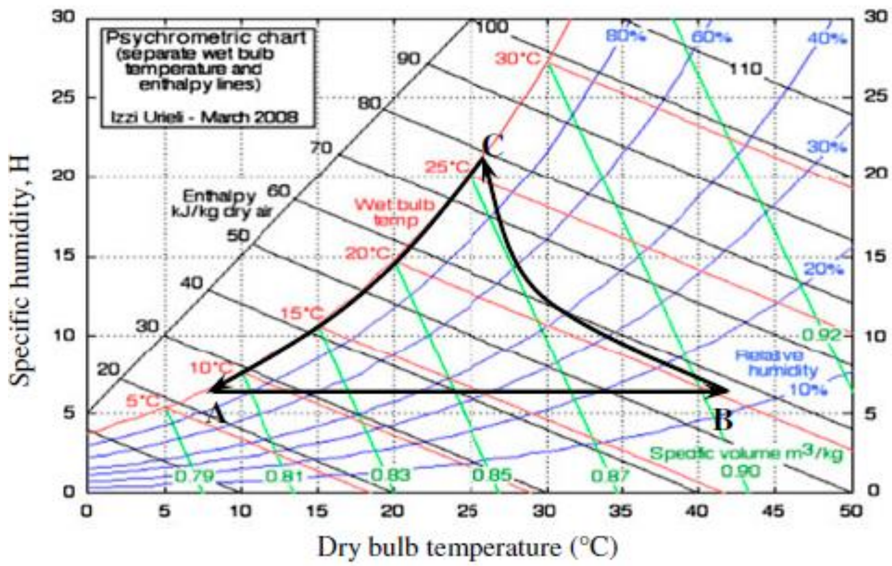

Figure 1.10: Air-heated CAOW system Psychometric chart [10]

iv. Air Heated, Open-Water Open-Air (OWOA) System

Figure 1.11 presents the air heated OAOW system. In this cycle, ambient air is heated it passes over the air-heater. The heated air enters the humidifier where it is cooled and humidified by the evaporated water vapour from the warm saline water sprayed over the packing material. Unevaporated water is discharged as brine from the dehumidifier. The humid air exits from the humidifier and enters into the dehumidifier where it further cooled and the moisture content is removed to produce distilled water. On the other hand, the low temperature saline water passing through the inner tube of dehumidifier get warm as it condenses the humid air. Air stream pass once through the system. As such, there is no connection of dehumidified air stream between the dehumidifier and the humidifier.

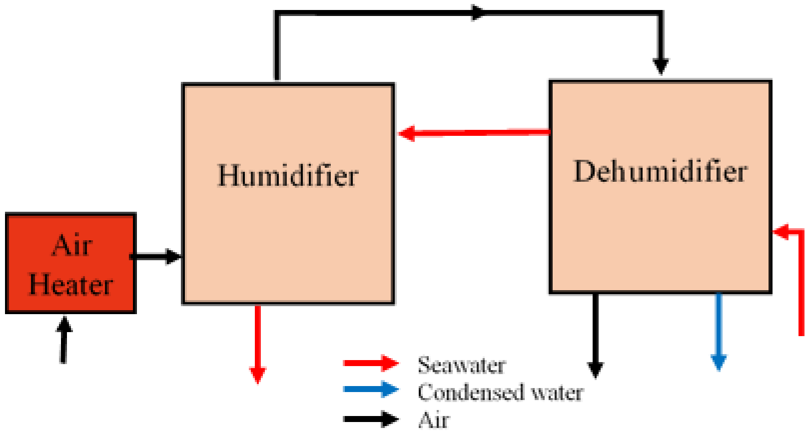

Figure 1.11: Air Heated, Open-Water Open-Air (OWOA) cycle.

1.4.2 Modification of Basic Cycles

The performance of basic HDH systems can be improve through the cycle modifications of basic HDH and some of the modified HDH cycles will be discuss in this section.

i. Modified water heated Closed-Water Open-Air (CWOA) HDH Cycle

The modified water heated closed water open air HDH System as illustrated in Figure 1.12 is similar to the basic cycle of close water open air loop shown in Figure 1.8, except the modification made in the water loop. As presented in Figure 1.12, the low temperature saline water passes through the dehumidifier where it absorbs heat from the hot humidified air stream. Part of the preheated saline water is admitted into a make-up tank while the rest is rejected. The saline water in the tank is then heated and sprayed in the humidifier where part of it evaporates and the unevaporated seawater is collected, ducted and re-circulated back to the tank to close the water loop. Make-up water from the dehumidifier is admitted into the water heater intermittently to dilute the concentrated brine. This modification in water loop is expected to reduce the energy input to achieve the desire maximum saline temperature. The water loop modification can also solve the problem of ineffective condensation of water vapor. Therefore, the modified water heated cycle is expected to yield an improved both productivity and energy efficiency of the system.

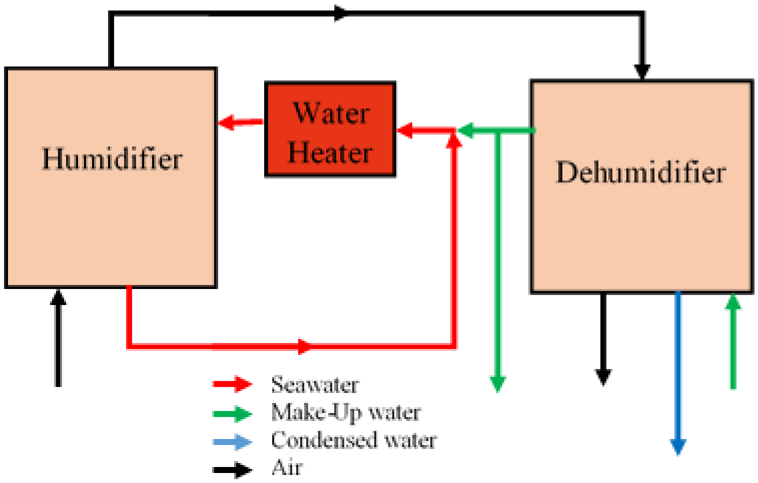

Figure 1.12: Modified water heated Closed-Water Open-Air (CWOA) HDH Cycle

ii. Modified Air Heated, Closed-Air Open-Water (CAOW) HDH Cycle

In modified air-heated CAOW system shown Figure 1.13, the air heater is inserted in between the humidifier and dehumidifier, and the humidified air leaving the humidifier is heated by the air heater before it enters into the dehumidifier. As the humidified air enters into dehumidifier, its moisture content is removed to produce distilled water while dry/dehumidified air leaves the dehumidifier and ducted into humidifier where it absorbed water vapor from the evaporated saline water. On the other hand, saline water enters passing through the dehumidifier gets preheated by gaining heat from the dehumidifying air. The warm saline water is then directed to humidifier where it is sprinkled over packing materials. Part of the saline water evaporated and the rest is discharged as brine. The modified air heated CAOW system is very similar to the basic air heated CAOW system shown in Figure 1.9, except the change in the location of the stream heater. The saline water temperature entering the humidifier is higher than that of air for both basic and modified air heated cycles (Figures 1.9 and 1.13). As a result, more efficient humidification process is achieved when compare to other cycles such as the one shown in Figure 1.11 where air temperature entering the humidifier is always greater than the water temperature entering the humidifier. Narayan et al.[14] in their work shows that heating the air leaving the humidifier is more efficient when compared to heating the air entering the humidifier.

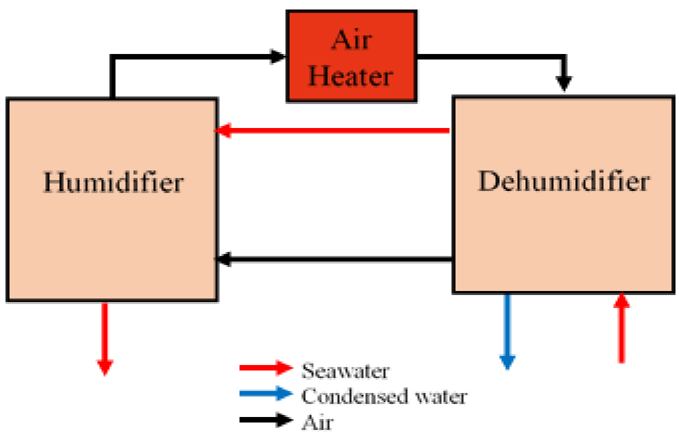

Figure 1.13: Modified Air Heated, Closed-Air Open-Water (CAOW) HDH Cycle

iii. Water Heated, Multi Effect Closed-Air Open-Water (CAOW) System

The idea of multi-effect HDH system was introduced to improve heat recovery by Müller-Holst [16]. Figure 14 shows the line diagram of this process, while the line A – E in Figure 1.15 illustrates the process on the psychometric chart. In this configuration, air stream is removed at different points from the humidifier and injected at the corresponding points on the dehumidifier. The stream extraction and injection resulted in small temperature gap that enables greater recovery of heat from the dehumidifier. As reported in [3,4,10], Tinox GmbH, a commercial water management company commercialized and marketed a water heated, multi effect CAOW system where they have recovered most of the energy required for humidification process. The energy demand of the system was brought down to a value of 120 kWh/m^3.

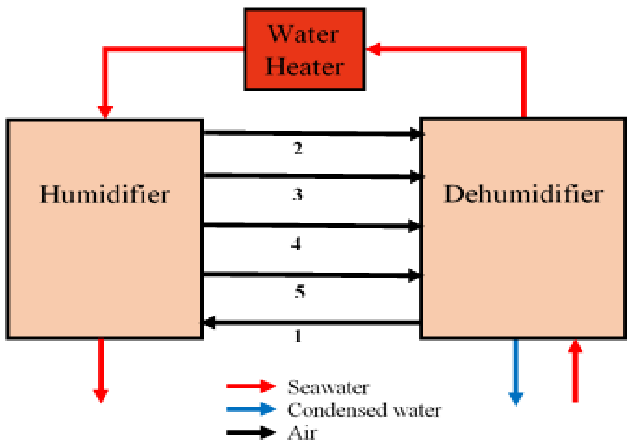

Figure 1.14: Water Heated, Multi Effect CAOW System

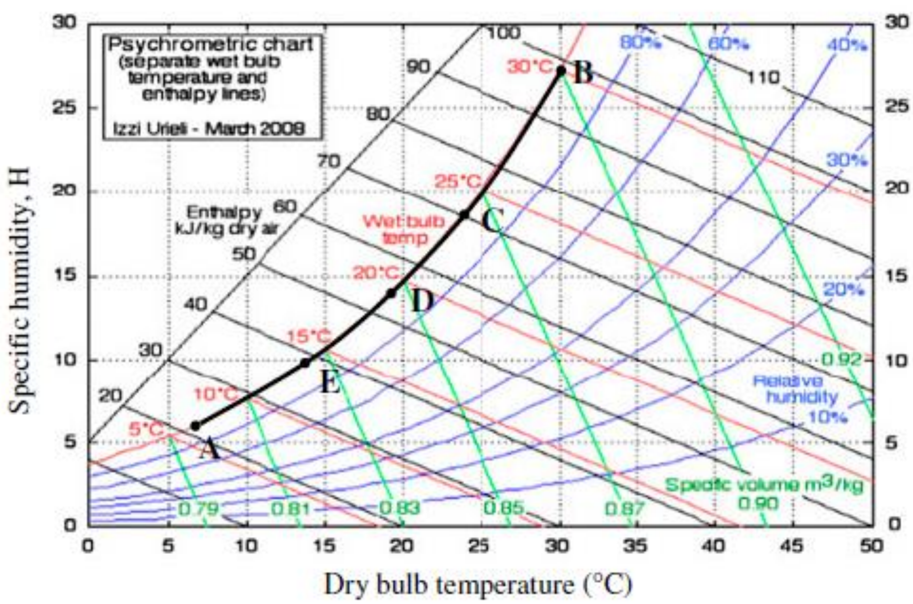

Figure 1.15: Water Heated, Multi Effect CAOW System Psychometric chart [10]

iv. Multistage heating and humidification cycle

Multistage heating and humidification cycle illustrated in Figure 1.16 is proposed by Chafik [18] to address the shortcomings of single-stage system (Figure 1.9). Figure 1.17 demonstrates this process on psychometric chart. In multistage heating and humidification system, air is heated in the air heater (solar collector), and then humidified in the humidifier. The heating and the humidification process are shown by line A - B and line B - C respectively on psychometric chart. The humidified air is then ducted to second air-heater and second humidifier where it is heated again and undergoes another humidification process as shown by line C - D and line D - E respectively. The humidified air is further channelled to the third air-heater and then to third humidifier for further heating and humidification as shown by line E - F and line F - G respectively, to reach a higher absolute humidity value. It is worth noting that absolute humidity of 15% and beyond can be achieve by the arrangement of several of such stages [3,10]. To achieve the similar humidity as a three-stage cycle, the single-stage cycle (Figure 1.9) has to attain high temperature at point H in Figure 1.17.

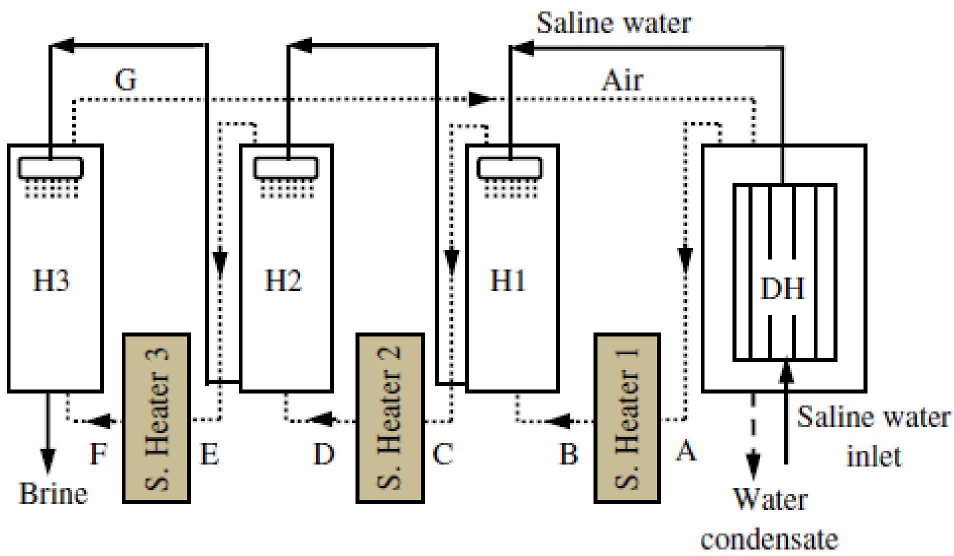

Figure 1.16: Multistage heating and humidification cycle [10]

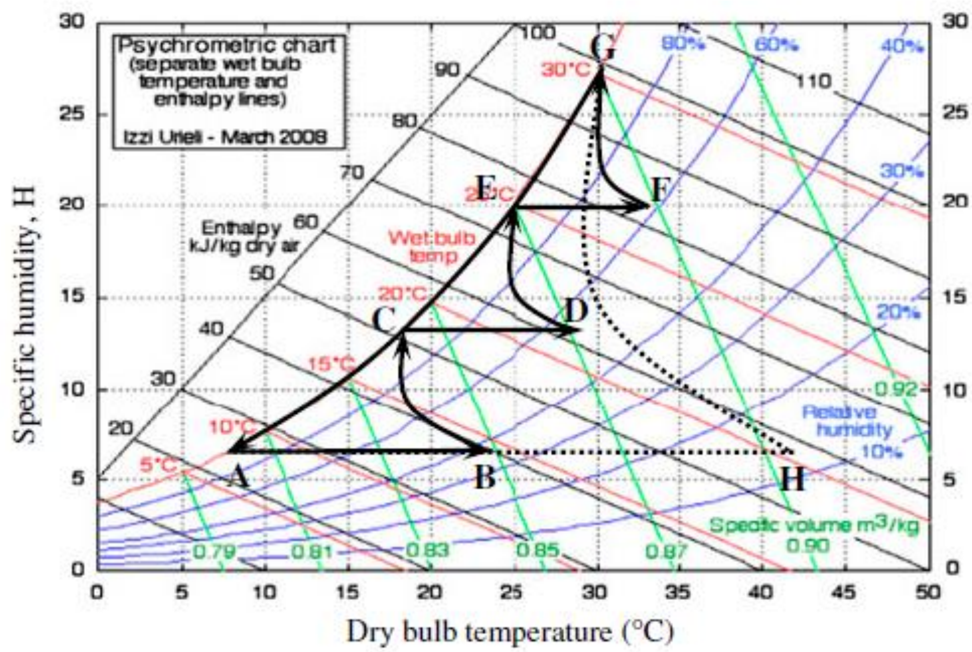

Figure 1.17: Psychometric chart for multistage heating and humidification cycle [10]

1.3 Heat Pump (HP) system

A heat pump (HP) is energy saving technology that conveys heat from a low to a high temperature level. HP systems are heat-generating devices that can be employed to heat water to be utilized in either space heating applications or domestic hot water [17]. Heat pumps extract heat from one medium and transfer the heat into another medium through a reverse refrigeration cycle. HP provide economical alternatives of recovering heat from different sources for use in different residential, industrial and commercial applications [18]. It provide one of the most practicable solutions to the greenhouse effect. It is the only known process that recirculates environmental and waste heat back into a heat production process; providing environmental friendly and energy efficient heating and cooling in applications ranging from process industries to commercial and domestic buildings [19].

In heat pump, the heat is transported by circulating a refrigerant through a cycle of evaporation and condensation. The refrigerant vapor and liquid mixture passes through the cold side heat exchanger (Evaporator), during which the refrigerant completely converted into vapor by absorbing heat from the medium the evaporator is in contact with. The refrigerant boils and evaporates at low temperature and pressure. The saturated vapor then flows into compressor, which increases the pressure and temperature of the saturated vapor to superheated gaseous state. The superheated vapor at high-pressure and temperature enters the hot side heat exchanger (condenser) producing heat for water or heating system, and in so doing changes state from superheated vapor into a liquid. The condensed vapor (liquid) passes through the expansion valve, which forces the liquid refrigerant to flash into a gas and liquid mixture, at a lower pressure and temperature. The cycle repeats. A schematic diagram of heat pump is shown in Figure 1.18.

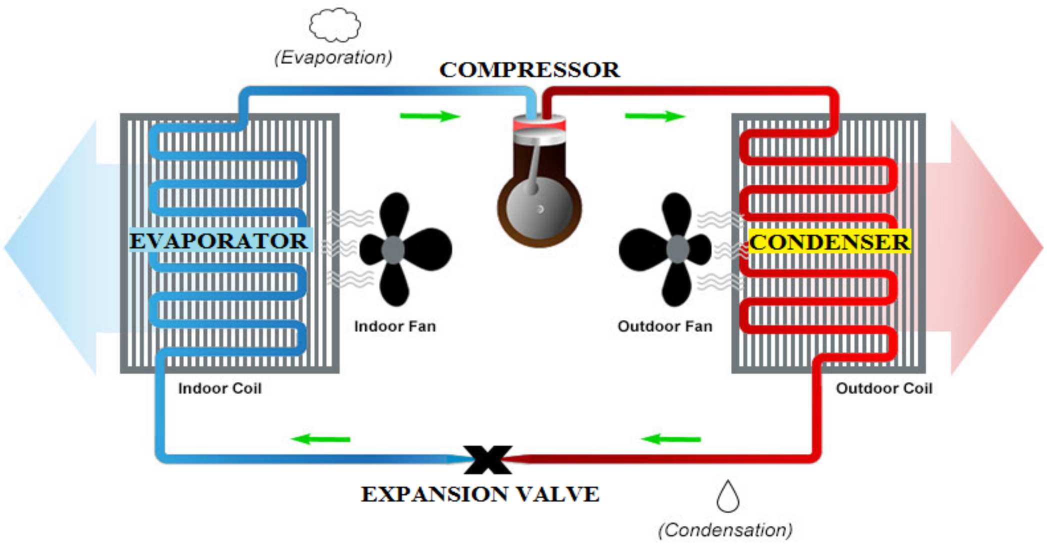

Figure 1.18: Schematic diagram of heat pump system (Prior Art) [20]

The Vapor-compression refrigeration is the mostly used cycle for refrigerators and heat pumps. There is an ideal vapor-compression refrigeration cycle and vapor-compression refrigeration cycle. An ideal vapor-compression refrigeration cycle consist of the following four processes:

1 – 2 isentropic compression of the refrigerant.

2 – 3 constant pressure heat rejection in the condenser

3 – 4 throttling process in an expansion valve at constant enthalpy

4 – 1 constant pressure heat addition in the evaporator

In addition, the following assumptions hold for an ideal vapor-compression cycle:

- irreversibilities within the compressor, evaporator and condenser are ignored
- frictional pressure drops are neglected
- refrigerant flows at constant pressure through the two heat exchangers (condenser and evaporator)
- negligible heat losses to the surroundings

The T-s and P-h diagrams of an ideal vapor-compression refrigeration cycle is shown in Figure 1.19 [21].

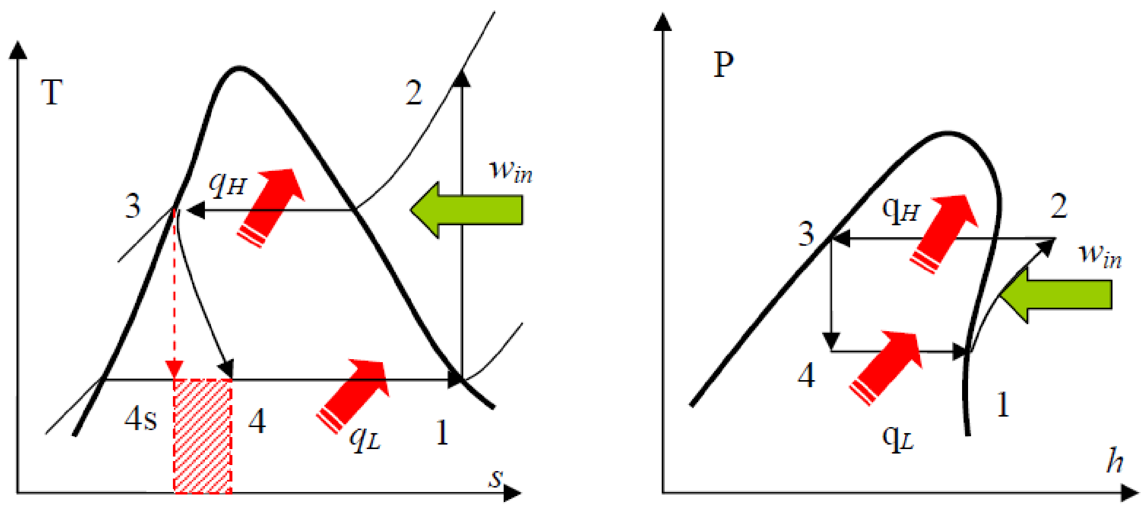

Figure 1.19: T-s and P-h diagrams for an Ideal process[21]

An actual vapor-compression cycle differs from the ideal vapor-compression refrigeration cycle due to irreversibilities in various components of the system. Figure 1.20 is the T-s diagram for actual vapor-compression cycle, while the summary of some of the main difference between the actual and ideal vapor-compression cycles are given below [21]:

- The refrigerant enters the compressor at state 1 in slightly superheated vapor, instead of saturated vapor in the ideal cycle.

- The line connecting the compressor to the evaporator (suction line) is very long. Therefore, there is significant heat transfer and pressure drop, process 6-1
- The degree of irreversibilities increases because, compression process is not internally reversible. However, the entropy generation (state 2) can be decrease by cooling the refrigerant during the compression process or by employing multi-stage compressor.
- In practice, the refrigerant exits condenser as sub-cooled liquid. This is shown by 3-4 in Figure 1.20. The cooling capacity increases by the sub-cooling process, which also stop any vapor/bubbles entering the expansion valve.
- Heat addition and rejection in the evaporator and condenser do not occur in constant pressure and temperature due to pressure drop in the refrigerant.

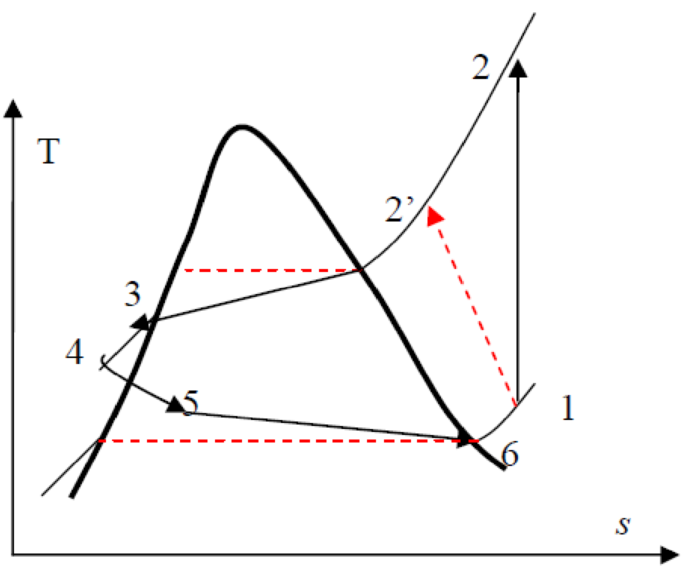

Figure 1.20: T-s diagram for an actual process

CHAPTER 2

2.0 LITERATURE REVIEW

2.1 The main components of HDH desalination system

Humidification-dehumidification desalination system is composed of several parts/components, which includes humidifier, dehumidifier, and stream heater. Each of these components will be reviewed in this section.

2.1.1 Humidifier of HDH system

Humidifier is one of the main part of HDH system. Humidifiers are devices, which increase the moisture content of air/carrier gas. They are commonly used in heating, ventilation, and air conditioning systems to attain a healthy and comfortable environment for workers and residents [22]. It has been used widely in industrial applications in which it is used to adjust the humidity level to prevent static electricity build-up in industries such as packaging, plastics, textiles, electronics, semiconductors, automotive manufacturing, pharmaceuticals, electrostatic painting, and powder coating. Humidifiers are used also to preserve material properties such as in paper industry to prevent paper curl shrinkage. It is also used in food industry to maintain foodstuff fresh. humidifiers can also be used in medical ventilators and hospital operating rooms [23]. Many devices are used for air humidification and they can be classified as packed bed or wetted element humidifiers [24,25], spray/atomizing humidifiers, spargers or bubble columns [26], and heating or steam element humidifiers. All these devices have the same operational principle. When the saline water comes in contact with unsaturated air in the humidifier, the humidity of the air increases. The diffusion of water vapour in unsaturated air is as a results of concentration difference between the air-water interface and water vapor in air. Therefore, the vapour pressure at the water-air interface and partial pressure of water vapor in air influence the water vapour mass transfer. If the temperature of air is lower than the temperature of water, then the air will be heated and humidified. If the dew point temperature of air is higher than the temperature of water (chilled water), the air will be cooled and dehumidified. If the water is circulated adiabatically (i.e. without being heated or cooled), it will approach the wet bulb temperature and the air will be cooled and humidified which is known as the air washer or evaporative cooling process.

Heating and steam element humidifiers is reported to consumed large amount of generated energy [24]. Spray or atomizing humidifiers face a problem of pressure drop because of atomizer nozzles [27]. Kreith and Boehm [27] provides the design procedures and different empirical correlations for spray towers. Xu et al. [28] carried out numerical and experimental investigations to analyse and predict the humidification process in spray tower. One-dimensional numerical model was developed for simulating the heat and mass conservation of humid air and water. The developed numerical model was found to be in good agreement against the obtained experimental results for the pressurized model spray tower. The model was used to predict the distributions of volumetric heat transfer coefficient and velocity of the droplet over the tower height. spray tower has also been used by Bonilla et al. [29], Javed et al. [30], Ben-Amara et al. [31], Younis et al. [32], and Orfi et al [33].

Owing to the low water holdup capacity of the humidifier unit, the efficiency of the spray tower is usually low. Thus, a packing material (packed bed) is introduced in the humidifier unit to overcome this drawback which raises the humidifier water holdup capacity and thereby specific humidity of air. Packed bed type humidifier is the most widely used humidification device in the HDH water desalination system. It is similar to the spray towers in which the water is sprayed in the form of droplets that falls under the force of gravity. While air flows in cross- flow arrangement [34,35] or counter flow arrangement, the water is mostly sprinkled from the top. The packing material increases the contact time and contact area and. Packed bed humidifier is a wetted element humidifier where the elements are made of random or structured packing material which has high surface area-to-volume ratio that increases the diffusion surface area. An effectiveness or efficiency defined to calculate the performance of an air humidifier [33,36,37],

$$\eta = \frac{\omega_{out} - \omega_{in}}{\omega_{out,sat} - \omega_{in}}$$

Where $\omega_{out,sat}$ is outlet humidity ratio at saturation, ω_{in} is inlet humidity ratio, and ω_{out} is outlet humidity ratio. An energy and exergy analysis has done to evaluate the performance of solar packed bed humidification desalination with pall rings as packing material [38]. It was noticed that the exergy efficiency increases with the reduction in tower length. Extraction of gas from humidifier has been considerably enhanced the gained output ratio [39]. Sharqawy et al. [23] conducted experimental and theoretical investigation of packed-bed cross-flow humidifier. The used packing material is the cross-fluted film fill. They calculated the humidification capacity, saturation efficiency, and Specific Electrical Energy Consumption using the experimental data of the outlet and inlet conditions for the water and air streams. They found that the Specific Electrical Energy Consumption is almost constant with variation of the mass flowrate ratio, packing thickness, and temperature of the water inlet within the investigated range of these parameters.

Table 2.1: Material used as packed bed towers in HDH systems

Packing material	Authors
zigzag packing (aluminum sheets)	Hossam et al. [40]
Gunny bag and saw dust	Muthusamy and Srithar [41]
Jute cloth	Rajaseenivasan and Srithar [42]
cross-fluted film fill	Sharqawy et al. [23], Aburub et al. [35]
plastic screens	EL-Shazly et al. [43]
Ceramic corrugated packing	Wu et al. [44]
Plastic packing	Chiranjeevi and Srinivas [45], Al-Enezi et al. [46], Yamali et al. [47]
Corrugated cellulose material	Ahmed et al. [48], Efat Chafik [37], Houcine et al. [49]
Cellulose paper	A.E. Kabee and Mohamed Abdelgaied [50] Hermosillo et al. [51]
Wooden shaving	Farid M., Al-Hajaj A [52]
Wooden, PVC, Gunny bag cloth	Amer et al. [53]
Honeycomb paper	Yuan G., Zhang H. [54], Dai and Zhang [55,56]
Ceramic Raschig rings	Khedr [57], Eslamimanesh A., Hatamipour M. [58]
Wooden slates packing	Hou and Zhang [59], Nawayseh et al. [60], Farsad S., Behzadmehr A. [61]
Canvas	Nafey et al. [62]
Wooden surface	Al-Hallaj et al. [52]
Indigenous structure	Garg et al. [63]
Thorn trees	Ben-Bacha et al. [64]
HD Q-PAC	Klausner [65]

Furthermore, an effectiveness model originally developed for cross-flow packed-bed cooling tower is adopted to estimate the number of transfer units of the humidifier and the effectiveness of the humidifier. In the humidifier of a HDH desalination system, Muthusamy and Srithar [66] have used the gunny bag and saw dust as packing material. They concluded that the humidifier with gunny bag has better mass transfer coefficient and productivity compared to the sawdust as packing material.

Amer et al. [53] investigated humidification-dehumidification desalination using several type of packing materials like plastic, wooden slates and gunny bag cloth. Higher humidifier proficiency was noticed with the wooden slates compared to the others. Zhani and Bacha [67] used textile material (viscose) as packed bed to increase the contact area between the air and water in a humidifier. The peak production rate of 21.75 kg/day has been collected in the HDH desalination. Other various packing materials used in the literatures includes; honeycomb paper [54], wooden shavings [68], indigenous structure [63], Raschig ring ceramic [58], wooden surface [52], canvas [62], corrugated and treated cellulose paper [51], thorn trees [69], and plastic pad [47]. Table 2.1 gives the summary of different packing materials used to enhance the effectiveness of humidifier in HDH desalination system.

In wetted element humidifiers, air is forced to flow across a water film so that water diffuses into the air stream as vapor. Orfi et al. [33] and Muller-Holst et al. [70] has use wetted-wall towers as humidifier their HDH systems. Using a polypropylene material, Muller-Holst et al. [70] construct a vertical hanging fleeces over which hot water is distributed. Air flowing in opposite direction in the humidifier absorbed water vapour and become saturated as it exit the humidifier. To improve the heat and mass exchange process, Orfi et al. [33] use a cotton wick to covered the wooden vertical wetted-walls. To always keep the vertical walls wetted, they reduces the velocity of flowing water through use of the capillary effect. Humidification efficiency of almost 100% was obtained in their study.

For bubble column humidifier, the water is filled in a column and the air stream is injected into a column containing water to form small bubbles. Small equipment volume is required of bubble column because; bubble column enhances heat transfer and mass transfer processes, and surface area [71]. Some investigators [36,72–74] have proposed the use bubble columns in HDH desalination systems. experimentally investigation of the performance of a bubble column humidification process was conducted by El-Agouz and Abugderah [36]. At different operating conditions they measured the humidification efficiency of the system. They have use a nozzle diameter of 10 mm and total nozzles of 32. Increasing the temperature of water in the column is reported to increase the humidification efficiency. Air velocity as well as air temperature are also reported to influence the humidification efficiency. A novel multistage stepped bubble column humidifier was recently developed by Abd-ur-Rehman and Al-Sulaiman [75] for air humidification. The performance of single stage, double stage and three-stage bubble humidifier were compared against each other in terms of absolute humidity. Double stage and three-stage bubble humidifier recorded increments in the absolute humidity of 7-9% and 18-21% respectively over the one-stage bubble column humidifier. In another development, using biomass as source of energy, Rajaseenivasan and Srithar assessed the performance bubble column HDH desalination system [76]. In another investigation, they used solar energy to powered the bubble column HDH desalination system [77]. In the later, they found out that they can reach a peak specific humidity gain of 0.187 kg_{water}/k_{gair}, if they use concave turbulators in the solar air heater. Without concave turbulators in the solar air heater, they can only reach a peak specific humidity gain of about 0.11 kg_{water}/k_{gair}. The system can provide a maximum freshwater of 20.61 kg/m^{2}day.

2.1.2 Dehumidifier of HDH system

Dehumidifier is another component of HDH system for the dehumidification of water vapour in the humid air to obtained condensed distilled water. Dehumidifiers made of different materials and heat transfer surfaces have been investigated and tested. Bubble column dehumidifier has been used for dehumidification purpose [73]. The most commonly used dehumidifier are flat-plate and finned-tube heat exchangers [36,70,78,79]. Shell and tube heat exchanger has also been used to improved heat recovery and enhanced condensation of vapors [80]. Mounted copper tubes on a stack of plates [15], Packed bed direct contact heat exchangers [33] and long tube with longitudinal fins [81] have also been used.

In bubble dehumidifier, humid air is directed into column of cold water. The vapor in the air bubble condenses as it passes through the water column. The temperature of the water column can be kept constant by passing coolant through the coiled tube immersed in the water column. An experimental and theoretical investigation of bubble column dehumidifier was presented by Narayan et al. [73]. They developed thermal resistance model, and the model was further simplified by Tow and Lienhard [74] by neglecting the gas-side resistance. The bubble column dehumidifier effectiveness was measured for different air inlet temperature, various superficial velocity and bubble column water height. Dehumidifier effectiveness and heat flux were found to decrease and increase respectively, with increasing temperature of air inlet and superficial velocity. Sharqawy and Liu [71] examined the performance of bubble column dehumidifier experimentally. The influence of column height, absolute pressure, and superficial velocity on the system performance was assessed. Higher absolute pressure was reported to results in a larger size bubble column dehumidifier.

A finned-tube type air coolers (dehumidifiers) has been used by Chafik [78,79] where seawater passing through the tube get heated by the humid air. Muller-Holst et al. [70] uses propylene material to make a double webbed slabs flat-plate heat exchanger (dehumidifier). Rajaseenivasan and Sritha [76] used shell and coil type heat exchanger, where the shell is made from hollow pipe having a diameter of 0.15 m and the coil tube is fabricated from copper tube having a diameter of 6 mm. Recently, Kabeel and Abdelgaied [50] used a radiator type cross-flow heat exchanger consists of a finned flat copper tube matrix. The dimensions of the radiator are 40 cm × 38 cm × 10 cm height. The radiator is covered with a galvanized sheet in the form of a pyramid of both directions to control the passage of humidified air over the radiator and the condensate water is collected down the dehumidifier to obtain distillate water. The cooling water passes inside the tubes of the radiator, but the humid air passes outside the tubes of the radiator in the cross direction. All sides of dehumidifier are insulated with a fiberglass of 5 cm thick to reduce the loss in heat between a dehumidifier and its surrounding.

direct contact packed bed heat exchangers is another type of heat exchanger used in [33,82,83], because of the degradation of the film condensation heat transfer in the presence of carrier gas. Threlkeld [84] presents differential equations governing the dehumidifier, while Pacheco-Vega et al. [85] summarized the correlations for heat-transfer coefficients and friction factor which may be used for dehumidifiers. McQuiston [86,87] developed a standard method which consists of multi-column multi-row finned-tube compact heat exchangers, and adopted Colburn j-factors along with wet-bulb temperatures, dry-bulb temperatures, flow rate, fin spacing and other dimensions to predicts heat and mass transfer rates.

2.1.3 Heaters

Most of the existing HDH systems are driven by solar energy for heating the air stream or water stream and in some cases for heating the both stream. Therefore, solar heaters for HDH system will be discussed in this section.

2.2 HDH System powered by Solar Heater

Solar heaters are generally used to increase the temperature of any medium. For HDH desalination system, the carrier medium or water stream, or both stream has to be heated. The devices and the materials used to provide thermal energy (heater) for the carrier medium and the water stream is another essential component of humidification-dehumidification desalination system.

2.2.1 Solar Air Heater

To elevate air temperature, solar air heaters can used. Heating the air will increases the capacity of air to absorb more water vapor. Different types and designs of solar collectors integrated with humidification dehumidification desalination system have been used as solar air heaters. Ben-Amara et al. [88] presented a novel solar air collector for humidification-dehumidification desalination process. They investigated the influence of the ambient temperature, inlet air humidity, the air mass flow rate, wind velocity, the inlet air temperature, and the solar radiation on the collector efficiency. solar air heater of a single pass connected to the packed-bed HDH desalination system has been assessed in

[89]. The overall exergetic efficiency was found to increases with decrease in inlet air temperature, through the increase in tower diameter and reduction in the length of the tower. Flat plate solar air heater of double-pass has also been used in [90]. Compared to a single-pass solar air heater, double-pass solar air heater has been reported to have increased the system productivity by 8%. In another development, the impact of flat plate double-pass solar air heater, feed water mass flow rate, amount of the water inside the storage tank, process air mass flow rate, initial water temperature, and cooling water mass flow rate on the system productivity was examined in [47]. Al-Sulaiman et al. [91] theoretically investigated the performance of two layouts of humidification dehumidification desalination systems integrated with solar air collector of parabolic trough type. The parabolic trough solar air heater was positioned before the humidifier in the first layout, and parabolic trough solar air heater was located after the humidifier in the second layout. On average, the first layout and the second layout recorded maximum gained output ratio of 1.5 and 4.7 respectively. The performance of air-heated HDH unit has also been investigated experimentally by Antar and Sharqawy [92] using both single and two-stage modes solar evacuated tube collectors. The pressure drops in fittings and pipelines and the heat losses were reported to significant affect the system performance. Productivity of 3.5 and 6 L/day was obtained from the single-stage and two-stage systems, respectively. Experimental study to assessed the performance a small scale air-heated HDH desalination system was conducted by Li et al. [93] using a novel design solar air collector made of dual-wall glass evacuated tube. Outlet air temperature and relative humidity were reported to increase with increase in the water temperature sprayed in the humidifier.

energy storage phase change material (PCM) integrated with solar air heater has been used in HDH desalination system [94]. It was reported that PCM material (inbuilt storage energy) thickness of 8 cm placed below the absorber plate is enough to provide a constant output temperature throughout the day and night and thereby enhanced the overall performance of the system. Rajaseenivasan et al. [95] has examined the performance of an integrated solar collectors of single purpose and dual purpose, and a bubble column humidifier. They have considered three cases in their work. In case one, they examined the performance of solar air-heater humidification-dehumidification desalination system. In case two, they modified the case one by integrating the solar air-heater with turbulators. In the third case, they integrate the HDH system with dual-purpose solar collector equipped with turbulators. The reported system productivity for the case III, II, and I, are about 23.92, 20.61, and 16.32 kg/m^{2}day respectively, while the system gained output ratio of 3.3, 2.8 and 2 were reported for case III, II, and I respectively.

Srithar and Rajaseenivasan [77] also developed a bubble column HDH coupled with and without solar air heater. They assessed the influence of turbulators, air flowrate and water depth in humidifier on the system performance. Their results shows that a reduction in humidifier water depth elevates the water temperature and thereby specific humidity. It was reported that rise in air flowrate and the creation of turbulence in the flow caused by turbulator enhances the solar air heater outlet temperature. A maximum distillate production of 20.61 kg/m^2-day was reported in the study. More recently, Elsafi [96] theoretically assessed the performance of a co-generation unit for the generation of power and production of freshwater. The system under study is an integrated concentrated photovoltaic-thermal (CPVT) collectors and air-heated humidification-dehumidification desalination system. The cost of system's products were estimated based on exergy-costing analysis. 0.289 \$/kWh and 0.01 \$/L were reported to be the system power generation and water production cost respectively.

2.2.2 Solar Water Heater

Extensive studies on HDH desalination system equipped with solar water heating has been conducted for years. Solar water heaters integrated with a HDH desalination system are used to elevate the water temperature going to the humidifier. Solar water heating HDH system has attracts greater attention in comparison to solar air heating HDH system [3], because water has higher heat capacity as compared to air [97]. Three units of HDH desalination system were constructed in Jordan and Malaysia [15]. The used solar collector in the work is that of flat plate collector, used to elevate the water temperature up to about 80 ^{o}C before been sprayed over packed-bed materials in the humidifier using a simple distributor. A solar collector of flat-plate tubeless type having a total area of 2m^2 has been used to increase water temperature to about 70 °C [52]. Using a flat-plate solar collector having an area of 1.15 m^2, Abdel Dayem [98], experimentally tested HDH desalination system under different weather conditions at Makkah. The system was reported to be capable of producing freshwater of 9 L/day-m^2 and solar energy of about 1.6 L/kWh. Water production cost of about 0.5 \$/litre was reported. Cost and performance investigation of HDH desalination cycle was performed by Zubair et al. [99] using solar collectors of evacuated tube type for water heating. The evacuated tubes consist of 30 tubes per collector. The impact of the geographical location, effectiveness of both dehumidifier and humidifier, as well as the number of collectors, on the system productivity was investigated. The maximum and minimum annual water production was found to be 19,445

L and 16,430 L respectively. Depending on the considered location, the freshwater production cost was found to varied from 0.032 to 0.038 $/litre of freshwater. Their results also show a maximum GOR of about 2.7. The designs and constructions of a two-stage pilot plant HDH desalination system driven by solar collector having area of 80 m^2 was investigated in [100]. The unit assessment was carried out on hot and cold days and recorded a peak freshwater production of 7.25 ($L/day \cdot m^2$). About 20% increase in the system productivity was reported for the two-stage unit compared to single-stage unit. Farid et al. [81] uses solar collector of flat plate type having area of 1.9 m^2 to elevate water temperature for humidification dehumidification desalination system. They studied the influence of humidifier, condenser, and number of solar collector on the system productivity, and their unit was found to be capable of producing 12L/day-m^2 of freshwater.

2.2.3 Combined Water-Air Solar Heater

There are cases where both water and air are heated using solar collectors. For example, in Suez City, Egypt a HDH desalination test rig was designed, constructed and tested at various operating and climatic conditions in [62]. In their system, concentrated solar collector was used to heat water, whereas flat plate solar collector was used to heat air. They assessed the impact of the cooling water flowrate, the air flowrate, feed water flowrate, as well as the climatic conditions on the system. Two double passes corrugated absorber solar air collector of 1.4 square meter each and evacuated tubes solar water collector has been employed to assessed the performance of an indirect solar dryer coupled with HDH desalination system [50]. The evacuated tube solar water collector consists of 15 tubes (58 mm diameter and 1800 mm length). The air leaving the drying unit is ducted to the humidifier for humidification process as shown in Figure 2.1. Their results shows two-stage dryer recorded about 71.78% improvement in moisture removal as compared to single stage dryer. Increasing the air flowrate from 50 to 75 m^3/h was reported to have increase the freshwater productivity from 29.55 to 42.3 L/day. Based on a series of researches since the year 2007, HIMIN Solar Co. Ltd and Chinese Academy of Sciences designed, constructed and tested A HDH desalination system [101]. The system consists of an air heater field comprising a total number of 72 evacuated tubes solar collectors having a total of 100-m^2 surface area, and water heater field containing a total number of 10 evacuated tubes solar collectors having a total of 14-m^2 surface area, for air and water heating respectively. The air heater could heat the air up to a temperature of about 118 °C. The system productivity was investigated for different climatic conditions. For a mean solar radiation of about 550 W/m^2, the system was reported to be capable of producing about 1200 L of freshwater per day. To enhances the production of freshwater and make HDH system more flexible, Zhani and Ben Bacha [67] uses solar air heater collectors of flat-plate type of 16-m^2 field, and solar water heater collectors of flat-plate type of 12-m^2 field to elevates air and water temperatures respectively. The test rig was investigated at various operating and climatic conditions. The system cost analysis was also performed. The assessed system can produced freshwater of 20 L/day and freshwater production cost was to be 0.08 €/L. a solar collector of dual-purpose was employed to powered HDH desalination system by Rajaseenivasan and Srithar [42]. The used solar collector is capable of simultaneously heating both water and air in the system. Concave and convex turbulators was introduced in the air-flow field to enhance the performance of the system. A peak system productivity of about 15.23 kg/m^2-day of freshwater was recorded in their study. In another development, a solar concentrator of cylindrical/curved Fresnel lens type was used for supplying heat to the humidification compartment of a multi-stage HDH desalination cycle [44]. For a mean solar radiation intensity of about 867 W/m^2, the system can reach a maximum GOR and peak productivity of 2.1 and 3.4 Liters per hour respectively.

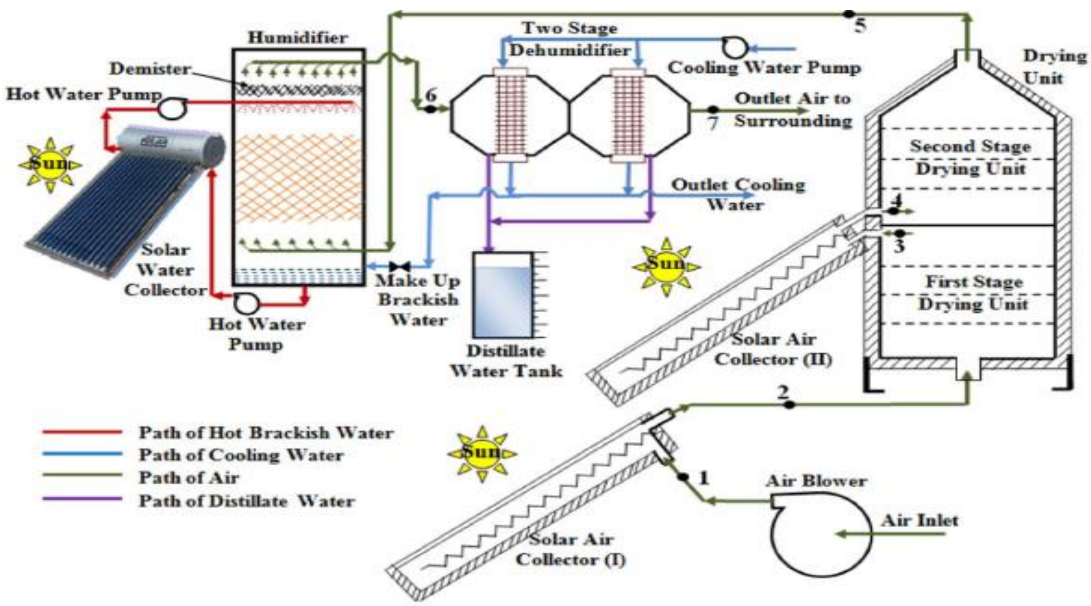

Figure 2. 1: Diagram of two-stage indirect solar dryer with reheating coupled with humidification-dehumidification desalination systems [50] **.**

2.3 Refrigeration cycle Integrated with HDH system

Integrating HDH system with air conditioning system can improve the attractiveness of the integrated system, since the system could be used to achieve multiple objectives, such as water desalination and space cooling process. In this regard, the performance of a hybrid vapor compression air conditioning system and HDH desalination system was evaluated by Nada et al. [102] experimentally. The evaporator of the air conditioner was used to condense the water vapor in the flowing humid air. A steam boiler was used to generate steam for air humidification process, while three air heaters are employed to heat the incoming ambient air before humidification process. Their findings revealed that increasing mass flow rate and specific humidity of air improves the refrigeration capacity, the compressor work, and the desalinated water productivity. Relative humidity and temperature of the supplied air also enhances the rate of fresh water production. Experimental correlations in terms of operating parameters are developed for several system performance indices. The main shortcoming of this system is the fact that the entire system is an intensive energy consuming system.

The performance analysis of a novel type of air-heated HDH desalination system coupled with heat pump was carried out by Gao et al. [103]. In this system, the humidified air from is condensed in the evaporator and in the pre-condenser to generate freshwater. Solar photovoltaic as well as heat pump condenser are used to elevate the air temperature. Saline water is also pre-heated as it passes through the condenser to recover some energy. The unit consumed about 0.5kW of electricity to produce about 60 L/day of desalinated water. However, the system operate with the help of solar PV system.

The assessed the performance of a dehumidifying unit couple with heat pump presented by Habeebullah [104]. The system can provides freshwater ranging from 0.618 m^3/day to 2.23 m^3/day by extracting/condensing water vapor present in an atmospheric air. The exiting air from the dehumidifier is cold and was utilized to provide cooling comfort to an office building. However, the rejected energy from the condenser is not utilized.

Chiranjeevi and Srinivas [105], theoretically investigated the performance of HDH system integrated with solar water heater (SWH) and vapor absorption refrigerator's (VAR's) for water desalination and space conditioning process. The study analyzed single stage and double stages HDH desalination system with the option of using chilled and normal water for dehumidification process. The study recommended that the dehumidification process in the second stage should be performed using chilled water. The work also recommended low evaporator temperature, high saline water temperature and medium humidifier efficiency for enhanced energy conversion. The reported EUF for single stage and double stages are 0.18 and 0.33 respectively. The maximum system productivity is 50 L/hr and the energy available for space conditioning is about 200 watts. However, the system is assisted by solar water heater, and it is vapor absorption refrigeration.

The performance of heat pump operated HDH desalination system was presented by Lawal et al. [106]. In their study, the energy rejected from the condenser was utilized as heat source for the seawater flowing to the humidifier, while the cooling effect of the evaporator was is used to lower the temperature of incoming seawater to the dehumidifier for effective condensation of humid air in the dehumidifier. Two different HDH layouts were considered in the study. Their findings indicated a maximum GOR of 8.88 and 7.63 for modified air heated and water heated cycle, respectively at a humidifier and dehumidifier effectiveness of 80%. An exergo-economic analysis of two layouts of humidification-dehumidification desalination plants integrated with vapor compression heat pump was also performed by Lawal et al. [107], and determined the components with highest and lowest exergy destruction. The cost of fresh water production varied from 4.61$/m3 to 14.95 $/m3 depending on the HDH layout used.

Dehghani et al. [108], presented theoretical analysis of direct contact HDH desalination system driven by heat pump using the ε-NTU heat and mass transfer correlations. The influence of fresh water temperature and flow rate ratio and saline water temperature on the specific electrical energy consumption (SEEC) and recovery ratio (RR) are investigated. Their results show an optimum RR of 5.8% and SEEC of 335.4 kW.hr/m3. He et al. [109], theoretically performed an investigation on heat pump driven HDH desalination system. They built mathematical models based on energy and mass transfer in and out of the major components of the integrated system. Their results show a maximum system freshwater production of 82.12 kg of freshwater per hour, and a peak GOR of 5.14 attained at pressure ratio of 4. The system productivity enhances to 106.53 kg/h when the pressure ratio was increase to 5. The system is direct contact HDH desalination system and not non direct contact HDH desalination system.

2.4 Research Objective

From the aforementioned literature, most of the existing humidification-dehumidification desalination system is driven by solar energy, and without a unit for storing energy during the day, the energy source to the system becomes a challenge. In most cases, constant supply of water is demanded of desalination system. One of the ways to handle this challenge is through the recovery of the abundant waste heat to power the desalination system. This ensures the needed constant supply of sweet-water at all time. Therefore, this work experimentally and theoretically investigates the performance of HDH desalination system coupled with a heat pump system. The waste heat from the condenser of the heat-pump (HP) is employed as the source of input energy to elevate the temperature of the saline water, while the evaporator of the heat pump is used as a pre-cooler to supplied chilled water needed for effective condensation of fresh water.

It is clear from the literature that HDH has been integrated with heat pump by few investigators/researchers. However, in most of the studies, the condenser is used to heat air. In some cases, solar energy is employed to assist the heating process with heat pump, while in others, electrical heating elements are coupled with the heat pump to deliver the necessary heat to the air/seawater. There are other cases where the heat rejected by the condenser of heat pump is not utilized at all. A review of existing studies also reveals that, there is no single study that has experimentally investigated the performance of heat pump integrated HDH system where rejected heat from the condenser of heat pump is utilized to heat saline water without auxiliary heating. Furthermore, the performance metrics of the integrated HDH desalination system has not been properly investigated. Hence, the motivations for this work are set. The main objectives of the current work are:

- To design, and construct a lab-scale humidification dehumidification desalination system coupled with a heat pump.
- To evaluate the performance of the built integrated desalination unit at different system operating and design conditions.
- To develop an analytical model based on mass and energy balance for different HDH-HP layouts.
- To evaluate the performance of various novel configurations of HDH desalination systems integrated with the heat pump cycle.
- To perform second law analysis (exergy analysis) for selected existing HDH cycle arrangements coupled with the heat pump system, to identify the degree of irreversibility associated with various components of the systems.

- To carry out an exergy-economic analysis for a selected existing configurations of HDH cycle augmented with heat pump system and evaluate their performance in terms of freshwater cost.

2.5 Research Methodology

The above mentioned research objectives are achieved through the following steps:

- A comprehensive literature review on humidification dehumidification (HDH) desalination system and heat pump (HP) system.
- Experimental design.
- A detailed design of HDH components. That is sizing of humidifier and dehumidifier.
- Sizing of heat pump system
- Manufacturing of the designed HDH components and heat pump system.
- Assembling of the integrated experimental set up (HDH and HP).
- Instrumentation of the built set-up
- Testing and evaluating the system performance
- Developing the theoretical model describing energy and mass transfer across each component of the integrated system.
- Evaluating the performance of the integrated system based on energy analysis
- Evaluating the performance of the integrated system based on exergy analysis
- Estimating the product cost through exergo-economic analysis of the integrated system.

CHAPTER 3

3.0 Theoretical Investigation of Water and Modified Air Heated HDH Systems Coupled With Heat Pump

In this chapter, two known basic configurations of HDH system are integrated with heat pump system. The two HDH systems are the closed air open water (CAOW) water-heated cycle and the modified air-heated cycle. Each of the two HDH systems is connected to a heat pump system which supplied the heating and cooling for the HDH system. This integration is aimed at improving the overall thermal performance of the HDH system. The performance of the two integrated systems are predicted from the mathematical models based on first law of thermodynamics. The models described energy and mass transfer across various components of the integrated systems. A parametric study is conducted to investigate the influence of various system operating parameters, including water and air flowrate, seawater temperature, and refrigerant flow rate, on the system performance such as gained output ratio, recovery ratio, Specific Electrical Energy Consumption and cost of freshwater production.

3.1 System Description

The proposed systems are shown in Figs. 3.1 & 3.2. They consists of two subsystems, namely: (i) the heat pump cycle, and (ii) the desalination (HDH) system. The heat pump system consists of a compressor, a condenser, an evaporator, and an expansion valve. On the other hand, the desalination system comprises of a humidifier, dehumidifier, pumps, and fan/blower. The source of heat for desalination process is the condensing vapor of the refrigerant R134a, ammonia (or any other substances with low vaporization temperature) at the condenser of the heat pump. The combined system is based on the utilization of the two heat exchangers of the vapor compression system, the evaporator absorbs heat from the incoming seawater to cool it to state 1w to improve the condensation process in the dehumidifier through higher temperature difference between this stream and the hot humid air entering at state 2a. In addition, the vapor compression system condenser rejects heat to further heat the seawater leaving the dehumidifier at state 2W to its maximum temperature at state 3W before it is sprayed in the humidifier. The energy input to the combined system is basically mechanical work in the compressor of the vapor compression system.

3.1.1 Humidification-Dehumidification Desalination Process

The HDH system investigated in this work includes Water heated, Closed Air Open Water (CAOW) HDH Cycle, and the Modified Air heated, Closed Air Open Water (CAOW) HDH Cycle. For water heated HDH cycle, shown in Fig. 3.1, seawater is initially cooled down to bottom system temperature, as it passes through the evaporator of heat pump, and transfers heat to the refrigerant within the tubes of the evaporator. The cold seawater is then flows through the dehumidifier tubes, where it is pre-heated by the condensing vapor carried by the humidified air. The pre-heated seawater is then passed through the condenser of the heat pump, to raise its temperature to its top temperature, due to the heat transfer from the compressed refrigerant in the condenser to the seawater outside the condenser tubes. The heated seawater is sprinkled over packing material in the humidifier used to increase the surface area for effective heat and mass transfer. Part of the seawater evaporates in the air stream and the remains of seawater is discharged as brine from the bottom of the humidifier. Air circulated by fan/blower enters the humidifier in a counter flow direction and through the packing material where it is heated and humidified as it comes in direct contact with the sprayed hot seawater. The warmed humid air leaves through the top of the humidifier to the dehumidifier where the humid air condenses on outer surface of the seawater finned tube coil heat exchanger. The condensed fresh water is collected and measured in fresh water basin. The cold air is then discharged from the dehumidifier to commence the next cycle.

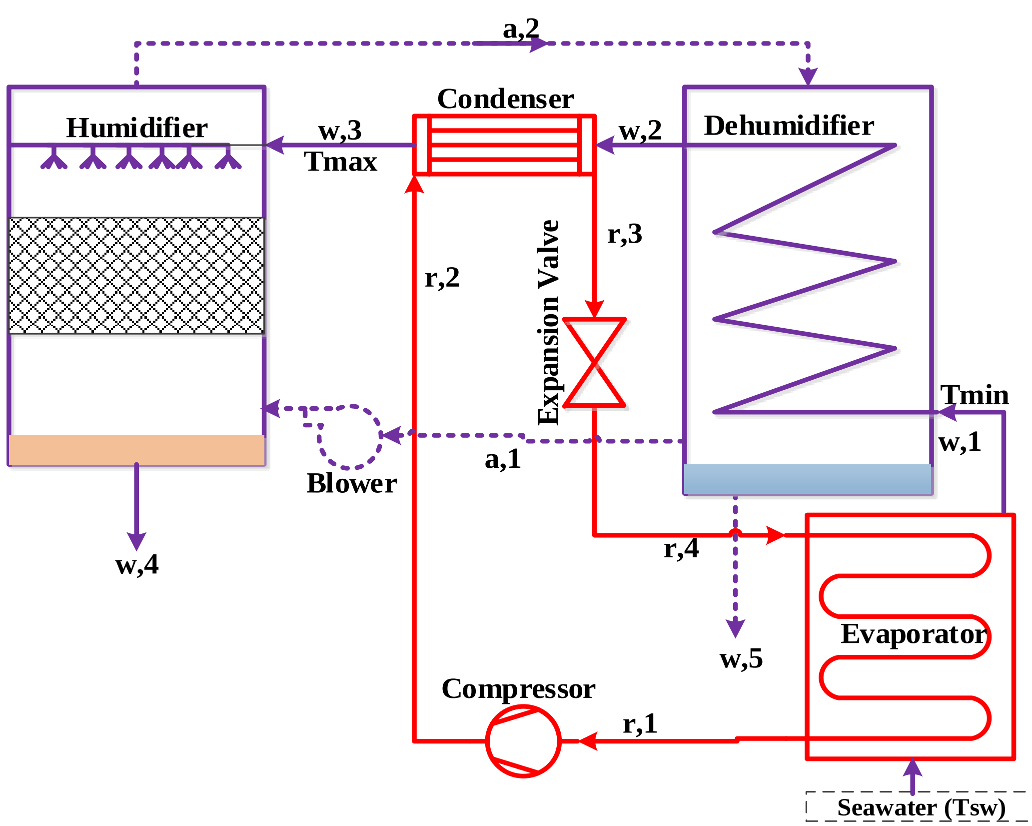

Figure 3. 1: Schematic diagram of a combined Water heated, Closed Air Open Water (CAOW) HDH Cycle and Heat pump

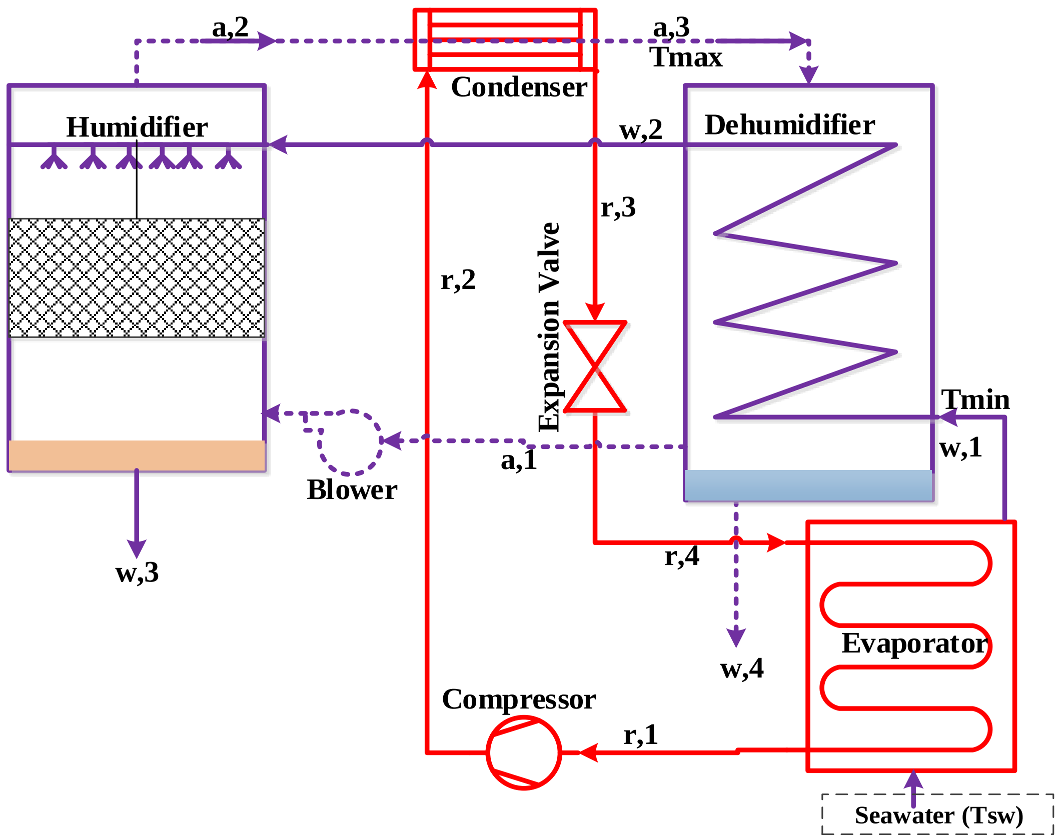

Figure 3. 2: Schematic diagram of a combined Modified Air heated, Closed Air Open Water (CAOW) HDH Cycle and Heat pump

The modified air heated cycle is shown in Fig. 3.2, is different from the water heated cycle since the heat rejected in the condenser does not heat seawater, it heats air leaving the humidifier such that the maximum temperature is for air at state a,3. This way, effective condensation of the humid air takes place in the dehumidifier that witnesses the maximum temperature difference between humid air and cold seawater. Besides, seawater is heated to higher temperature as it leaves the dehumidifier and it is directed to the humidifier to preheat the air leading to effective humidification. A previous study [14] shows that this system is thermodynamically superior in terms of its higher GOR compared to water heated system.

3.1.2 Heat Pump Cycle

For the heat pump cycle, the liquid refrigerant leaving the expansion valve undergoes phase change in the evaporator, where the refrigerant evaporates by absorbing heat from the incoming seawater. The vaporized refrigerant is then compressed in the compressor. The compressed refrigerant then condenses in the condenser heat exchanger by giving off its latent heat to the pre-heated seawater that leaves the dehumidifier in the case of Water heated HDH Cycle (while it heats air in the case of modified air heated cycle). The condensed refrigerant expands through the expansion valve and is returned to the evaporator of the heat pump to complete the cycle. The schematic diagram of the two cycles is shown in Figs. (3.1 & 3.2).

3.2 Mathematical Model

To model the water-heated and air-heated HDH cycles depicted in Figs. 3.1 & 3.2, the following assumptions are taken into consideration:

I. Heat losses to the surroundings are neglected.

II. Pumping and fan powers are negligible compared to compressor power input

III. The system runs in a steady-state condition.

IV. Kinetic and potential energy terms are neglected in the energy balance.

The presented model is based on a thermodynamic analysis where mass and energy balances are applied on each of the cycle components presented in Figs. 3.1 & 3.2

Humidifier:

The mass and energy balance of the humidifier is given as

$$\dot{m}_{w,3} = \dot{m}_a(\omega_{a,2} - \omega_{a,1}) + \dot{m}_{w,4} \tag{1}$$

$$\dot{m}_w h_{w,3} - \dot{m}_b h_{w,4} = \dot{m}_a(h_{a,2} - h_{a,1}) \tag{2}$$

Note that

$$\dot{m}_{w,4} = \dot{m}_b \tag{3}$$

$$\dot{m}_{s,w} = \dot{m}_{w,1} = \dot{m}_{w,2} = \dot{m}_{w,3} = \dot{m}_w \tag{4}$$

Dehumidifier:

The mass and energy balance of the humidifier can be express as

$$\dot{m}_{fw} = \dot{m}_{w,5} = \dot{m}_a(\omega_{a,2} - \omega_{a,3}) \tag{5}$$

$$\dot{m}_w(h_{w,1} - h_{w,2}) = \dot{m}_{fw} h_{w,5} + \dot{m}_a(h_{a,3} - h_{a,2}) \tag{6}$$

Evaporator:

The mass and energy balance of the evaporator is given as

$$\dot{m}_r = \text{constant} \tag{7}$$

$$\dot{Q}_{evap} = \dot{m}_r(h_{r,1} - h_{r,4}) = \dot{m}_w(h_{sw} - h_{w,1}) \tag{8}$$

Compressor:

The power consumed by the compressor can be expressed as:

$$\dot{W}_{comp} = \dot{m}_r\left(h_{r,2} - h_{r,1}\right) \tag{9}$$

Condenser:

For the heat rejection by the condenser, the following expression on the energy balance in the condenser can be used:

$$\dot{Q}_{cond} = \dot{m}_r\left(h_{r,2} - h_{r,3}\right) = \dot{m}_w\left(h_{w,3} - h_{w,2}\right) \tag{10}$$

In case of modified air heated cycle, the last term in Eq. (10) is replaced by $\dot{m}_a(h_{3a} - h_{2a})$

Expansion (Throttling) Valve:

Throttle valve is a constant enthalpy device. The energy balance on the expansion valve can be express as:

$$h_{r,4} = h_{r,3} \tag{11}$$

The effectiveness of the humidifier is defined as the ratio of actual enthalpy change of either stream ($\Delta\dot{H}$) to maximum possible enthalpy change ($\Delta\dot{H}_{max}$), and may be expressed as [11,34,35,110]:

$$\varepsilon_H = \max\left\{\frac{h_{a,out} - h_{a,in}}{h_{a,out,ideal} - h_{a,in}}, \frac{h_{w,in} - h_{w,out}}{h_{w,in} - h_{w,out,ideal}}\right\} \tag{12}$$

Similarly the effectiveness of the dehumidifier can be expressed as [11,34,35,110]:

$$\varepsilon_D = \max\left\{\frac{h_{a,in} - h_{a,out}}{h_{a,in} - h_{a,out,ideal}}, \frac{h_{w,out} - h_{w,in}}{h_{w,out,ideal} - h_{w,in}}\right\} \tag{13}$$

where the ideal outlet air enthalpy ($h_{a,out,ideal}$) is calculated when the outlet air is fully saturated at the water inlet temperature, while the ideal outlet seawater enthalpy ($h_{w,out,ideal}$) is calculated when its temperature is equal to the inlet air dry-bulb temperature.

The System Performance Index Used

Gain Output Ratio (GOR)

The energy performance for HDH and other thermal desalination systems is tagged as the gained output ratio. GOR is the most important performance indicator for HDH system. it is defined as the ratio of latent heat of evaporation of the distillate produced to the total energy input into the system, and it is generally expressed as:

$$GOR = \frac{\dot{m}_{fw} h_{fg}}{\dot{E}_{in}} \tag{14}$$

For this system, GOR can be expressed as [109,111]:

$$GOR = \frac{\dot{m}_{fw} h_{fg}}{\dot{W}_{comp}} \tag{15}$$

The specific work consumption (sW)

The specific work consumption is the amount of electrical energy (in kJ) consumed to produce one kilogram of fresh water, and can be expressed as [112]:

$$SW = \frac{\dot{w}_{comp}}{\dot{m}_{fw}} \tag{16}$$

The GOR of the current system can be expressed in terms of SW, which is given as:

$$\mathrm{GOR} = \frac{\mathrm{h_{fg}}}{\mathrm{SW}} \tag{17}$$

Recovery Ratio (RR)

The recovery ratio is another performance indicator of HDH system, which is defined as the ratio of produced fresh water flow rate to the seawater flow rate, and can be expressed as:

$$\mathrm{RR}(\%) = \frac{\dot{\mathrm{m}}_{\mathrm{fw}}}{\dot{\mathrm{m}}_{\mathrm{sw}}} \times 100 \tag{18}$$

Mass flowrate ratio (MR)

Mass flowrate ratio is defined as the ratio of seawater mass flow rate to the circulating dry air mass flow rate in the cycle, can be expressed as:

$$\mathrm{MR} = \frac{\dot{\mathrm{m}}_{\mathrm{sw}}}{\dot{\mathrm{m}}_{\mathrm{a}}} \tag{19}$$

The presented equations were solved using the commercial software, Engineering Equation Solver (EES) that uses accurate equations to model the properties of moist air and water. EES is a numerical solver, and it uses an iterative procedure to solve the equations. The calculations converge if the relative equation residuals is lesser than 10^{-6} or if change in variables is less than 10^{-9} [14].

3.3 Results and discussion

The following values are assumed throughout this work, and their value will be specified if otherwise: the condensing (High) pressure which is the pressure at which the refrigerant change phase from a vapor to a liquid, is assumed to be 1378 kPa (200 psi), while the evaporating (low) pressure which is the pressure at which the refrigerant change phase from a liquid to a vapor, is assumed to be 240 kPa (35 psi). The relative humidity, humidifier effectiveness, dehumidifier effectiveness, and refrigerant mass flow rate are assumed to be 100%, 80%, 80%, and 0.05kg/s respectively. The used refrigerant is R-134a. It has been shown that the use of pure water properties instead of seawater properties does not significantly affect the performance of the HDH cycle [113]. In fact, calculations showed that the change in peak GOR, when using 35000 ppm seawater properties, is less than 1% as compared to that when using pure water, while all of the general trends remained unchanged [114]. Hence, this approximation is used in this work.

To ensure that the presented model has good prediction capability, the HDH models are validated against the work of Sharqawy et al. [11]. The validated results are shown in Figs. 3.3 (a & b) for water heated and modified air heated cycle respectively. The present models produce the same trends and are in good agreement with the work of Sharqawy et al. [11], as shown in Figs. (3.3a,b). No percentage deviations are observed for the validation of heat pump model against an example and a problem taken from Cengel and Boles [115]. After model validations, the heat pump model is then coupled with HDH model to provide a combined HDH-heat pump system as sketched in Figs. (3.1 & 3.2). The performance of the combined system (HDH and heat pump cycles) are presented in Figs. 3.4 to 3.14

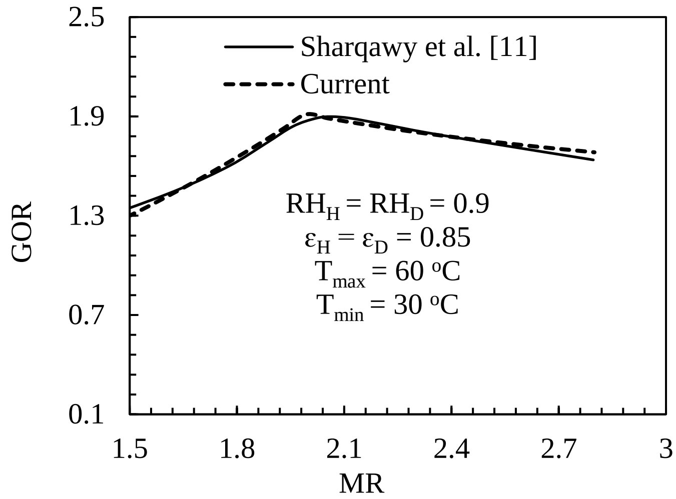

Fig. 3.3(a): Water heated cycle

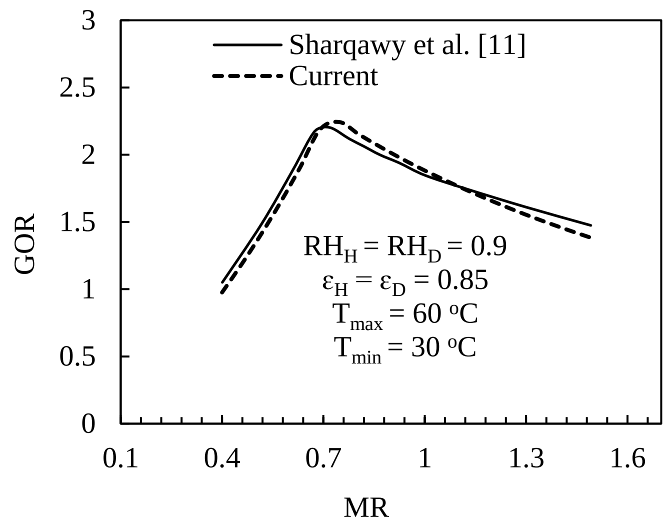

Fig. 3.3(b): Modified Air heated cycle

Figure 3. 3: Effect of mass flowrate ratio on gain output ratio

One of the major performance indicators of HDH system is the gained output ratio (GOR). Improving the GOR of HDH system represents a contribution toward industrialization of the system, and to the academic literature. Figs. 3.4(a & b) show the influence of mass flow rate ratio (MR) on the gain output ratio at different feed water flowrates for both water heated and modified air heated cycles respectively. The mass flow rate ratio indicates the right amount of water to be sprayed in the humidifier, so that air is humidified to the extent needed as per the humidifier effectiveness [11]. As observed from both figures, increasing MR leads to increase in the GOR of the system to its peak value, and then decreases with further increase in MR for a fixed feed water flow rate. The decrease in GOR with increasing MR may be due to flooding of the system caused by too much water supply with insufficient air supplied and vice versa. The peak value of the GOR signifies the optimum flow rate of circulating air and feed water. It can also be observed that higher feed water flowrates yield greater values of GOR, because of higher water evaporation, which leads to higher productivity, and consequently higher GOR. At optimum MR, the influence of feed water flowrate in more pronounced for water heated cycle when compared to modified air heated cycle, where feed water flowrate effect is not significant. Optimum MR in Fig. 3.4(a) is noticed to shift slightly to left by increasing feed water flow rate. This happens because at a higher water flow rate, more air flow is required to absorb additional water vapor to approach saturation condition. Therefore, the optimum MR value decreases. For example, for water flow rate of 0.1 kg/s and an optimum MR = 1.4, the air flow rate is 0.071 kg/s; however, this value increases to 0.23 kg/s for a water flow rate of 0.3 kg/s at an optimum MR value of 1.3.

The modified air heated cycle portrays higher peak value of the gain output ratio, due to the fact that less amount of energy is required for heating the humidified air compared to the heating water for water-heated cycle. It is well known that humid air is better heated, which also leads to an increase in the pre-heat feed water temperature in the dehumidifier, leading to reduced overall energy needed to produce the same quantity of condensate thereby increasing the GOR of the system. The comparison between water and modified air heated cycle can be made at feed water flow rate of 0.3kg/s, where we observed GOR of 7.426 at optimum MR of 1.3, and GOR of 8.463 at MR of 0.63 for water and modified air-heated cycles, respectively. It can also be observed that depending on the value of MR, a higher value of GOR can be achieved for either water heated or modified air-heated system. For instance, at MR value of 1.5 and Mw of 0.7 kg/s, we attained a GOR of 5.147 and 3.351 for water heated or modified air-heated cycles, respectively, while at MR value of 0.4 and Mw of 0.7 kg/s, we attained a GOR of 3.535 and 4.798 for water heated or modified air-heated cycles respectively. It can also be noticed Figs. 3.4(a & b) that the air heated cycle has a lower optimum mass flow rate ratio compared to the water heated cycle. This is due to the considerably larger volumetric flow rate of air in the air-heated cycle compared to the water heated cycle. Larger air flowrates means lower MR, and consequently lower optimum MR.

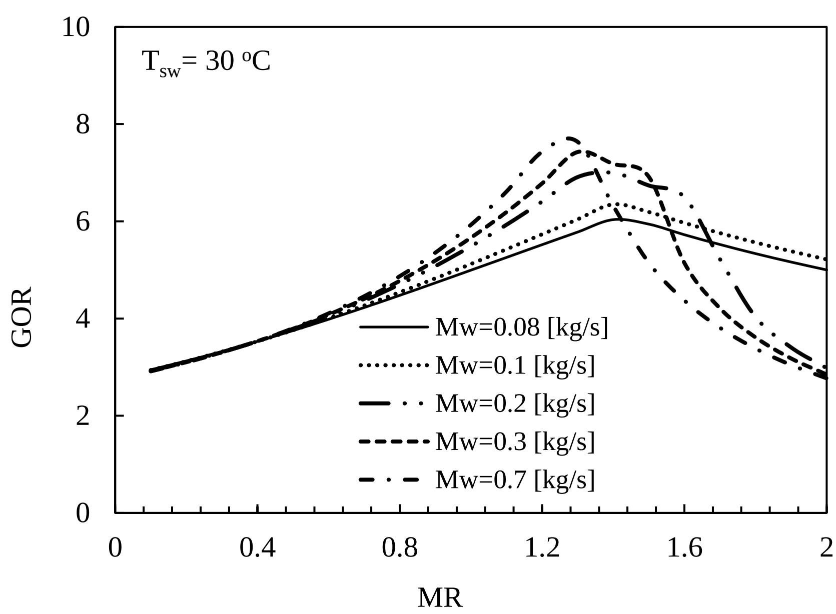

Fig. 3.4(a): Water heated cycle

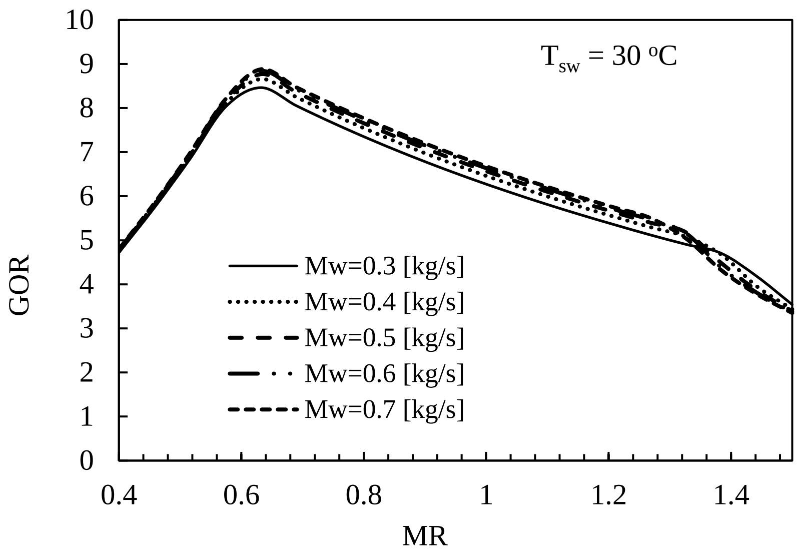

Fig. 3.4(b): Modified Air heated cycle

Figure 3. 4: Influence of mass flow rate ratio on gain output ratio

The impact of seawater temperature on GOR at different mass ratios is depicted in Figs. 3.5(a & b) for both water-heated and modified air-heated cycles. As observed, increasing the seawater temperature enhance the GOR of the system. However, optimum GOR exists at which further increase in seawater temperature will lead to decreases in GOR. On the other hand, higher seawater temperature may result in less effective condensation in the dehumidifier due to low temperature difference. The peak GOR value is observed to slightly increase with MR as seen in water-heated cycle, and differs as observed from modified air-heated cycle. Increasing the seawater temperature favors better GOR because less amount of energy will be required to raise the seawater temperature entering the humidifier at its maximum value. Figs. 3.5 (a & b) also give information on the right water and air flow rates to run the system for a particular seawater temperature (seasonal temperature change). For instance, in summer season where the seawater temperature is expected to be above 30°C, Fig. 3.5(a) suggests to run the system at mass ratio of 1.4

(around m_w of 0.1 kg/s and m_a of 0.07 kg/s). Whereas in winter, where the seawater temperature is around 20-22 ^oC, the system is recommended to be operated at mass flowrate ratio of 1.0.

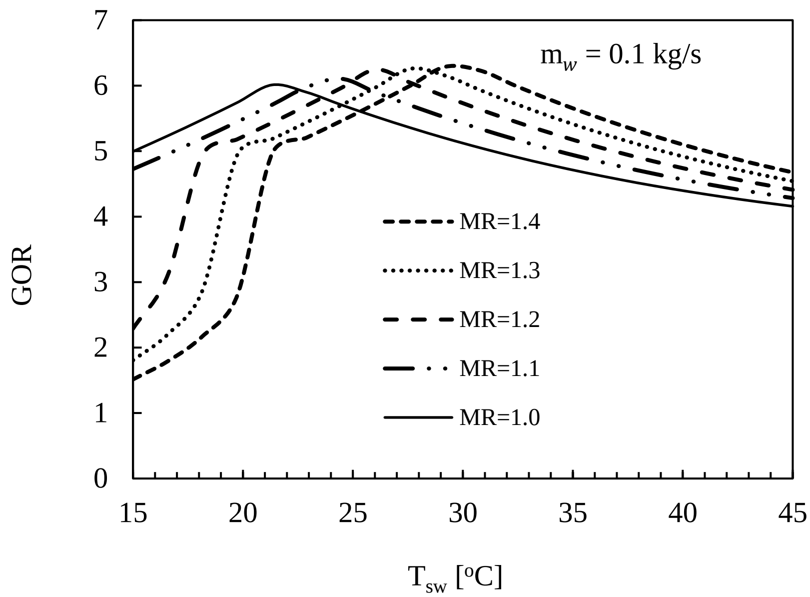

Fig. 3.5(a): Water heated cycle

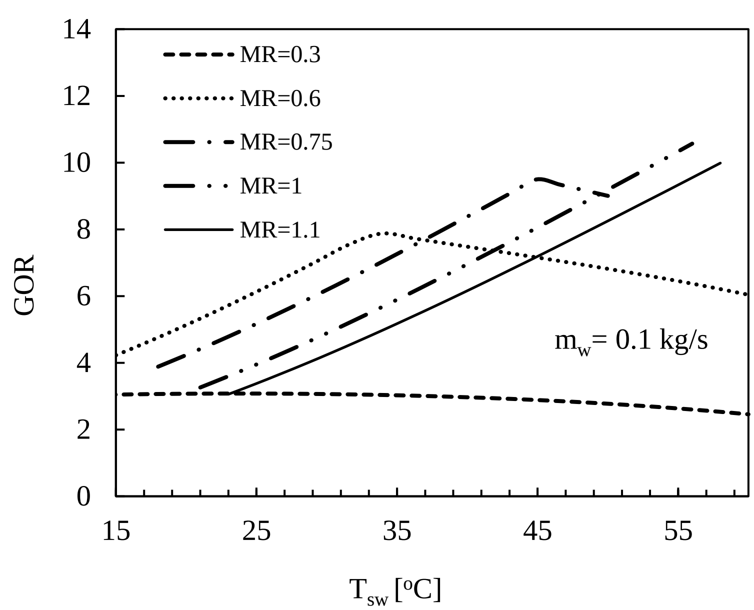

Fig. 3.5(b): Modified Air heated cycle

Figure 3. 5: Effect of feed seawater temperature on gain output ratio

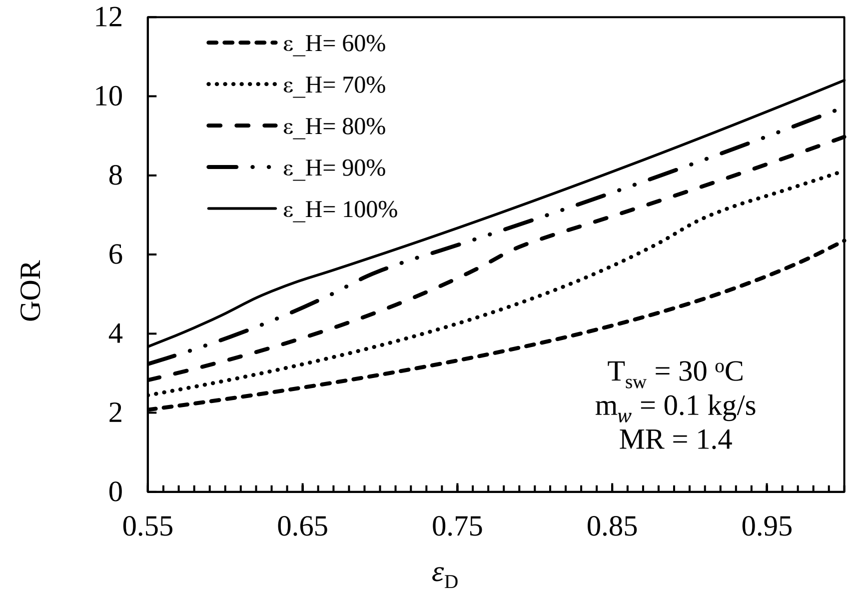

Fig. 3.6(a): Water heated cycle

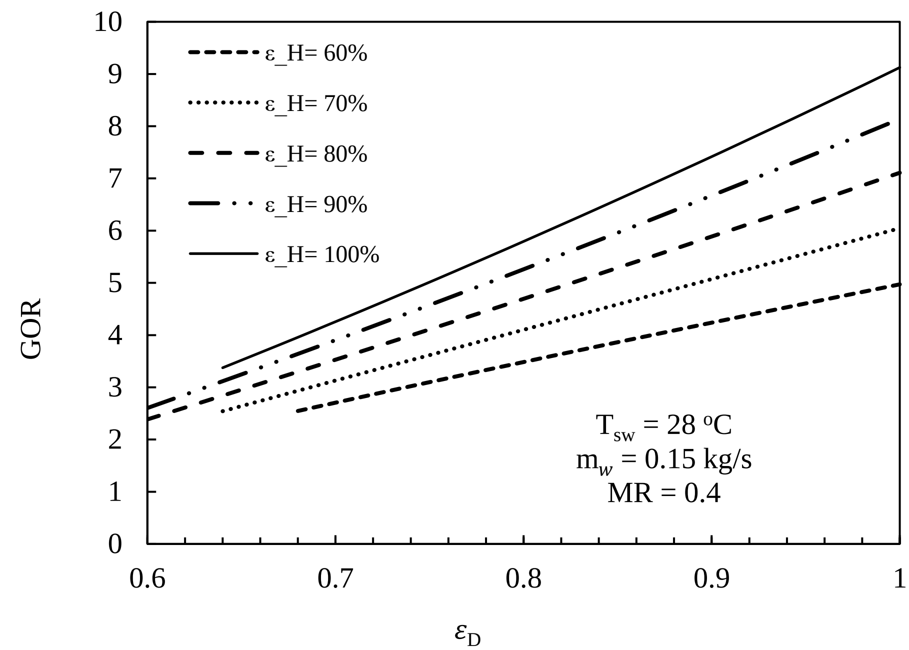

Fig. 3.6(b): Modified Air heated cycle

Figure 3. 6: Effect of components effectiveness on gain output ratio

Figs. 3.6(a & b) shows the influence of humidifier effectiveness and the dehumidifier effectiveness on the gain output ratio. GOR is observed to increase with increasing both humidifier effectiveness and the dehumidifier effectiveness. The effect of components effectiveness on GOR is noticed to be greater at higher effectiveness values, and lower at lower effectiveness values. A closed examination of the figures shows that the dehumidifier effectiveness is more effective as compared to humidifier effectiveness, which matches prior observations in the literature [14]. For example, for water heated cycle, at 60% dehumidifier effectiveness, increasing humidifier effectiveness from 60 – 100% improve the GOR by about 50.3%, while at humidifier effectiveness of 60%, increasing the dehumidifier effectiveness from 60 – 100% improve the GOR by about 128%. High effectiveness of both humidifier and the dehumidifier portrayed important advantages in terms of GOR. However, large areas are needed for the high effectiveness, hence; the initial cost of the system is expected to be high.

The effect of mass flowrate ratio (MR) at different feed water flowrates on the top system temperature is presented in Figs. 3.7(a & b). For the water heated cycle, the optimum top system temperature is observed to occur at the same MR (MR of 1.4) for all feed water flow rates. For the case of modified air-heated cycle, the top temperature is observed to increase significantly with increasing MR, because it is easy to heat humidified air compared to water due to its low specific heat. It can also be observed that at higher feed water flow rate, the effect of MR on the top temperature observed to be less compared to lower feed water flowrate for both cycle. In all cases, decreasing the feed water flow rate leads to increase in the top temperatures. This is due to increase in the water residence time (dwelling time) in the condenser heat exchanger, which permits more exchange of heat to raise the top temperature. In other words, to transfer the same rate of energy, decreasing the mass flow rate requires high temperature difference for a given value of specific heat (C_P).

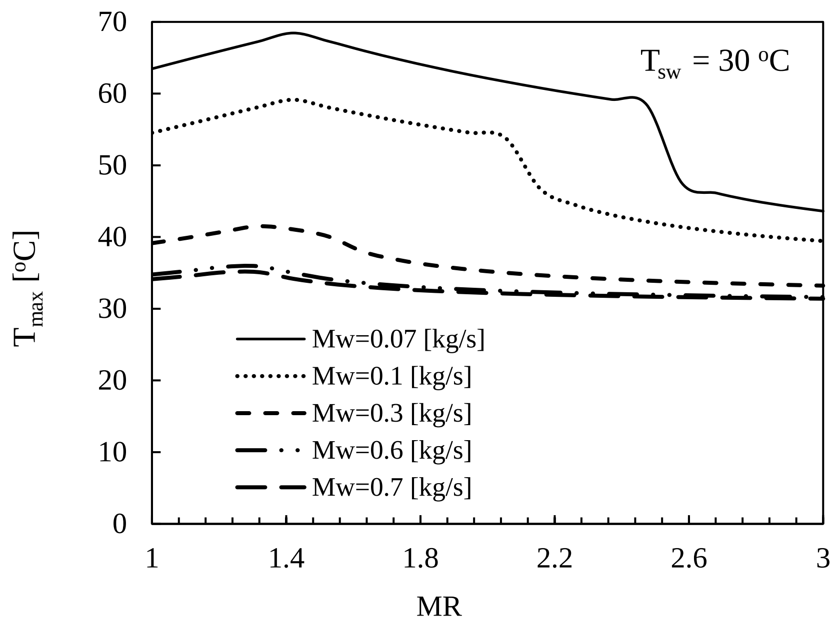

Fig. 3.7(a): Water heated cycle

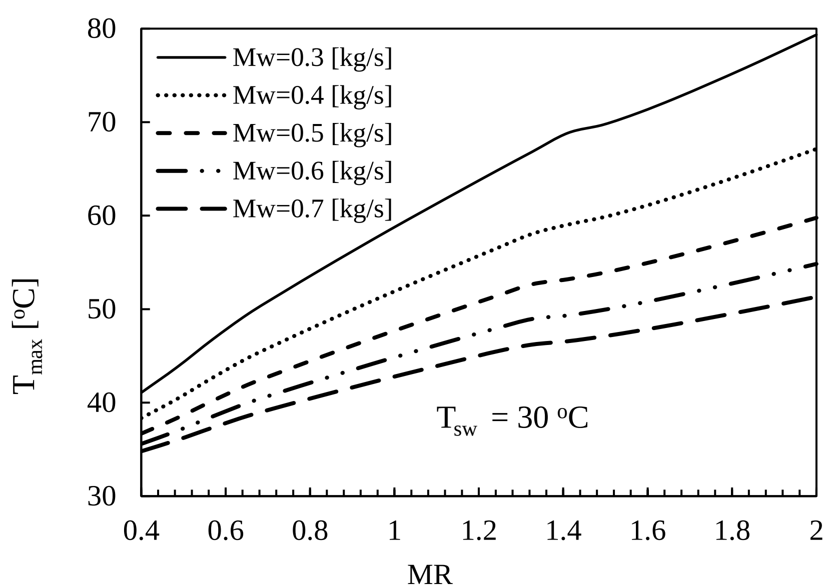

Fig. 3.7(b): Modified Air heated cycle

Figure 3. 7: Influence of mass flow rate ratio on top system temperature

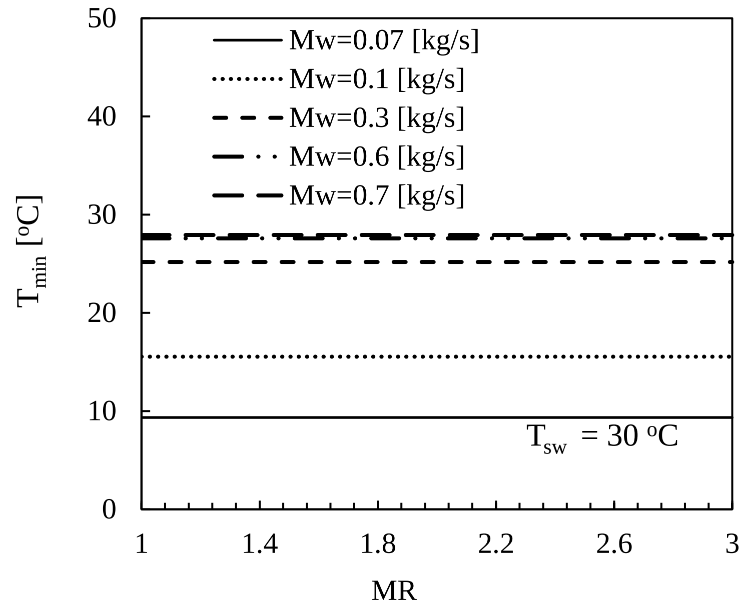

Fig. 8(a): Water heated cycle

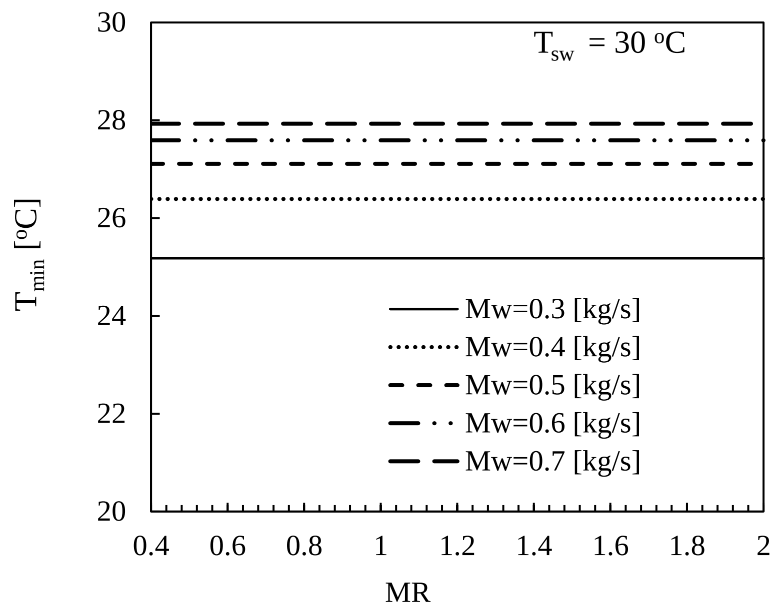

Fig. 3.8(b): Modified Air heated cycle

Figure 3. 8: Effect of mass flow rate ratio on bottom system temperature

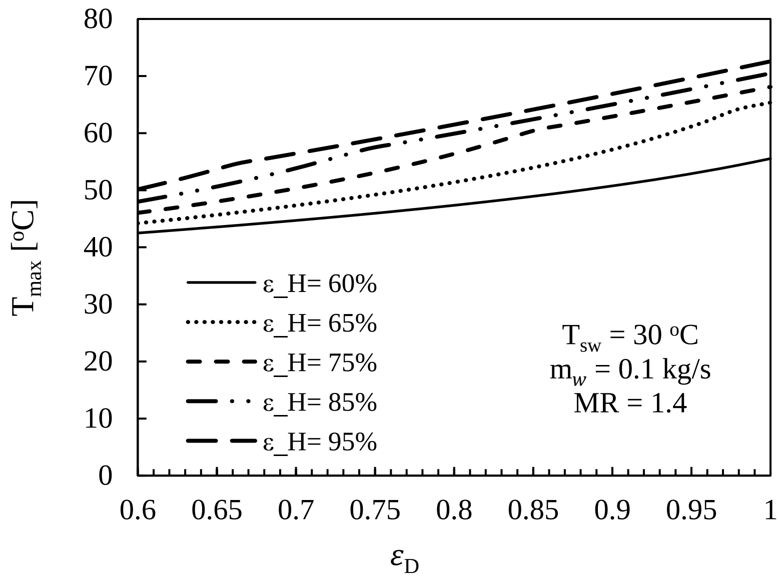

Fig. 3.9(a): Water heated cycle

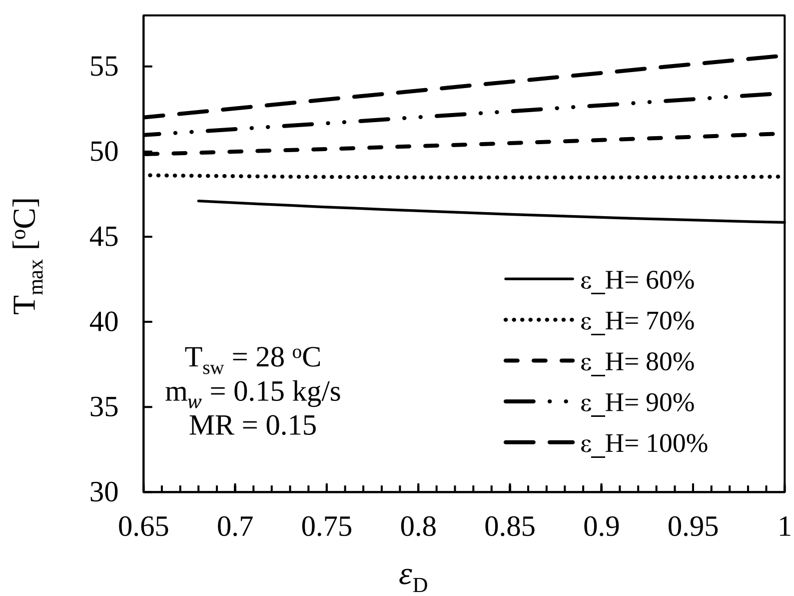

Fig. 3.9(b): Modified Air heated cycle

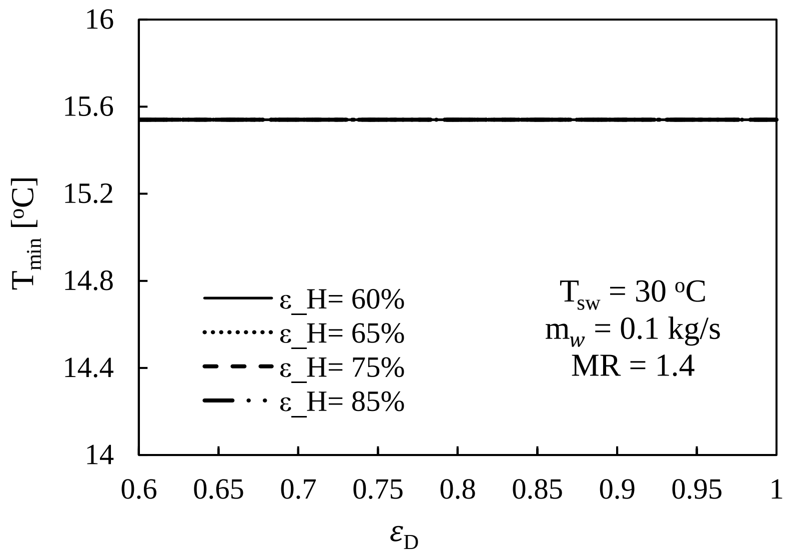

Fig. 3.9(c): Water heated cycle

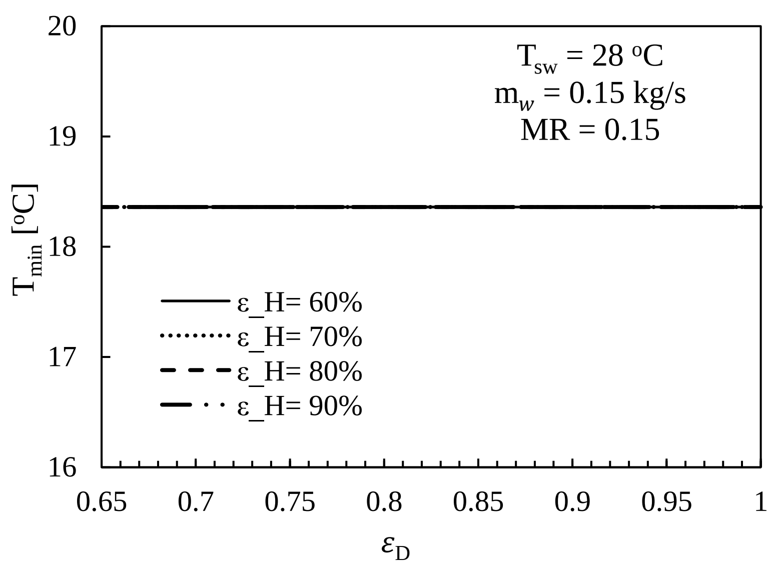

Fig. 3.9(d): Modified Air heated cycle

Figure 3. 9: Influence of components effectiveness on top and bottom system temperature

Figs. 3.8(a & b) display the effect of mass flow rate ratio at different feed water flow rate on the bottom temperature (lowest seawater temperature of the system). The effect of MR is noticed to be insignificant of system bottom temperature (seawater temperature leaving the evaporator into the dehumidifier), because heat pump evaporator is an independent component from HDH cycle. However, seawater flow rate significantly influences the system bottom temperature, especially at lower water flow rate. System bottom temperatures is observed to be lowest at lowest feed water flow rate, because low feed water flow rate signifies lager residence/dwelling time that allows better exchange of heat at the evaporator heat exchangers.

The effect of humidifier and dehumidifier effectiveness on the system top temperature is presented in Figs. 3.9(a & b). Higher effectiveness of both humidifier and dehumidifier encouraged better system top temperature for both water and modified air-heated cycles, since higher component effectiveness will result in better heat exchange. Increasing the effectiveness of both components provides higher humidified air temperature in the humidifier, and condensation of evaporated water in the dehumidifier, which improve the pre-heating temperature and consequently the top temperature of the system. However, the influence of humidifier and dehumidifier effectiveness on bottom temperature of the system as demonstrated in Figs. 3.9(c & d) suggested independency of system bottom temperature on effectiveness of both humidifier and dehumidifier for both modified air and water-heated cycles since the selection of the evaporator is independent of HDH system component selection.

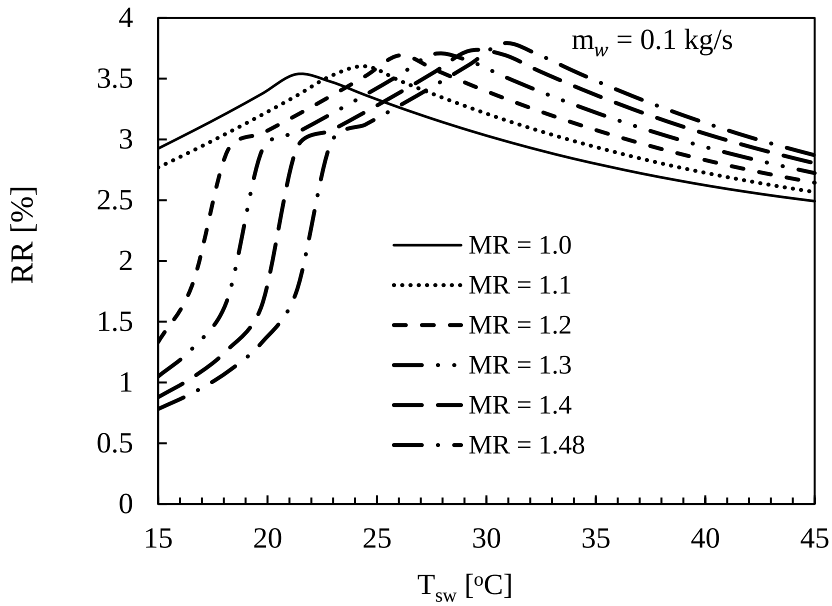

Fig. 3.10(a): Water heated cycle

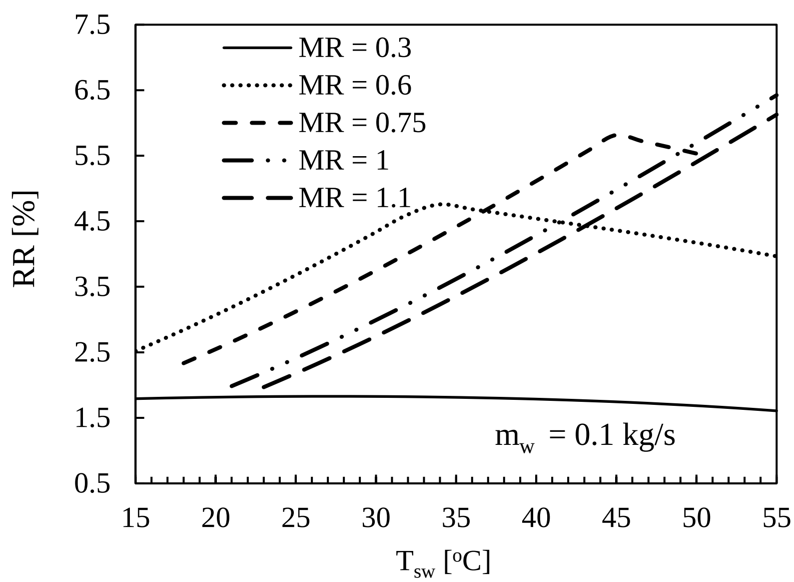

Fig. 3.10(b): Modified Air heated cycle

Figure 3. 10: Effect of feed seawater temperature on recovery ratio

Another important parameter that plays a vital role in evaluating the performance of HDH system is the recovery ratio (RR), which is defined as the ratio of produced fresh water flow rate to feed seawater flow rate. Presented in Figs. 3.10(a & b) is the effect of MR and feed water temperature on the recovery ratio for both water and modified air-heated cycles. The RR increases with increasing seawater temperature, because high feed seawater temperature results in higher system top temperature, which provides better evaporation for humidification, leading to more distillate, and consequently higher RR. However, peak recovery ratio exists at which further increase in seawater temperature decreases recovery ratio. The peak RR suggest the best MR to be used for a particular weather season. For instance, in winter where the weather temperature is well below 20^{o}C, MR of 1.0 or less may be used in accordance to (Fig. 3.10a).

Refrigerant flow rate can significantly influence the rejected heat in the condenser. The combined effect of refrigerant flow rate and seawater temperature on the gain output ratio is presented in Figs. 3.11(a & b). Increasing the refrigerant flow rate reduces the GOR of the system, due to increase in power demand by the compressor. The figure also suggested the optimum seawater temperature (30 ^{o}C) to operate the system. Furthermore, decreasing seawater temperature enhances the GOR of the system, because less energy will be needed in the evaporator to achieve the required bottom temperature of the system.

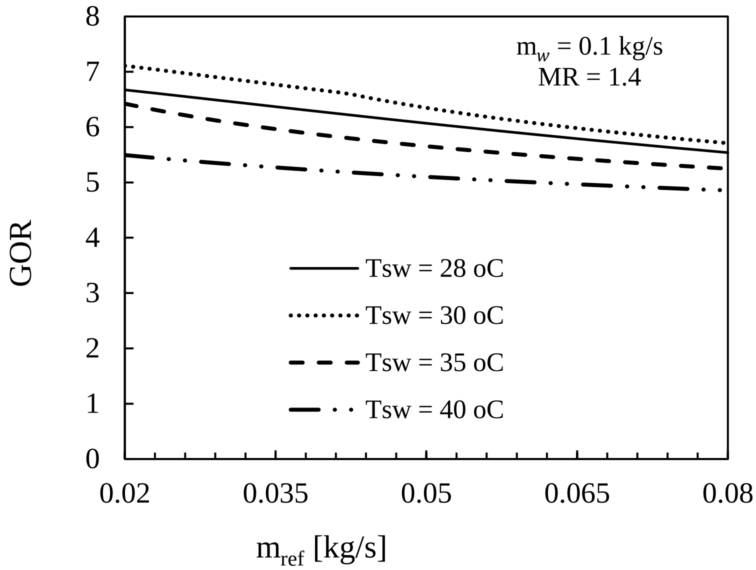

Fig. 3.11(a): Water heated cycle

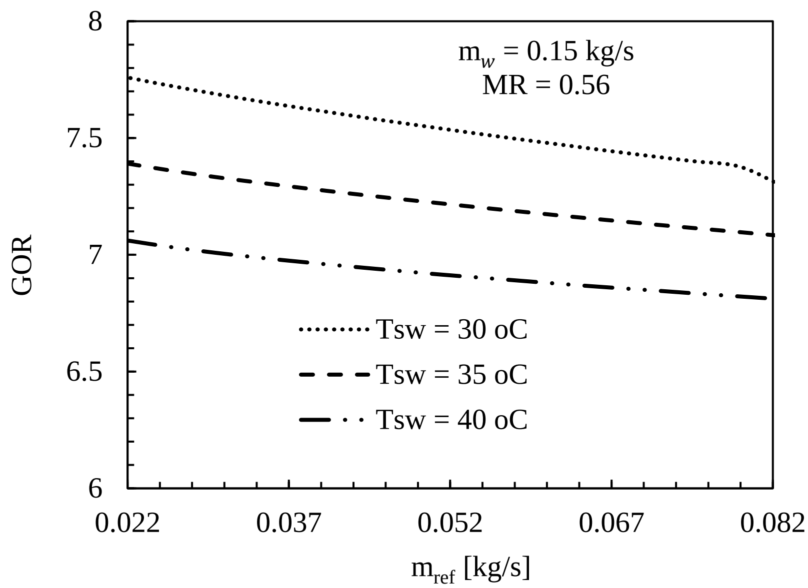

Fig. 3.11(b): Modified Air heated cycle

Figure 3. 11: Influence of refrigerant flow rate ratio on gain output ratio

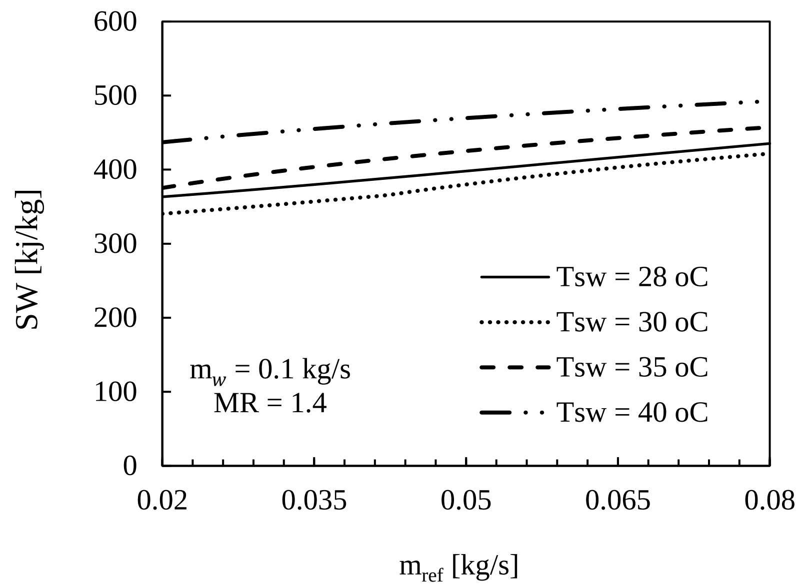

Fig. 3.12(a): Water heated cycle

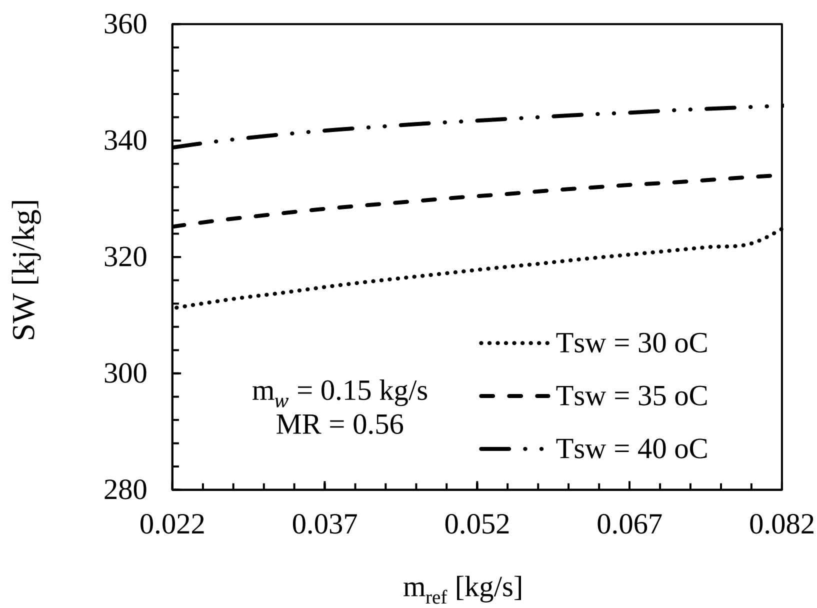

Fig. 3.12(b): Modified Air heated cycle

Figure 3. 12: Influence of refrigerant flow rate ratio on specific work

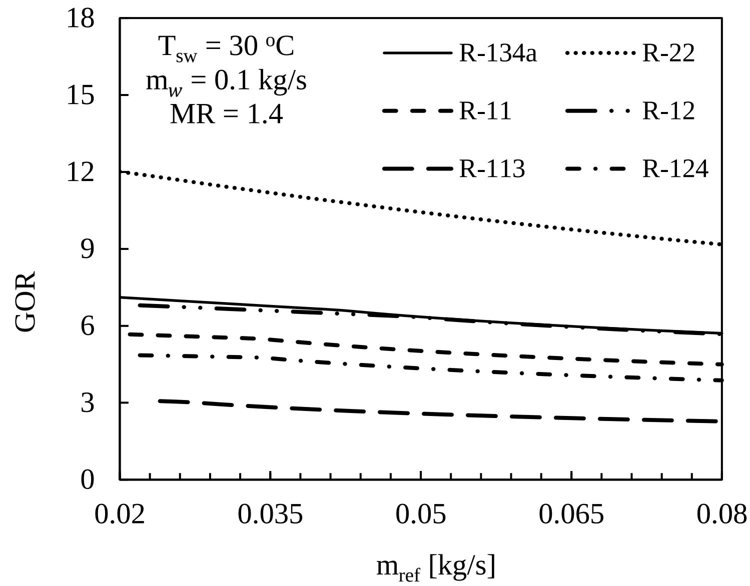

Fig. 3.13(a): Water heated cycle

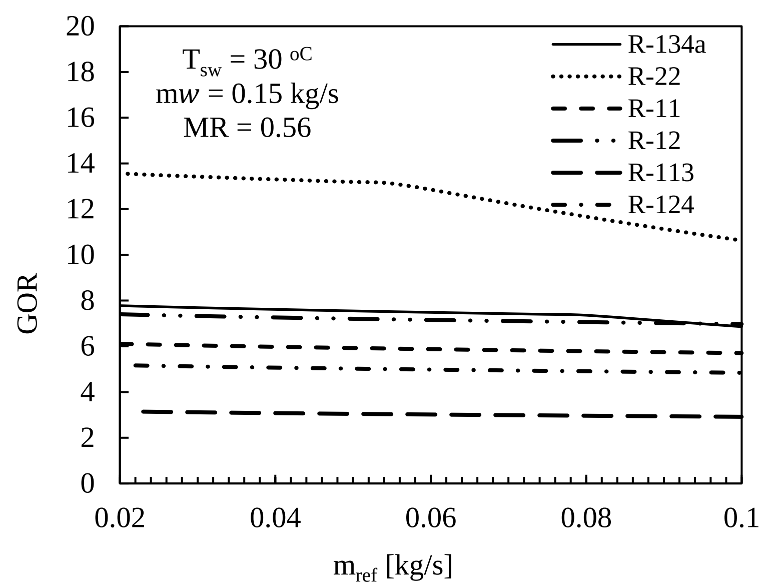

Fig. 3.13(b): Modified Air heated cycle

Figure 3. 13: Effect of refrigerant flow rate ratio on gain output ratio

Presented in Figs. 3.12(a & b) is the influence of refrigerant flow rate and seawater temperature on the specific work of the system. The specific work consumption (SW) is the amount of energy consumed to produce one kilogram of fresh water. Increasing the refrigerant flow rate increases the amount of energy consumed by the compressor to produce one kilogram of fresh water. Thus, high refrigerant flow rate means high demand of compressor power. Similar to Figs. 3.11(a & b), Figs. 3.12(a & b) also suggested that low energy would be needed to produce fresh water if the heat pump is operated at lower temperatures.

Every refrigerant has different properties; as such, their behavior and performance differs from one to another. To select the right refrigerant, the effects of different refrigerants were investigated on GOR and SW, and the obtained results are presented in Figs. 3.13 & 3.14(a, b), respectively. It can be observed that increasing the refrigerant flow rate decreases the GOR of the system and increase the SW, due to increase in the compressor work required to compress the refrigerant. As noticed from Figs. 3.13(a & b), the refrigerant that gives the best GOR (maximum GOR of 13.547 at m_{ref} of 0.02 kg/s) and SW (maximum SW of 222 kJ/kg at m_{ref} of 0.1 kg/s) is chlorodifluoromethane (R-22), while trichlorotrifluoroethane (R-113) produces the least value of the gain output ratio (maximum GOR of 3.142 at m_{ref} of 0.023 kg/s) and highest value of specific work consumption (maximum SW of 815.4 kJ/kg at m_{ref} of 0.1 kg/s). However, based on health and environmental safety, R-22 is not adopted in this work. Therefore, Tetrafluoroethane (Freon 134a) is used throughout this study because of its relatively high GOR (maximum GOR of 7.778 at m_{ref} of 0.02 kg/s), relatively low SW (maximum SW of 344.7 kJ/kg at m_{ref} of 0.1 kg/s), better health and environmental safety, and its availability.

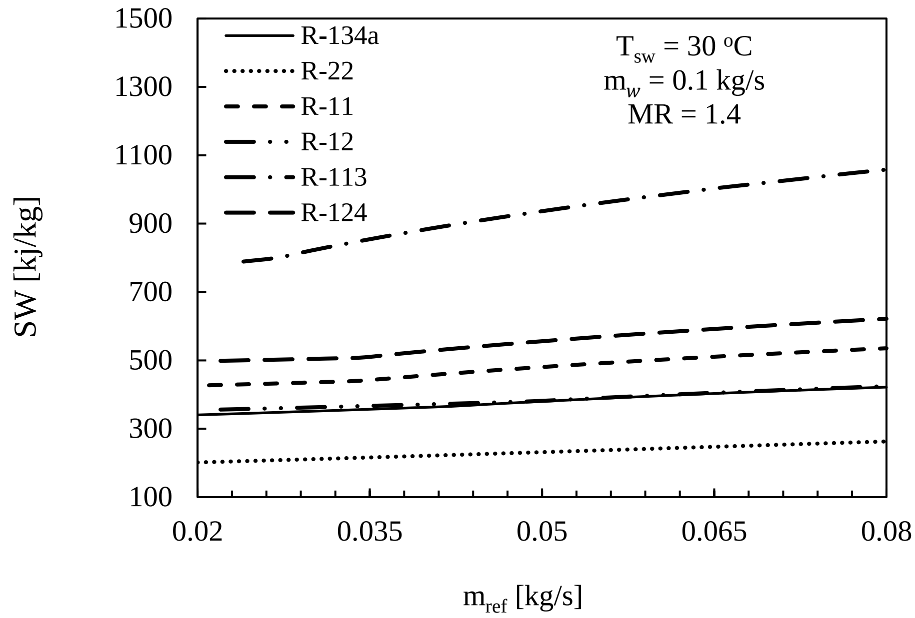

Fig. 3.14(a): Water heated cycle

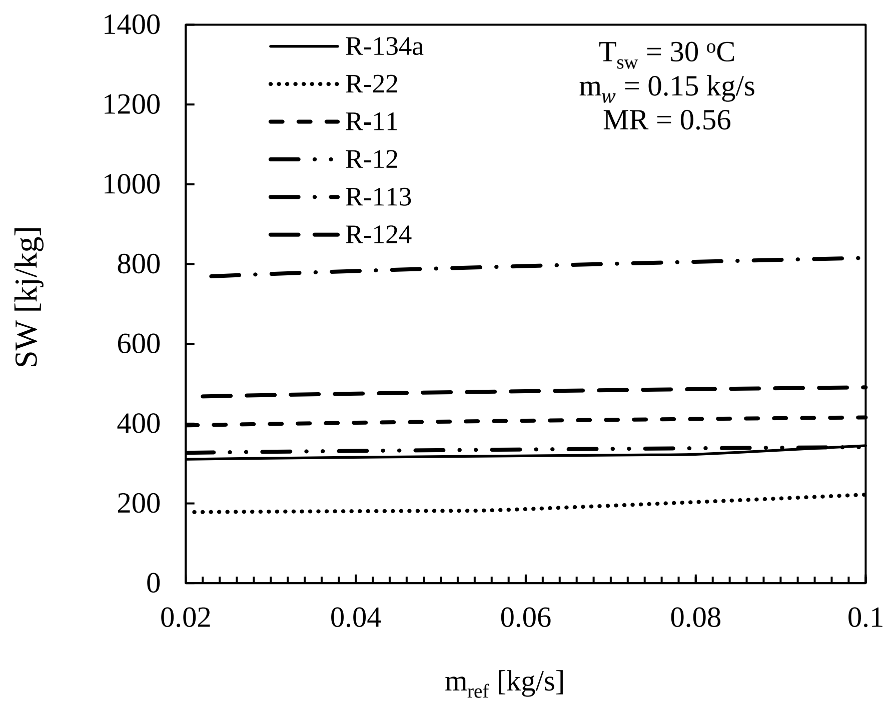

Fig. 3.14(b): Modified Air heated cycle

Figure 3. 14: Effect of refrigerant flow rate ratio on specific work

Cost of desalinated water

In this section, the cost of fresh (desalinated) water from the proposed hybrid HDH-HP system is estimated, taking into consideration several design and operational variables. The economics of mechanically driven heat pump is directly related to the capital cost of the unit and the cost of the input energy ($/kWh) [104]. The capital cost of a typical desalination plant includes items such as the cost of the supply equipment, costs such as piping, tanks, pumps and land and building costs if indoor space is required. The costs may also include shipping, construction, services, etc [99]. The total estimated capital (purchasing and manufacturing) costs include installation cost for the purposed plants are presented in Table 3.1. These costs are based on both the real purchasing prices and assumptions made from the cited references. The following assumptions were made while performing the economic analysis of the system:

- The unit cost of electricity (COE) is 0.07$/kWh [116], 0.09 [117], (0.04-0.09) $/kWh [5]. The upper limit is characteristic of European countries and the lower limit can be found in the Gulf States and the United States [5].
- The annual operator salary (P_S) is 6000$/year [116], with the plant using a single operator for a small plant according to the proposed design.
- The yearly maintenance cost is estimated to be 1.5% of the capital cost [116].
- The annual management cost is estimated as 20% of the labor cost [5,116,118].
- Zero pretreatment costs is assumed [118].
- The interest rate (i) is 5% [116,118].

- The plant life expectancy (n) is 15 years [104], 20 years [99,116–118], 30 years [5].
- The plant availability (f) is 90% [5,118].
- The land costs may be ignored assuming outdoor location and operating in a rural deserted area [99].

The economic analysis performed in the current study is based on the procedure presented in [5].

Table 3. 1: Capital investment cost for HDH-HP plant.

Item Description	Price (US $)	Ref
Control devices	80	[118]
Packed Bed Humidifier	133	[118]
Dehumidifier	70	[118]
Finned Tube Coil Heat Exchangers	120	[-]
Pipes, Fittings	35	[118]
Water Tanks	260	[-]
Pumps And Blowers	345	[118]
Accessories	33	[118]
Heat Pump Units Equipment	7465	[-]
Total	8541	

Capital cost and equipment costs

The capital cost (Cc) includes the purchase cost of major equipment, auxiliary equipment, construction, management, etc given in Table 3.1. The annual capital cost or fixed charges (C_F) of the system can be determined by multiplying the capital cost given in Table 3.1 and the amortization factor(α).

Operating costs

The operating costs include the following items; labor, energy, spare parts, amortization or fixed charges, and miscellaneous. The energy costs is the cost of energy consumption by the system. The consumed electrical energy for the compressor is presented in Figures 12. Note that the unit is in kJ/kg, which can be converted to kWh/kg by dividing the former by a factor of 3600.

The amortization charges also known to as capital recovery factor (CRF) [119] can be expressed as [5,116–119]:

$$\alpha = \frac{i(i+1)^n}{(i+1)^n - 1} \tag{20}$$

Where α is the amortization factor, i is the interest rate and n is the amortization years (life of the system). The following expressions may be used to calculate various components of product cost per annum [5]:

The annual capital cost (C_F);

$$C_F\left(\frac{\$}{yr}\right) = C_c(\$) \times \alpha\ (yr^{-1}) \tag{21}$$

The annual electric power cost (EPC);

$$EPC\left(\frac{\$}{yr}\right) = COE\left(\frac{\$}{kWh}\right) \times \frac{SW}{3600}\left(\frac{kWh}{kg}\right) \times f \times Product\left(\frac{kg}{day}\right) \times 365 \tag{22}$$

The annual labor cost (L_C);

$$L_C\left(\frac{\$}{yr}\right) = \mathcal{L}\left(\frac{\$}{kg}\right) \times f \times \text{Product}\left(\frac{kg}{day}\right) \times 365 \tag{23}$$

Where $\mathcal{L}$ is the specific cost of operating labor ($/kg) which can be calculated from;

$$\mathcal{L}\left(\frac{\$}{kg}\right) = \left(\frac{\text{Operator salary}\left(\frac{\$}{yr}\right)}{\text{Product}\left(\frac{kg}{day}\right) \times 365}\right) \tag{24}$$

The total annual cost (C_T);

$$C_T\left(\frac{\$}{yr}\right) = C_F\left(\frac{\$}{yr}\right) + PC\left(\frac{\$}{yr}\right) + L_C\left(\frac{\$}{yr}\right) \tag{25}$$

The unit product cost (C_P);

$$C_P\left(\frac{\$}{kg}\right) = \left(\frac{C_T\left(\frac{\$}{yr}\right)}{f \times \text{Product}\left(\frac{kg}{day}\right) \times 365}\right) \tag{24}$$

The results obtained for the cost analysis of the proposed two hybrid systems (water heated and the modified air-heated HDH cycles driven by HP) are shown in Figures 3.15 – 3.17. While Figure 3.15 presented the effect of refrigerant mass flowrates on the cost of the desalted water, Figure 3.16 illustrates the influence of the systems lifetime on the produced fresh water cost. Variation of cost of electricity on the cost of the system productivity is shown in Figure 3.17.

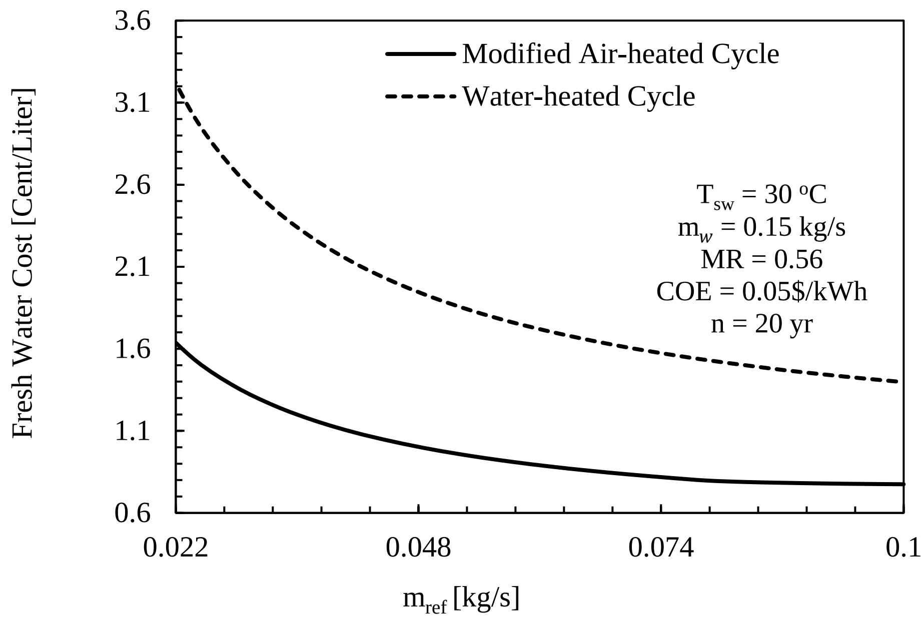

Figure 3. 15: Effect of Refrigerant flowrate on freshwater cost

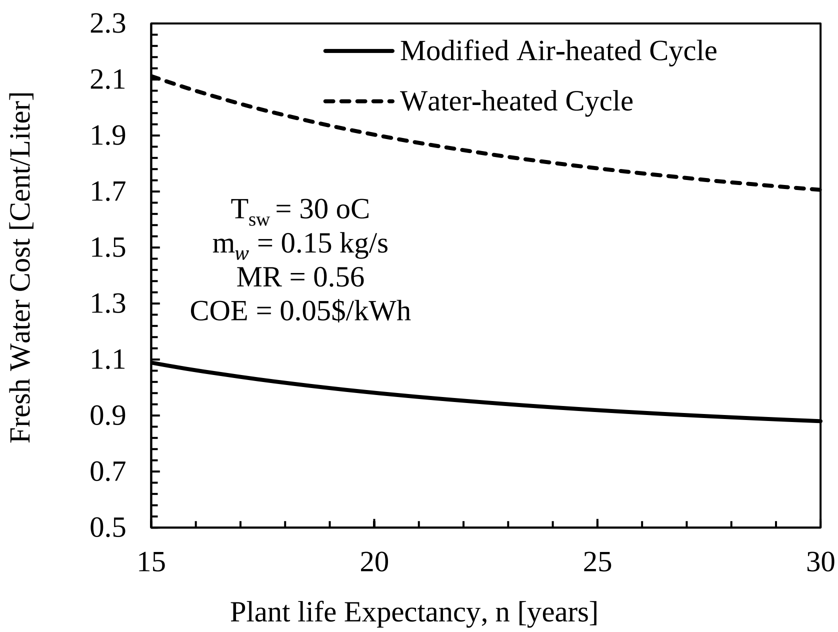

Figure 3. 16: Effect of Plant lifetime on desalted water cost

It can be noticed in Fig. 3.15 that increasing the refrigerant mass flowrate leads to declines in the cost of the freshwater. Although, at high refrigerant flowrates, the specific power consumed by the compressor is high, leading to a high product cost according to Eq. 22. However, the effect of system capacity on the cost of freshwater overcomes that of specific power consumption by the compressor. Therefore, the reduction in the product cost due to increase in the flowrate of the refrigerant can be attributed to the fact that at low refrigerant flow rate, the plants/systems capacity is low, leading to a higher cost of desalted water. Larger plant capacity reduces the capital cost for unit product [5]. For the modified air-heated cycle, the fresh water cost decreases from 0.01746 - 0.007747 $/L, representing about 125% reduction in the product cost. The variation of distillated water cost with plant life expectancy is shown in Fig. 3.16. It can be observed that the cost of desalted water decreases by increasing the plant lifetime. In fact, the expected lifetime for the different desalination plant components and their spent duration depend on the good manufacturing quality, the resistance of different components to corrosion and on the adopted maintenance program [118]. The percentage reduction in the product cost is about 24% for the both cycles, when the plants life is increase from 15 to 30 years. The most critical parameters in cost evaluation are the fixed charges (amortization) and the energy cost [5]. Therefore, it is important to understand the variation of the product cost against the input energy cost because the price of electricity is differs for every locality.

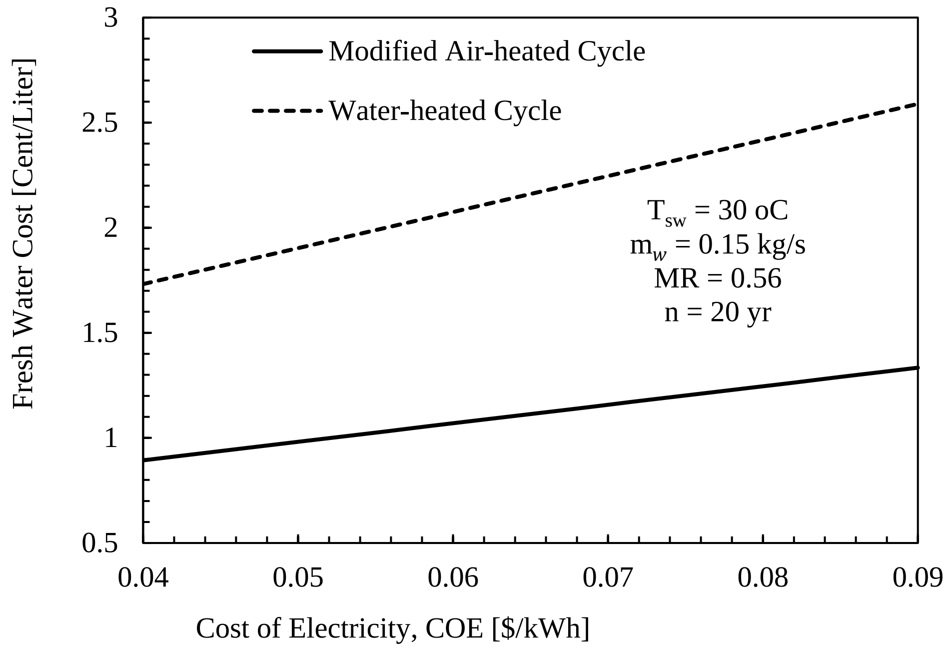

Figure 3. 17: Impact of electricity cost on cost freshwater

The effect of energy cost on the freshwater cost is presented in Fig. 3.17. It can be noticed that high cost of electricity leads to a high product cost and vice versa. This is very clear from Eq. 22 where cost of electricity has a direct correlation with the annual electric power cost. The price of desalted water will be almost double (about 50%) if the COE is increases from 0.04 – 0.09 $/kWh for both air and water. From Figures 3.15-3.17, it is obvious that the modified air-heated cycle has a better (lower) cost of distilled water production as compared to the water heated cycle. This suggested that the energy demand of water-heated cycle is higher than that of air-heated cycle due to the smaller heat capacity of the air than that of the water.

CHAPTER 4

4.0 Exergo-economic Analysis of Water and Modified Air heated HDH Systems coupled with heat pump

In this section, exergo-economic analysis of two configurations of humidification-dehumidification (HDH) desalination systems driven by a vapor compression heat pump (HP) is presented and discussed. The systems are the closed-air open-water water-heated HDH cycle coupled with a heat pump (HP-HDH-WH), and closed-air open-water modified air-heated HDH cycle, integrated with heat pump system (HP-HDH-AH). For the purpose of comparison, a conventional closed-air open-water (CAOW) electric water-heated HDH system (E-HDH-WH) is also presented. Exergy destruction, exergetic efficiency and product cost were evaluated for each system. The influence of system input parameters such as mass flowrate ratio, dehumidifier effectiveness, compressor isentropic efficiency, and feed water temperature on Second-Law efficiency and exergy destruction associated with the major components of the systems were analyzed. The impact of input cost parameters on the price of desalted water was investigated using two different approaches.

4.1 System Description

The system under investigation consists of heat pump system, and an HDH desalination system. The configurations of HDH cycle considered are; the water-heated system (HP-HDH-WH) and the modified air heated (HP-HDH-AH) desalination units. The schematic line diagram of the integrated systems is demonstrated in Figures 4.1 and 4.2. For these systems, the condensing refrigerant vapor in the condenser of the heat pump provides the necessary heat required for desalination process. The refrigerant in the evaporator vaporized by absorbing heat from the incoming seawater, thereby lowering the temperature of seawater exiting the evaporator, which consequently enhances the condensation process in the dehumidifier. As the seawater passes through the dehumidifier, it is preheated by the condensing vapor from the humidified air. The preheated water is either channeled directly to the humidifier (modified air heated cycle) or it is further heated in the condenser to its top system temperature before it enters into the humidifier (water heated cycle). The saline water is sprayed over a packing material, where a portion of the seawater evaporates into the air stream and the rest is rejected as brine from the humidifier.

On the other hand, the dehumidified air stream leaving the dehumidifier is circulated by fan/blower to the humidifier, and flows through the packing bed, where it becomes saturated with the vapor generated in the humidifier. The warm humid air either leaves the humidifier to the dehumidifier directly (water heated cycle) or passes through the condenser of the heat pump where it is further heated to its top system temperature before going to the dehumidifier (modified air heated cycle). The vapor present in the humid air is condensed and collected as a distillate, while the dehumidified air is ducted out of the dehumidifier to the humidifier to continue the cycle. The schematic diagram of the electrically driven water heated HDH system, which provides the basis for the comparison, is illustrated in Figure 4.3.

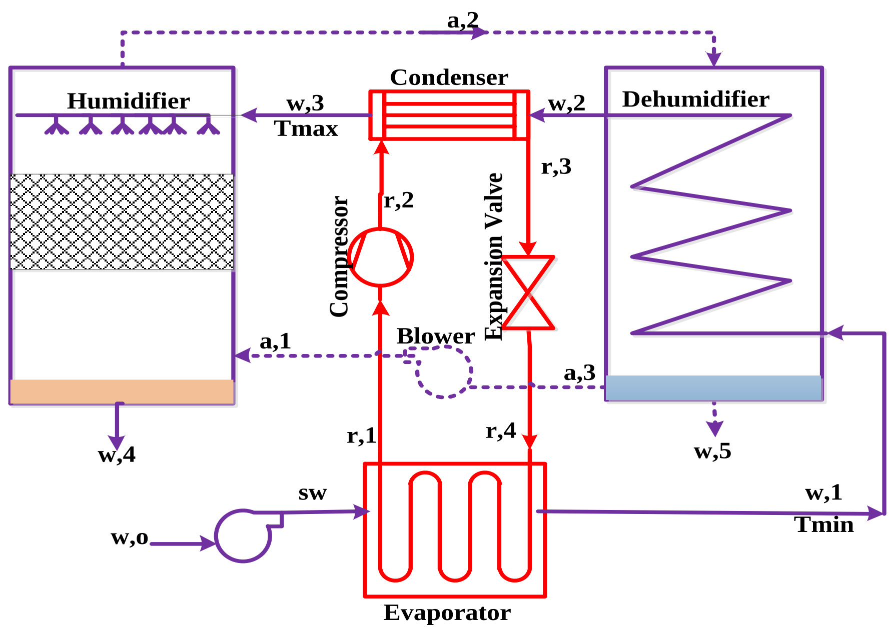

Figure 4. 1: Schematic diagram of an integrated HP-HDH-WH plant

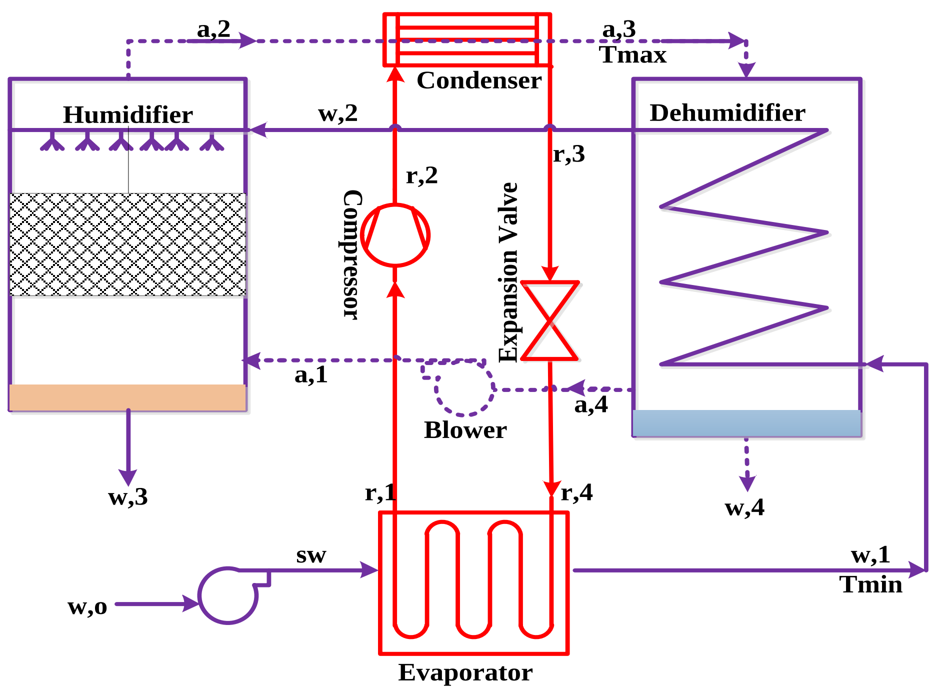

Figure 4. 2: Schematic diagram of an integrated HP-HDH-AH unit.

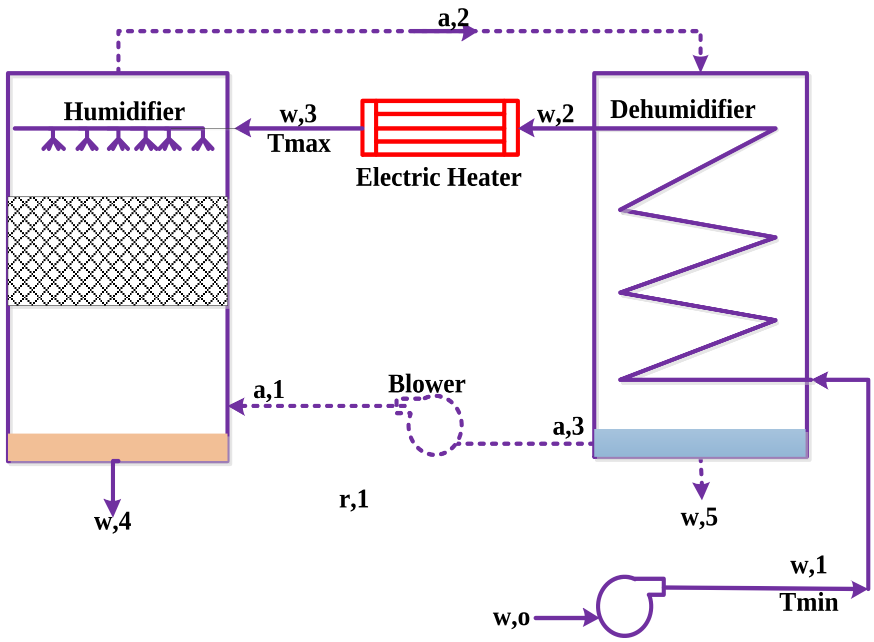

Figure 4. 3: Schematic diagram of a conventional E-HDH-WH system

4.2 Mathematical models and assumptions

The following assumptions are made in the current analysis [106]: Heat losses to the surroundings are neglected. The system runs in a steady-state condition. The kinetic and potential energy terms are neglected in the energy balance. The condensing (high) pressure is 1378 kPa (200 psi), while the evaporating (low) pressure is 240 kPa (35 psi). The relative humidity, humidifier effectiveness, dehumidifier effectiveness, and refrigerant mass flow rate are assumed to be 100%, 85%, 87%, and 0.05kg/s, respectively. The refrigerant used is R-134a. The feed water mass flow rate is 0.18 kg/s with a salinity of 35 g/kg. The mass flowrate ratio is unity and water inlet temperature is 27 °C. The dead state for each stream is taken at standard conditions of atmospheric pressure and temperature of 25 °C [120]. The isentropic compressor efficiency is taken to be 85% [115]. Engineering equation solver

(EES) software with updated seawater properties compiled by Sharqawy et al. [121] has been used for the solving the equations.

4.2.1 First-law analysis:

The mass and energy balance for the main components of the proposed HDH desalination systems are as follows[106]:

The Mass and Energy balance for the humidifier can be expressed as,

$$\dot{m}_w h_{w,in} - \dot{m}_b h_b = \dot{m}_a \left(h_{a,out} - h_{a,in} \right) \tag{1}$$

$$\dot{m}_b = \dot{m}_w - \dot{m}_{fw} \tag{2}$$

Mass and Energy balances for the dehumidifier are:

$$\dot{m}_{fw} = \dot{m}_a \left(\omega_{a,in} - \omega_{a,out} \right) \tag{3}$$

$$\dot{m}_w \left(h_{w,in} - h_{w,out} \right) = \dot{m}_{fw} h_{fw} + \dot{m}_a \left(h_{a,out} - h_{a,in} \right) \tag{4}$$

While the Mass and Energy balances of the condenser (heater) are:

$$\dot{m}_{r,in} = \dot{m}_{r,out} = \dot{m}_r \tag{5}$$

$$\dot{Q}_{cond} = \dot{m}_r \left(h_{r,in} - h_{r,out} \right) = \dot{m}_w \left(h_{w,out} - h_{w,in} \right) \tag{6}$$

The Energy balance for the evaporator (pre-cooler):

$$\dot{Q}_{evap} = \dot{m}_r \left(h_{r,out} - h_{r,in} \right) = \dot{m}_w \left(h_{w,in} - h_{w,out} \right) \tag{7}$$

And the Energy balance for the compressor, and throttling valve, respectively are,

$$\dot{W}_{comp} = \dot{m}_r\left(h_{r,out} - h_{r,in}\right) \tag{8}$$

$$h_{r,in} = h_{r,out} \tag{9}$$

Since the number of unknowns is more than the number of equations, then supplementary equations are needed to solve the equations. These supplementary equations can be obtained from the effectiveness of components.

The effectiveness of the humidifier is defined as the ratio of actual enthalpy change of either stream ($\Delta\dot{H}$) to maximum possible enthalpy change ($\Delta\dot{H}_{max}$), and can be expressed as [11,106,110]:

$$\varepsilon_H = \max\left\{\frac{h_{a,out} - h_{a,in}}{h_{a,out,ideal} - h_{a,in}}, \frac{h_{w,in} - h_{w,out}}{h_{w,in} - h_{w,out,ideal}}\right\} \tag{10}$$

Similarly, the effectiveness of the dehumidifier as [11,106,110]:

$$\varepsilon_D = \max\left\{\frac{h_{a,in} - h_{a,out}}{h_{a,in} - h_{a,out,ideal}}, \frac{h_{w,out} - h_{w,in}}{h_{w,out,ideal} - h_{w,in}}\right\} \tag{11}$$

where the ideal outlet air enthalpy ($h_{a,out,ideal}$) is calculated when the outlet air is fully saturated at the water inlet temperature, while the ideal outlet for seawater enthalpy ($h_{w,out,ideal}$) is calculated when its temperature is equal to the inlet air dry-bulb temperature.

The Gain Output Ratio (GOR) is defined as the ratio of latent heat of evaporation of the distillate produced to the total energy input into the system. For this system, it can be expressed as:

$$\mathrm{GOR} = \frac{\dot{m}_{fw} h_{fg}}{\dot{W}_{Total}} \tag{12}$$

Where,

$$\dot{W}_{Total} = \dot{W}_{Comp} + \dot{W}_{Pump} + \dot{W}_{Fan}$$

The Specific Electrical Energy Consumption (SEEC) is the total electrical energy (in kWh) used to produce one cubic meter (m^3) of fresh water, and can be given as:

$$\mathrm{SEEC} = \frac{\dot{W}_{Total}}{\dot{V}_{freshwater}} \tag{13}$$

Where

$\dot{V}_{freshwater}$ $(m^3/hour)$ is the volumetric flowrate of the condensate.

4.2.2 Second-law analysis:

From the second law of thermodynamics, exergy can be defined as the maximum useful work which can be obtained from a system (a flow of material or energy) as it comes to an equilibrium state with a reference environment [122–124]. Exergy analysis measures the extent of irreversibility in terms of exergy destruction, which can be evaluated by applying exergy-balance on each component. The exergy destruction associated with each component of the system can be calculated as [125,126]:

$$\dot{X}_{dest} = \sum_{in} \dot{X} - \sum_{out} \dot{X} \tag{14}$$

The flow exergy content of a flow stream ($\dot{X}$) is a summation of both physical and chemical exergy as the salt concentration changes during the cycle. For a control volume system, the mathematical expressions of physical ($\dot{X}_{ph}$) and chemical exergy ($\dot{X}_{ch}$) can be given as follows [127]:

$$\dot{X}_{ph} = \dot{m}[(h - h_0) - T_0(s - s_0)] \tag{15}$$

$$\dot{X}_{ch} = \sum_{i}^{n} w_s(\mu^* - \mu_i^0) \tag{16}$$

where s and μ and w_s are the entropy, chemical potential and mass fraction, respectively. The subscript/superscript "0" refers to the dead state. The superscript "*" represents the properties determined at the dead state but at the same composition or concentration of the initial state.

The exergy destroyed at different components of the system is expressed as shown below:

Exergy balance for the humidifier:

$$\dot{X}_{dest,Hum} = \dot{X}_{w,in} + \dot{X}_{a,in} - \dot{X}_{w,out} - \dot{X}_{a,out} \tag{17}$$

Exergy balance for the dehumidifier:

$$\dot{X}_{dest,Dehum} = \dot{X}_{w,in} + \dot{X}_{a,in} - \dot{X}_{w,out} - \dot{X}_{a,out} - \dot{X}_{fw,out} \tag{18}$$

Exergy balance for the evaporator:

$$\dot{X}_{dest,Evap} = \dot{X}_{w,in} + \dot{X}_{r,in} - \dot{X}_{w,out} - \dot{X}_{r,out} \tag{19}$$

Exergy balance for the condenser (for HP-HDH-WH):

$$\dot{X}_{dest,Cond} = \dot{X}_{w,in} + \dot{X}_{r,in} - \dot{X}_{w,out} - \dot{X}_{r,out} \tag{20}$$

Exergy balance for the condenser (for HP-HDH-AH):

$$\dot{X}_{dest,Cond} = \dot{X}_{a,in} + \dot{X}_{r,in} - \dot{X}_{a,out} - \dot{X}_{r,out} \tag{21}$$

Exergy balance for the compressor:

$$\dot{X}_{dest,Comp} = \dot{X}_{r,in} + \dot{W}_{Comp} - \dot{X}_{r,out} \tag{22}$$

Exergy balance for the expansion valve:

$$\dot{X}_{dest,EXV} = \dot{X}_{r,in} - \dot{X}_{r,out} \tag{23}$$

Another performance indicator for the second law analysis is the exergetic efficiency. The exergetic efficiency is defined as the ratio of useful exergy output to the inlet exergy to the system. It can be expressed as [125,126]:

$$\eta_{II} = \frac{\dot{X}_{out,useful}}{\dot{X}_{in}} \tag{24b}$$

$$\eta_{II} = \frac{\dot{X}_{Product}}{\dot{X}_{Source}} \tag{24b}$$

Where the useful exergy output is the exergy associated with the system productivity, while the inlet exergy is the exergy accompanying the input power to the compressor, pump and blower, and the exergy of inlet water and air. Equation (24b) is ratio of exergy of the process product to the exergy supplied to the system [128].

4.2.2.1 Thermodynamic Parameters:

The following thermodynamic parameters can be used for exergetic assessment of a thermal system [129–131]:

(a) The fuel depletion ratio (β): It is defined as the ratio representing the exergy consumption of ith component to the fuel exergy rate input power to the system. It can be expressed as,

$$\beta_i = \frac{\dot{X}_{dest,i}}{\dot{W}_{Comp}} \tag{25}$$

(b) The relative irreversibility ratio (χ): It is defined as the ratio of exergy consumption of ith component to the the total exergy destruction rate of the system. It can be written as,

$$\chi_i = \frac{\dot{X}_{dest,i}}{\dot{X}_{dest,total}} \tag{26}$$

(c) The productivity lack (δ): It is the ratio of the exergy consumption of ith component to the exergy of products (freshwater produced). It is expressed as,

$$\delta_i = \frac{\dot{X}_{dest,i}}{\dot{X}_{product}} \tag{27}$$

(d) The exergetic factor (ξ): It is defined as the ratio of exergy consumption of ith component to the exergy input to the component and the input power. It is written as,

$$\xi_i = \frac{\dot{X}_{dest,i}}{\dot{W}_{Comp} + \dot{X}_{i,in}} \tag{28}$$

(e) The exergetic improvement potential (Γ): The exergetic improvement potential shows the potential improvement of ith component from an exergetic point of view considering the losses ratio expressed in Eq. (28). This is expressed as,

$$\Gamma_i = 1 - \xi_i \tag{29}$$

4.2.3 Exergo-economic analysis:

In this analysis, each stream is treated as flowing costs like flowing exergy and energy. Each component is analyzed separately and the cost of each stream entering or leaving the component is evaluated. Exergy-based cost analysis is aimed at determining the cost of products and irreversibilities (exergy destroyed) associated with energy conversion processes. To model the cost of fresh water production, the following assumptions are adopted:

- The cost of intake water is assumed zero [96].
- The unit cost of electricity (COE) is 0.045$/kWh [5,132].
- Zero pretreatment costs are assumed [118].
- Plant availability is assumed to be 90% with a life expectancy of 20 years [118].
- The interest rate (i) is 5% [116,118].
- Energy cost of any useless flow (such as blowdown) is considered as zero [133].

- The power consumed by pump and fan/blower is 750 W and 50 W [96], respectively.

- Specific cost of operating labor, ($\mathcal{L}$) = 0.1 \$/m^3 [116].

- The annual maintenance cost is estimated to be 1.5% of the capital cost [116].

- The annual management cost is estimated at 20% of the labor cost [5,116,118,134].

To carryout thermo-economic analysis, the following cost parameters need to be determined:

Fixed costs/Investments:

As a first step in the Exergo-economic analysis, the capital cost of each major and supplementary equipment is estimated. The capital costs Z (\$) involved both purchasing cost and running cost of the equipment. Table 4.1 summarizes the fixed cost for different components of the system as obtained from [99,118,120]. Multiplication of capital cost and capital recovery factor (amortization factor) (α) leads to the annual capital cost or fixed charges $\mathrm{Z_{Annual}}$ (in \$/yr). The amortization factor (α) can be express as [106,119,120]:

$$\alpha = \frac{\mathrm{i(i+1)^n}}{\mathrm{(i+1)^n - 1}} \tag{30}$$

where α is the amortization factor, i is the interest rate and n is the expected lifetime of the system (amortization period).

Thus, the annual capital cost can be written as:

$$\mathrm{Z_{Annual}\ (in\ \$/yr) = Z_{Component} \times \alpha} \tag{31}$$

The rate of fixed charges can be evaluated as:

$$\dot{Z} = \frac{Z_{Annual}}{365 \times 24 \times \text{Å}} \tag{32}$$

Where Å is the plant availability.

4.2.3.1 Cost Flow Method (C-F-M):

The cost flow method has been applied to analyze different desalination systems and the approach offers the following advantages over traditional methods [119]; (a) it is more comprehensive from an economic standpoint and allows the evaluation of each stream cost at any intermediate state in the system, as shown in Table 4.2, (b) it highlights the involvement of each component in the final cost and offers an opportunity to identify the cost concentrated components, (c) this method can reduce the capital investment through optimization of the localize cost-intensive areas, like component-based entropy generation minimization.

Equations for Stream Cost

The cost of each stream is determined by combining the cost of fuel streams and the rate of fixed charges of the components producing these streams. A cost balance equation is applied to each component, to evaluate the cost of output stream (in $/s). The general form of the cost balance equation used to calculate output streams can be expressed as [120]:

$$\dot{C}_P = \sum \dot{C}_{fliud} + \dot{Z} \tag{33}$$

The following Eqs. (34-45) is the applications of Eq. (33) to each component of HP-HDH water heated system presented in Figure 4.1. The same procedure can be applied to the components of other HDH plants (Figures 4.2 and 4.3). The first component to produce a stream with a definite exergy and cost values in the system is the pump. The cost of seawater stream leaving the feed pump include the intake stream cost, pump fixed cost and electricity cost. Thus, the stream exiting the feed pump can be expressed as:

$$\dot{C}_{sw} = \dot{C}_0 + \dot{C}_{elect}\dot{W}_{FP} + \dot{Z}_{FP} \tag{34}$$

The cost balance equation for feed stream leaving the evaporator can be written as,

$$\dot{C}_{w1} = \dot{C}_{sw} + \dot{C}_{r1} + \dot{C}_{r4} + \dot{Z}_{Evap} \tag{35}$$

Because the evaporator has two outlets, an additional auxiliary equation based on equality of average costs of the inlet and outlet refrigerant stream is needed for the solution. This equation can be expressed as:

$$\frac{\dot{C}_{r4}}{\dot{X}_{r4}} = \frac{\dot{C}_{r1}}{\dot{X}_{r1}} \tag{36}$$

The cost balance equation for the dehumidifier can be written as,

$$\dot{C}_{w5} = \dot{C}_{w1} + \dot{C}_{a2} - \dot{C}_{w2} - \dot{C}_{a3} + \dot{Z}_{Dehum} \tag{37}$$

The dehumidifier has three outlet streams (feed stream, dehumidified air, and distillate) leaving the dehumidifier. Thus, two more auxiliary equations based on equality of average costs of the streams are needed for the solution. These equations are,

$$\frac{\dot{C}_{w2}}{\dot{X}_{w2}} = \frac{\dot{C}_{w1}}{\dot{X}_{w1}} \tag{38}$$

$$\frac{\dot{C}_{a2}}{\dot{X}_{a2}} = \frac{\dot{C}_{a3}}{\dot{X}_{a3}} \tag{39}$$

The cost balance equation for feed stream leaving the condenser/heater can be written as:

$$\dot{C}_{w3} = \dot{C}_{w2} + \dot{C}_{r2} + \dot{C}_{r3} + \dot{Z}_{Cond} \tag{40}$$

The condenser has two outlet streams, thus one more auxiliary equation based on equality of average costs of the inlet and outlet refrigerant stream is required for the solution. It is given as,

$$\frac{\dot{C}_{r3}}{\dot{X}_{r3}} = \frac{\dot{C}_{r2}}{\dot{X}_{r2}} \tag{41}$$

The cost balance equation for the humidifier can be written as,

$$\dot{C}_{w4} = \dot{C}_{w3} + \dot{C}_{a1} - \dot{C}_{a2} + \dot{Z}_{Hum} \tag{42}$$

The humidifier has two outlet streams (brine stream and humidified air) leaving the humidifier. Thus, one additional auxiliary equation based on equality of average costs of the stream is needed for the solution. Based on the assumption that the exergy cost of the blowdown is zero, because it has no further utility, we take $\dot{C}_{w4} = 0)$ as the needed auxiliary equation.

The cost balance equation for the compressor and expansion valve, can be respectively written as,

$$\dot{C}_{r2} = \dot{C}_{r1} + \dot{C}_{elect}\dot{W}_{Comp} + \dot{Z}_{Comp} \tag{43}$$

$$\dot{C}_{r4} = \dot{C}_{r3} + \dot{Z}_{EXV} \tag{44}$$

The final product cost C_5 (in \$/m^3) can be evaluated as [119,120]:

$$C_{reshwater} = \frac{\dot{C}_{w5}}{\dot{V}_{w5}} = \frac{\dot{C}_{freshwater}}{\dot{V}_{freshwater}} \tag{45}$$

where $\dot{V}_{freshwater}$ $(m^3/hour)$ is the volumetric flowrate of the condensate.

4.2.3.2 El-Dessouky and Ettouney Method (E-E-M)

For the purpose of comparison, we also present cost analysis described in [5]. This approach is simple and treats the whole plant as a single unit instead of components-wise. The production cost depends on the processing capacity, site characteristics, and design features. The product cost is divided into the direct/indirect cost and annual operating cost. In E-E-M, product cost is obtained by dividing the total cost (comprising the cost of equipment, the labor cost, operation and maintenance costs) by the plant capacity.

The annual capital cost ($\dot{Z}_f$): This cost can be obtained by multiplying capital costs by amortization factor. It can be expressed as

$$\dot{Z}_f(\$/yr) = Z(\$) \times \alpha\ (1/yr) \tag{46}$$

The annual electric power cost ($\dot{C}_{Elect}$): It is expressed as,

$$\dot{C}_{Elect}(\$/yr) = COE\ (\$/kWh) \times \frac{SEEC}{3600}(kWh/m^3) \times f \times \dot{V}_{fw}\ (m^3/day) \times 365 \tag{47}$$

The annual labor cost ($\dot{C}_L$): This can be written as,

$$\dot{C}_L(\$/yr) = \mathcal{L}(\$/m^3) \times f \times \dot{V}_{freshwater}\ (m^3/day) \times 365 \tag{48}$$

The total annual cost ($\dot{C}_T$), is some of the above cost elements,

$$\dot{C}_T(\$/yr) = \dot{Z}_f(\$/yr) + \dot{C}_{Elect}\ (\$/yr) + \dot{C}_L(\$/yr) + \dot{C}_{mt}(\$/yr) + \dot{C}_{mg}(\$/yr) \tag{49}$$

Now, the unit product cost (C_P) can be written as,

$$C_P(\$/m^3) = \left(\frac{\dot{C}_T(\$/yr)}{f \times V_{freshwater}\ (m^3/day) \times 365\ (day/yr)}\right) \quad (50)$$

Table 4. 1 Capital investment cost for HP-HDH and E-HDH plants [99,118,120]

Item Description	E-HDH-WH system	HP-HDH-WH system	HP-HDH-AH system
Packed Bed Humidifier	133 US $	133 US $	133 US $
Dehumidifier	500 US $	500 US $	500 US $
Water Tanks	200 US $	200 US $	200 US $
Flowmeters	230 US $	230 US $	230 US $
Pumps	150 US $	150 US $	150 US $
Blowers/fans	100 US $	100 US $	100 US $
Pipes, Fittings	35 US $	35 US $	35 US $
Accessories	33 US $	33 US $	33 US $
Semi Hermetic Compressor	-	1200 US $	1200 US $
Shell and Tube Condenser	-	600 US $	600 US $
Shell & Tube Evaporator	-	600 US $	600 US $
Expansion Valve	-	100 US $	100 US $
Electric Heater	48 US $	-	-

4.3 Results and discussion

This section contains the results of our findings from the study. Figure 4.4 illustrates the influence of dehumidifier effectiveness on both the GOR and SEEC of HP-HDH-AH, HP-HDH-WH, and E-HDH-WH desalination systems. It is important to emphasize that GOR is one of the major performance indexes of HDH system. It represents the ratio of latent heat of evaporation of the distillate produced to the total energy input into the system, while the SEEC represents the amount of electrical energy consumed to produce one kg of fresh water.

Figure 4.4 (a & b) indicates that both HP-HDH-AH and HP-HDH-WH units portrayed superior performance in term of GOR and SEEC as compared to the E-HDH-WH system, with HP-HDH-AH attaining the highest GOR and lowest SEEC. This is because a lower amount of energy is required to heat the humidified air as compared to heating water in the case of the water-heated cycle. Furthermore, the improvement in the performance of HP-HDH-AH and HP-HDH-WH systems over the E-HDH-WH cycle is because of better condensation of water vapor in the dehumidifier, leading to higher productivity, and consequently higher GOR and lower SEEC. Increasing the effectiveness of the dehumidifier leads to a better system performance especially the HP-HDH-AH. This may be due to better vapor condensation process in the dehumidifier.

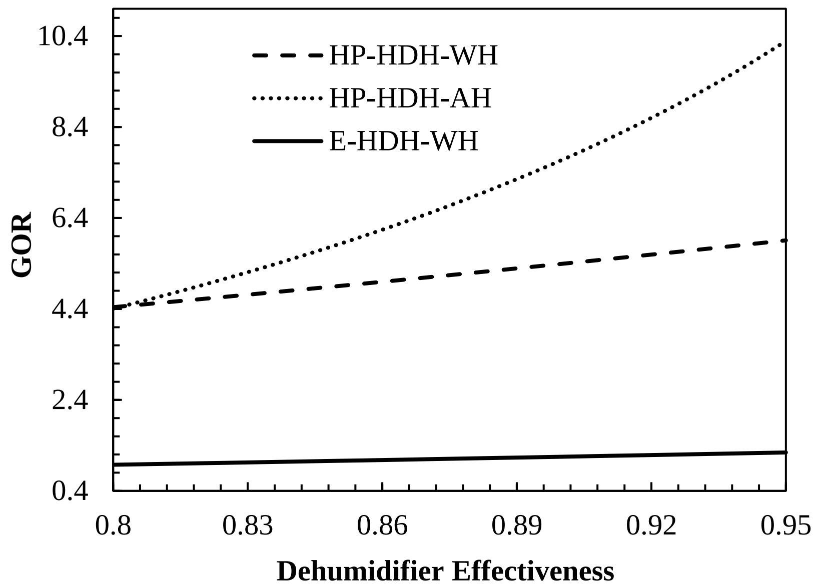

Figure 4. 4a: Effect of dehumidifier effectiveness on gain output ratio

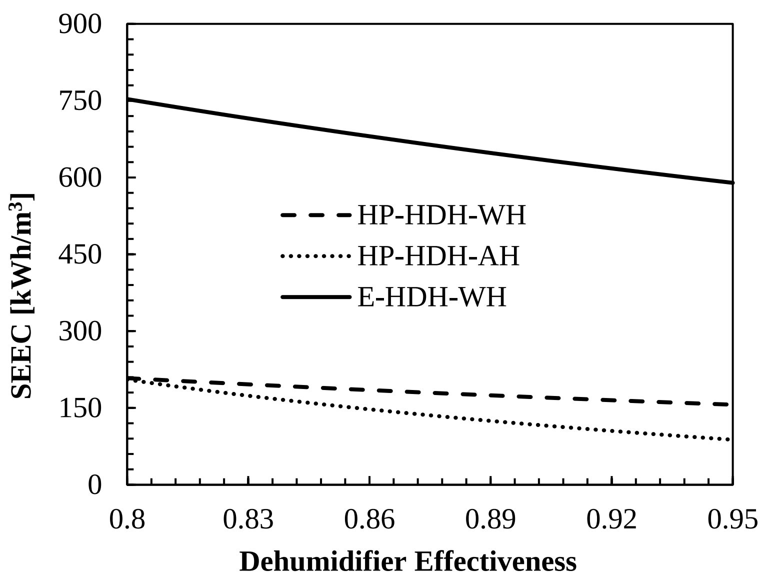

Fig. 4.4b: Effect of dehumidifier effectiveness on Specific Electrical Energy Consumption

Figure 4. 4: Effect of dehumidifier effectiveness on (a) GOR and (b) SEEC

4.3.1 Second-Law Analysis

Based on the assumptions and conditions presented in the mathematical model section, the major source of irreversibility in each of the major components of the system is presented in Figure 4.5. The system inefficiencies can be measured by exergy destruction. Knowing the sources of irreversibilities provides the useful information needed to improve the component performance by eliminating/mitigating the causes. It is obvious that the entropy generation associated with the humidifier, dehumidifier, expansion valve, compressor, condenser, evaporator and heater are all of the same order of magnitude, which shows that special attention must be paid to all the components when designing the systems. However, on a relative scale, the highest irreversibility occurs in the evaporator as compared to other components. This result is presented better in Figure 4.6 (a and b), which shows the percentage exergy destruction in each component of the systems. The high exergy destruction in the evaporator can be attributed to the temperature differences between the streams, friction, heat exchanged with the surroundings and higher entropy generation associated with the energy needed for vapor condensation. Expansion valve appears to be another component associated with high exegy destruction, due to the throttling process. The compressor is also noticed to be associated with high irreversibility. Another major source of irreversibility in the system occurs in the condenser, due to high energy loss to the coolant during the condensation process, in order to operate the cycle. This calls for special attention when selecting this type of components, since the components of inferior performance can considerably reduce the overall performance of the whole system.

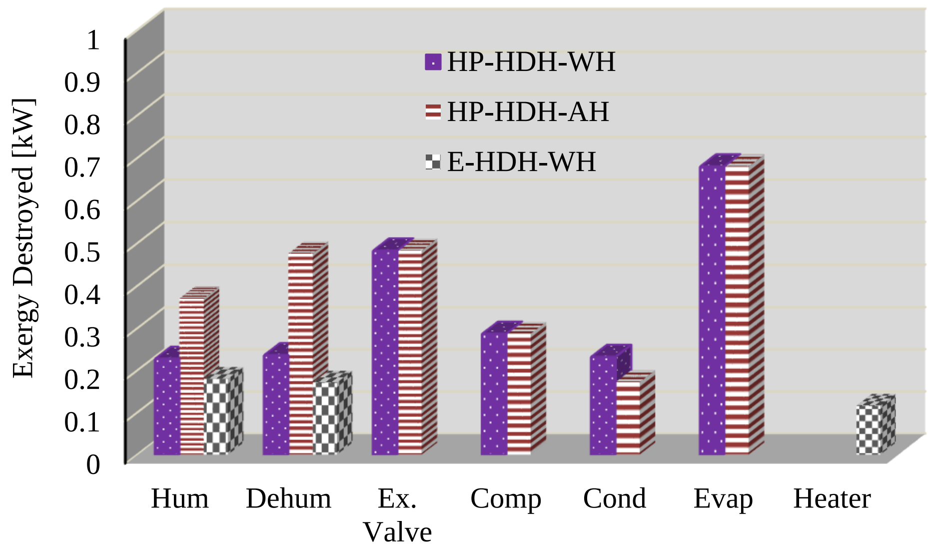

Figure 4. 5: Exergy destroyed at each main component of the systems

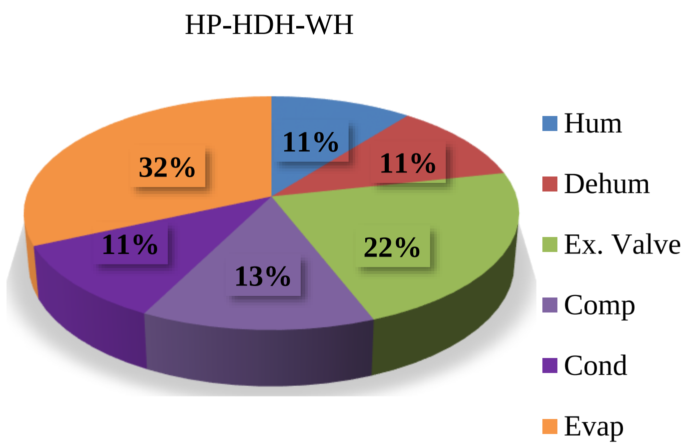

4.6(a)

HP-HDH-AH

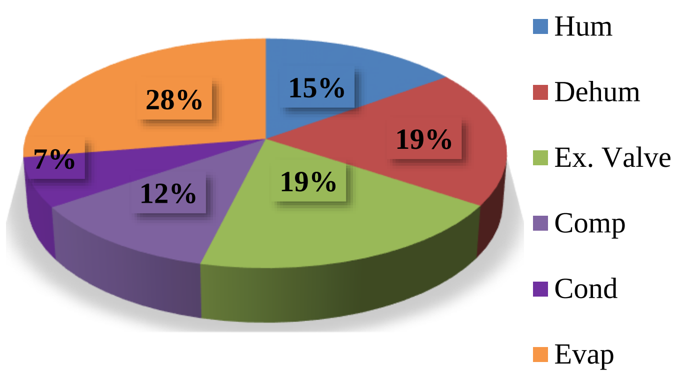

4.6(b)

E-HDH-WH

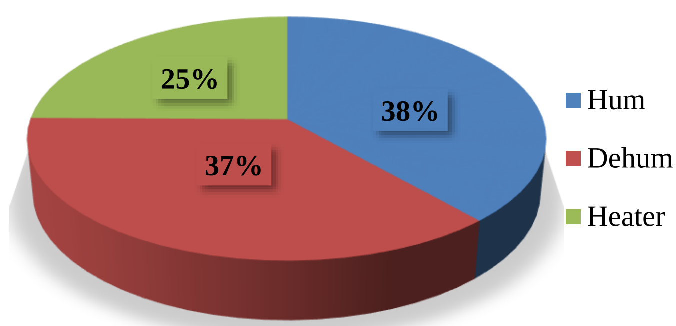

4.6(c)

Figure 4. 6: Exergy destruction by percentage in each component of (a) HP-HDH water heated, (b) HP-HDH air heated, and (c) E-HDH water heated

As presented in Figures 4.5 and 4.6 (c), the order of magnitude of entropy generation within the humidifier, dehumidifier and the heater is identical to those obtained in the previous study [135]. It is worth noting that exergy destroyed within the compressor can be greater than any other component if we change the operating conditions or consider lower values of compressor isentropic efficiency, as presented in Figures 4.7(a & b) for the case of HP-

HDH-WH and HP-HDH-AH, respectively. In fact, entropy generated in the compressor can be more than 130% higher than that generated at the evaporator, if we consider a compressor isentropic efficiency of 50%, dehumidifier effectiveness of 95% and humidifier effectiveness of 90%. Such case of high exergy destruction in the compressor can be attributed to the reciprocating compressor being used in the system. The losses are huge due to friction between the cylinder and piston rings, and losses due to wire drawing effect during suction and delivery of the refrigerant, which changes the entropy of the system and increases the irreversibility of the system. Although, the lubricant is used to minimize these losses, still frictional losses are more prominent in reciprocating compressors.

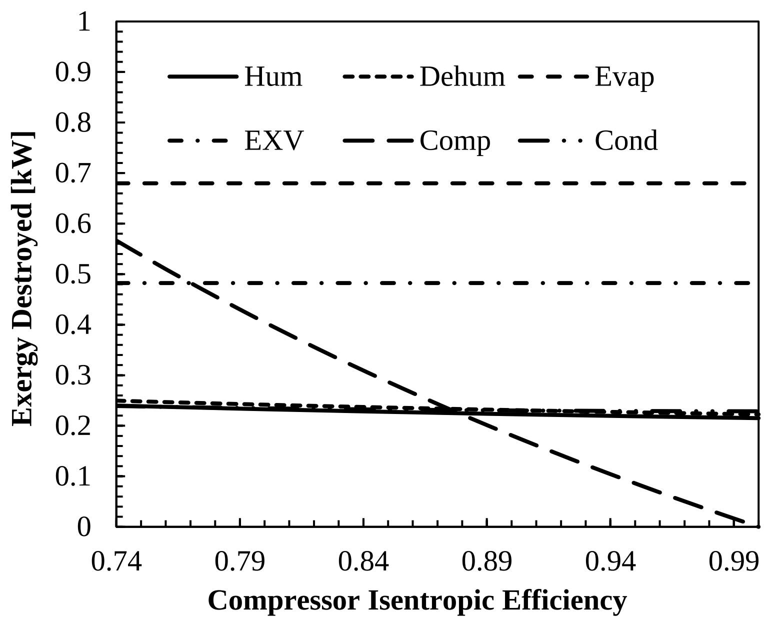

Fig. 4.7(a): HP-HDH water-heated cycle

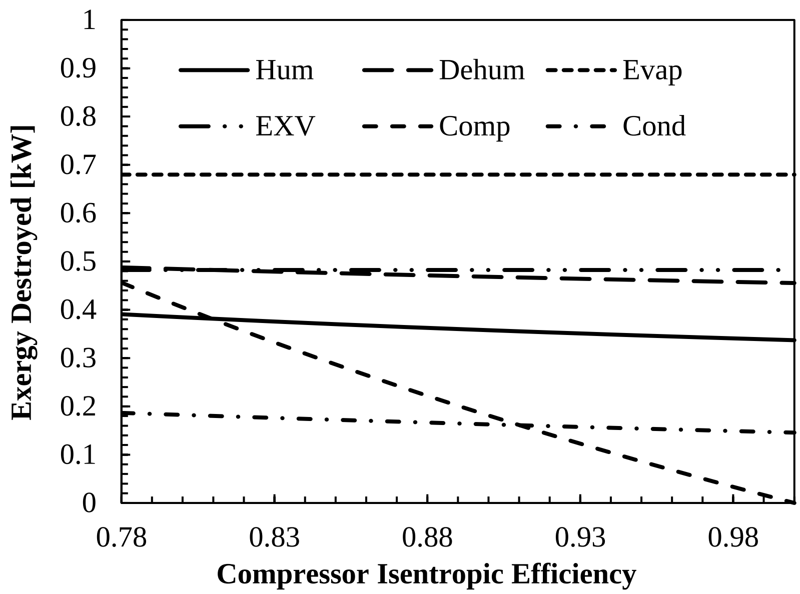

Fig. 4.7(b): HP-HDH air-heated cycle

Figure 4. 7: Effect of Isentropic efficiency of compressor on the exergy destroyed within the major components

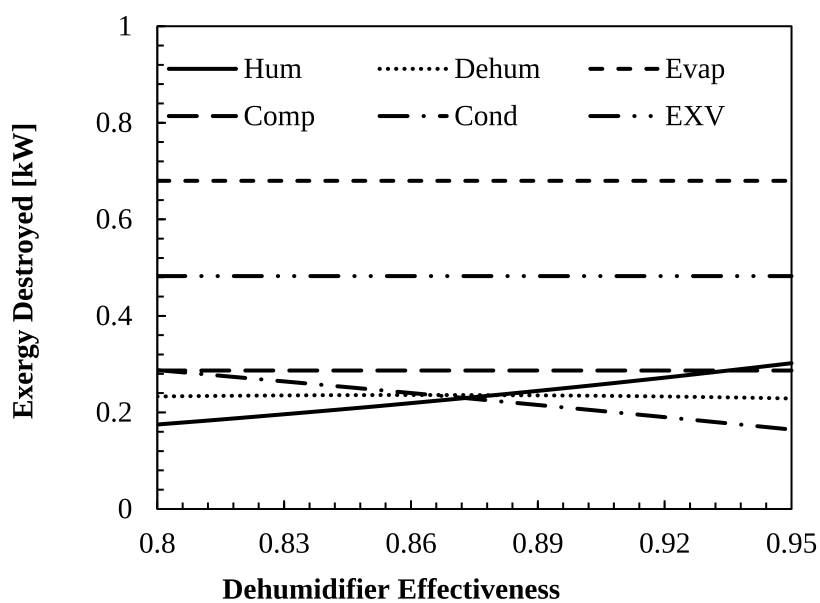

Fig. 4.8(a): HP-HDH water-heated cycle

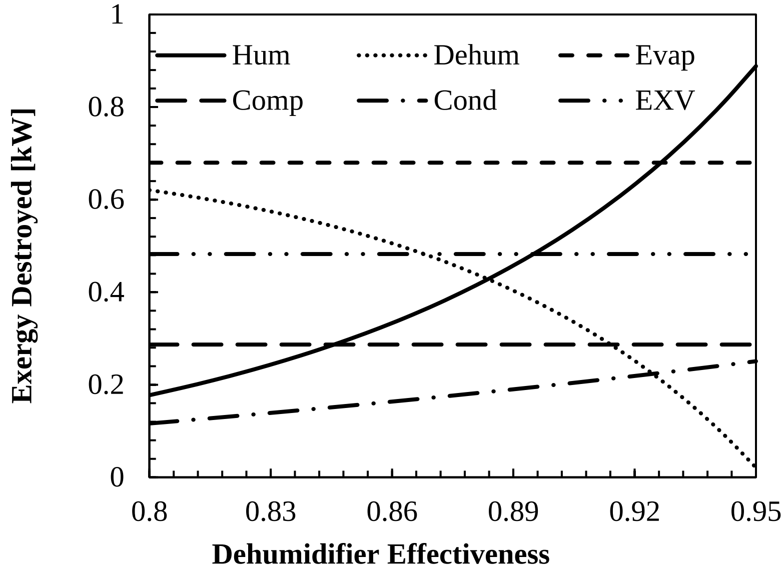

Fig. 4.8(b): HP-HDH air-heated cycle

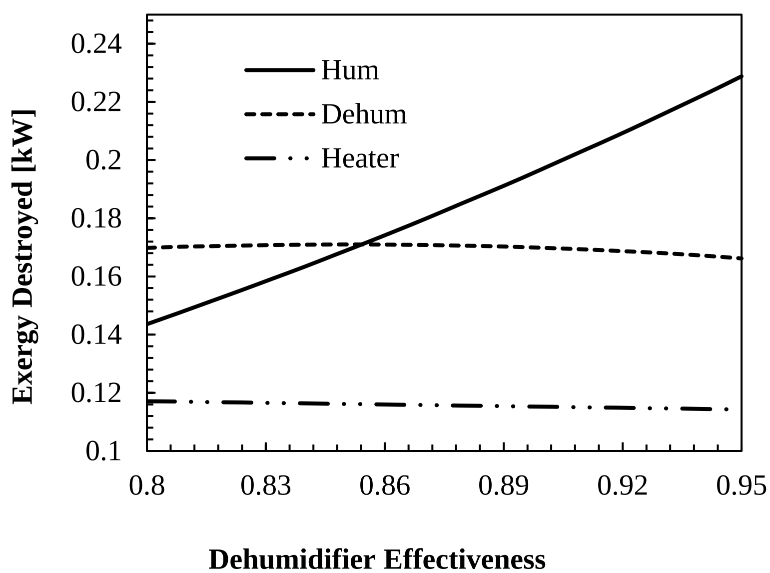

Fig. 4.8(c): E-HDH water-heated cycle

Figure 4. 8: Effect of effectiveness of dehumidifier on the exergy destroyed within the major components

The influence of variation in dehumidifier effectiveness on the exergy destruction within each component of the system is illustrated in Figure 4.8. It is obvious that the effectiveness of the dehumidifier has no relationship with the entropy generation within the expansion valve, evaporator and compressor, since these components are not a direct function of the dehumidifier. However, the variation in dehumidifier effectiveness influences the exergy destruction in the humidifier and dehumidifier considerably, especially for the HP-HDH-AH cycle. For HP-HDH-WH cycle, the exergy destruction in the humidifier is greater than that in the dehumidifier (for $\varepsilon_D > 87.89\%$), and vice versa (for $\varepsilon_D < 87.89\%$). Similar characteristic is portrayed in the case of HP-HDH-AH and E-HDH-WH systems at $\varepsilon_D = 88.68\%$ and $\varepsilon_D = 85.53\%$ respectively.

These findings simply show that the source of irreversibility in the humidifier can be higher or lower than that within the dehumidifier depending on the effectiveness of the dehumidifier. It can also be noticed that the magnitude of irreversibility within the dehumidifier decrease towards zero as the dehumidifier effectiveness increases. Zero and negative exergy destruction in the dehumidifier shows that the component cannot be further improved, as such the designer should focus on enhancing the effectiveness of the humidifier in order to improve the performance of the system.

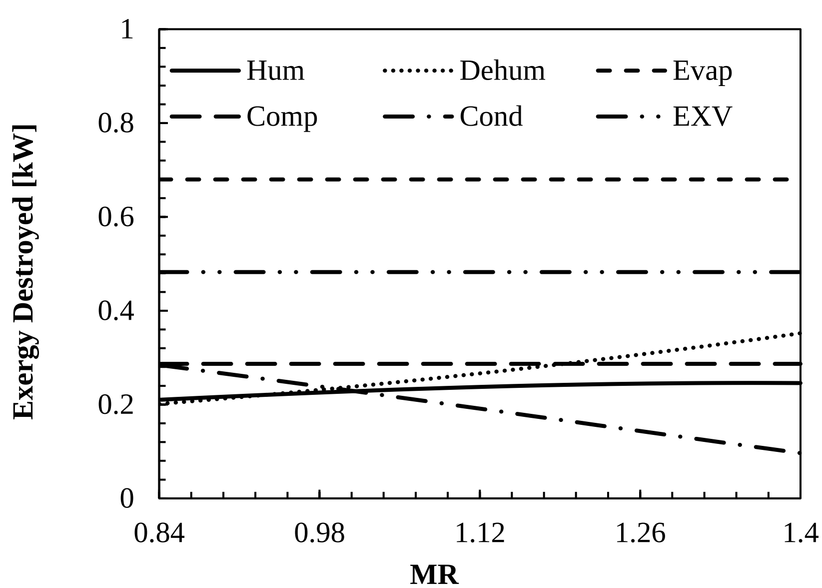

Fig. 4.9(a): HP-HDH water-heated cycle

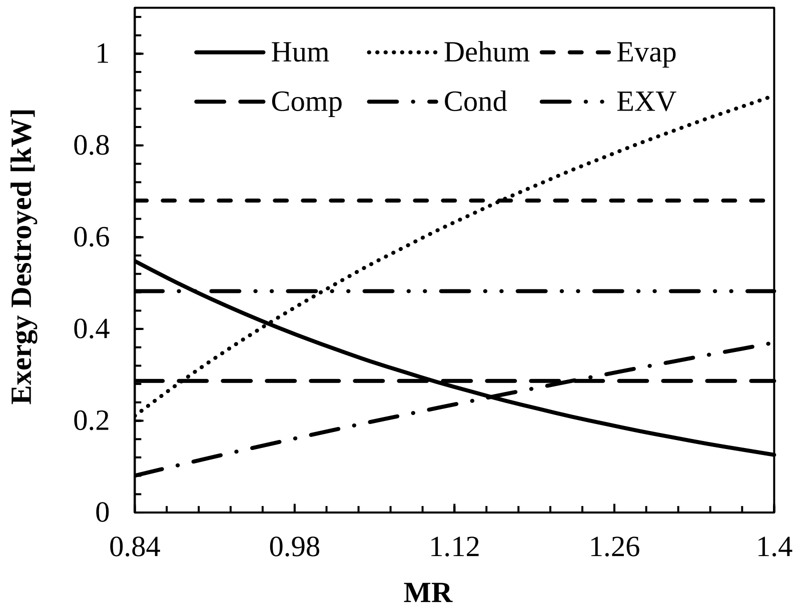

Fig. 4.9(b): HP-HDH air-heated cycle

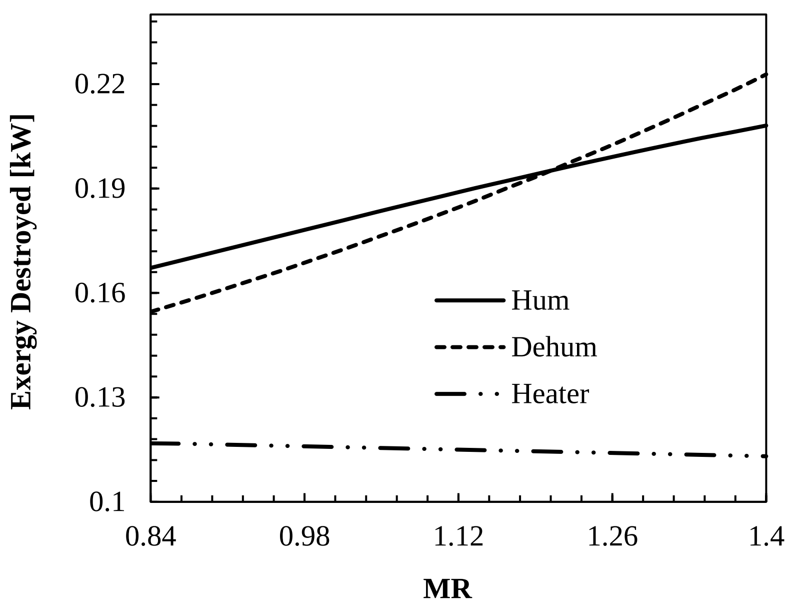

Fig. 4.9(c): E-HDH water-heated cycle

Figure 4. 9: Influence of MR on the exergy destroyed within the major components

Another important parameter that influences the performance of HDH system is the mass flowrate ratio (MR), which represents the ratio of mass flowrate of feed water to the mass flowrate of the circulating air. The impact of MR on the exergy destroyed within the major components of the three systems is shown in Figure 4.9. It can be seen that the exergy destructions in the expansion valve, evaporator and compressor are insensitive to the variation of the mass ratio of the flowing streams. The variation in MR affects the exergy destruction at the humidifier, dehumidifier and condenser of the systems. Increasing the mass ratio resulted in an increase in vapor generation and condensation in the humidifier and dehumidifier, respectively, leading to an increase in mixing of fluids and the degree of irreversibility in both components. However, for HP-HDH-WH unit, the exergy destruction in the dehumidifier is found to be greater than that of the humidifier at MR > 0.99 and vice versa at MR < 0.99. Similar behavior is observed in the case of HP-HDH air heated and E-HDH water heated cycles at MR = 0.96 and MR = 1.22, respectively.

It should be noted that exergy destruction in the dehumidifier can be higher or lower than that in humidifier depending on the mass flow rate ratio. For both HP-HDH water heated cycle and HP-HDH air heated system, the exergy destruction associated with the humidifier tends to approach zero as MR increases. This shows that the limiting component depends on the mass flow rate ratio. Hence, the effectiveness of the humidifier cannot be further increased, therefore, the designer should concentrate on improving the dehumidifier in order to improve the overall performance of the plant. It should be noted that the limiting component effectiveness may switch depending on operating conditions of the system. The exegy destruction in the humidifier is predominantly contributed by mixing of fluids, which results in a loss of useful available energy. This result shows that increasing MR will lead to increase in irreversibility associated with the humidifier. However, in some case as observed in Figure 4.9 (b), the MR has exceeded the optimum value. Therefore, we observe a decrease in exergy lost with an increase in MR.

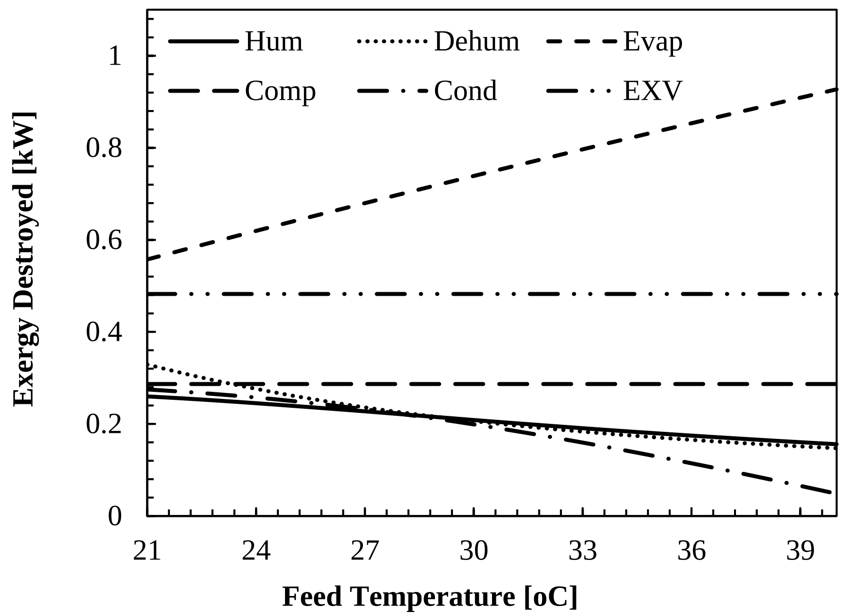

Fig. 4.10(a): HP-HDH water-heated cycle

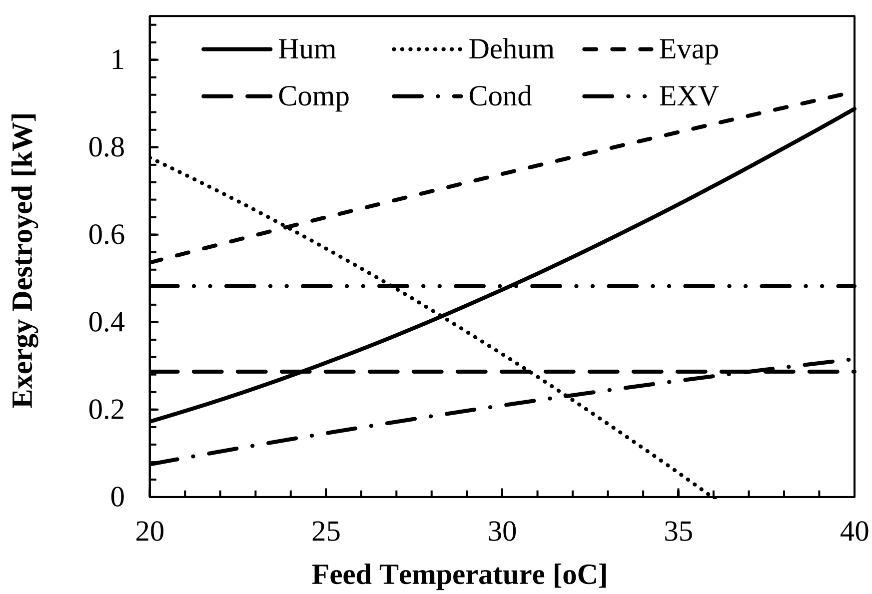

Fig. 4.10(b): HP-HDH air-heated cycle

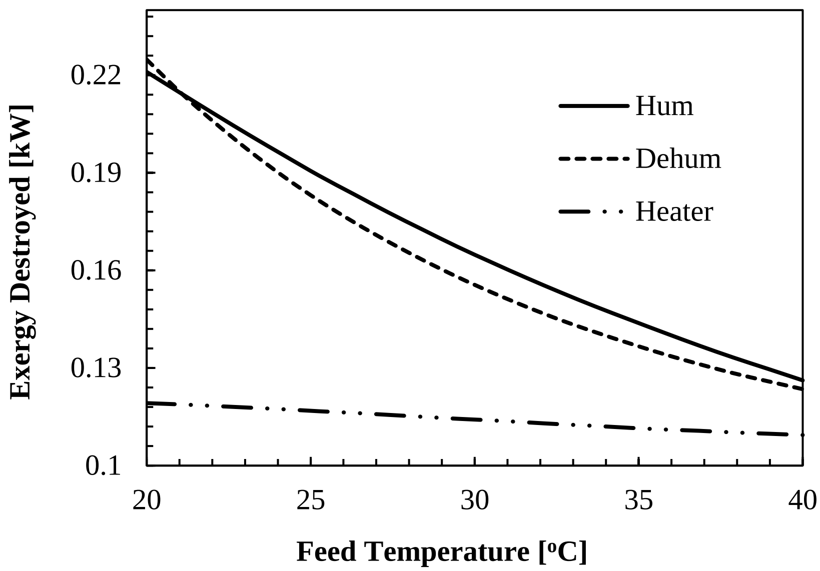

Fig. 4.10(c): E-HDH water-heated cycle

Figure 4. 10: Impact of Feed Temperature on the exergy destroyed within the major components

The variation in feed water temperature with the degree of irreversibility in the humidifier, dehumidifier, expansion valve, compressor, condenser, evaporator, and the heater are demonstrated in Figure 4.10. It can be noticed that the irreversibility within the humidifier, dehumidifier, evaporator, and condenser is very sensitive to variation in feed water temperature, with the highest exergy destruction recorded in the evaporator for HP-HDH water-heated and HP-HDH air-heated cycles, due to a large temperature difference, which causes greater losses during the heat transfer process. Therefore, the temperature difference should be kept as small as practical e.g. in evaporators and condensers to minimize entropy generation in those components. Exergy lost in both the humidifier and dehumidifier are observed to be more sensitive to the change in feed water temperature for the case of HP-HDH air-heated cycle and E-HDH water-heated cycle. In all the three systems, exergy destruction in the dehumidifier is observed to decrease with an increase in the feed water temperature. This is because of decline in the temperature difference between the hot humid air and feed water entering the dehumidifier. Heater, expansion valve and compressor are observed to be less sensitive to the variation in the feed water temperature.

.

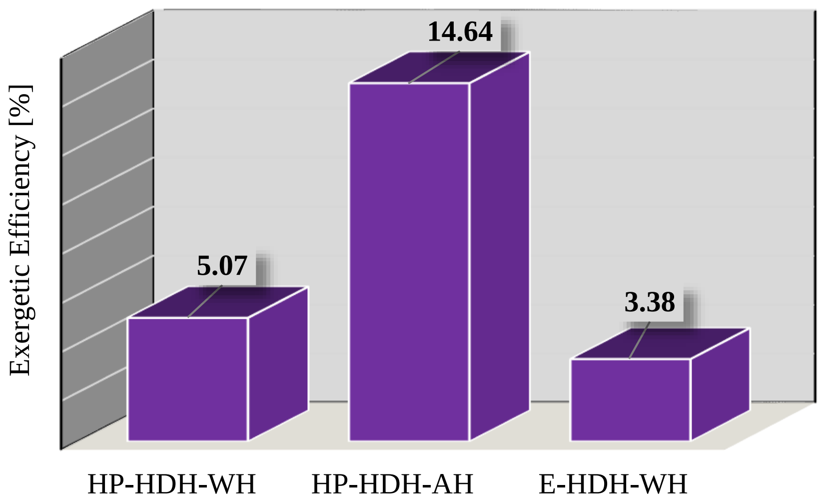

Figure 4. 11: Second law efficiency of each system

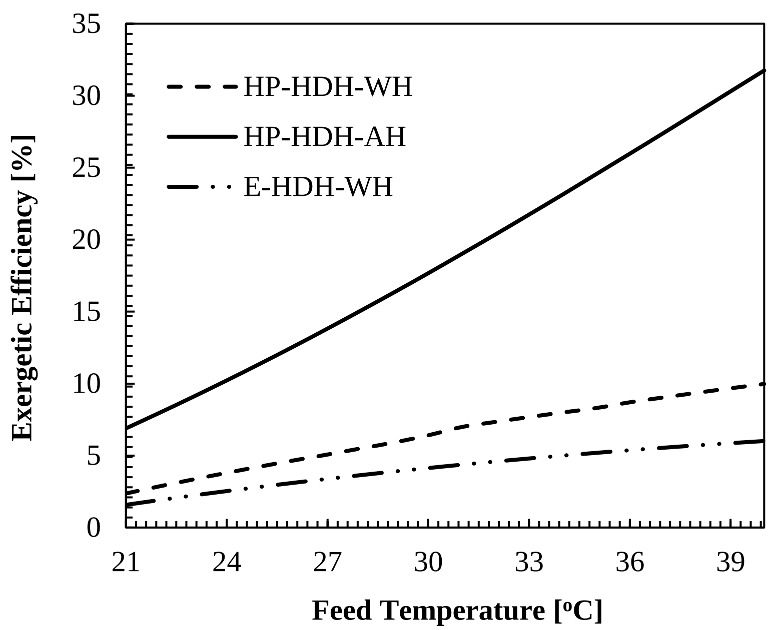

Figure 4. 12: Second law efficiency of each system

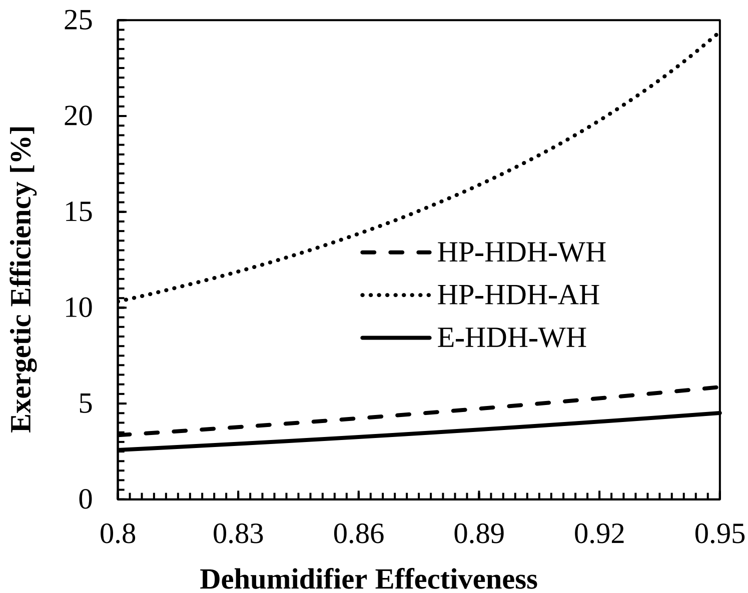

Figure 4. 13: Second law efficiency of each system

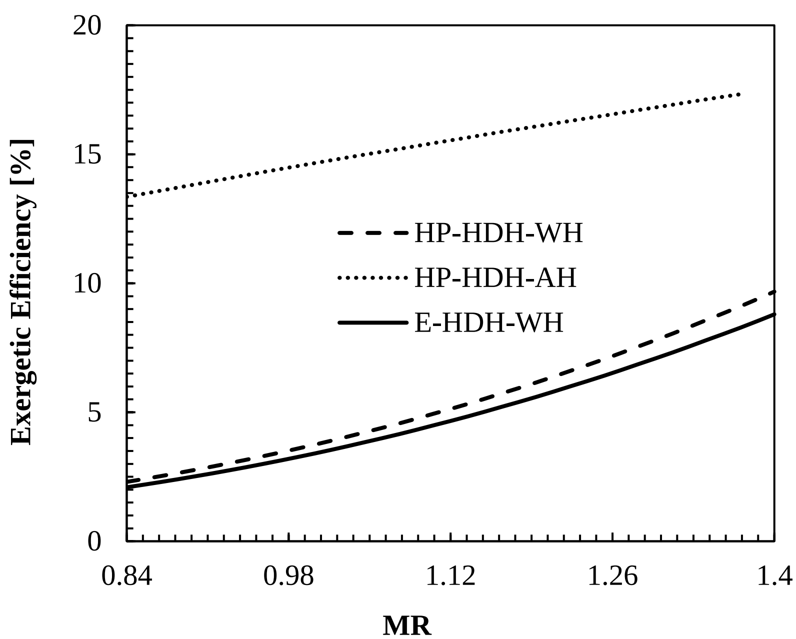

Figure 4. 14: Second law efficiency of each system

The exergetic efficiency measures the performance of the system from a thermodynamic prospective. The results obtained based on our initial assumptions, is illustrated in Figure 4.11. It is obvious that HP-HDH air-heated cycle produces the highest second-law efficiency, reaching an exergetic efficiency of about 14.64%. The exergetic efficiency of both HP-HDH water-heated and E-HDH water-heated cycles were found to be about 5.07% and 3.38% respectively. These results are in agreement with the previous work presented in [120,126]. The high exergetic efficiency attained in HP-HDH air-heated cycle can be attributed to high condensate and low SEEC, as presented in Figure 4.4. The variation of feed water temperature, dehumidifier effectiveness, and mass ratio with the exergetic efficiency of each system is presented in Figures (4.12) to (4.14). The HP-HDH air-heated cycle attained the highest second-law efficiency as compared to other cycles as we varied the feed water temperature, dehumidifier effectiveness, and mass ratio. Increasing feed water temperature, dehumidifier effectiveness, and MR increase the exergetic efficiency of all the systems, with HP-HDH air-heated cycle being the most sensitive to the variation in feed water temperature, dehumidifier effectiveness, and MR. For instance, increasing the feed water temperature from 21 to 40 ^{o}C leads to about 360% increment in exergetic efficiency (6.89%-31.75%).

4.3.1.1 Thermodynamic parameters

The various thermodynamic parameters such as the fuel depletion ratio, the productivity lack, the exergetic improvement potential, and the exergetic factor used for the exergetic assessment of the desalination plants are illustrated in Table 4.2. The conditions at which they are evaluated are as presented in the mathematical modeling. In the case of HP-HDH-WH and HP-HDH-AH, it is obvious from Table 4.2 that the component with the highest and least fuel depletion ratio, productivity lack, and the exergetic factor is the evaporator and the condenser of the heat pump, respectively at the evaluated conditions. Whereas, in the case of E-HDH-WH, both the humidifier and the dehumidifier of the system are the components that possess the largest fuel depletion ratio, productivity lack, and the exergetic factor. These results (fuel depletion ratio) are in a very good agreement with the findings presented in Figure 4.6, where the components with the highest and the lowest exergy destruction ratios/relative irreversibilities are the evaporator and the condenser respectively for both HP-HDH-WH and HP-HDH-AH systems, while for the E-HDH-WH the component associated with the largest exergy destruction is the humidifier and the dehumidifier of the system.

Table 4. 2: Results of some exergetic performance parameters for the HP/E-HDH systems

HP-HDH-WH					
	Fuel Depletion Ratio (β)	Relative Irreversibility (χ)	Productivity Lack (δ)	Exergetic Factor (ξ)	Improvement Potential (Γ)
Expansion Valve	0.2251	0.2249	235.3	0.1098	0.8902
Compressor	0.1338	0.1337	139.9	0.08888	0.9111
Condenser	0.1083	0.1082	113.2	0.04433	0.9557
Evaporator	0.3173	0.317	331.7	0.1736	0.8264
Humidifier	0.1062	0.1061	111	0.01471	0.9853
Dehumidifier	0.1101	0.1101	115.2	0.01548	0.9845
HP-HDH-AH					
Expansion Valve	0.2251	0.1955	14.95	0.1098	0.8902
Compressor	0.1338	0.1162	8.888	0.08888	0.9111
Condenser	0.08036	0.0698	5.337	0.00941	0.9906
Evaporator	0.3173	0.2755	21.07	0.1736	0.8264
Humidifier	0.1727	0.15	11.47	0.02353	0.9765
Dehumidifier	0.222	0.1929	14.74	0.0293	0.9707
E-HDH-WH					
Electric Heater	0.01413	0.2483	22.21	0.01263	0.9874
Humidifier	0.02193	0.3854	34.47	0.00819	0.9918
Dehumidifier	0.02084	0.3663	33.77	0.00792	0.9921

It is worth noting that a component with least exergetic factor has a high potential for improvement and vice versa. Therefore, our findings as presented in Table 4.2 suggested that the components with a high potential for improvement are humidifiers, closely followed by the dehumidifier for the HP-HDH-WH system. For the HP-HDH-AH layout, condenser, followed by the humidifier are components with high potential for improvement, while dehumidifier, closely followed by the humidifier are components with high potential for improvement in the case of E-HDH-WH configuration.

4.3.2 Thermo-economic Analysis

For the evaluation of freshwater cost produced from each plant, the cost flow approach and convectional (El-Dessouky and Ettouney) method has been adopted. In cost flow analysis, the cost balance equations are used to determine the cost of each stream in order to achieve the product cost. The cost flow evaluation method is reported to be more elaborative and useful because it enables the component level cost optimization [119]. This method has been used earlier by several authors [119,120,136,137] to analyze the cost of desalinated water for several desalination systems. Our findings from the cost analysis is presented in this section. Table 4.3 summarizes the investment cost rate of the main components needed in the system. For both HP-HDH water-heated and HP-HDH air-heated systems, it can be noticed from Table 4.3 that compressor has the highest investment cost rate of $0.0122/h, followed by the condenser and the evaporator with cost rate of 0.0061$/h. Fan/blower records the least investment cost rate of $0.001/h.

For the E-HDH water-heated plant, the component with the highest investment cost rate is the dehumidifier with the cost of $0.005 per hour, due to large surface heat transfer area needed for the condensation process, while the component with the least rate of investment cost is the electric heater (0.00049$/h). The monetary costs of the individual stream across the three plants are illustrated in Table 4.4, and the monetary costs of the product were found to be 0.1894, 0.2801, and 0.2802$/h for E-HDH water-heated, HP-HDH water-heated and HP-HDH air-heated cycles, respectively, using the cost flow method.

Table 4. 3: The rate of investment cost for the main components of HDH-HP/E plants

Item Description	**Values ($/h)**		
	E-HDH-WH cycle	**HP-HDH-WH cycle**	**HP-HDH-AH cycle**
Packed Bed Humidifier	0.001354	0.001354	0.001354
Dehumidifier	0.005089	0.005089	0.005089
Water Tanks	0.002036	0.002036	0.002036
Flowmeters	0.002341	0.002341	0.002341
Pumps	0.001527	0.001527	0.001527
Blowers/fans	0.001018	0.001018	0.001018
Semi Hermetic Compressor	-	0.012210	0.012210
Shell and Tube Condenser	-	0.006107	0.006107
Shell & Tube Evaporator	-	0.006107	0.006107
Expansion Valve	-	0.001018	0.001018
Electric Heater	0.0004885	-	-

The cost of desalinated water was evaluated by dividing the monetary cost of condensate of each system by their corresponding mass flowrate of the condensate. The cost of the product from each plant is demonstrated in Figure 4.15. The product cost from HP-HDH-water heated system was found to be 6.55$/m^3 and 6.22 $/m^3 for the cost flow method and convectional method, respectively. The cost of desalted water from HP-HDH-air heated plant was found to be 5.04$/m^3 and 4.81$/m^3 for the cost flow method and traditional approach, respectively. However, the freshwater cost from the electrically water heated HDH unit was found to be 14.69 $\$/m^3$ and 14.61$\$/m^3$ for the cost flow approach and a convectional method, respectively.

Table 4. 4: The monetary costs of each stream from the HP-HDH and E-HDH plants

Stream	Values ($/h)		
	E-HDH-WH cycle	HP-HDH-WH cycle	HP-HDH-AH cycle
$\dot{C}_0$	0	0	0
$\dot{C}_{sw}$	-	0.01653	0.01653
$\dot{C}_{w,1}$	0.01653	0.1098	0.1098
$\dot{C}_{w,2}$	2.005	1.862	10.89
$\dot{C}_{w,3}$	2.17	2.024	0
$\dot{C}_{w,4}$	0	0	0.2802
$\dot{C}_{w,5}$	0.1894	0.2801	-
$\dot{C}_{a,1}$	44.86	67.8	101.6
$\dot{C}_{a,2}$	47.03	69.82	112.5
$\dot{C}_{a,3}$	44.85	67.8	112.7
$\dot{C}_{a,4}$	-	-	101.6
$\dot{C}_{r,1}$	-	0.03316	0.03316
$\dot{C}_{r,2}$	-	0.08823	0.08823
$\dot{C}_{r,3}$	-	0.0675	0.0675
$\dot{C}_{r,4}$	-	0.05405	0.05405

Our findings also show that the cost of freshwater production can be as low as 2.42$\$/m^3$, 5.29$\$/m^3$ and 11.61$\$/m^3$ for HP-HDH air-heated, HP-HDH water-heated, and E-HDH water-heated systems, respectively, when the system is operated at the dehumidifier effectiveness and humidifier effectiveness of 95% and 90%, respectively. Although, the monetary cost of freshwater of HP-HDH air-heated cycle was found to be the highest among the three systems investigated in this study. However, the final product cost of the same system was found to be the least, due to its higher condensate mass flowrate.

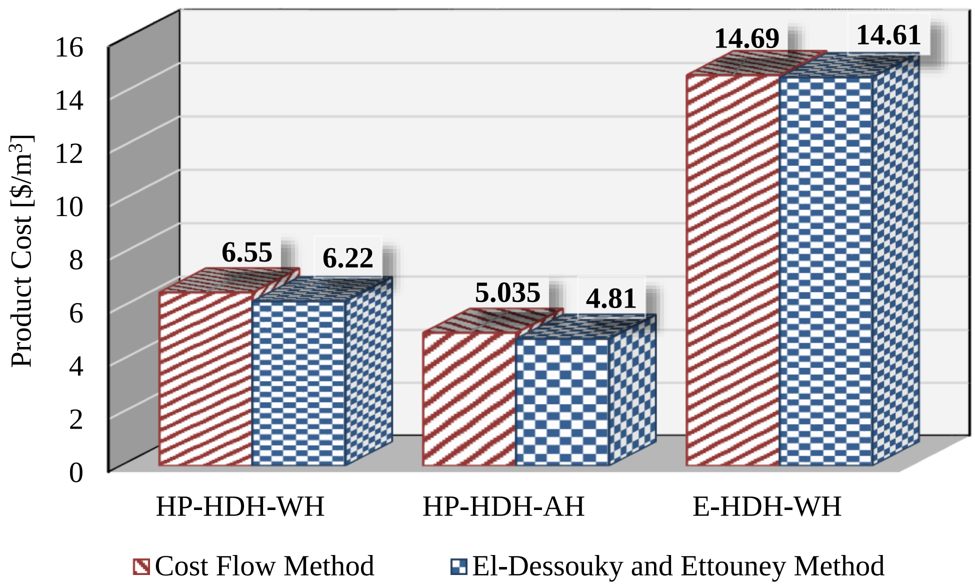

Figure 4. 15: cost of freshwater

It is essential to investigate how cost input parameters influence the cost of desalinated water. Therefore, it is important to understand the variation of the product cost with the cost of electricity, since the price of electricity may differ from one location to another. It is also a good idea to investigate the variation in product cost with plant life expectancy, because each plant may have different life expectation. As such, we investigated the impact of input energy cost (cost of electricity) and plant life expectancy on the cost of freshwater. The cost of desalinated water of each plant with the variation in the cost of electricity are demonstrated in Figure 4.16 for both cost flow approach and convectional method.

As expected, the cost of freshwater from each plant increases linearly with increase in the cost of electricity. This is an indication that the energy consumes by the system has direct relationship with the performance (product cost) of the system. The percentage increment in the product cost when the cost of electricity increases from 0.04 to 0.09$/kWh was found to be about 227.8%, 138.5%, and 122.3% for E-HDH water-heated, HP-HDH water-heated and HP-HDH air-heated desalination plants respectively. This suggested that the energy demand of water- heated cycles is higher than that of the air-heated cycle, because of the lower air heat capacity as compared to the heat capacity of water.

The product cost from E-HDH water-heated plant is observed to be more sensitive to the input energy cost when compared to HP-HDH water-heated and HP-HDH air-heated desalination plants. This may be attributed to the fact that the energy required to increase the water temperature for E-HDH water-heated desalination plant has a direct relationship with the input electricity, whereas, the input electricity for HP-HDH water-heated and HP-HDH air-heated desalination plants has an indirect relationship with energy needed to increase/decrease the water/air temperature in the system.

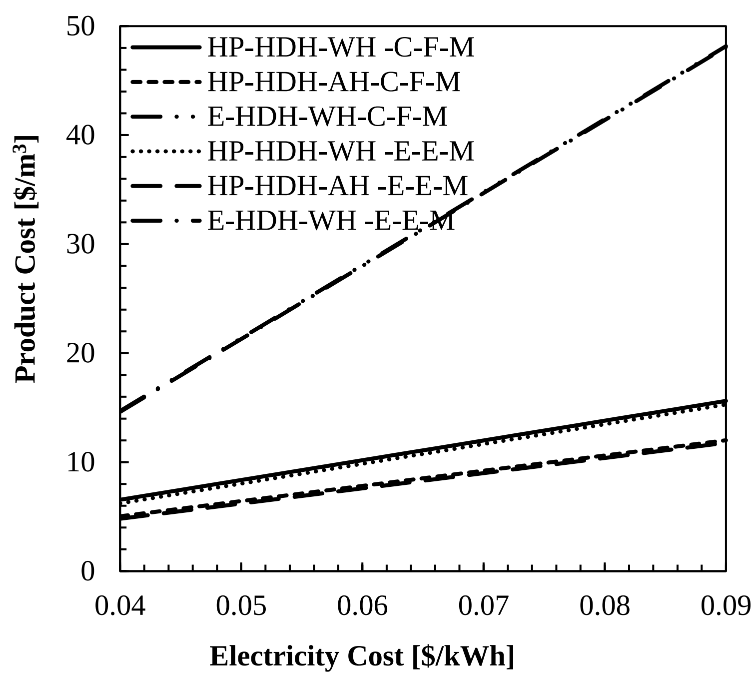

Figure 4. 16: Effect of cost of electricity on desalted water cost

The variations of product cost with the plant lifetime expectation are illustrated in Figure 4.17 for both the cost flow approach and convectional method. It can be noticed that the longer the lifetime of the plant, the lower the cost of desalinated water. Increasing the lifetime of the plant from 15 to 30 years resulted in reduction in the product cost from 5.49$/m^3 to 4.61$/m^3 (representing percentage reduction of about 19%), 7.14$/m^3 to 6.00$/m^3 (representing 19% percentage decrement), and 14.95$/m^3 to 14.44$/m^3 (representing percentage reduction of 4%) for HP-HDH air-heated, HP-HDH water-heated, and E-HDH water-heated desalination plants, respectively. This finding shows that plant lifetime expectation has lesser effect on the plant product cost when compared to the cost of electricity.

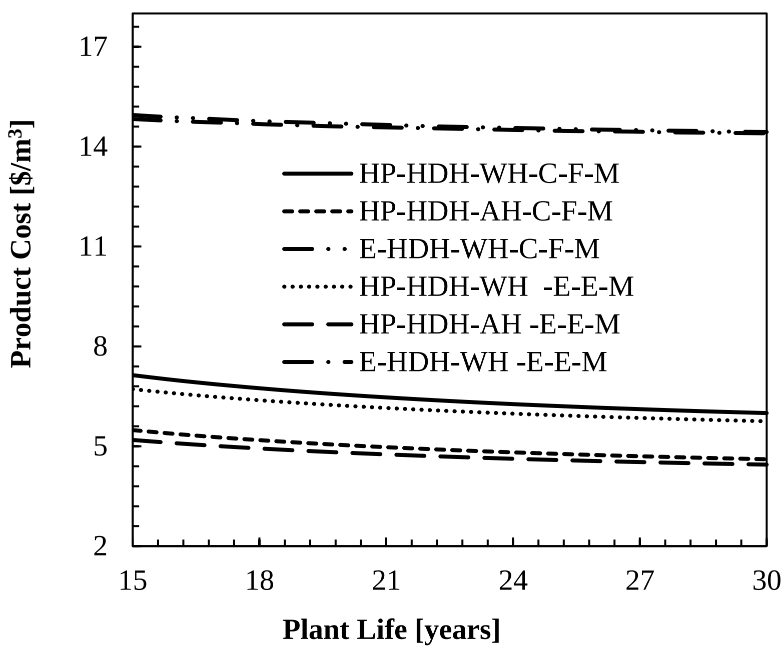

Figure 4. 17: Influence of plant life expectancy on freshwater cost

CHAPTER 5

5.0 Water heated HDH System Integrated with heat pump with Energy Recovery Option

In this section, the analysis of Closed Air Open Water (CAOW) Water heated HDH system driven by vapor compression heat pump is presented. The integrated system is equipped with a brine heat exchanger (BHX) to recover thermal energy from the rejected brine. The influence of various system operating parameters on both thermal and economic performance of the system are investigated. The selected operating parameters includes; mass flowrate ratio, seawater temperature, humidifier effectiveness, brine heat exchanger effectiveness, unit cost of electricity and expected plant life, while the selected performance indices includes; gained output ratio, recovery ratio, rate of desalinated water, Specific Electrical Energy Consumption, and the cost of freshwater production.

5.1 System Description

The proposed HDH desalination system integrated with a heat pump cycle is depicted in Fig. 5.1. The coupled system consists of two loops; the HDH desalination loop and the vapor compression refrigeration loop. For the HDH desalination loop, temperature of the incoming seawater drops to a system minimum temperature as it passes via the evaporator. The low temperature seawater then flows into the dehumidifier where it absorbed latent heat and is accordingly preheated by the condensing vapor carried by the humid air. The preheated seawater leaves the dehumidifier and flows into a brine heat exchanger (BHX), where it is further preheated to a higher temperature (System A). Seawater leaving the brine heat exchanger passes through the heat pump condenser, where it gains heat rejected by the refrigerant from the condenser and its temperature is elevated to the system top temperature. Then, hot seawater is sprayed in the humidifier, where part of the sprayed water evaporates and the rest is rejected as brine at the brine pool at the bottom of the humidifier. The discharged brine is utilized to either preheat the seawater leaving the dehumidifier (System A) or preheat the dehumidified air entering the humidifier (System B). Air from the dehumidifier flows in a counter flow direction through the humidifier, where it is saturated with water vapor. The humidified air is blown to the dehumidifier where the condensation of the water vapor contained in the air takes place. The condensed vapor is collected as distillate, while the cooled humid air enters the humidifier to complete the cycle. For the refrigeration cycle, the refrigerant evaporates in the evaporator as it absorbed heat from the incoming seawater. The refrigerant is then compressed in the compressor to elevate its pressure. Afterward, the refrigerant is cooled in the condenser upon giving off its latent heat to raise the seawater temperature. The cooled refrigerant is then throttled to the evaporation pressure and returned to the evaporator to complete the loop. It is important to mention that the conventional refrigerant to air heat exchangers usually found in vapor compression units are replaced by refrigerant to seawater heat exchangers. It is equally worth mentioning that further modification to current systems integration could provide desalted water and energy for space conditioning (space heating/cooling). For instance, the thermal energy associated with the discharged brine can be used for space heating or drying purpose instead of its utilization for seawater preheating. Or the air loop be open loop such that the dehumidified air leaving the dehumidifier (usually leaves at low temperature) can be employ in space cooling.

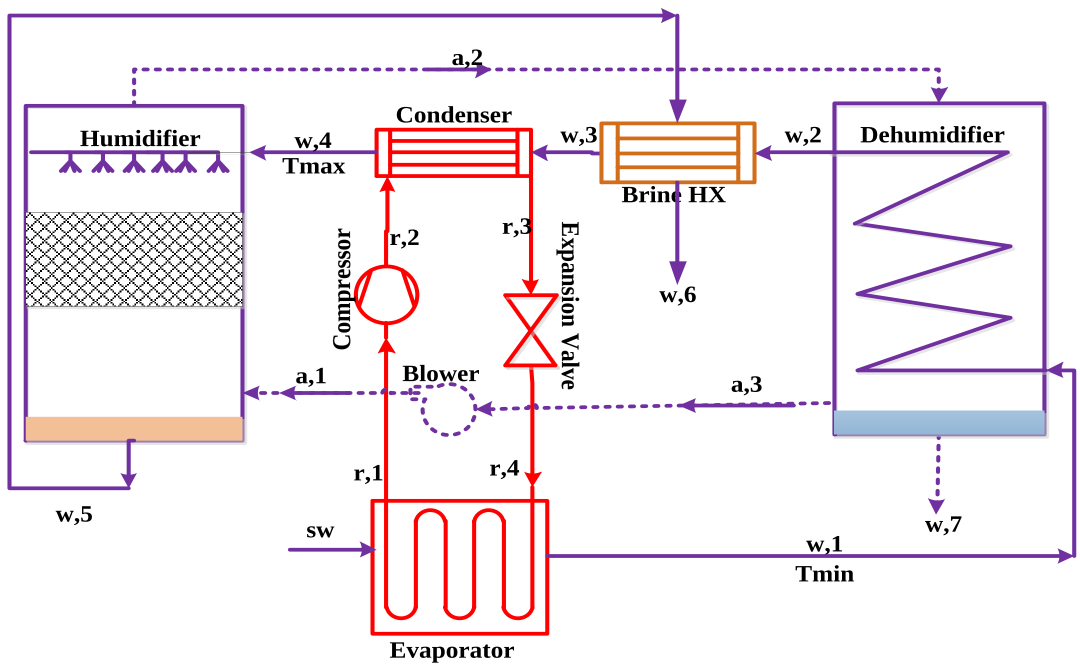

System A

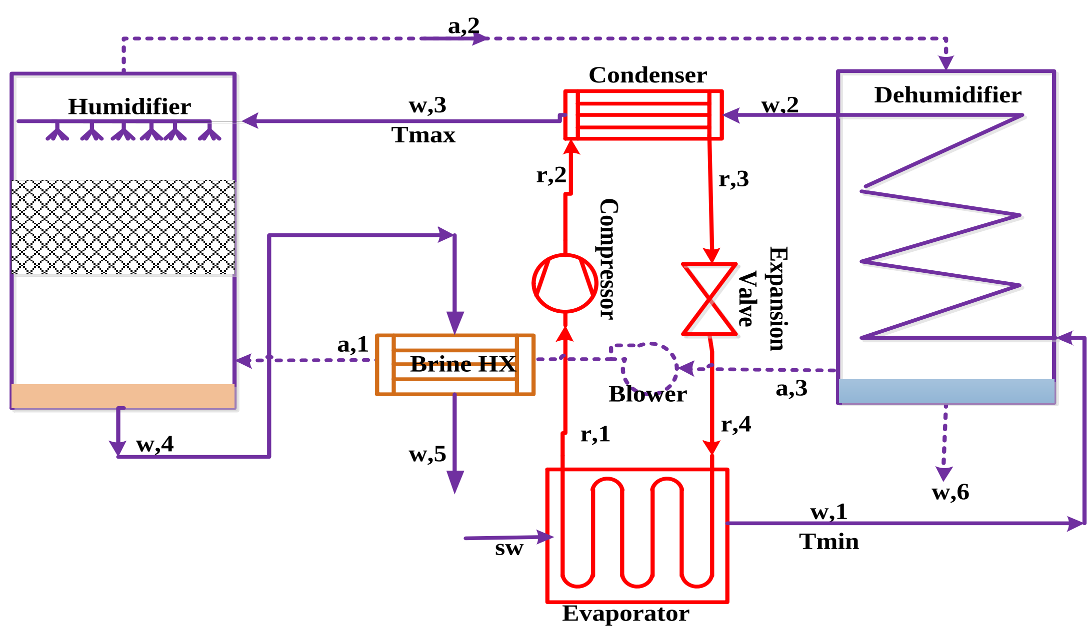

System B

Figure 5. 1: Schematic of the proposed system

5.2 Mathematical model

The following assumptions have been adopted during the mathematical modeling of the proposed system [106]: the system is operating at steady state. No heat losses to the surroundings. No potential and kinetic energy terms. The high and low pressure sides of the heat pump system are 200 and 35 psi, respectively. The relative humidity, the refrigerant mass flow rate, the effectiveness humidifier, dehumidifier and brine heat exchanger are assumed to be 100%, 0.05kg/s, 50%, 80%, and 80%, respectively. The refrigerant in the vapor compression system is R-134a. The inlet temperature of seawater is 27 °C with a salinity of 35 g/kg. Other operating conditions are presented in their respective figures.

The mass and energy balance equations for the main components of the system are presented in the following section [106]:

Humidifier:

$$\dot{m}_a\left(h_{a,out} - h_{a,in}\right) = \dot{m}_w h_{w,in} - \dot{m}_b h_b \quad (1)$$

$$\dot{m}_b = \dot{m}_w - \dot{m}_{fw} \quad (2)$$

Dehumidifier:

$$\dot{m}_{fw} = \dot{m}_a\left(\omega_{a,in} - \omega_{a,out}\right) \quad (3)$$

$$\dot{m}_{fw} h_{fw} + \dot{m}_a\left(h_{a,out} - h_{a,in}\right) = \dot{m}_w\left(h_{w,in} - h_{w,out}\right) \quad (4)$$

Brine Heat Exchanger:

$$\dot{m}_b\left(h_{b,in} - h_{b,out}\right) = \dot{m}_w\left(h_{w,out} - h_{w,in}\right) \tag{5}$$

Condenser:

$$\dot{m}_r = \dot{m}_{r,in} = \dot{m}_{r,out} \tag{6}$$

$$\dot{Q}_{cond} = \dot{m}_w\left(h_{w,out} - h_{w,in}\right) = \dot{m}_r\left(h_{r,in} - h_{r,out}\right) \tag{7}$$

Evaporator:

$$\dot{Q}_{evap} = \dot{m}_w\left(h_{w,in} - h_{w,out}\right) = \dot{m}_r\left(h_{r,out} - h_{r,in}\right) \tag{8}$$

Compressor, and Expansion valve:

$$\dot{W}_{comp} = \dot{m}_r\left(h_{r,out} - h_{r,in}\right) \tag{9}$$

$$h_{r,out} = h_{r,in} \tag{10}$$

The following expressions are used for evaluating the components effectiveness.

Humidifier effectiveness [11]:

$$\varepsilon_H = \max\left\{\frac{h_{a,out} - h_{a,in}}{h_{a,out,ideal} - h_{a,in}}, \frac{h_{w,in} - h_{w,out}}{h_{w,in} - h_{w,out,ideal}}\right\} \tag{11}$$

Dehumidifier effectiveness [11]:

$$\varepsilon_D = \max\left\{\frac{h_{a,in} - h_{a,out}}{h_{a,in} - h_{a,out,ideal}}, \frac{h_{w,out} - h_{w,in}}{h_{w,out,ideal} - h_{w,in}}\right\} \tag{12}$$

Brine Heat Exchanger effectiveness:

$$\varepsilon_{BHX} = \max\left\{\frac{T_{w,out} - T_{w,in}}{T_{b,in} - T_{w,in}}, \frac{T_{b,in} - T_{b,out}}{T_{b,in} - T_{w,in}}\right\} \tag{13}$$

The ideal air outlet enthalpy ($h_{a,out,ideal}$) is evaluated when the outlet air is fully saturated at the water inlet temperature, and the ideal water outlet enthalpy ($h_{w,out,ideal}$) is estimated when its temperature is equal to the temperature of the inlet air dry-bulb.

The investigated system performance indices are the Gained Output Ratio (GOR), Productivity, Recovery Ratio (RR), and Specific Electrical Energy Consumption (SEEC). Their respective mathematical expression are as follows:

Gained Output Ratio (GOR): Is the product of produced freshwater and latent heat of vaporization divided the energy input [106,107,109,111]:

$$\mathrm{GOR} = \frac{\dot{m}_{fw} h_{fg}}{\dot{W}_{Comp} + \dot{W}_{Pump} + \dot{W}_{Fan}} \tag{14}$$

Recovery Ratio (RR) is the ratio of produced freshwater to feed water flowrates[106,107,109,111]:

$$\mathrm{RR} = \frac{\dot{m}_{fw}}{\dot{m}_{w}} \tag{15}$$

The Specific Electrical Energy Consumption (SEEC) is ratio of electrical energy consumed to produce one kilogram/cubic meter of fresh water [106,107]:

$$\mathrm{SEEC} = \frac{\dot{W}_{Comp} + \dot{W}_{Pump} + \dot{W}_{Fan}}{\dot{V}_{freshwater}} \tag{16}$$

Where

$\dot{V}_{freshwater}$ (m^3/hour) is the volumetric flowrate of the condensate.

The following expressions are used to evaluate the unit product cost [106,107]: The cost analysis involves the cost of energy consumed by the system, the capital cost, labor/operational cost, management cost, maintenance cost and the cost of freshwater production.

The following conditions are assumed for the cost analysis adopted from [107]: The electricity cost is 0.045$/kWh. No pretreatment costs. The plant availability and life expectancy is 90% and 20 years, respectively, while the interest rate (i) is 5%. The pump and fan/blower power is 750 W and 50 W, respectively. The operating labor specific cost, annual maintenance cost, and annual management cost is 0.1 $/m^3, 1.5% of the capital cost, and 20% of the labor cost, respectively.

For the current system, the energy cost involves the cost of electricity consumed by heat pump, blower, and pumps. The capital cost includes the cost of equipment's/main components such as humidifier, dehumidifier, heat pump, water pumps, pipes, fittings, air blower and water tanks. To evaluate the capital cost capital recovery factor (amortization factor) is required which can be calculated from:

Amortization factor (α):

$$\alpha = \frac{i(i+1)^n}{(i+1)^n - 1} \tag{17}$$

Annual capital cost:

$$\dot{Z}_f(\$/yr) = Z(\$) \times \alpha\ (1/yr) \tag{18}$$

The summary of fixed capital cost of the plants main components is presented in Table 5.1 as adopted from [102]:

Annual electric power cost ($\dot{C}_{Elect}$):

$$\dot{C}_{Elect}(\$/yr) = COE\ (\$/kWh) \times \frac{SEEC}{3600}(kWh/m^3)\ \times Å \times \dot{V}_{fw}\ (m^3/day) \times 365 \quad (19)$$

The annual labor cost ($\dot{C}_L$):

$$\dot{C}_L(\$/yr) = \mathcal{L}(\$/m^3) \times Å\ \times \dot{V}_{fw}\ (m^3/day) \times 365 \quad (20)$$

The total annual cost ($\dot{C}_T$):

$$\dot{C}_T(\$/yr) = \dot{Z}_f(\$/yr) + \dot{C}_{Elect}\ (\$/yr) + \dot{C}_L(\$/yr) +\ \dot{C}_{mt}(\$/yr)\ + \dot{C}_{mg}(\$/yr) \quad (21)$$

Where $\dot{C}_{mt}$and $\dot{C}_{mg}$ is the annual maintenance and management costs, respectively.

Therefore, unit product cost (C_P):

$$C_P(\$/m^3) = \left(\frac{\dot{C}_T(\$/yr)}{Å\ \times V_{fw}\ (m^3/day) \times 365\ (day/yr)}\right) \quad (22)$$

5.3 Results and Discussion

The mathematical modeling of the HDH desalination system driven by heat pump was performed by solving the above set of presented mathematical equations using Engineering equation solver (EES) software [138]. EES has a complete library of thermo-physical properties for different fluids including brine, real fluids, and moist air. The results obtained for the proposed desalination systems are analyzed and discussed to examine the impacts of the various system operating parameters, such as mass flowrate ratio, seawater temperature, humidifier effectiveness, and effectiveness of brine heat exchanger on the system performance, including gained output ratio, fresh water productivity, recovery ratio, and Specific Electrical Energy Consumption. Furthermore, the findings for the cost of fresh water production was equally presented and discussed. The specific system operating conditions are given on each figure for consistency. It is important to state that if we remove the brine heat exchanger added at the exit/inlet of the dehumidifier, the results match with the work of [106,107]; thus validating the mathematical model used in this work.

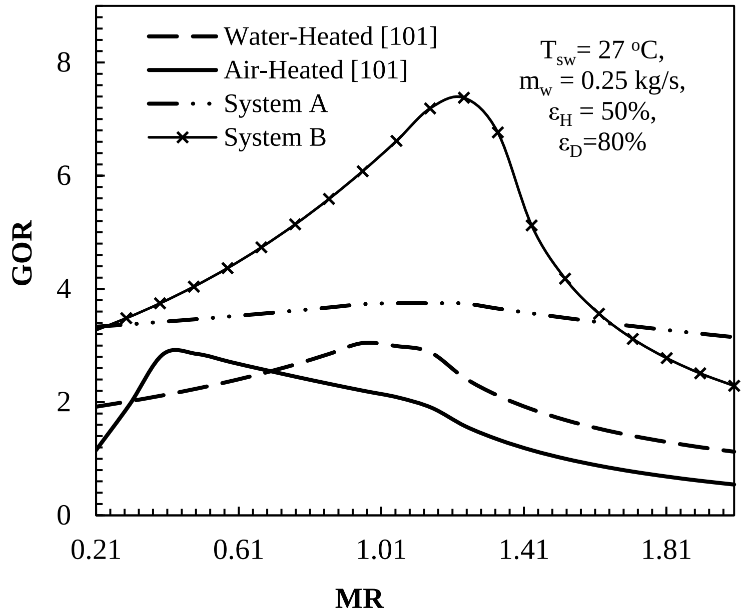
Water-Heated [101]
Air-Heated [101]
System A
System B
T_{sw}= 27 ^oC,
m_w = 0.25 kg/s,
ε_H = 50%,
ε_D=80%
GOR
MR
0.21
0.61
1.01
1.41
1.81
0
2
4
6
8

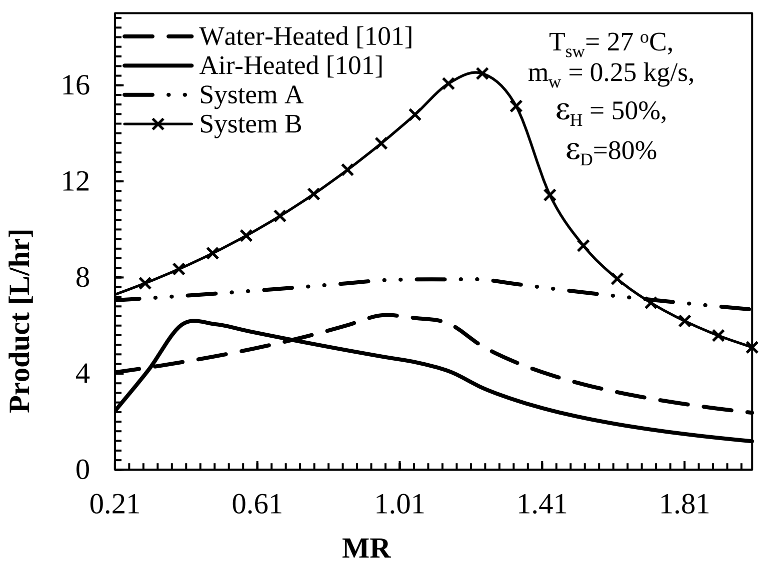
Water-Heated [101]
Air-Heated [101]
System A
System B
T_{sw}= 27 ^oC,
m_w = 0.25 kg/s,
ε_H = 50%,
ε_D=80%
Product [L/hr]
MR
0.21
0.61
1.01
1.41
1.81
0
4
8
12
16

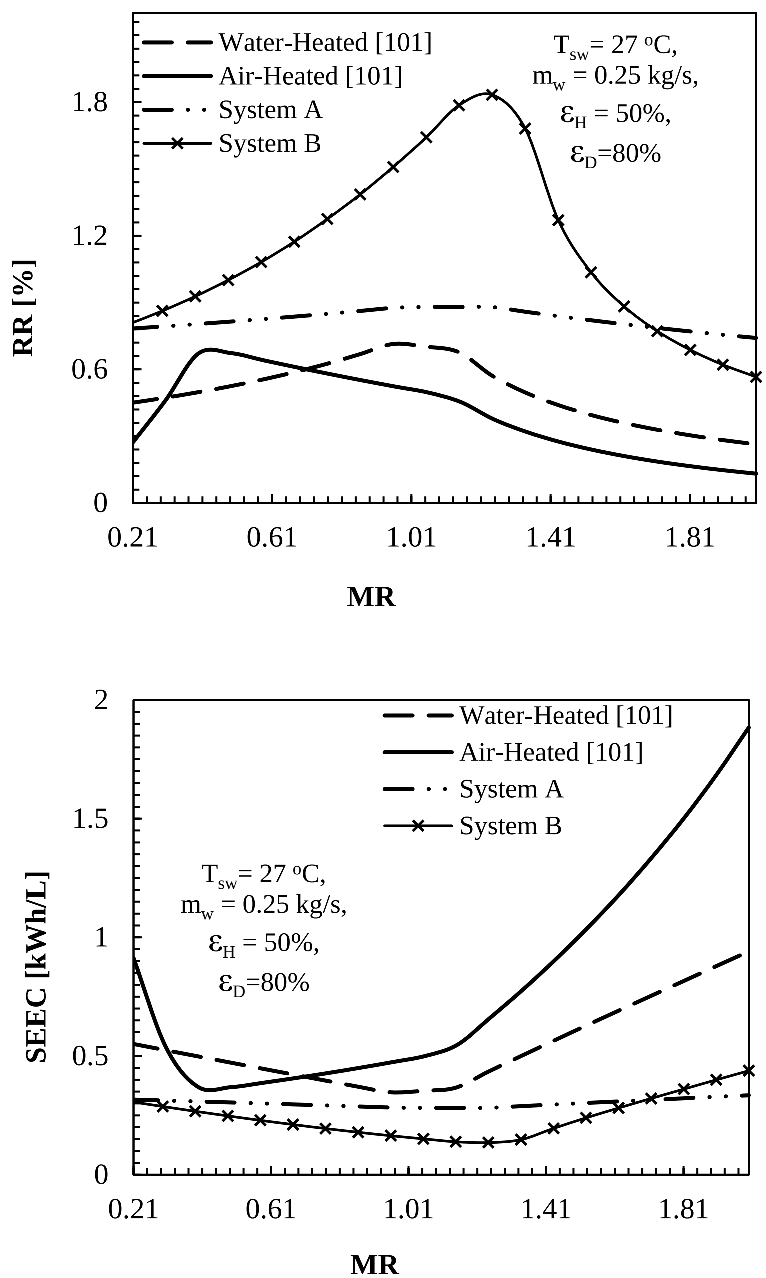

Figure 5. 2: Effect of Mass Ratio on GOR, productivity, RR and Specific Electrical Energy Consumption

The performance of the proposed desalination systems against those presented by [106] is illustrated in Figure 5.2. It is obvious that when operating the systems at the same conditions, the current systems (A and B) provides superior performances in terms of GOR, freshwater production rate, RR and SEEC when compared to water heated (WH-HDH-HP) and modified air heated (AH-HDH-HP) systems operated by heat pump. For instance, at operating conditions where the system maximum GOR is 3.04 and 2.85 for water and air heated HDH systems respectively, the maximum GOR for systems A and B is 3.75 and 7.38 respectively. On the other hand, the best values for water heated, modified air heated, system A and system B are; 6.43L/hr, 6.06,L/hr 7.92L/hr and 16.49L/hr for productivity; 0.71%, 0.67%, 0.88% and 1.83 for RR; and 0.34 kWh/L, 0.37 kWh/L, 0.28 kWh/L and 0.14 kWh/L for Specific Electrical Energy Consumption, respectively. In fact, systems with low SEEC demands lower energy requirement to provide the same system output, when compared to those with higher SEEC. Therefore, lower SEEC value is the best and it's demand of any thermal systems.

The above systems comparison were made at humidifier and dehumidifier effectiveness of 50% and 80% respectively. The performance of the proposed systems becomes closer or even inferior to that of water heated system [106] at higher humidifier effectiveness. In fact, at 59.16% humidifier effectiveness and mass ratio of unity, both the proposed system A and water heated HDH system [106] portrayed the same performance. Beyond 59.16% humidifier effectiveness, the performance of system A becomes inferior to that of water heated system [106]. Similarly, the proposed system B shows superior performance in comparison to water heated system for humidifier effectiveness of 91.25% and below. Beyond 91.25% humidifier effectiveness, the performance of water heated system supersede that of proposed system B. These findings portrayed the limit of components effectiveness at which energy recovery becomes a necessity and beneficial. At low humidifier effectiveness (below 59.16% and 91.25% for system A and system B respectively), the thermal energy associated with the rejected brine is far greater than that accompanying the seawater/air leaving the dehumidifier, due to ineffectiveness of the humidifier. High thermal energy associated with the discharged brine signifies low humid air temperature exiting the humidifier. Therefore, using the thermal energy accompanying the discharged brine to preheat the seawater/air becomes advantageous, and improve the thermal performance of the systems. On contrary, at higher humidifier effectiveness (above 59.16% and 91.25% for system A and system B respectively), the discharged brine thermal energy is lower than the thermal energy associated with the seawater/air exiting the dehumidifier. Therefore, using the rejected brine becomes disadvantageous and deteriorate the overall thermal performance of the system. If BHX is employed above limiting case of components effectiveness, the seawater/air flowing to the condenser/humidifier respectively will gives out it accompanying thermal energy to the discharged brine, thereby leading to poor system performance. Similar findings were obtained for the dehumidifier effectiveness at a fixed value of humidifier effectiveness, since the thermal energy of the seawater/air exiting the dehumidifier has direct correlations with the effectiveness of the dehumidifier.

The thermal energy accompanying the seawater leaving the dehumidifier of system A is always lower than that of the discharged brine as long as the dehumidifier effectiveness is fixed below 63.6% for a fixed humidifier effectiveness of 80%. In this regard (less than 63.6% dehumidifier effectiveness), energy recovery from the rejected brine become a necessity to enhance the thermal performance of the proposed system A. However, at a fixed humidifier effectiveness of 80%, the performance of system B is always superior to that water heated system irrespective of dehumidifier effectiveness. These findings shows that to adopt the proposed system A, the effectiveness of humidifier and dehumidifier must be below 59.16% and 63.6% respectively. For system B, there is no limitation for dehumidifier effectiveness, while the humidifier effectiveness must be below 91.25%. These values of components effectiveness are the conditions that is favorable for the proposed desalination systems based on the comparison with the water heated system [106].

At the same system operating conditions, it is obvious that the performance of system B supersedes that of both system A and the water heated system [106]. The reason for the higher performance of system B may be attributed to the fact that less thermal energy is required for heating the air in comparison for heating water because of higher specific heat capacity of water. Therefore, for the same value of recovered thermal energy from the brine, air is heated to a higher temperature as compared to that of heating the water. Higher air temperature increases the ability of air to carry more water vapor, thus increasing the mass transfer to the dehumidifier, and consequently higher distillation rate, and higher system performance. Hence, for the same quantity of freshwater produced, system B utilizes lower overall energy, thereby improving the GOR and other performance metrics of the system.

The influence of mass flowrate ratio on the performance of proposed systems is present in Figures (5.3-5.6). It can be noticed that increasing the mass ratio initially increases the GOR, productivity and recovery ratio, and decreases the Specific Electrical Energy Consumption, up to the optimum mass ratio where maximum GOR, productivity and recovery ratio, and minimum Specific Electrical Energy Consumption occurred. Further increase in MR from the optimum value leads to decrease in the GOR, productivity and recovery ratio, and increase in Specific Electrical Energy Consumption of the system. The initial increment in the GOR may be predominantly due to decrease in the rate of air supplied for the given seawater flowrate. The decrease in air flowrate leads to increase in MR, decrease in required heat input, and consequently increase in the system GOR. The initial increase in water production rate is because of low air flowrate (high MR), which allows enough water vapor to comes in contact with the air and get humidified (saturated with water vapor) in the humidifier. The low air flowrates allows hot saline water heating the air effectively and leads to high specific humidity, and subsequently higher rate of condensation. The increase in recovery ratio is because of the increase in system productivity (rise in desalinated water produced). Further increase in MR after the optimum MR leads to reduction in GOR due to insufficient air supply, which resulted in flooding in the humidifier such that air is saturated and cannot carry more water vapor. The optimum MR indicates the MR value where the supplied air is just enough to carry the maximum water vapor generated from feed water. Optimum MR gives the right amount of air supplied and saline water flowrates to yield maximum system performance.

For system A, it can be observed that low feed water flowrate is encouraged for better system performance. For this system A, high water flow rate will result in lower temperature of water to be sprayed in the humidifier, which reduces the humidity ratio of the air and consequently the general performance of the system performance (GOR and other system performance metrics). For system B, high seawater flow rate improves the overall performance of the system. The improvement in GOR may be attributed to the fact that at high water flowrate, water temperature to be sprayed decreases, however, air enters the humidifier at relatively higher temperature, which increases the capacity of air to carry more vapor and high mass transfer to the dehumidifier. Consequently, more freshwater is produce, and higher GOR is achieved.

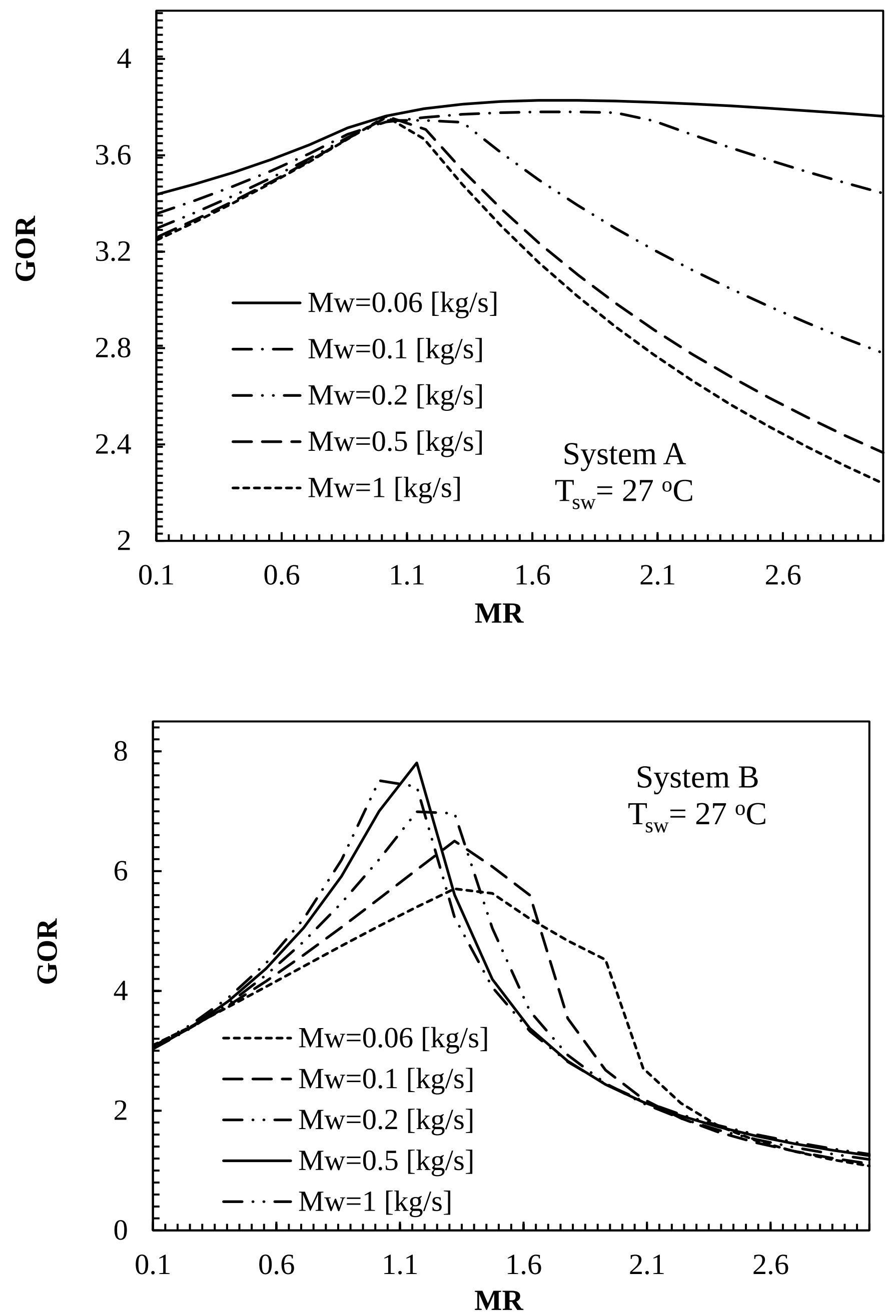

Figure 5. 3: Impact of Mass flowrate ratio on gained output ratio

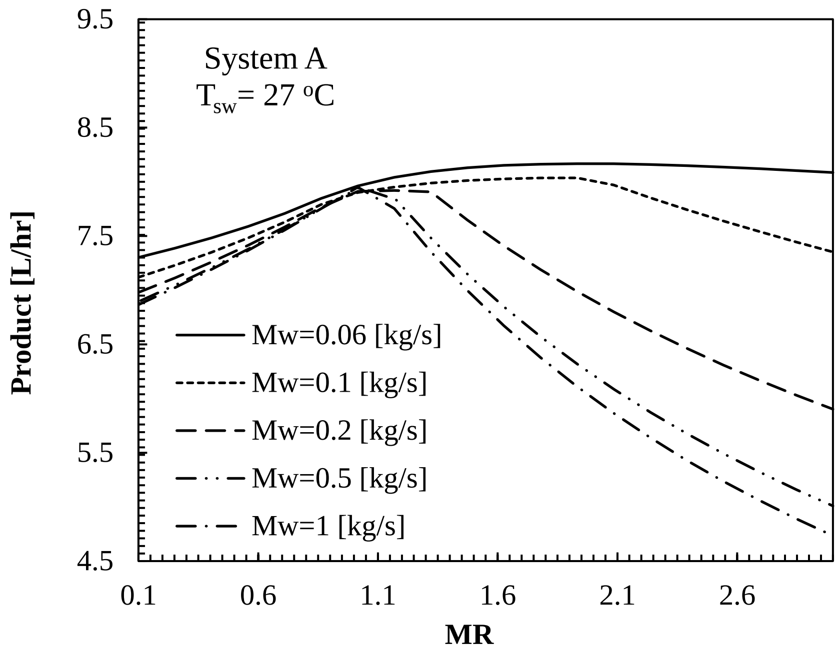

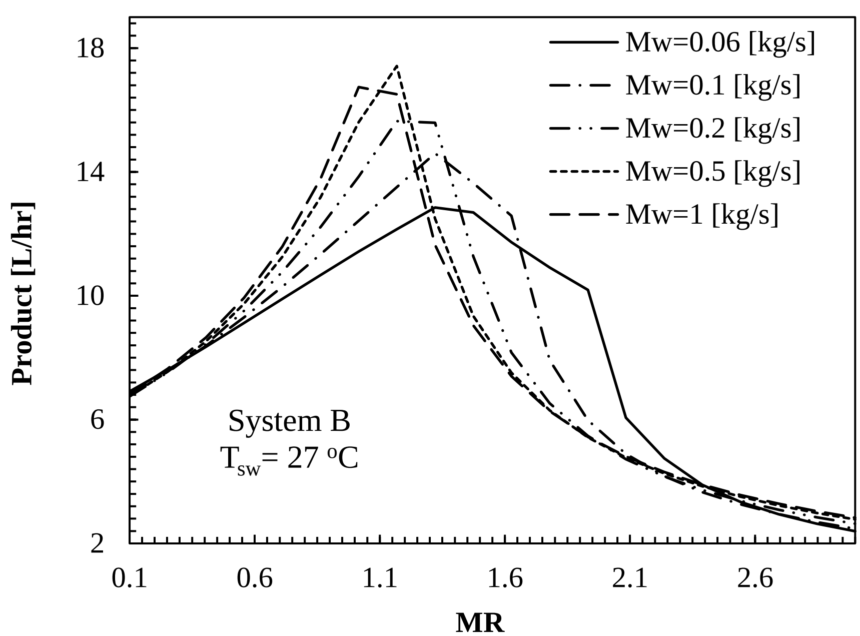

Figure 5. 4: Influence of Mass ratio on the rate of freshwater production

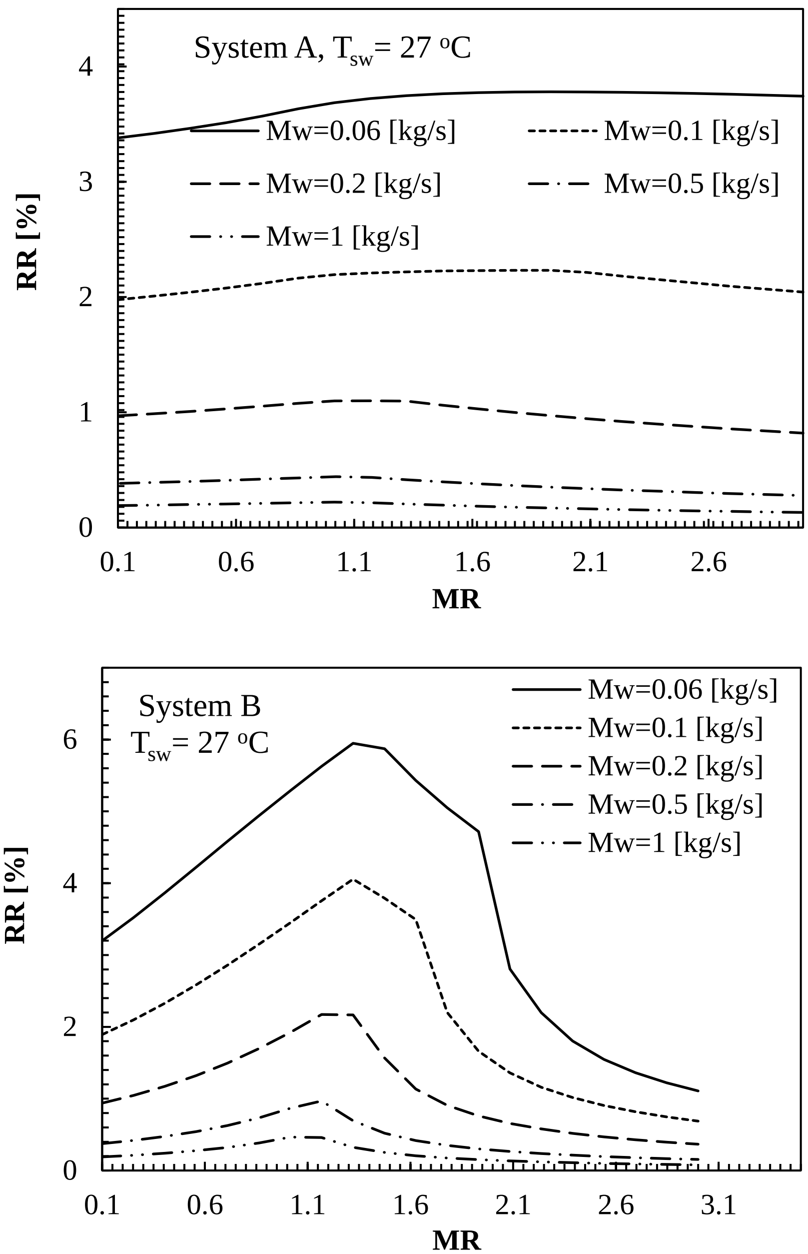

Figure 5. 5: Effect of Mass flowrate ratio on recovery ratio

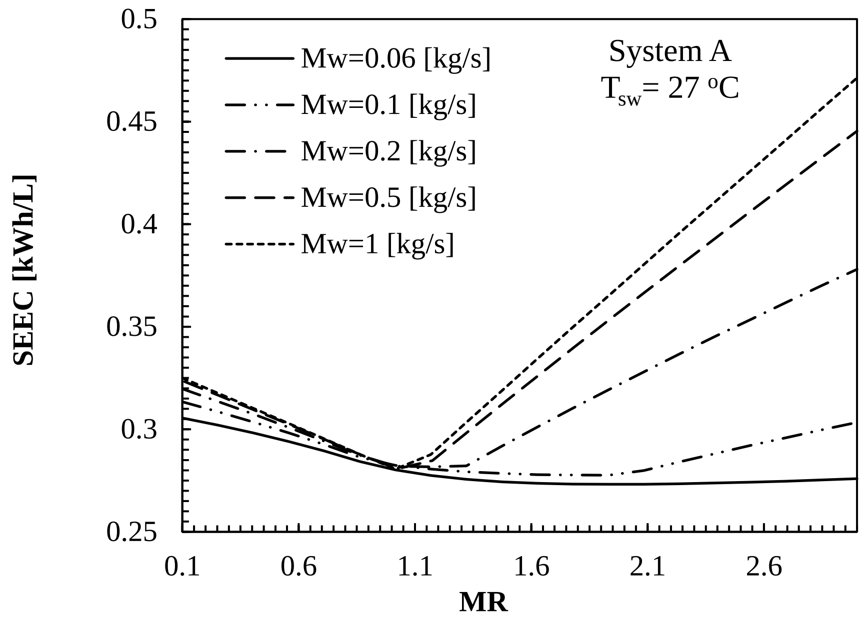

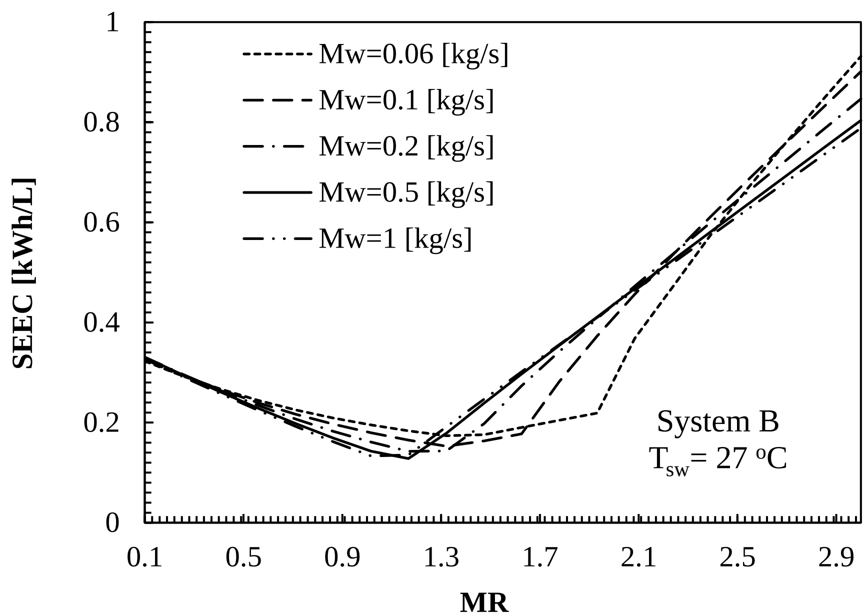

Figure 5. 6: Influence of Mass flowrate ratio on Specific Electrical Energy Consumption

The influence of inlet seawater temperature to the dehumidifier on the gained output ratio, rate of freshwater production, recovery ratio, and Specific Electrical Energy Consumption is depicted in Figures (5.7 – 5.10). For system A, higher temperature of inlet seawater leads to higher gained output ratio, recovery ratio and productivity, and lower Specific Electrical

Energy Consumption. The increase in GOR of the system with increasing seawater temperature is due to the less input energy required to attained top system temperature at high seawater temperature. Pre-heating the seawater temperature also decreases the energy required to reach top system temperature, thereby and consequently the increase in system GOR. Higher seawater temperature indicates higher top temperature of the system, which leads to higher evaporation process in the humidifier, thus higher fresh water production rate. Therefore, the increase in the system productivity may also resulted in an increase in GOR of the system, because GOR is a function of both system productivity and input energy. The increase in the rate of freshwater production due to increase in seawater temperature also leads to increase in recovery ratio, which is a function of freshwater flowrate and seawater flowrate. The decrease in Specific Electrical Energy Consumption with increase in seawater temperature is due to the lower energy demand by the high seawater temperature to attain the same top system temperature. For system B, optimum temperatures exist at which the best system performance metrics are attained. The optimum temperature increases and shifted to the right for higher MR. This may be because, at a higher mass flowrate ratio, more air flow is demanded to absorb extra water vapor to attained saturation condition at high seawater temperature. In surmise for systems (A and B), low Specific Electrical Energy Consumption is desirable, while higher productivity, gained output ratio and recovery ratio is encourage.

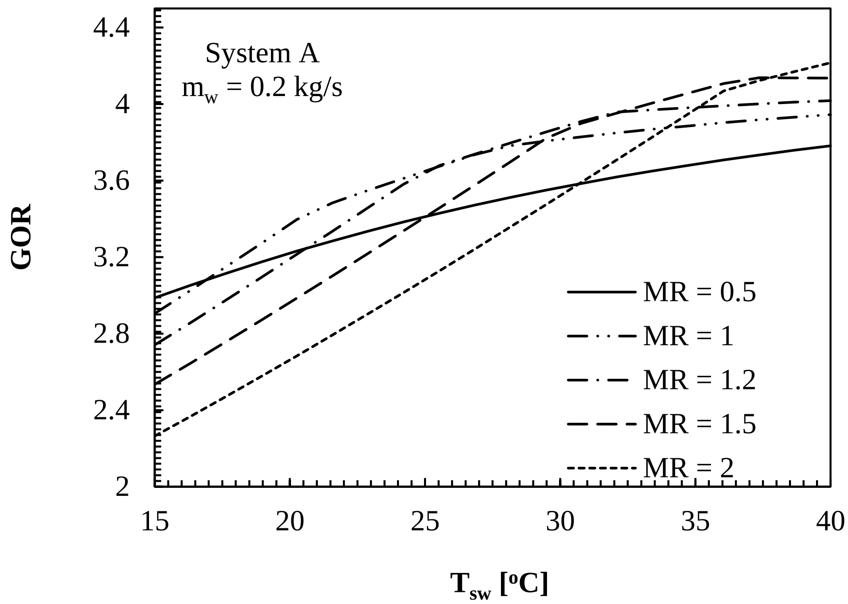

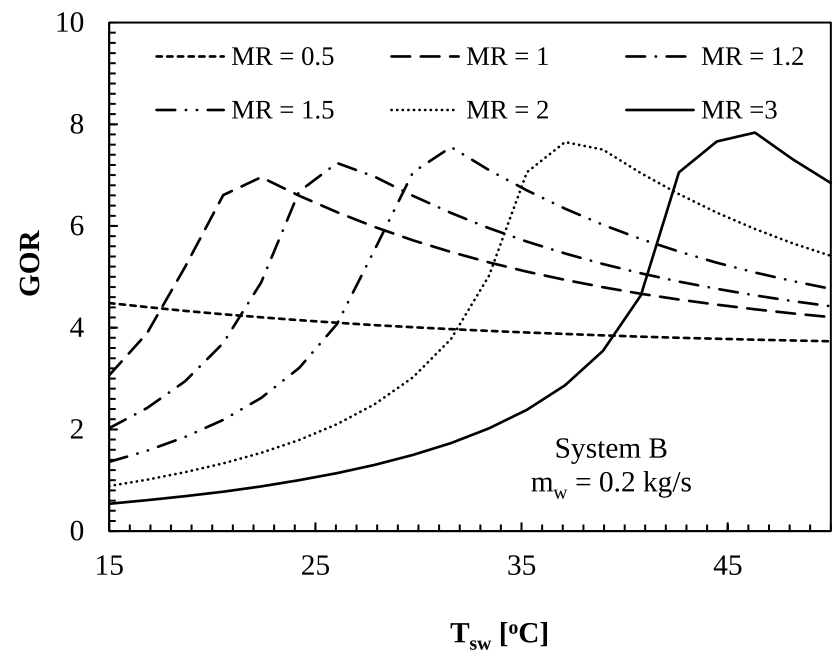

Figure 5. 7: Impact of inlet seawater temperature on gained output ratio

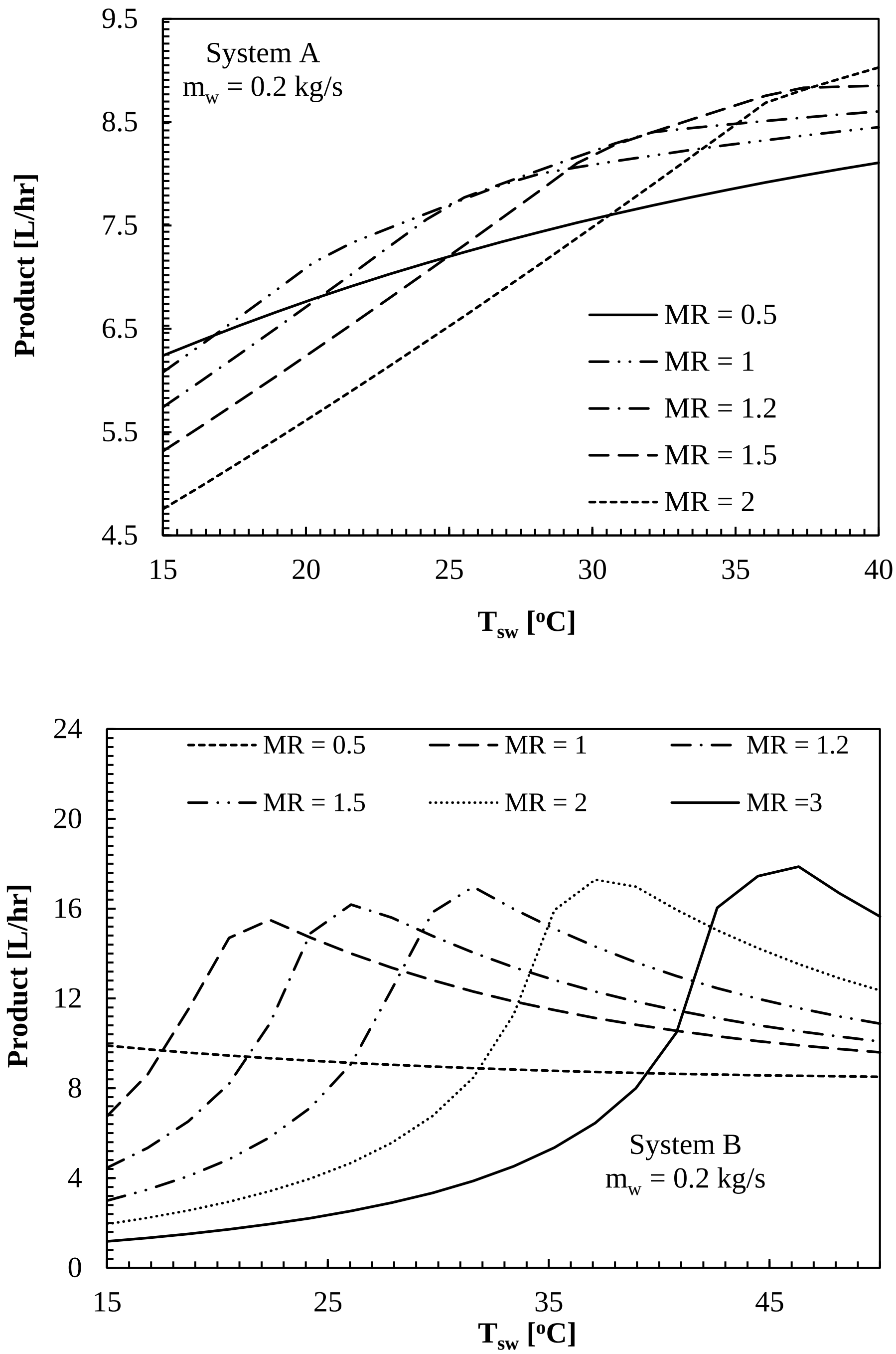

Figure 5. 8: Effect of inlet seawater temperature on productivity

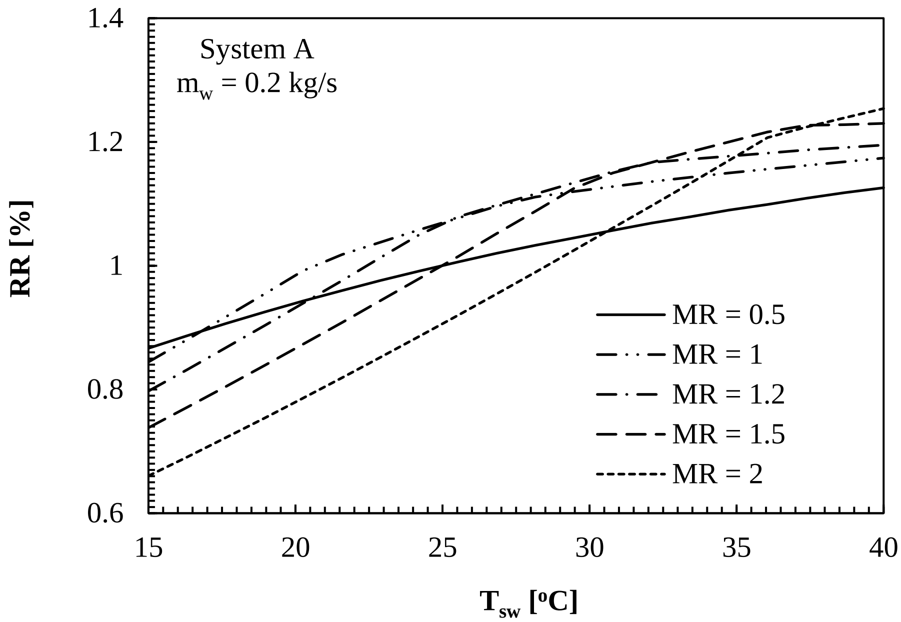

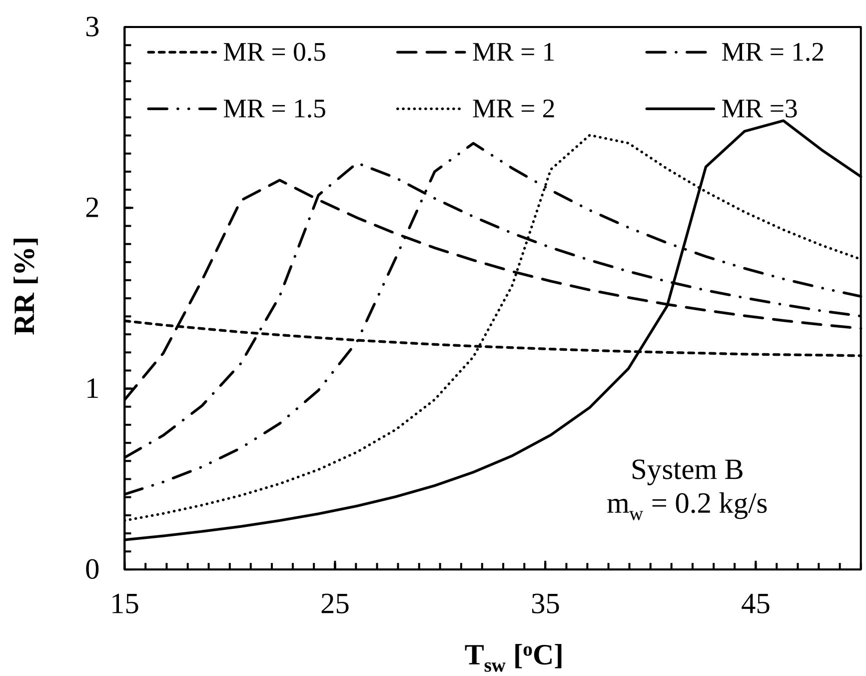

Figure 5. 9: Impact of inlet seawater temperature on recovery ratio

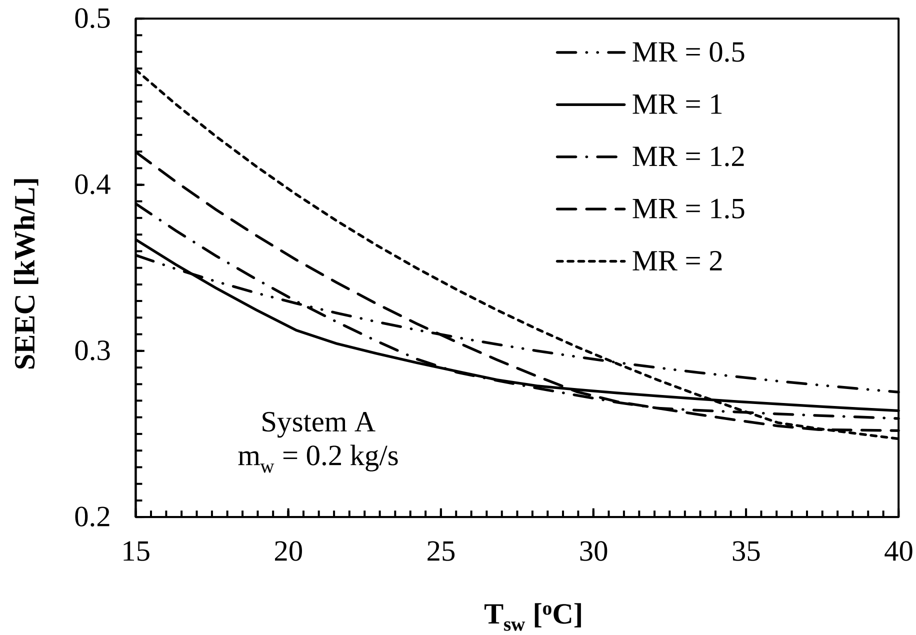

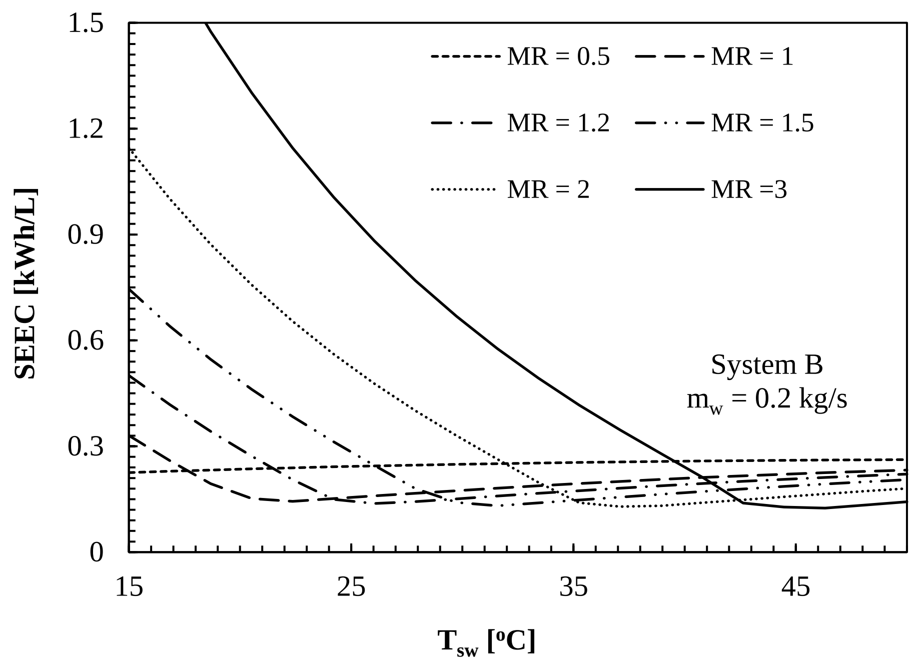

Figure 5. 10: Effect of inlet seawater temperature on Specific Electrical Energy Consumption

Illustrated in Figure 5.11 is the impact of humidifier effectiveness on the GOR, RR, productivity and Specific Electrical Energy Consumption, while Figure 5.12 demonstrates the effect of effectiveness of brine heat exchanger on the GOR of the system. It is obvious that higher humidifier effectiveness leads to higher GOR, recovery ratio and rate of freshwater production, and decreases the energy demand of the systems. The GOR increase with increase in humidifier effectiveness because higher humidifier effectiveness means air exit the humidifier at higher temperature and higher humidity ratio, which indicated that more water vapor will be carried by the air to be condense in the dehumidifier. In other words, high humidifier effectiveness means better functionality of the humidifier. Its better functionality leads to high humid air temperature exiting the humidifier, which creates high temperature difference across the dehumidifier, and consequently high distillation rate, which also leads to better system recovery ratio. It can be noticed from Figure 5.12 that the peak GOR increases with higher effectiveness of brine heat exchanger, due to high rate of heat exchange/transfer between the brine and the seawater/dehumidified air at higher BHX effectiveness.

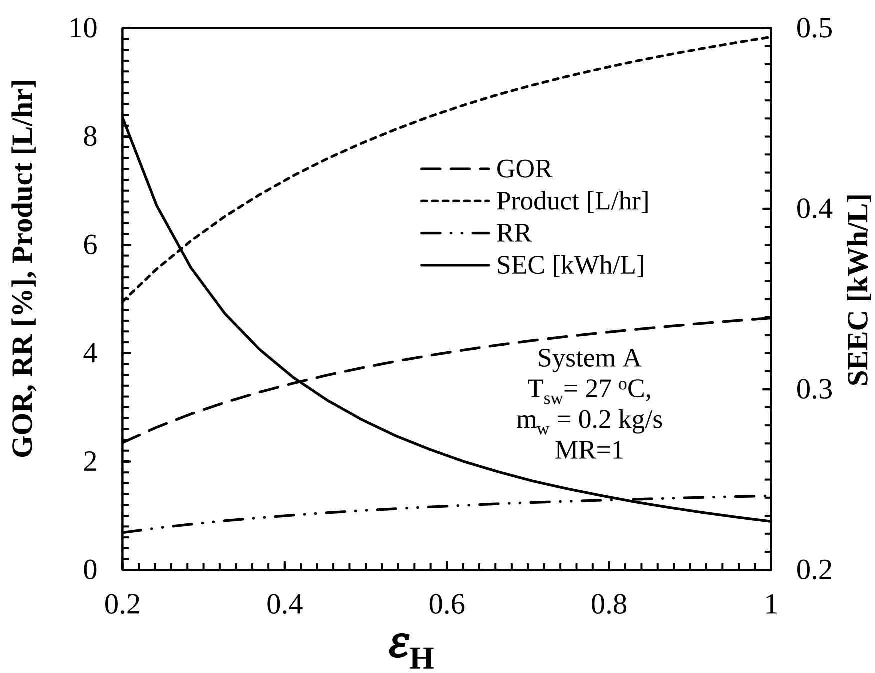

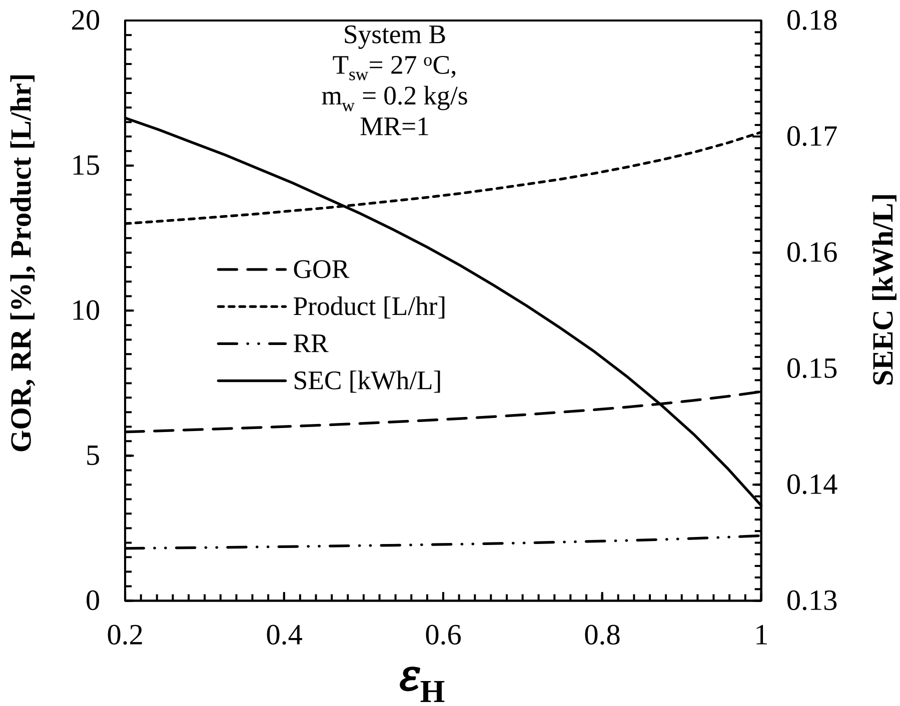

Figure 5. 11: Influence of humidifier effectiveness on system performance

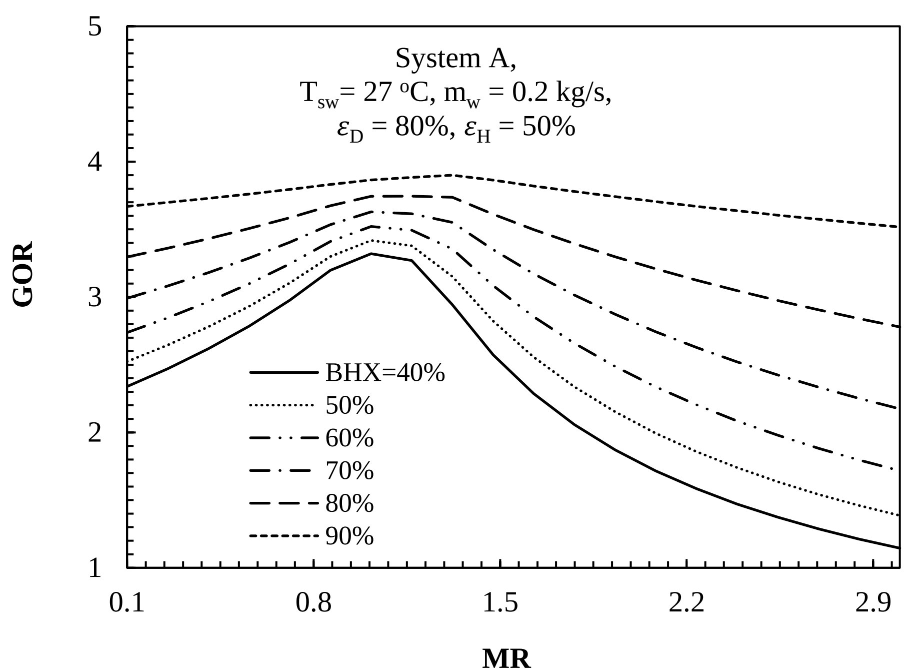

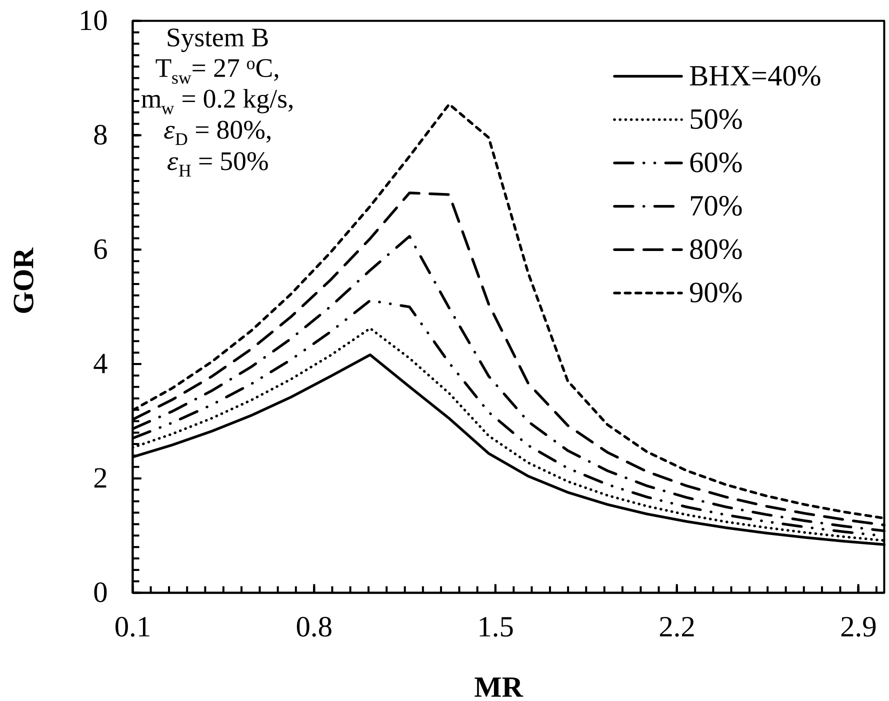

Figure 5. 12: Effect of Brine heat exchanger effectiveness on GOR

The cost of freshwater production for the proposed system is evaluated, and the obtained results for the cost analysis are graphically represented in Figures (5.13-5.15). The desalted water cost is based on the assumptions made from the cited references. The cost of freshwater production from the proposed desalination systems (A and B) is first compared with those from water heated and modified air heated desalination system presented by [106], at the same system operating conditions displayed in Figure 5.13 and at unit electricity cost of 0.045\$/kWh. The cost of desalinated water from the proposed system A, system, water heated plant and modified air heated unit was found to be 11.29\$/m^3, 8.16\$/m^3, 13.01\$/m^3 and 12.73\$/m^3, respectively. The cost of desalted water from the proposed system A is about 15.23% less than that of the water heated desalination plant, and 11.29% lower than that of modified air heated desalination unit. Similarly, the price of freshwater production from system B is about 59.44% and 56% less than that of water heated plant and modified air heated unit respectively. This low cost of freshwater production of system A and system B in comparison to the other presented systems is due to the thermal energy recovery from the rejected brine.

Table 5. 1: Capital investment cost for the main components of plants

Item Description	Prices (US $)	
	System A	System B
Packed Bed Humidifier	133	133
Dehumidifier	500	500
Water Tanks	200	200
Flowmeters	230	230
Pumps	150	150
Blowers/fans	100	100
Pipes, Fittings	35	35
Accessories	33	33
Semi Hermetic Compressor	1200	1200
Shell and Tube Condenser	600	600
Shell & Tube Evaporator	600	600
Expansion Valve	100	100
Brine heat exchanger	600	600

Figure 5.14 demonstrates the effect of variation in unit cost of electricity on the cost of desalted water. The cost of electricity consumed by a desalination plant greatly influence the price of freshwater production by the plant. The electricity cost is an important parameter to be considered when evaluating the cost of freshwater, because the unit cost

of electricity varies across different parts of the world or when the subsidy decreases/increases in other places. In this study, the cost of electricity is varied from 0.04$/kWh to 0.09$/kWh [139]. The upper limit (0.09$/kWh) is peculiar to most countries in Europe and the lower limit (0.04$/kWh) is associated with those countries in the Gulf States. For system A, the cost of desalinated water is found to be as high as 25$/m^3 when buying electricity at the rate of 0.09$/kWh, which represent about 152% increment in freshwater production cost (9.92 $/m^3) when buying energy at the rate of 0.04$/kWh. Similarly for system B, increasing the cost of electricity from0.04$/kWh to 0.09$/kWh increases the product cost from 7.17$/kWh to 18.02$/kWh, which represent about 151.3% increment in the product cost. Therefore, regions with low cost of electricity is expected to produce freshwater at low cost from the desalination plant, and vice versa for the regions with high cost of energy. The results also revealed that for the same cost of electricity, the price of freshwater for system A is about 38% higher than that of system B. The lower cost of freshwater from system B is majorly due to high system distillation rate.

Plant life is another factor that may affect the cost of desalted water from the desalination system. The impact of expected plant life on the cost of desalinated water is presented in Figure 5.15. The variation in plant life leads to variation in the freshwater production cost. It can be noticed from Figure 5.15 that higher expected plant life signifies lower cost of desalinated water. Increasing the expected plant life from 15 years to 30 years leads to about 21.7% reduction in the freshwater production cost (from 12.43$/m^3 to 10.21$/m^3) for system A, while that for system B varies from 8.98$/m^3 to 7.38$/m^3. The expected life span of the plants depend on good manufacturing quality, resistance of different components to corrosion and on the adopted maintenance program [118]. It is important to mention that both HDH systems and vapor compression heat pump are not demanding in terms of maintenance.

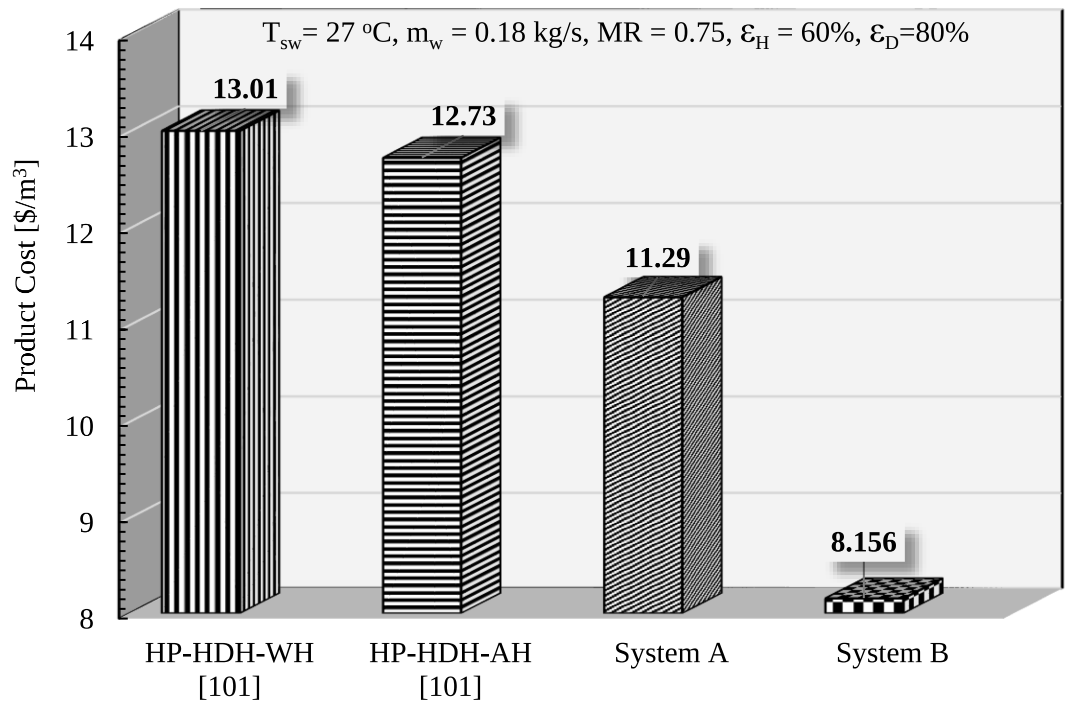

Figure 5. 13: Cost of desalinated water by various desalination plants

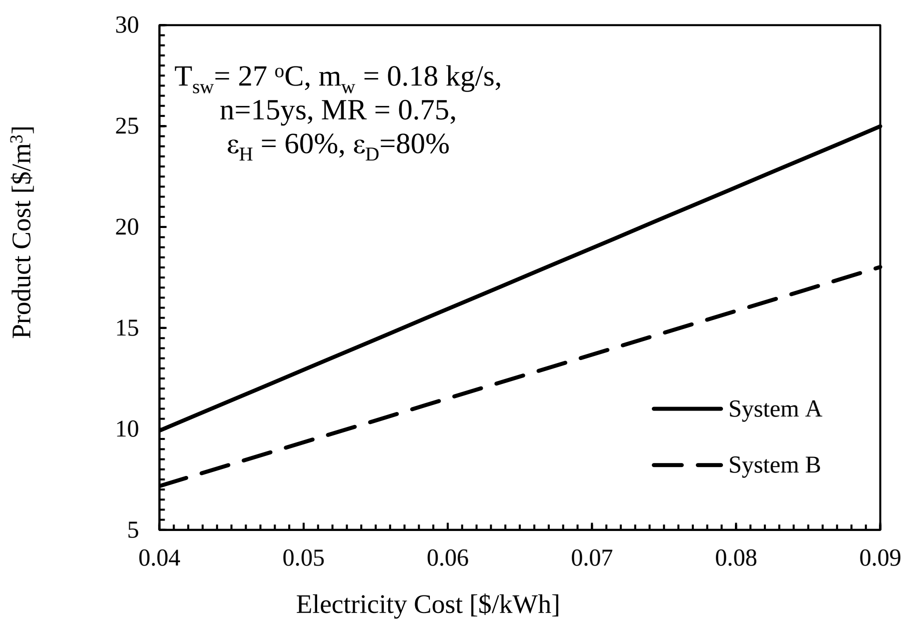

Figure 5. 14: Effect of energy cost on product cost

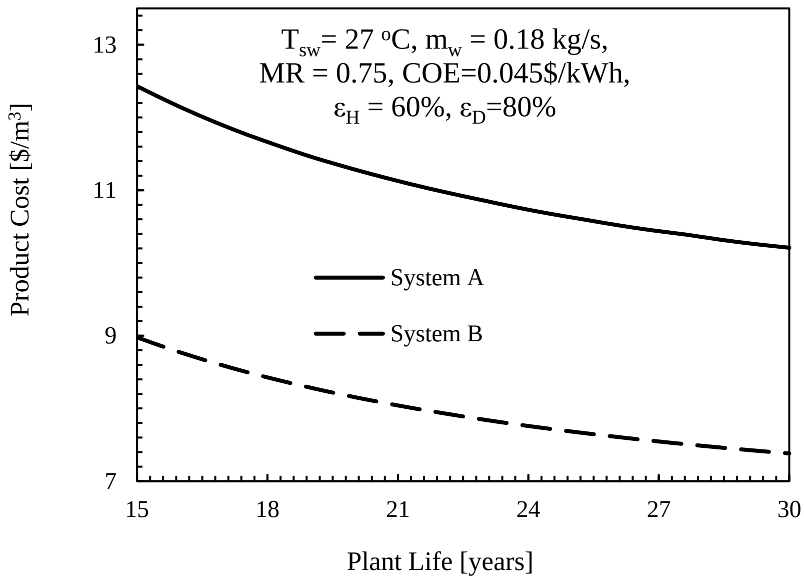

Figure 5. 15: Impact of plant life on product cost

CHAPTER 6

6.0 Heat Pump Driven Water heated HDH System with Different Layouts

The investigation of the performance of novel humidification dehumidification (HDH) desalination systems integrated with heat pump is presented in this chapter. Closed air open water (CAOW) water-heated HDH cycle is considered. The heat pump delivered the necessary heating and cooling loads to the HDH desalination unit. Three different layouts (system A, system B and system C) of water desalination units are proposed and evaluated theoretically at different system operating conditions, such as water temperature, water flowrate, mass flowrate ratio (MR), and humidifier effectiveness. The investigated performance metrics of the HDH desalination systems are the gained output ratio (GOR), freshwater production rate, specific electrical energy consumption (SEEC), recovery ratio (RR) and cost of freshwater production.

6.1 System Description

Three desalination systems (system A, system B and system C) are studied. Each of the system is integrated with a vapour compression refrigeration system (heat pump). Figures 6.1-6.3 shows the schematic line diagrams of the proposed desalination systems. System A is an Open Water Closed Air (OWCA) HDH cycle coupled with heat pump. The main components of system A are the humidifier, evaporator, condenser and compressor, while system B and system C are also OWCA cycle with the same components as system A, and in addition contained brine heat exchanger. The process of humidification and dehumidification takes place in the humidifier and heat pump evaporator. In system A, saline water at (state w,1) enters the condenser of the heat pump and get heated to a high temperature (state w,2). The heated saline water enters the humidifier and is sprayed over packing materials, where portion of the saline water evaporates and the rest is rejected as brine (state w,3). The dehumidified air at state (a,1) flows into the humidifier in a counter flow direction to the sprayed hot saline water. The air get heated and humidified as it come in contact with the vapor generated in the humidifier. The hot moist air exit humidifier (state a,2) and enters into the evaporator of heat pump, where the moisture contents contained in the air condenses to form freshwater by the cold refrigerant flowing through the tubes of the evaporator tubes. The dehumidified air leaves the evaporator at state (a,3) and flows into the humidifier for next cycle. In the case of system B, the thermal energy associated with the discharged brine is recovered to preheat the saline water from state (w,5) to state (w,1), whereas in system C, the recovered heat from the brine is utilized to preheat the dehumidified air from state (a,3) to state (a,1). The recovered thermal energy is expected to enhance the overall performance of the system because it will elevate the water and air temperature which increases moisture carrying capacity of the air.

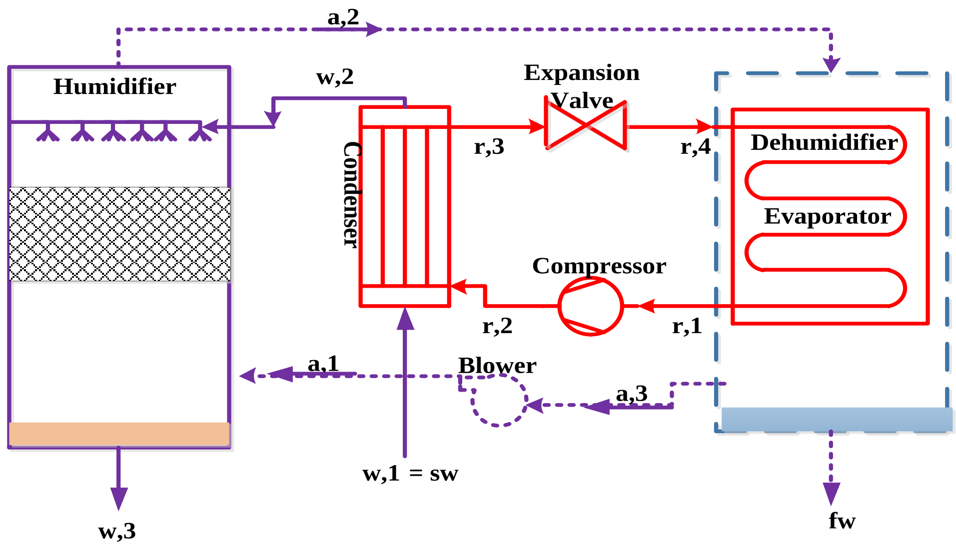

Figure 6. 1: Line diagram of system-A

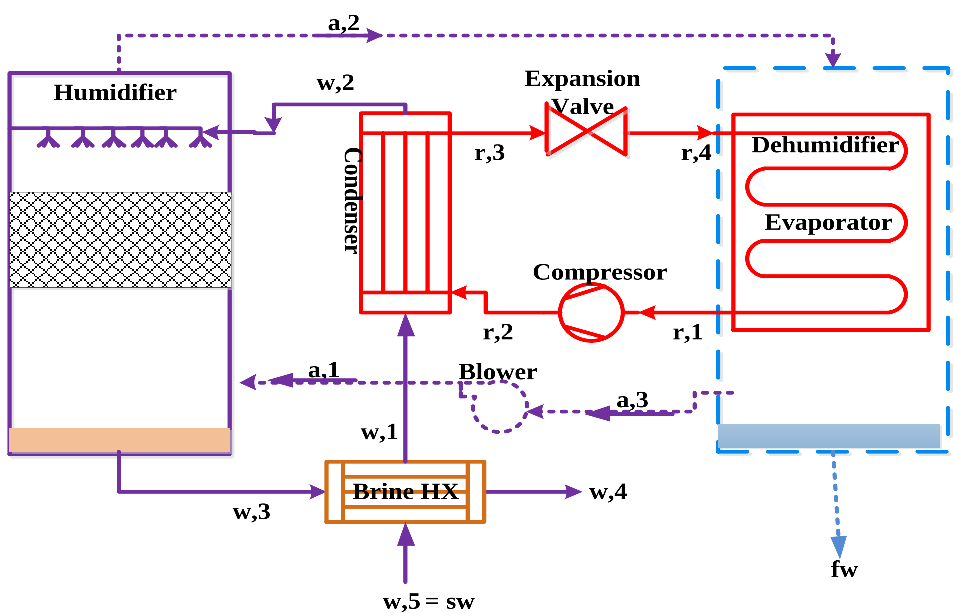

Figure 6. 2: Line diagram of system-B

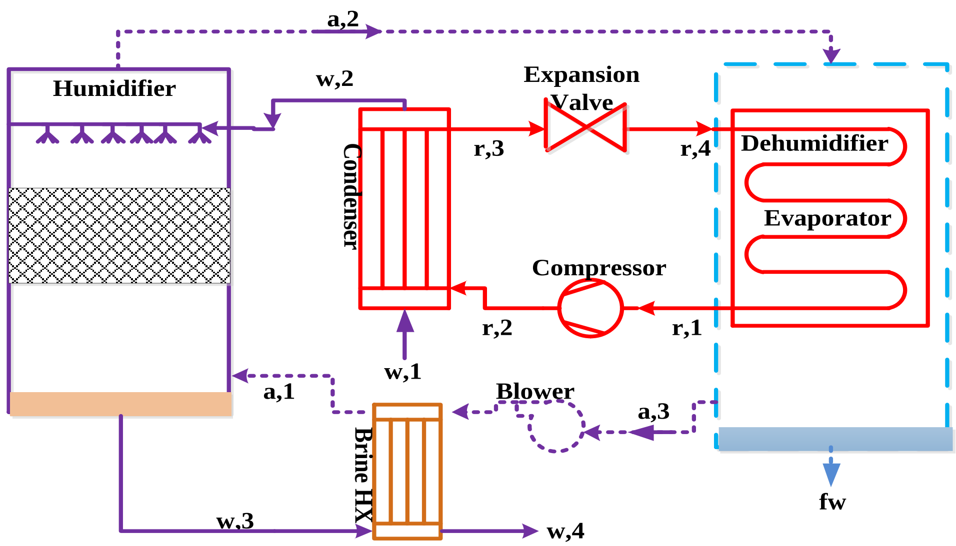

Figure 6. 3: Line diagram of system-C

6.2 Mathematical model

Heat and mass transfer analysis is performed to determine the performance of the proposed integrated desalination systems. The energy and mass balance model for each components of the system are presented and solved numerically to simulate the systems using an Engineering Equation Solver (EES) software: academic professional version 10.468. While modeling the systems, the following assumptions were made:

The system is operated at steady state. No heat losses to the surroundings. The potential and kinetic energy terms are negligible. The high and low pressure sides of the heat pump system are 200 and 35 psi, respectively. The refrigerant mass flow rate, the effectiveness of the humidifier and brine heat exchanger are taken to be 0.05kg/s, 70% and 80%, respectively. The adopted refrigerant is R-134a, and the isentropic efficiency of the compressor is considered to be 85%. The saline water inlet temperature is 30 °C having a salinity of 35 g/kg. The pump and fan powers are negligible compared to compressor input power.

The mass and energy balance for the main components in system A is presented as follows:

Humidifier

$$\dot{m}_a\left(h_{a,2} - h_{a,1}\right) = \dot{m}_w h_{w,2} - \dot{m}_b h_b \tag{1}$$

$$\dot{m}_{fw} = \dot{m}_w - \dot{m}_b$$

$$\dot{m}_a = \dot{m}_{a,1,2,3}\ ,\dot{m}_w = \dot{m}_{w,1,2,5}\ \&\ \dot{m}_b = \dot{m}_{w,3,4}$$

$$h_b = h_{w,3}$$

Evaporator:

$$\dot{m}_r h_{r,4} + \dot{m}_a h_{a,2} = \dot{m}_r h_{r,1} + \dot{m}_a h_{a,3} + \dot{m}_{fw} h_{fw} \tag{2}$$

Condenser:

$$\dot{Q}_{cond} = \dot{m}_r\left(h_{r,2} - h_{r,3}\right) = \dot{m}_w\left(h_{w,2} - h_{w,1}\right) \tag{3}$$

$$\dot{m}_r = \dot{m}_{r,1,2,..}$$

Compressor, and throttling valve:

$$\dot{W}_{comp} = \dot{m}_r\left(h_{r,2} - h_{r,1}\right) \tag{4}$$

$$h_{r,4} = h_{r,3} \tag{5}$$

Brine Heat Exchanger (System B):

$$\dot{m}_b\left(h_{w,3} - h_{w,4}\right) = \dot{m}_w\left(h_{w,1} - h_{w,5}\right) \quad (6)$$

Brine Heat Exchanger (System C):

$$\dot{m}_b h_{w,3} + \dot{m}_a h_{a,3} = \dot{m}_b h_{w,4} + \dot{m}_a h_{a,1} \quad (7)$$

Humidifier effectiveness:

$$\varepsilon_H = \max\left\{\frac{h_{a,out} - h_{a,in}}{h_{a,out,ideal} - h_{a,in}}, \frac{h_{w,in} - h_{w,out}}{h_{w,in} - h_{w,out,ideal}}\right\} \quad (8)$$

Brine Heat Exchanger effectiveness:

$$\varepsilon_{BHX} = \max\left\{\frac{T_{w,out} - T_{w,in}}{T_{b,in} - T_{w,in}}, \frac{T_{b,in} - T_{b,out}}{T_{b,in} - T_{w,in}}\right\} \quad (9)$$

The ideal air outlet enthalpy ($h_{a,out,ideal}$) is evaluated when the outlet air is fully saturated at the water inlet temperature, and the ideal water outlet enthalpy ($h_{w,out,ideal}$) is estimated when its temperature is equal to the temperature of the inlet air dry-bulb.

The following expression are used to evaluate the system performance parameters:

The Gained Output Ratio (GOR):

Is the product of produced freshwater and latent heat of vaporization divided by the energy input [106–109,111]:

$$GOR = \frac{\dot{m}_{fw} h_{fg}}{\dot{W}_{Comp}} \quad (10)$$

The Recovery Ratio (RR):

Is the ratio of produced freshwater to feed saline water flowrates [106–109,111]:

$$RR = \frac{\dot{m}_{fw}}{\dot{m}_{w}} \tag{11}$$

The Specific Electrical Energy Consumption (SEEC):

Is ratio of electrical energy consumed to produce one kilogram per meter cube of freshwater [106,107]:

$$SEEC = \frac{\dot{W}_{Comp} + \dot{W}_{Pump} + \dot{W}_{Fan}}{\dot{V}_{fw}} \tag{12}$$

Where

$\dot{V}_{fw}$ $(m^3/hour)$ is the volumetric flowrate of the condensate.

The expressions for evaluating the unit product cost are presented as follows. The product cost estimation is performed using the cost analysis presented by El-Dessouky and Ettouney [139]. The cost of freshwater is evaluated based on the cost of energy, capital cost, management cost, labor cost and maintenance cost, with the following assumptions:

Pretreatment cost is negligible; the cost of electricity is 0.045$/kWh. The plant life expectancy and availability is 20 years and 90%, respectively. The interest rate (i) is 5%. The blower and pump power is 50 and 750 Watts, respectively. The operating labor specific cost, annual maintenance cost, and annual management cost is 0.1 $/m^3, 1.5% of the capital cost, and 20% of the labor cost, respectively. The summary of fixed cost of the main components of system A, system B and system C are tabulated in Table 6.1.

To evaluate the capital cost, capital recovery factor (amortization factor) is required, which can be calculated as: Amortization factor (α):

$$\alpha = \frac{i(i+1)^n}{(i+1)^n - 1} \tag{13}$$

Annual capital cost:

$$\dot{Z}_f(\$/yr) = Z(\$) \times \alpha\ (1/yr) \tag{14}$$

Annual electric power cost ($\dot{C}_{Elect}$):

$$\dot{C}_{Elect}(\$/yr) = COE\ (\$/kWh) \times \frac{SEEC}{3600}(kWh/m^3)\ \times Å \times \dot{V}_{fw}\ (m^3/day) \times 365 \tag{15}$$

The annual labor cost ($\dot{C}_L$):

$$\dot{C}_L(\$/yr) = \mathcal{L}(\$/m^3) \times Å\ \times \dot{V}_{fw}\ (m^3/day) \times 365 \tag{16}$$

The total annual cost ($\dot{C}_T$):

$$\dot{C}_T(\$/yr) = \dot{Z}_f(\$/yr) + \dot{C}_{Elect}\ (\$/yr) + \dot{C}_L(\$/yr) +\ \dot{C}_{mt}(\$/yr)\ + \dot{C}_{mg}(\$/yr) \tag{17}$$

Where $\dot{C}_{mt}$and $\dot{C}_{mt}$ is the annual maintenance and management costs, respectively.

Therefore, unit product cost (C_P):

$$C_P(\$/m^3) = \left(\frac{\dot{C}_T(\$/yr)}{Å\ \times V_{fw}\ (m^3/day) \times 365\ (day/yr)}\right) \tag{18}$$

6.3 Results and Discussion

The performance evaluation of the proposed desalination systems is presented in this section. The impact of saline water temperature, saline water flowrate, mass flowrate ratio of saline water to air (MR) and humidifier effectiveness on system performance including fresh water yield, gained output ratio (GOR), recovery ratio (RR), specific electrical energy consumption (SEEC) and the product cost are presented and discussed. The obtained results are graphically represented in Figures (6.4-6.16).

Figure 6.4(a-d) demonstrates the variation of gained output ratio against the mass flowrate ratio of saline water to air and humidifier effectiveness. It is obvious from Figure 6.4(a-c) that component effectiveness highly influence the GOR of the system with higher humidifier effectiveness yielding higher GOR, especially at higher MR. The reason for increase in GOR with increase in humidifier effectiveness may be attributed to the increase in air temperature exiting the humidifier which improves the moisture carrying capacity of air as a result of better functionality of the humidifier. The increment in air moisture content resulted in higher heat and mass transfer to the evaporator surface, leading to higher condensation rate, and consequently higher GOR. It can also be noticed that increasing MR increases the GOR of the systems to the peak values and then decreases with further increase in MR. The maximum GOR of the system indicates the optimum mass flow rate ratio. The optimum MR is a ratio that provides the right amount of feed water and air to be supplied to the humidifier at the given operating conditions. It can also be observed that optimum MR varies with humidifier effectiveness, with higher effectiveness leading to a higher optimum MR. This signify that more water is sprayed and more vapor is generated, and the degree of air saturation increases. Increasing the humidifier effectiveness from 40% to 100% shifted the peaks of the GOR from 3.1 to 3.66, 3.56 to 3.87 and 3.58 to 3.66 for systems A, B and C respectively. These values correspond to about 19%, 9% and 2% increment in the maximum GOR of systems A, B, and C respectively. Increasing the MR from 0.1 to 1.3 leads to about 19% rise in the GOR for system A at 40% effectiveness. For the same system and at the humidifier effectiveness of 100%, there was an increment of about 6% in GOR when MR increases from 0.1 to 2.

Figure 6.4(d) shows a clear comparison between the three proposed desalination systems. System B shows a superior performance as compared to the other two desalination systems, while the performance of system C is better than that of system A (No heat recovery). The superior performance of system B is obviously due to the energy recovery from the discharged brine, which leads to higher top system temperature that increases the vapor generation air temperature within the humidifier, thereby increasing moisture content in the air. For system C, only air temperature is increase from the recovered heat, thus its inferior performance to system B. It can also be noticed that the performance of system C is the same as that of system A at 100% humidifier effectiveness (at high effectiveness). At high humidifier effectiveness, the thermal energy accompanying the brine is very low due to better functionality of the humidifier. This shows that energy recovered from the brine does not provide any benefit. Therefore, it is advisable to avoid heat recovery at high component effectiveness to decrease component (brine heat exchanger) capital cost and cost of freshwater production. However, system C outperformed system A significantly at lower humidifier effectiveness. This findings portrayed the benefit of heat recovery from the discharged brine, which is accompanied by high thermal energy, as a results of poor component effectiveness.

Figure 6.5(a-d) depicted the effect of MR and humidifier effectiveness on the system productivity. The Figures portrays similar observation as that of GOR presented in Figure 6.4(a-d). This is expected because the variation in the system GOR is majorly contributed by the variation in freshwater production. Therefore, the explanations given in Figure 6.4(a-d) are equally applicable to Figure 6.5(a-d). The maximum system productivity increases from 6.46 to 7.83kg/h, 7.59 to 8.40kg/h and 7.64 to 7.83kg/h when component effectiveness increases from 40% to 100% for systems A, B, and C respectively.

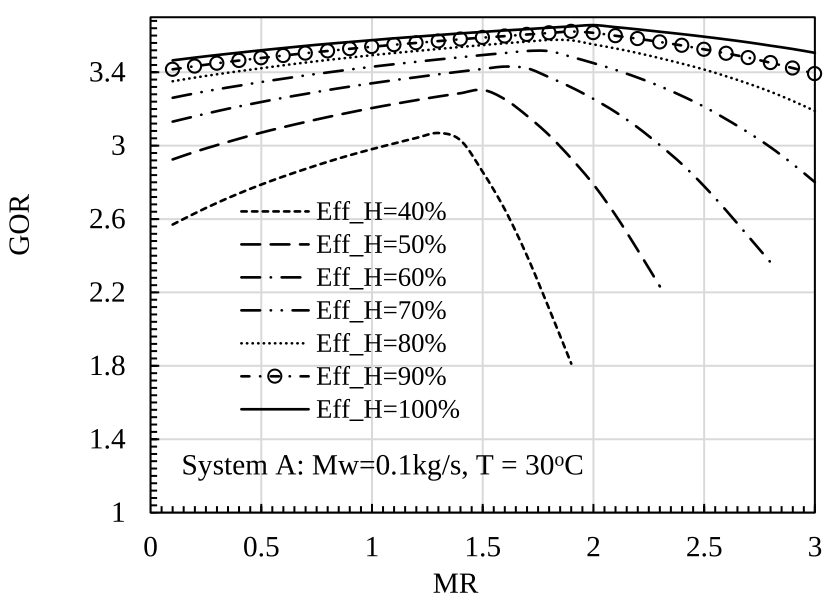

(a)

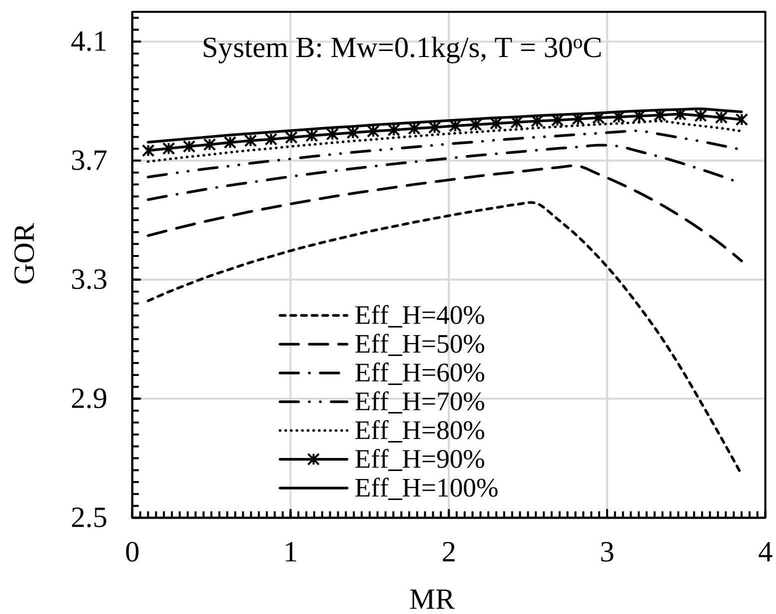
System B: Mw=0.1kg/s, T = 30°C
4.1
3.7
3.3
2.9
2.5
GOR
0
1
2
3
4
MR
Eff_H=40%
Eff_H=50%
Eff_H=60%
Eff_H=70%
Eff_H=80%
Eff_H=90%
Eff_H=100%

(b)

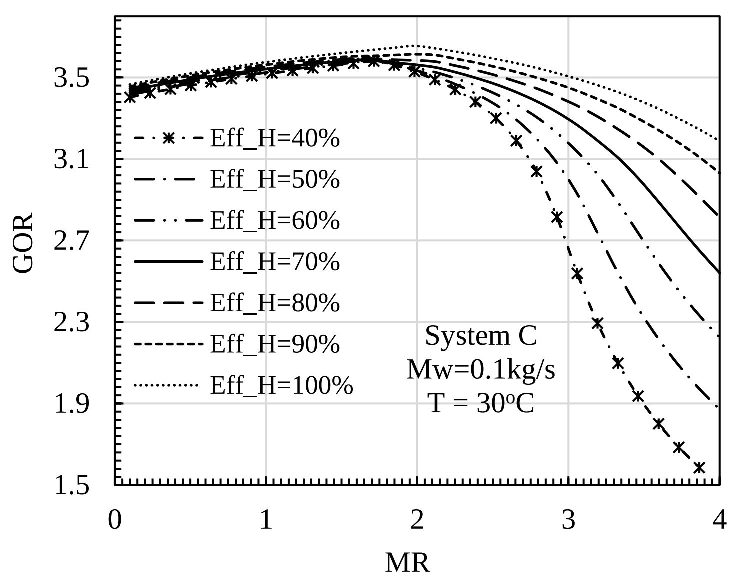
3.5
3.1
2.7
2.3
1.9
1.5
GOR
0
1
2
3
4
MR
Eff_H=40%
Eff_H=50%
Eff_H=60%
Eff_H=70%
Eff_H=80%
Eff_H=90%
Eff_H=100%
System C
Mw=0.1kg/s
T = 30°C

(c)

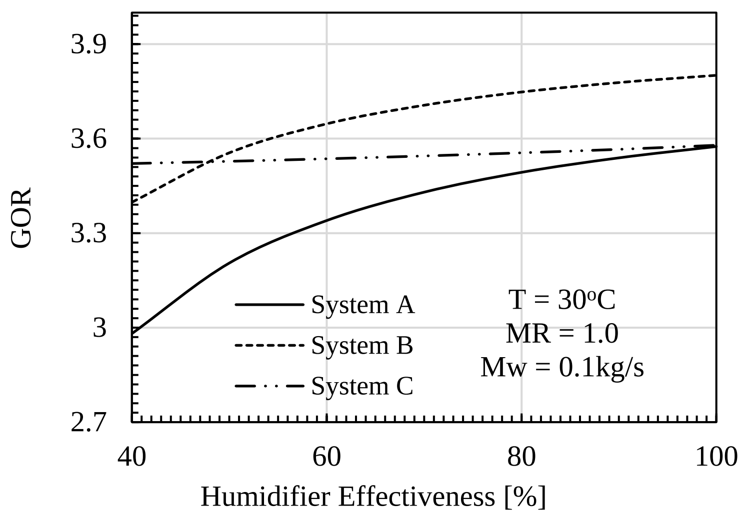

(d)

Figure 6. 4: Effect of ε_{hum} on the GOR of the (a) system A, (b) system B, (c) system C & (d) Combined

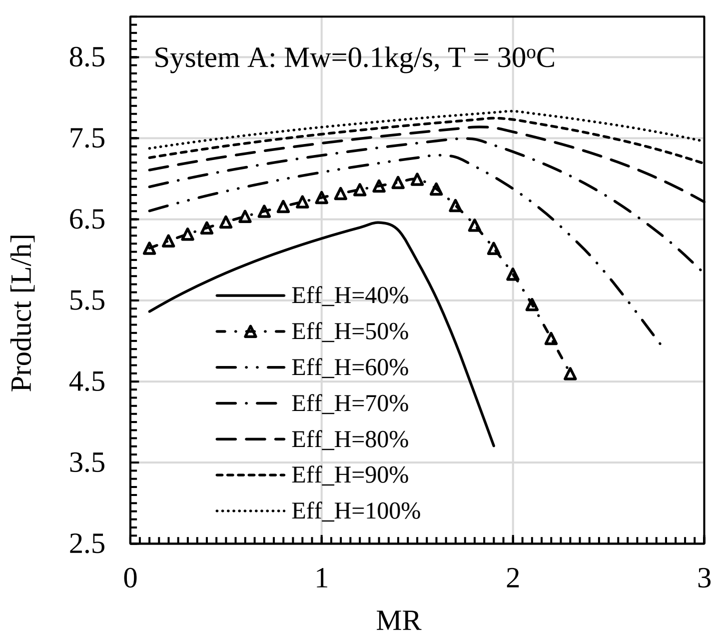

(a)

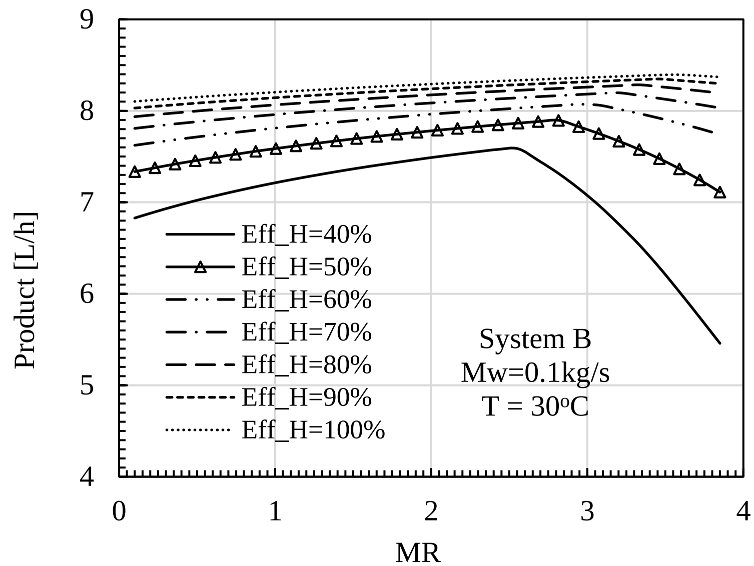
Product [L/h]
MR
Eff_H=40%
Eff_H=50%
Eff_H=60%
Eff_H=70%
Eff_H=80%
Eff_H=90%
Eff_H=100%
System B
Mw=0.1kg/s
T = 30oC

(b)

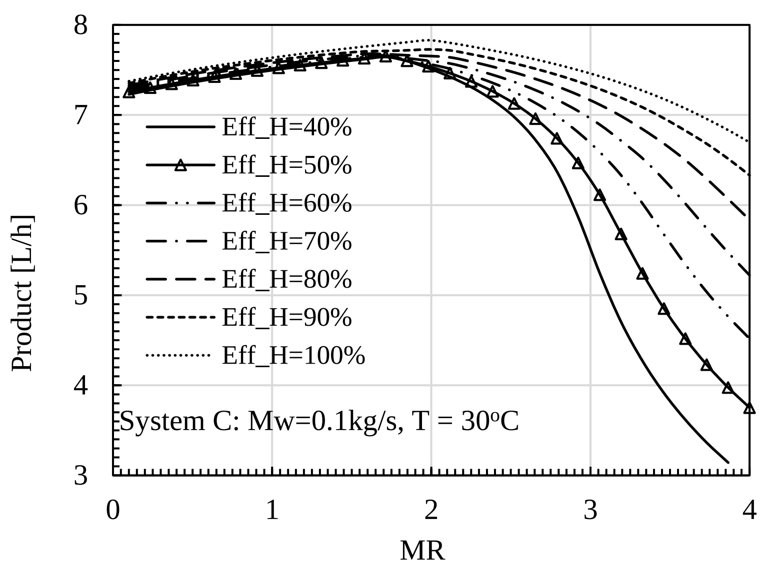
Product [L/h]
MR
Eff_H=40%
Eff_H=50%
Eff_H=60%
Eff_H=70%
Eff_H=80%
Eff_H=90%
Eff_H=100%
System C: Mw=0.1kg/s, T = 30oC

(c)

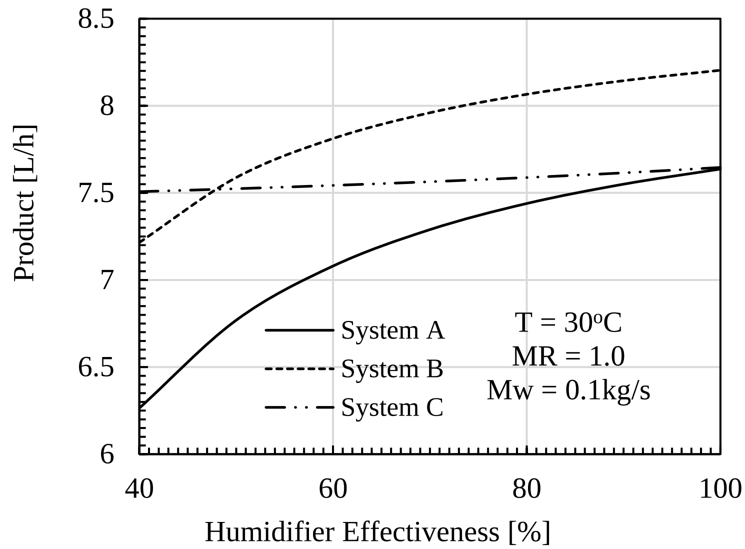

(d)

Figure 6. 5: Effect of ε_{hum} on the productivity of the (a) system A, (b) system B, (c) system C & (d) Combined

The variation of recovery ratio with MR and humidifier effectiveness is presented in Figure 6.6(a-d). The Figures reveals that increasing the humidifier effectiveness lead to increase in RR, which is an indication that more freshwater is produced per unit flowrate of the saline water. This means that the function of the plant is better at higher component effectiveness, which is attributed to more vapor formation. It is worth noting that higher humidifier effectiveness requires bigger surface areas, which may increase the initial capital investment of the component. The Figures also shows optimum MR that changes with component effectiveness, with higher optimum MR occurring at higher humidifier effectiveness. Raising the humidifier effectiveness from 40% to 100% shifted the peak recovery ratio from 1.8% to 2.2%, 2.1% to 2.33%, and 2.12% to 2.18% for systems A, B and C respectively.

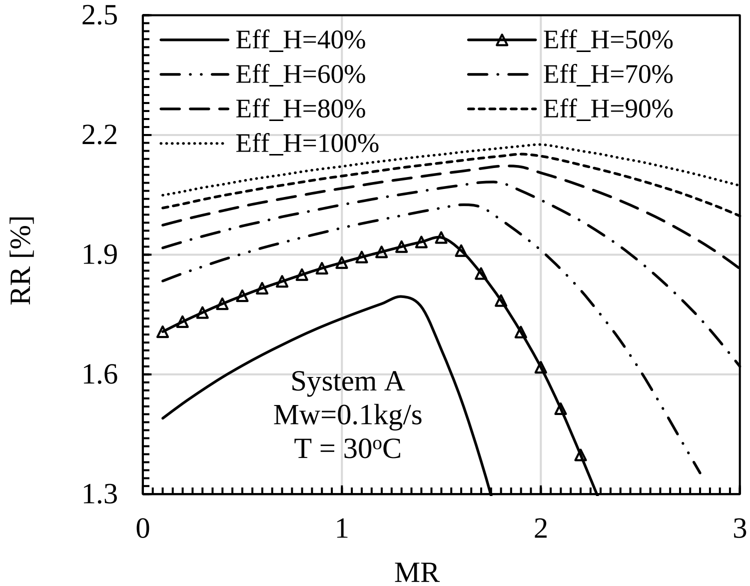

2.5
2.2
1.9
1.6
1.3
0
1
2
3
RR [%]
MR
Eff_H=40%
Eff_H=50%
Eff_H=60%
Eff_H=70%
Eff_H=80%
Eff_H=90%
Eff_H=100%
System A
Mw=0.1kg/s
T = 30°C

(a)

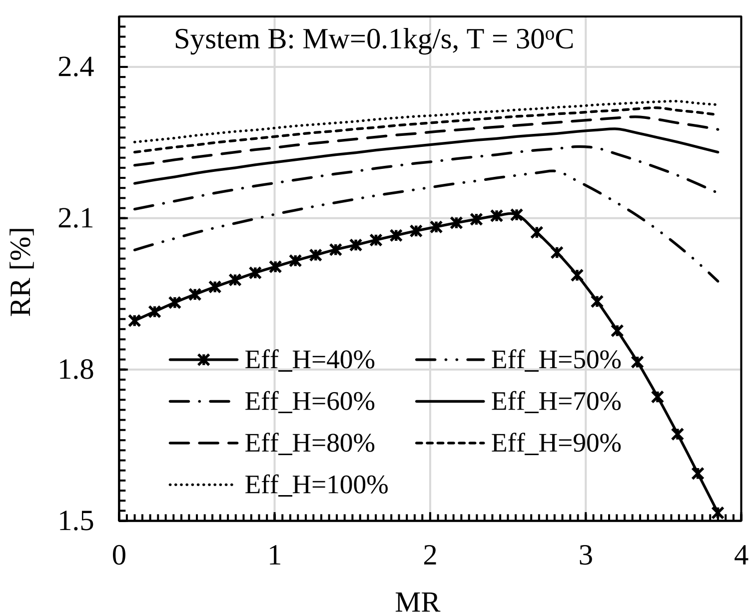

System B: Mw=0.1kg/s, T = 30°C
2.4
2.1
1.8
1.5
0
1
2
3
4
RR [%]
MR
Eff_H=40%
Eff_H=50%
Eff_H=60%
Eff_H=70%
Eff_H=80%
Eff_H=90%
Eff_H=100%

(b)

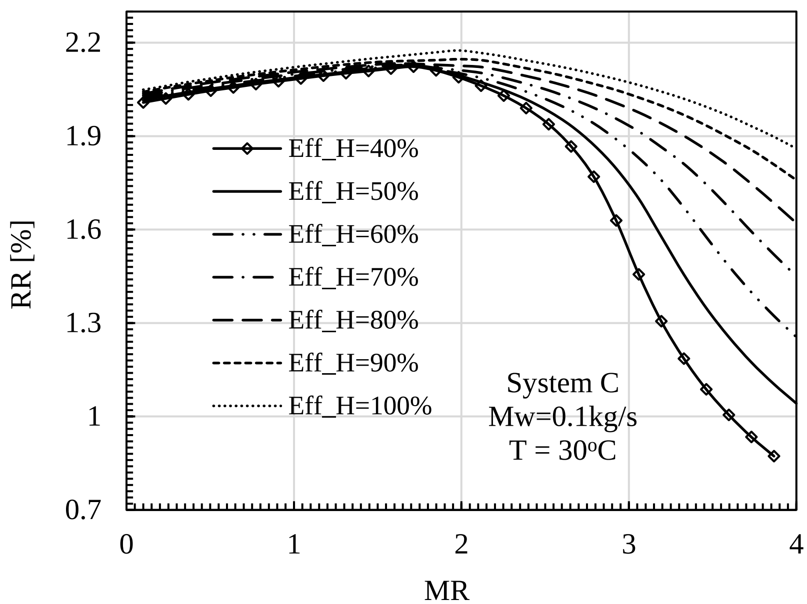

(c)

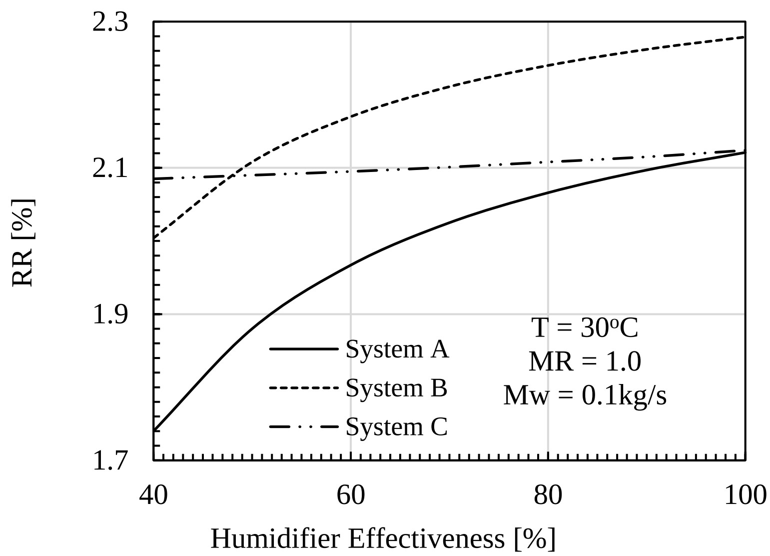

(d)

Figure 6. 6: Influence of ε_{hum} on the RR of the (a) system A, (b) system B, (c) system C & (d) Combined

Displayed in Figure 6.7(a-d) is the influence of MR and humidifier effectiveness on the specific electrical energy consumption of the system. By increasing the humidifier effectiveness from 40% to 100% the minimum value of specific electrical energy consumption drops to about 21%, 10% and 3% for system A, system B and system C respectively. Increasing the humidifier effectiveness decreases and shifted the minimum specific electrical energy consumption to higher system mass flowrate ratio of saline water to air. This shows that at low humidifier effectiveness, low optimum MR is required, since lower heating effects is demanded at low MR. In other words, higher humidifier effectiveness demands higher optimum MR to attain minimum SEEC. It is also obvious from Figure 6.7(d) that system B appeared to consume lesser electrical energy as compared to other systems (A and C), due to it higher freshwater productivity.

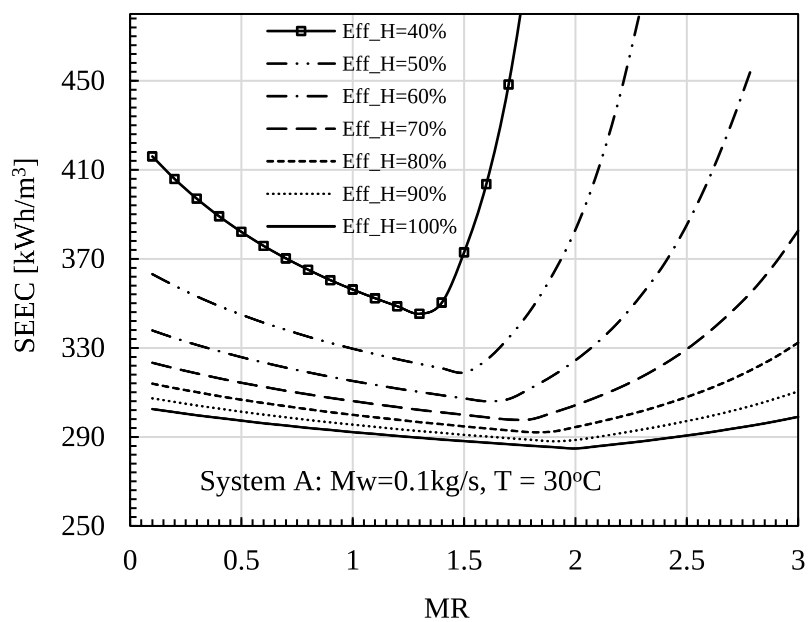

(a)

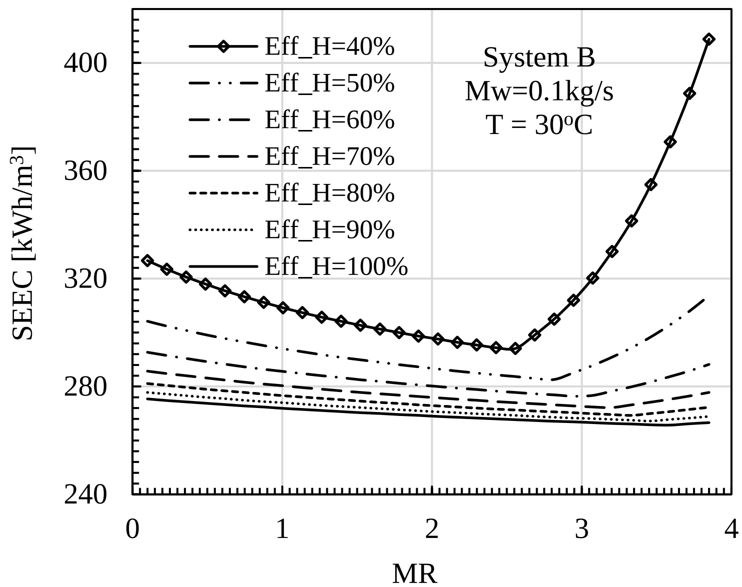

Eff_H=40%
Eff_H=50%
Eff_H=60%
Eff_H=70%
Eff_H=80%
Eff_H=90%
Eff_H=100%
System B
Mw=0.1kg/s
T = 30ºC
SEEC [kWh/m3]
400
360
320
280
240
0
1
2
3
4
MR

(b)

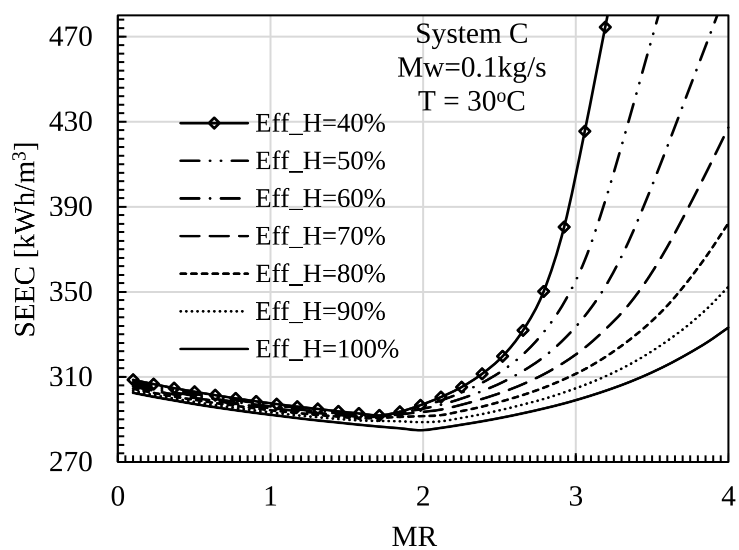

System C
Mw=0.1kg/s
T = 30ºC
Eff_H=40%
Eff_H=50%
Eff_H=60%
Eff_H=70%
Eff_H=80%
Eff_H=90%
Eff_H=100%
SEEC [kWh/m3]
470
430
390
350
310
270
0
1
2
3
4
MR

(c)

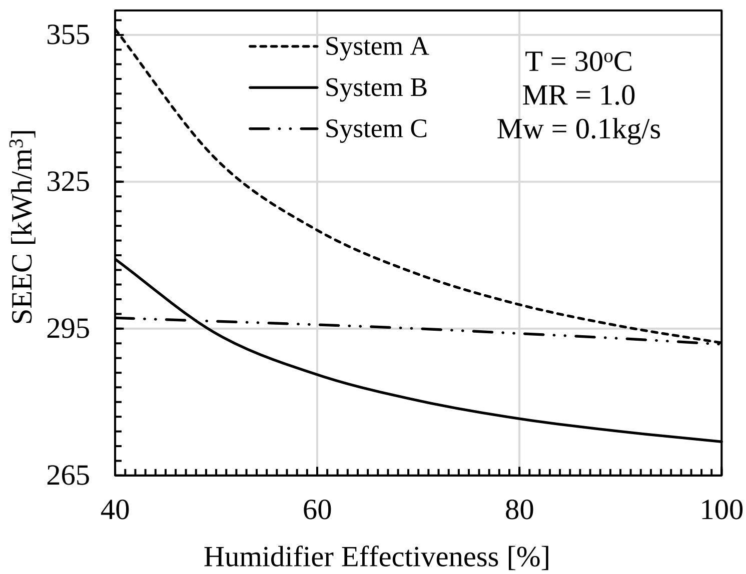

(d)

Figure 6. 7: Impact of ε_{hum} on the SEEC of the (a) system A, (b) system B, (c) system C & (d) Combined

Figure 6.8(a-d) demonstrates the variation of gained output ratio with mass flowrate ratio of saline water to air (MR) at different saline water flowrates. For different water flowrates, air flowrate is varied. This means that any variation in MR is caused by variation in air flowrate. The effect of this variation has been explained earlier in Figure 6.4(a-d). For the influence of saline water flowrate on the GOR, it can be noticed that low saline water flowrate yielded higher gained output ratio, as a results of higher rate of distillate production. The reason for the high distillation rate is explained in the next Figure 6.9(a-d). Declining the seawater flowrate increases and shifted the peak GOR to higher MR. Varying seawater flowrate from 0.075kg/s to 0.4kg/s decreases the maximum GOR from 3.59 to 3.38, 3.90 to 3.48, and 3.65 to 3.41 for systems A, B, and C respectively. These values corresponds to about 6%, 12%, and 7% percentage increment for systems A, B, and C respectively.

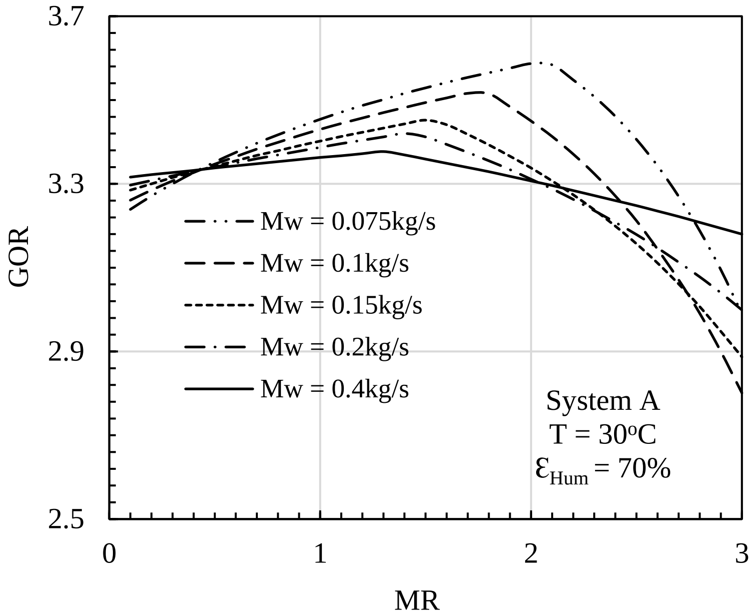
3.7
3.3
2.9
2.5
0
1
2
3
GOR
MR
Mw = 0.075kg/s
Mw = 0.1kg/s
Mw = 0.15kg/s
Mw = 0.2kg/s
Mw = 0.4kg/s
System A
T = 30°C
ε_Hum = 70%

(a)

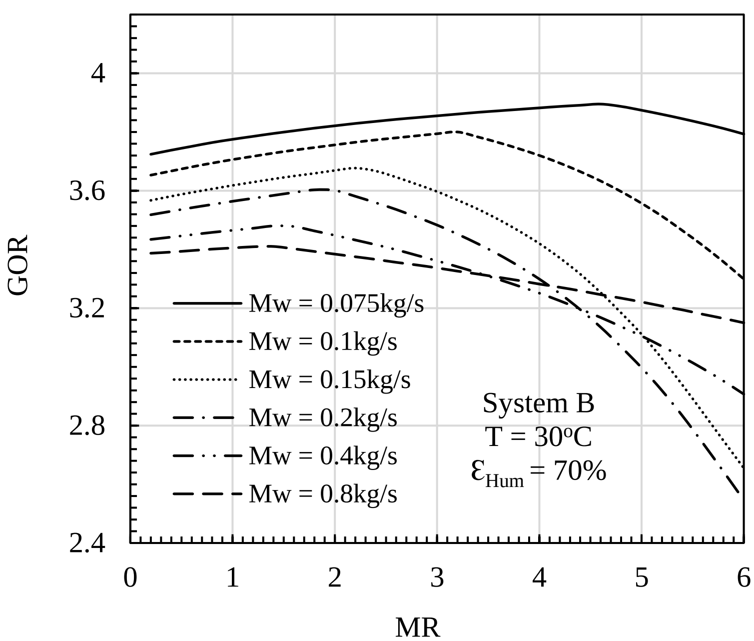
4
3.6
3.2
2.8
2.4
0
1
2
3
4
5
6
GOR
MR
Mw = 0.075kg/s
Mw = 0.1kg/s
Mw = 0.15kg/s
Mw = 0.2kg/s
Mw = 0.4kg/s
Mw = 0.8kg/s
System B
T = 30°C
ε_Hum = 70%

(b)

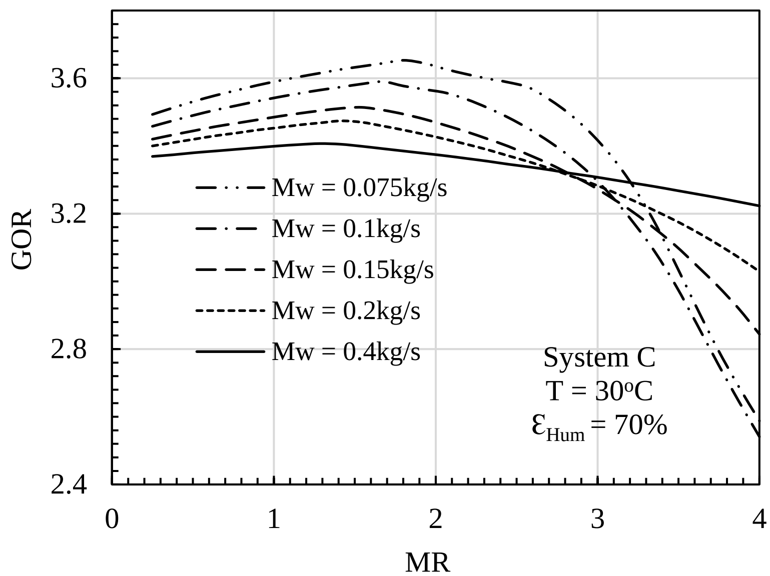

(c)

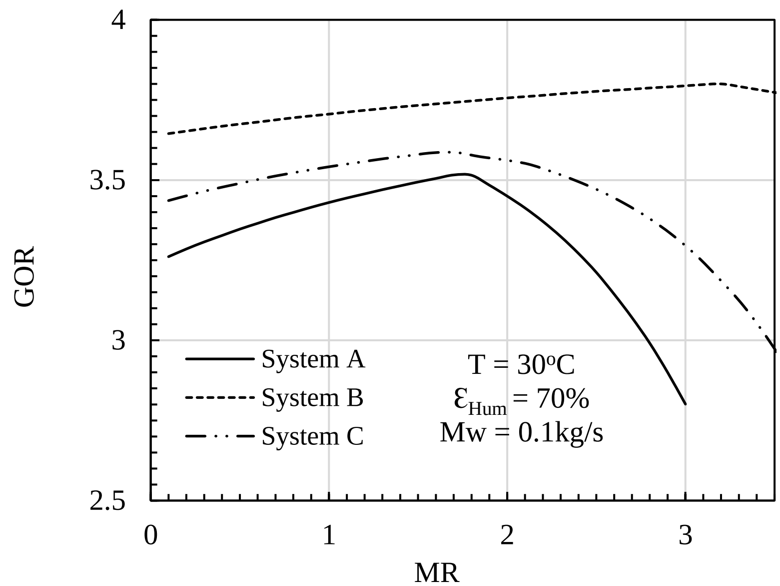

(d)

Figure 6. 8: Effect of MR on the GOR of the (a) system A, (b) system B, (c) system C & (d) Combined

Figure 6.9(a-d) presents the influence of MR (saline water flowrate to air flowrate) at different saline water flowrate on the system productivity. Increasing the saline water flowrate (0.4kg/s to 0.075kg/s) deteriorate the system productivity (percentage reduction of 6.9%, 14.1% and 8.1% for systems A, B, and C respectively). Reducing the saline water flowrate is observed to enhance and moved the peak system productivity to a higher MR. The improvement in the rate of distillate production at low saline water flowrate may be attributed to the fact that saline water at low flowrate experiences maximum heat transfer from the refrigerant in the condenser of the heat pump, thereby elevating the saline water temperature to a higher degree, and consequently enhances vapor generation as well as air temperature exiting the humidifier, which improves the distillate production.

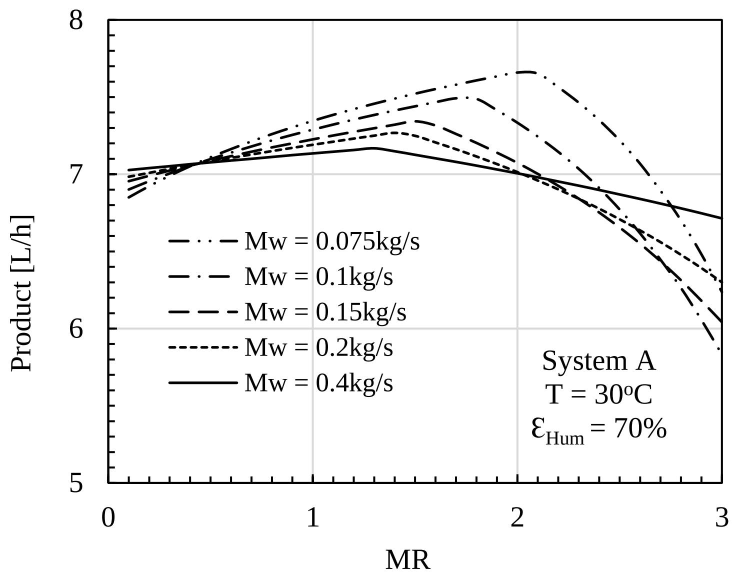

(a)

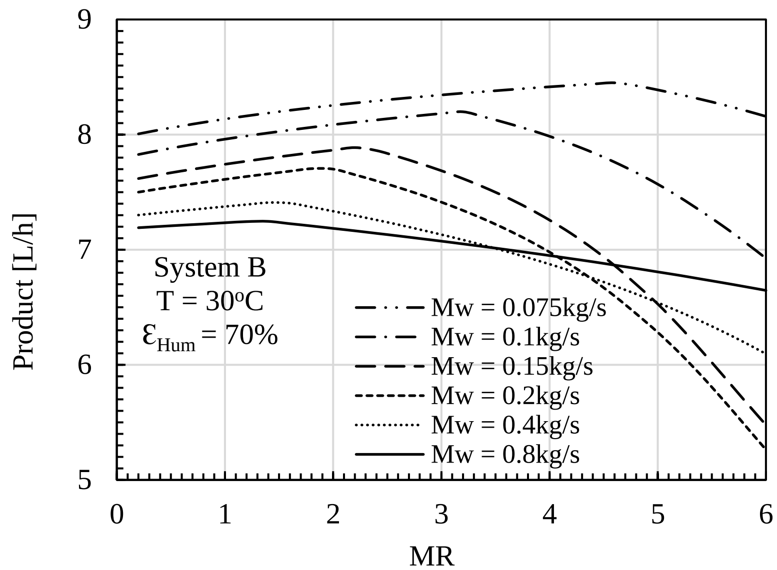
9
8
7
6
5
0
1
2
3
4
5
6
Product [L/h]
MR
System B
T = 30°C
ε_{Hum} = 70%
Mw = 0.075kg/s
Mw = 0.1kg/s
Mw = 0.15kg/s
Mw = 0.2kg/s
Mw = 0.4kg/s
Mw = 0.8kg/s

(b)

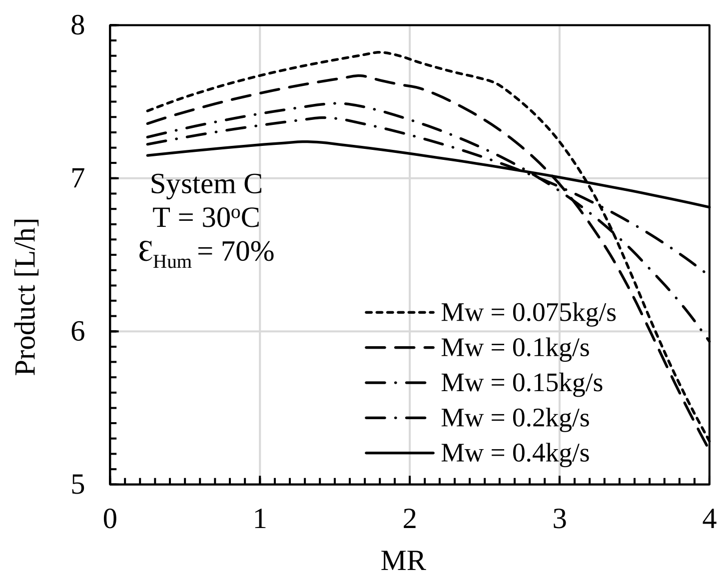
8
7
6
5
0
1
2
3
4
Product [L/h]
MR
System C
T = 30°C
ε_{Hum} = 70%
Mw = 0.075kg/s
Mw = 0.1kg/s
Mw = 0.15kg/s
Mw = 0.2kg/s
Mw = 0.4kg/s

(c)

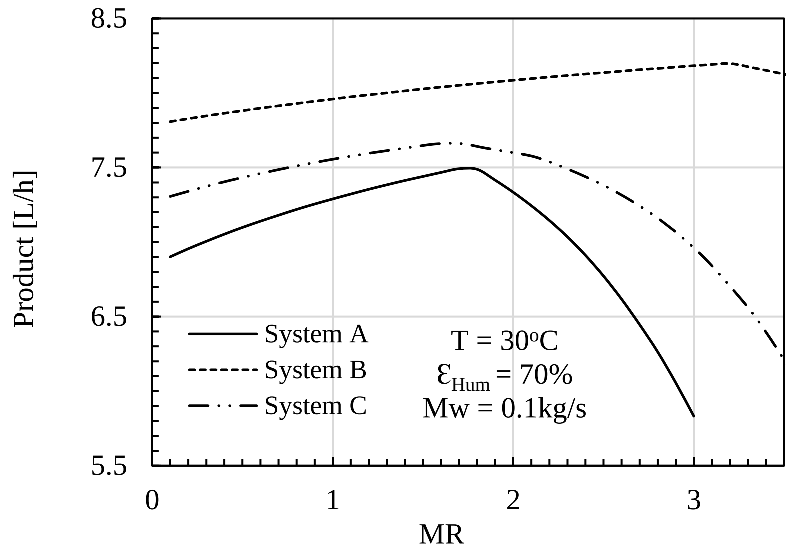

(d)

Figure 6. 9: Effect of MR on the productivity of the (a) system A, (b) system B, (c) system C & (d) Combined

The variations of recovery ratio with MR and seawater flowrate is demonstrated in Figure 6.10(a-d). Seawater flowrate is noticed to highly influence the recovery ratio of the system as we recorded about 470%, 500% and 480% percentage improvement on the recovery ratio of systems A, B, and C, respectively when the feed water flowrate decreases from 0.4 to 0.075kg/s. Similar to other previous observations, the maximum RR for each feed flowrate moves to a higher MR when the seawater flowrate decreases. The reduction in peak RR when the saline water flowrate increases is as a results of poor rate of freshwater production per feed water supplied at higher seawater flowrate, which is a direct effect of poor vapor generation due to low top system temperature.

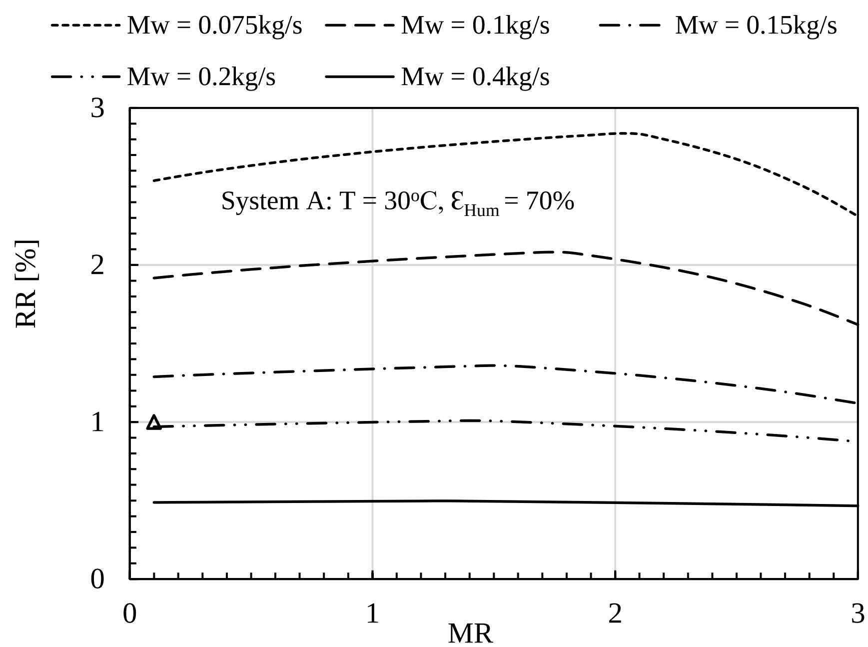

Mw = 0.075kg/s
Mw = 0.1kg/s
Mw = 0.15kg/s
Mw = 0.2kg/s
Mw = 0.4kg/s
System A: T = 30oC, ƐHum = 70%
RR [%]
MR
0
1
2
3

(a)

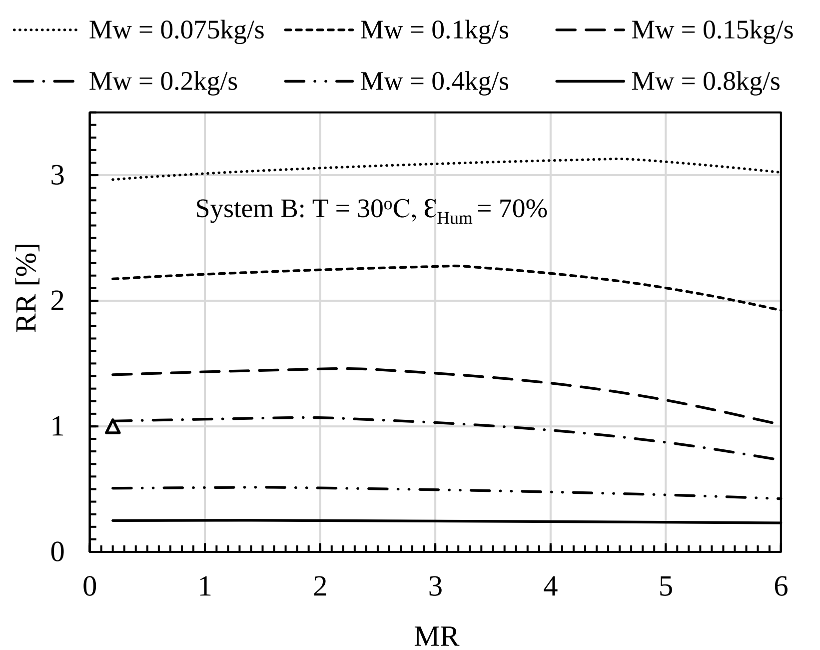

Mw = 0.075kg/s
Mw = 0.1kg/s
Mw = 0.15kg/s
Mw = 0.2kg/s
Mw = 0.4kg/s
Mw = 0.8kg/s
System B: T = 30oC, ƐHum = 70%
RR [%]
MR
0
1
2
3
4
5
6

(b)

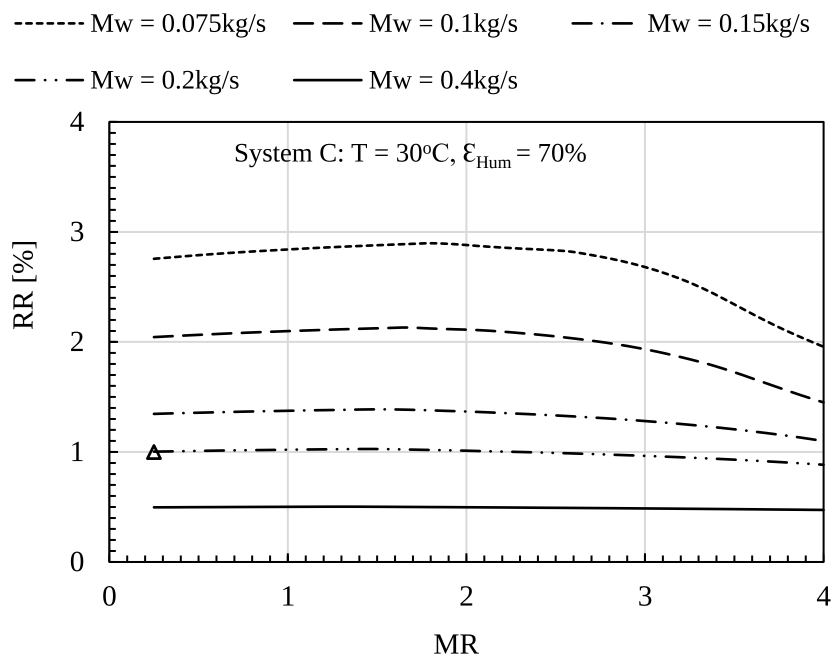

(c)

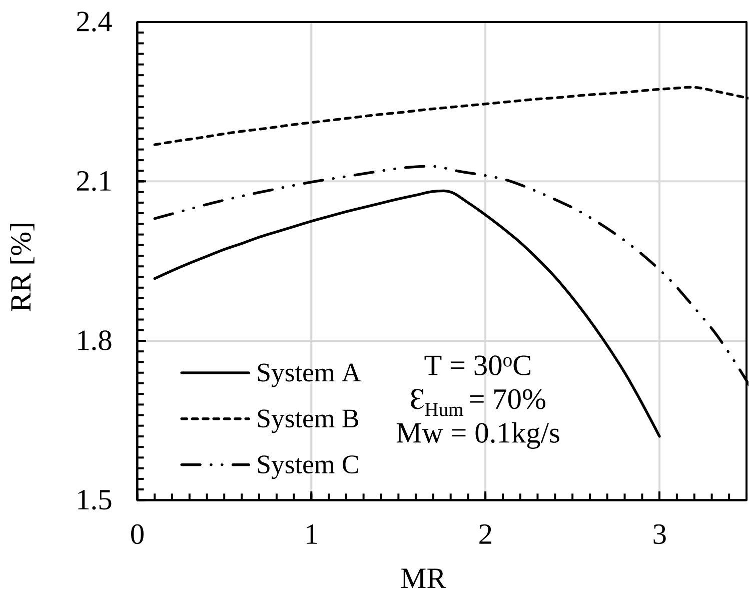

(d)

Figure 6. 10: Influence of MR on the RR of the (a) system A, (b) system B, (c) system C & (d) Combined

Figure 6.11(a-d) illustrates the effect of MR and seawater flowrate on the system specific electrical energy consumption. Increasing the saline water flowrate increases the SEEC of the system. Increasing the saline water flowrate also shifted the least SEEC to the left (low MR). Varying the seawater flowrate from 0.075 to 0.4kg/s of systems A, B, and C, increases the least SEEC from 291.3 kWh/m^3 to 311.3 kWh/m^3, 264 kWh/m^3 to 301.1 kWh/m^3 and 285.2 kWh/m^3 to 308.2kWh/m^3 respectively. The reduction in SEEC of the system with increasing seawater flowrate can be attributed to the low heat transfer (exchange) from refrigerant to the seawater at high seawater flowrate. This give rise to low saline water temperature to be sprayed in the humidifier, which leads to low air temperature and specific humidity (heat and mass transfer) exiting the humidifier that yielded low productivity, which resulted in high SEEC of the system.

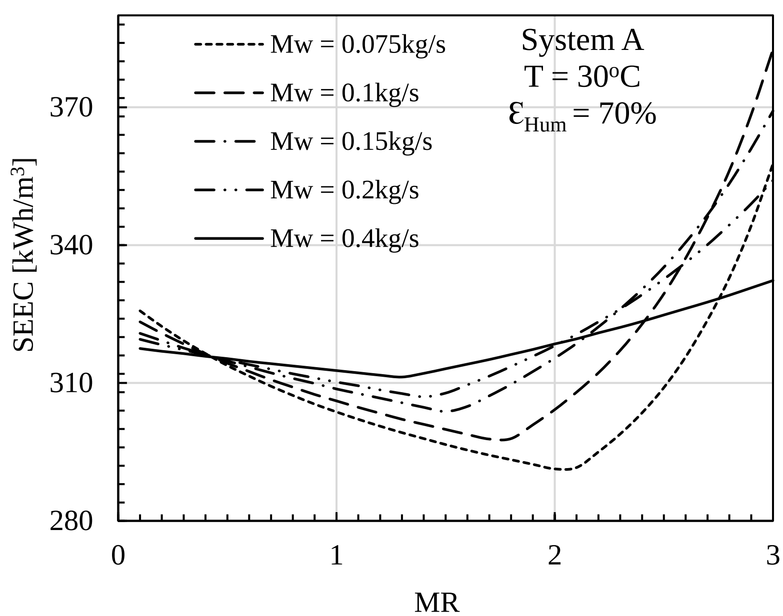

(a)

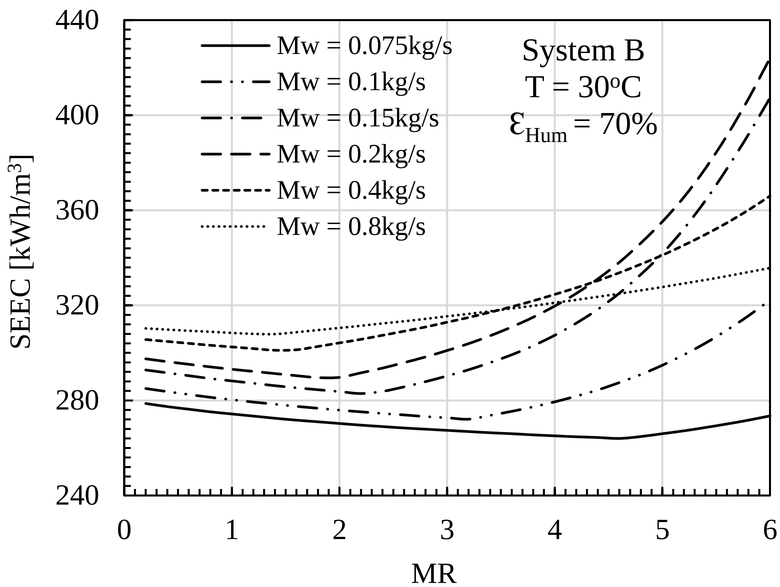
440
400
360
320
280
240
SEEC [kWh/m3]
0
1
2
3
4
5
6
MR
Mw = 0.075kg/s
Mw = 0.1kg/s
Mw = 0.15kg/s
Mw = 0.2kg/s
Mw = 0.4kg/s
Mw = 0.8kg/s
System B
T = 30oC
ƐHum = 70%

(b)

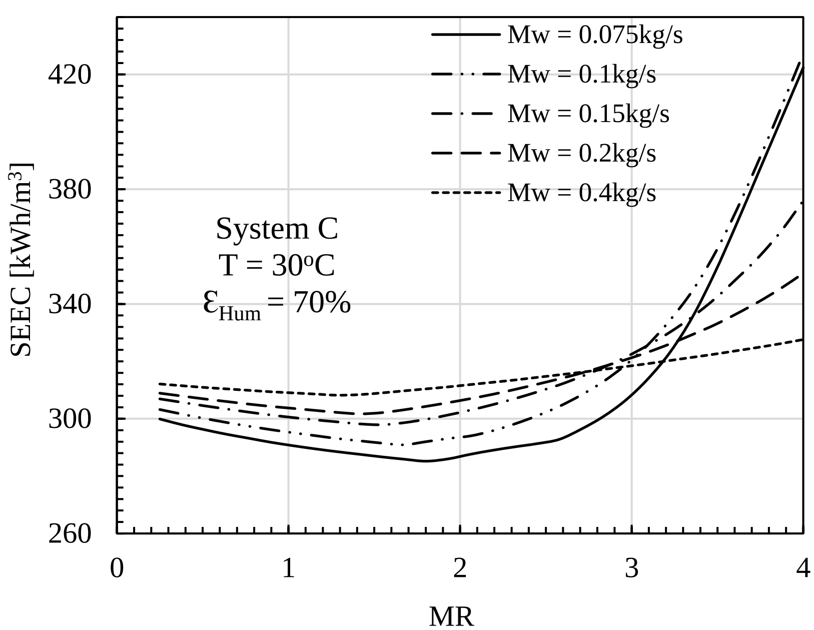
420
380
340
300
260
SEEC [kWh/m3]
0
1
2
3
4
MR
Mw = 0.075kg/s
Mw = 0.1kg/s
Mw = 0.15kg/s
Mw = 0.2kg/s
Mw = 0.4kg/s
System C
T = 30oC
ƐHum = 70%

(c)

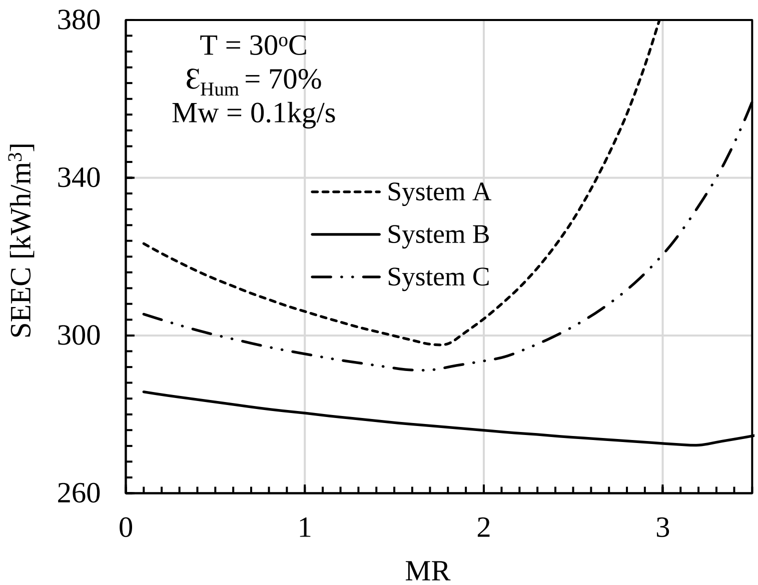

(d)

Figure 6. 11: Impact of MR on the SEEC of the (a) system A, (b) system B, (c) system C & (d) Combined

The effects of the seawater temperature and MR on the gained output ratio are shown in Figure 6.12(a-d). For all the three proposed systems, GOR is observed to increase with increasing seawater temperature. Increasing the saline water temperature from 20^{o}C to 40^{o}C at MR of 2.5 enhances the GOR from 2.29 to 3.75, 3.45 to 3.90, and 2.36 to 3.80 for systems A, B, and C respectively. The increment in the GOR of the systems is mainly due to variation in freshwater production rate. Therefore, any improvement in freshwater production rate will enhances the GOR of the system.

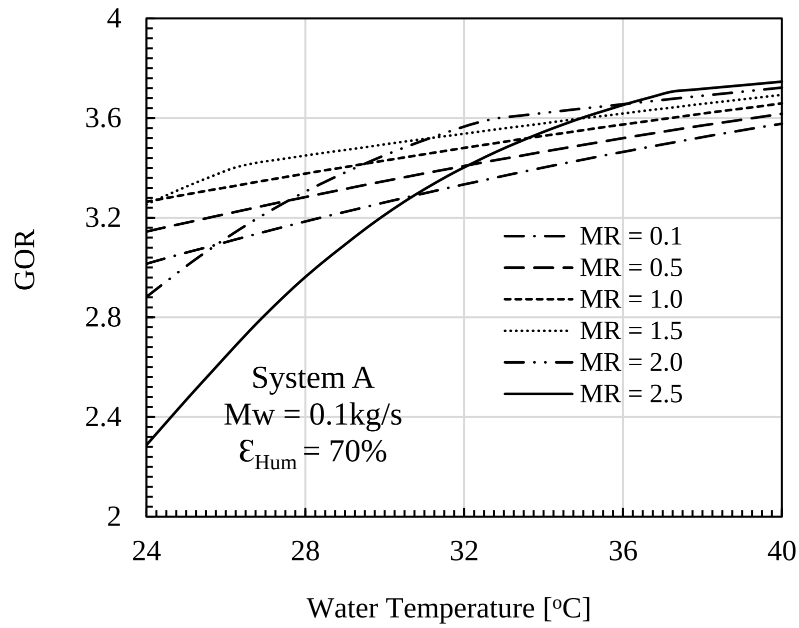

4
3.6
3.2
2.8
2.4
2
24
28
32
36
40
GOR
Water Temperature [^{o}C]
MR = 0.1
MR = 0.5
MR = 1.0
MR = 1.5
MR = 2.0
MR = 2.5
System A
Mw = 0.1kg/s
ε_{Hum} = 70%

(a)

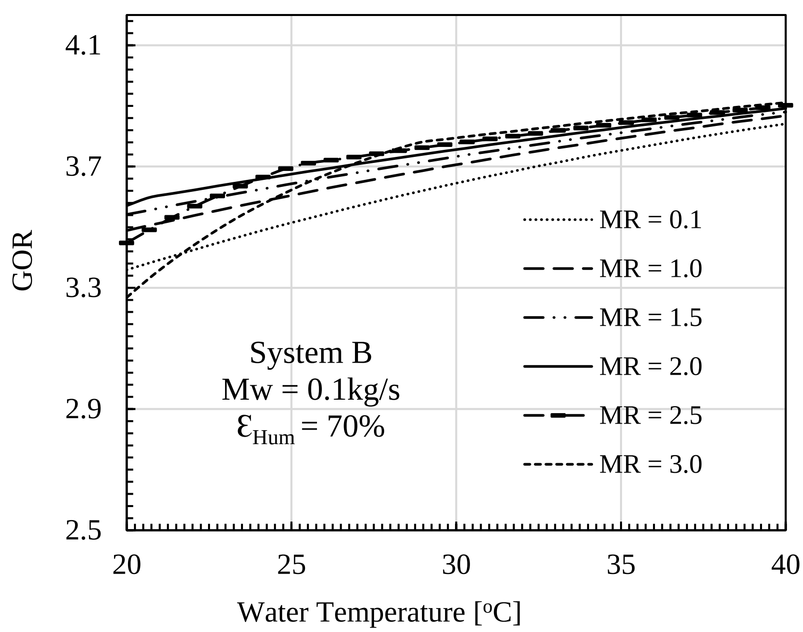

4.1
3.7
3.3
2.9
2.5
20
25
30
35
40
GOR
Water Temperature [^{o}C]
MR = 0.1
MR = 1.0
MR = 1.5
MR = 2.0
MR = 2.5
MR = 3.0
System B
Mw = 0.1kg/s
ε_{Hum} = 70%

(b)

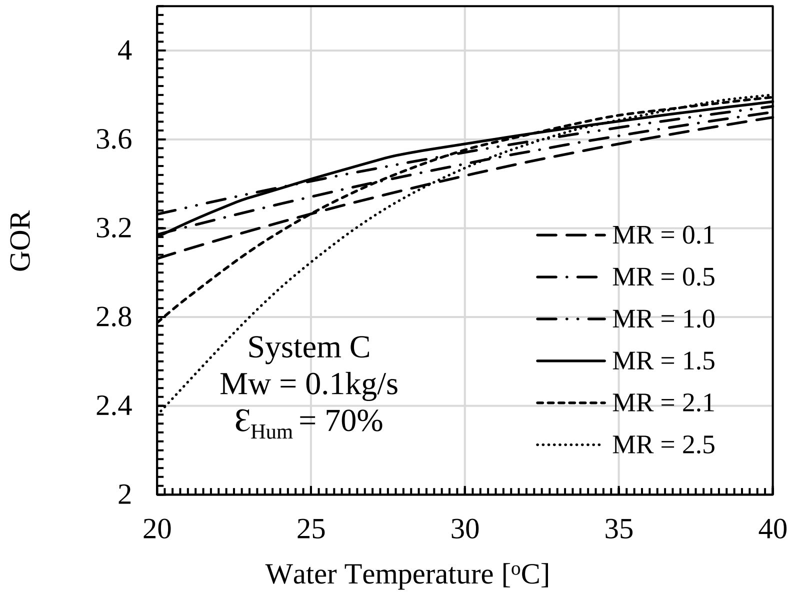

(c)

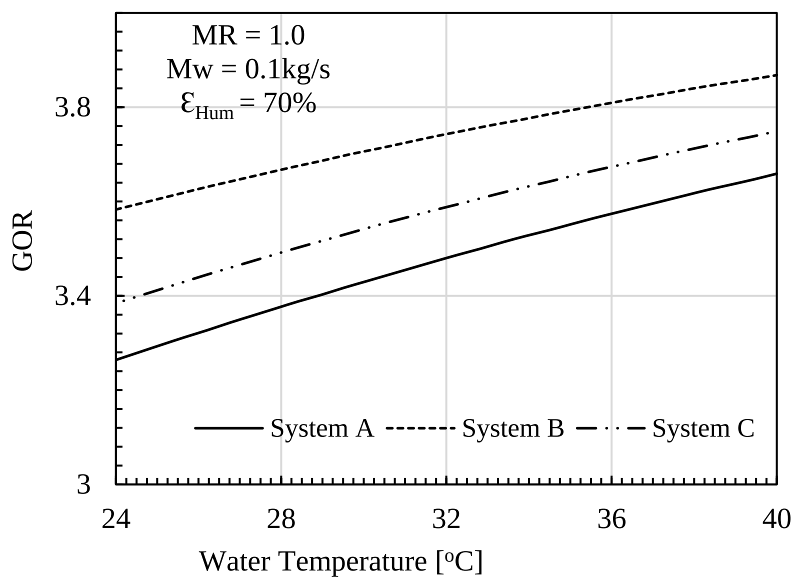

(d)

Figure 6. 12: Effect of T_{sw} the GOR of the (a) system A, (b) system B, (c) system C & (d) Combined

Figure 6.13(a-d) shows the variation of rate of freshwater production against the MR and seawater temperature. For MR of 2.5, raising the seawater temperature from 20°C to 40°C increases the freshwater productivity by 71.1%, 15.7% and 68.6% for systems A, B, and C respectively. This increment in system productivity may be due to increase in air temperature and humidity ratio. This increases the mass transfer to the evaporator surface, which improves the condensation rate and consequently the increase in the rate of freshwater production. The Figures also shows that MR affect system productivity considerably, especially at low temperatures. However, at higher temperatures, MR does not have much influence the GOR of the system. A closer look at the Figures shows that optimum MR exist at different seawater temperatures. Hence, when operating the system at any given temperature, it important to select the right optimum MR that will yield high productivity.

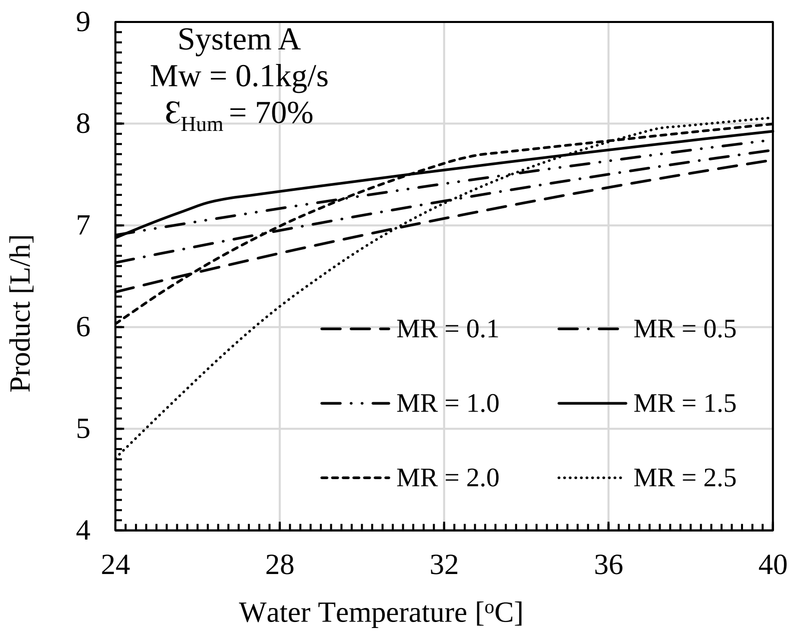

(a)

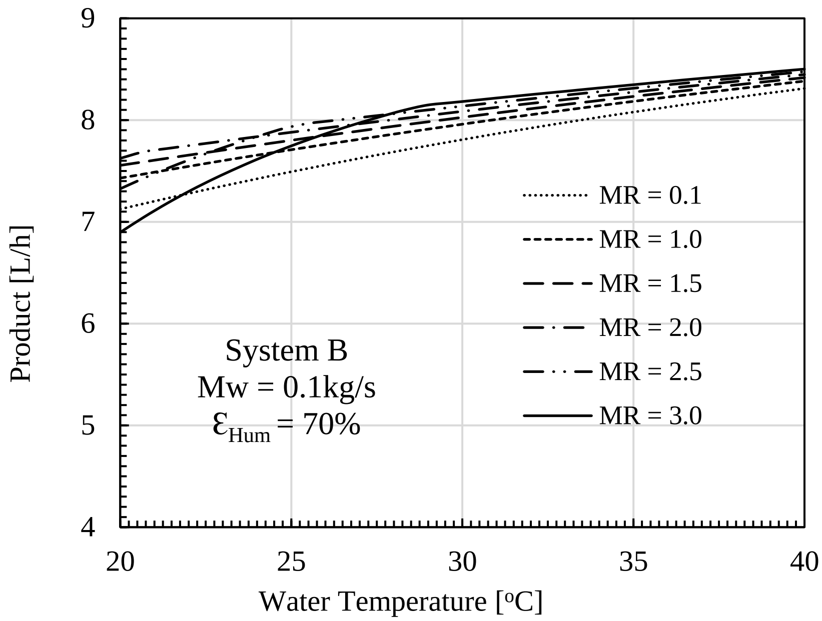
9
8
7
6
5
4
Product [L/h]
20
25
30
35
40
Water Temperature [oC]
System B
Mw = 0.1kg/s
ƐHum = 70%
MR = 0.1
MR = 1.0
MR = 1.5
MR = 2.0
MR = 2.5
MR = 3.0

(b)

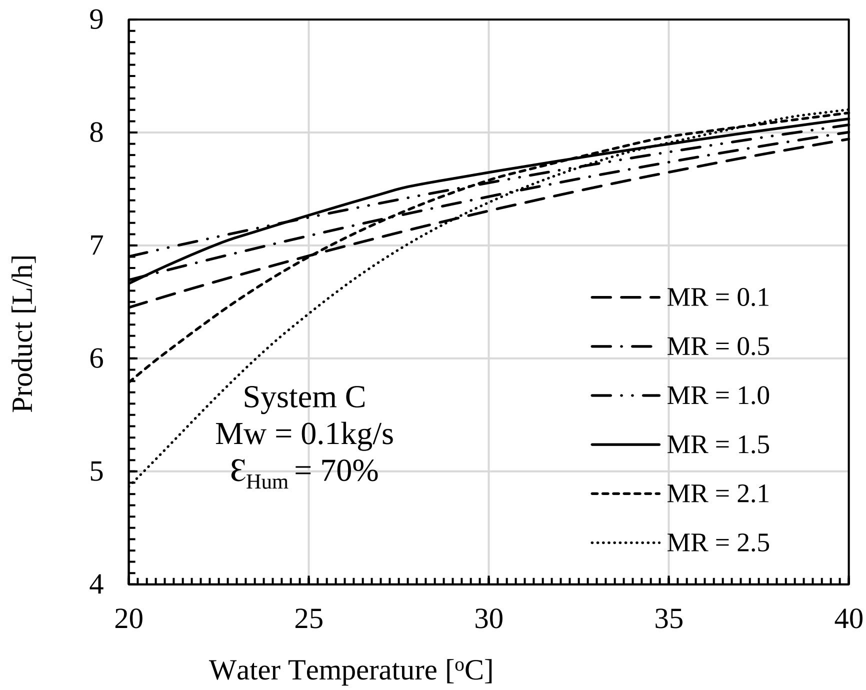
9
8
7
6
5
4
Product [L/h]
20
25
30
35
40
Water Temperature [oC]
System C
Mw = 0.1kg/s
ƐHum = 70%
MR = 0.1
MR = 0.5
MR = 1.0
MR = 1.5
MR = 2.1
MR = 2.5

(c)

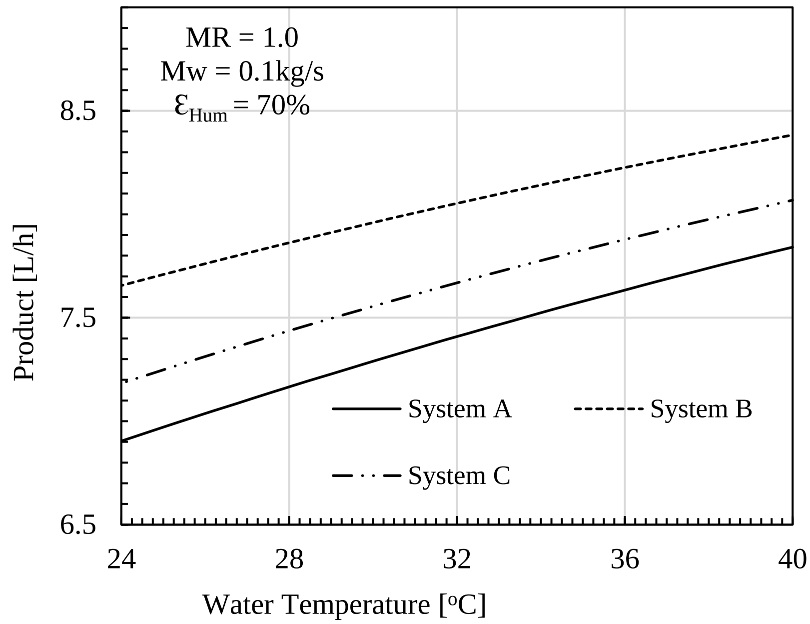

(d)

Figure 6. 13: Effect of T_{sw} on the productivity of the (a) system A, (b) system B, (c) system C & (d) Combined

The effects of MR and seawater temperature on the system recovery ratio are shown in Figure 6.14(a-d). Recovery ratio as the ratio of freshwater produce to the seawater supply, varies with saline water temperatures and MR. it can be noticed that higher seawater temperatures resulted in higher freshwater recovery ratio. For MR of 2.5, the percentage increment in system recovery ratio when saline water temperature increases from 20^{o}C to 40^{o}C is 71.2%, 15.7%, and 68.6% for systems A, B, and C respectively. This is an indication that more freshwater is produced per seawater supplied at high temperature due to high rate of condensation. In other words, less freshwater is produced per feed water supplied at low temperature.

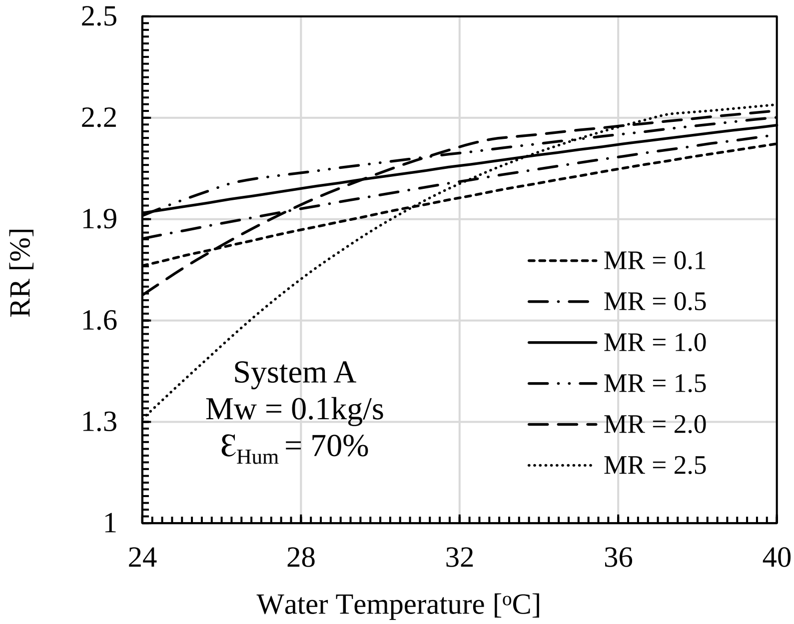
2.5
2.2
1.9
1.6
1.3
1
RR [%]
24
28
32
36
40
Water Temperature [oC]
MR = 0.1
MR = 0.5
MR = 1.0
MR = 1.5
MR = 2.0
MR = 2.5
System A
Mw = 0.1kg/s
ε_{Hum} = 70%

(a)

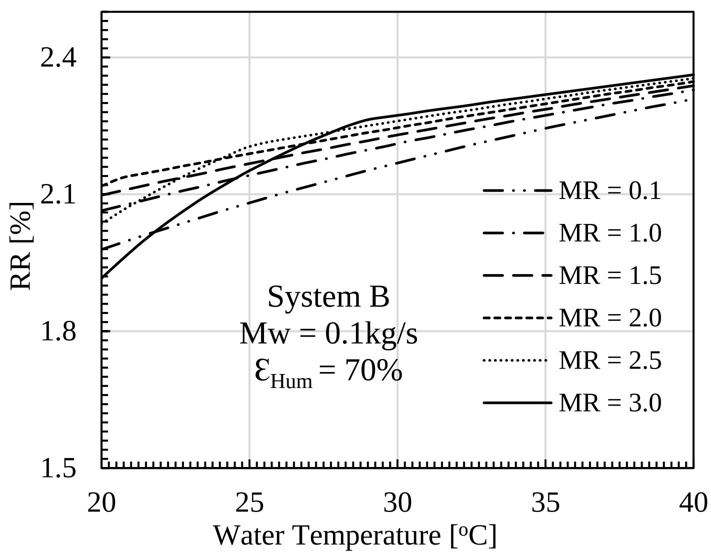
2.4
2.1
1.8
1.5
RR [%]
20
25
30
35
40
Water Temperature [oC]
MR = 0.1
MR = 1.0
MR = 1.5
MR = 2.0
MR = 2.5
MR = 3.0
System B
Mw = 0.1kg/s
ε_{Hum} = 70%

(b)

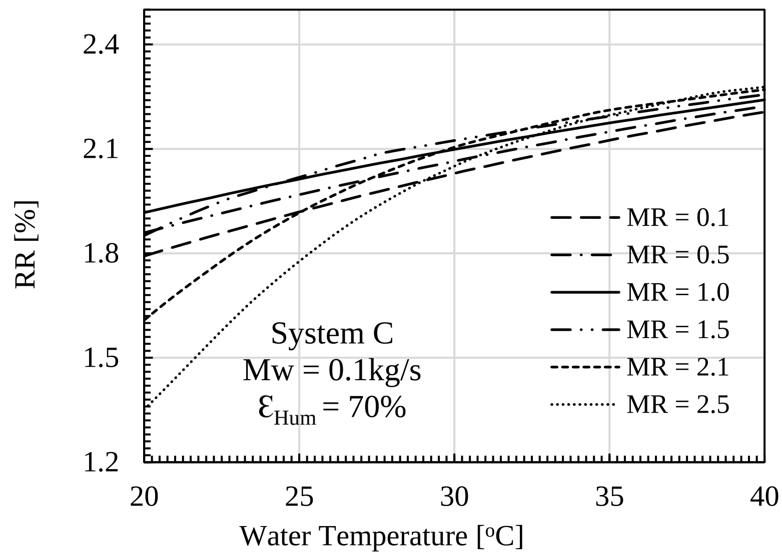

(c)

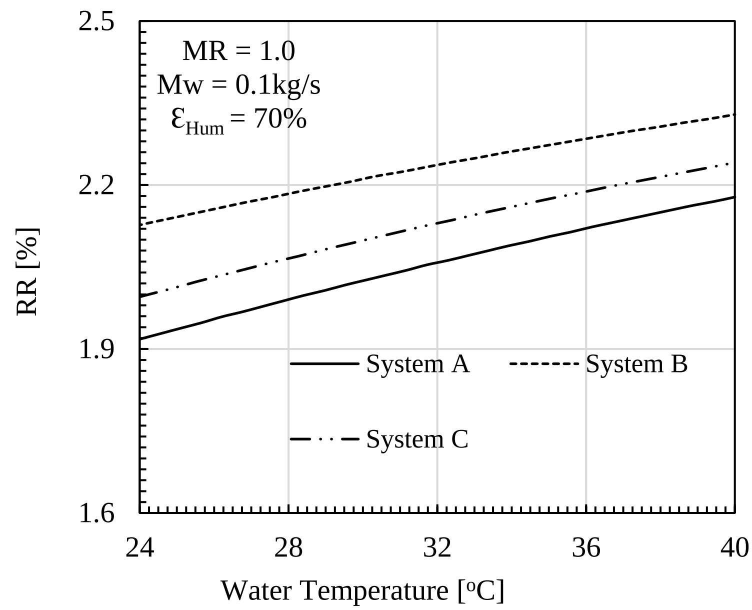

(d)

Figure 6. 14: Influence of T_{sw} on the RR of the (a) system A, (b) system B, (c) system C & (d) Combined

Presented in Figure 6.15(a-d) is the impact of seawater temperature and MR on the Specific Electrical Energy Consumption of the system. Increasing the seawater temperature decreases the SEEC of the system due high evaporation rate of seawater, high mass transfer to the evaporator surface, and high distillation rate of freshwater at elevated seawater temperature. The system SEEC decreases from 473.7kWh/m^3 to 276.8 kWh/m^3, 304.6 kWh/m^3 to 263.2 kWh/m^3, and 458.6 kWh/m^3 to 272 kWh/m^3 when the saline water temperature increases from 20°C to 40°C for systems A, B, and C respectively.

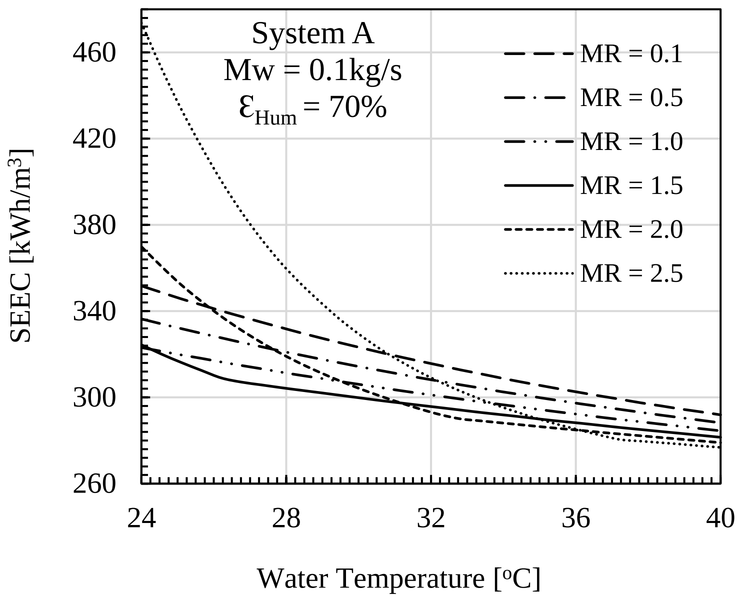

(a)

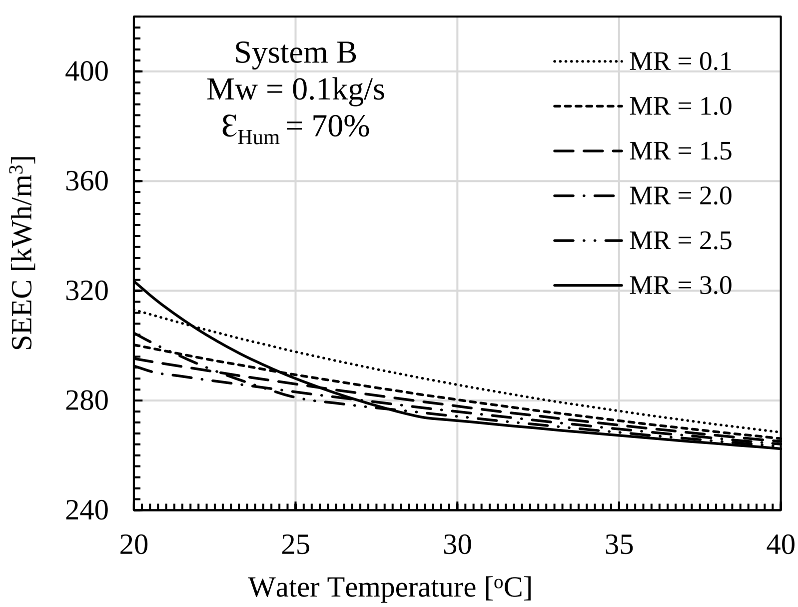

(b)

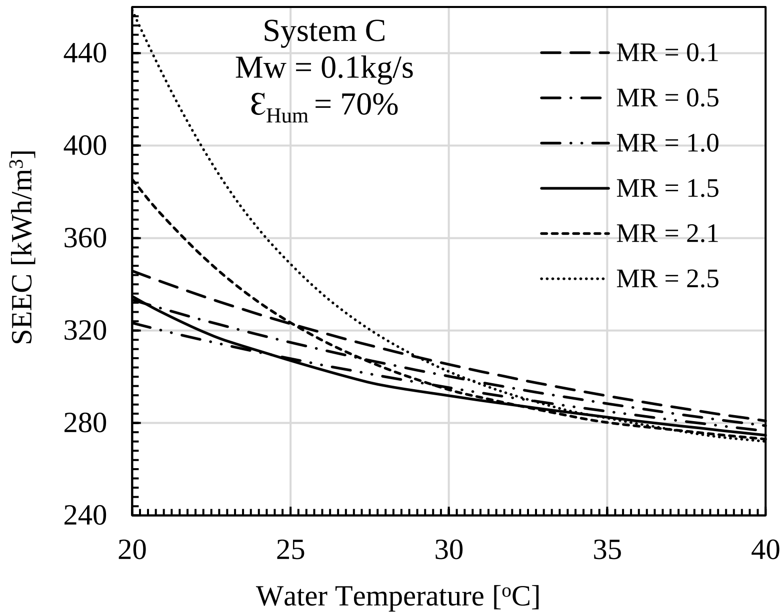

(c)

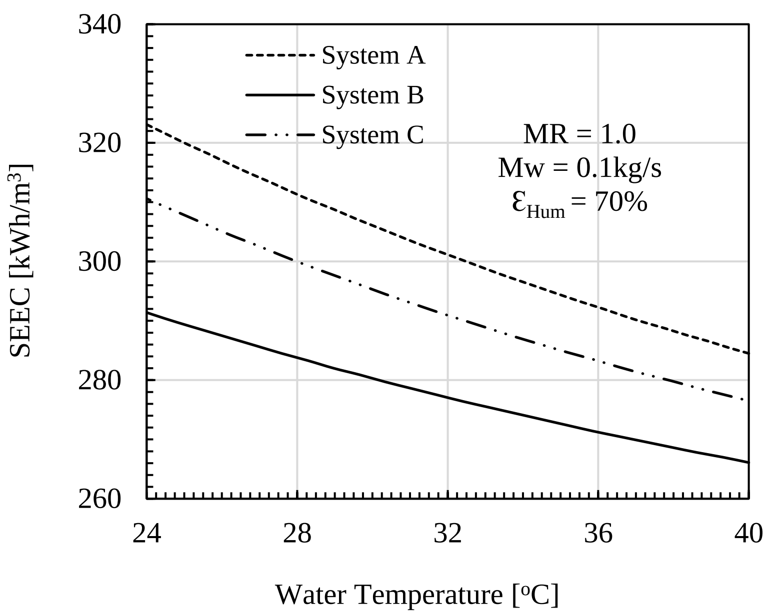

(d)

Figure 6. 15: Impact of T_{sw} on the SEEC of the (a) system A, (b) system B, (c) system C & (d) Combined

The variation in price of freshwater production from system A, system B, and system C with MR, saline water temperature, humidifier effectiveness, electricity cost and plant life expectancy are shown in Figure 6.16(a-e). The system operating conditions are specified on each Figures. It is obvious from Figure 6.16(a-c) that the MR, humidifier effectiveness and saline water temperature greatly influence the price of freshwater by the systems. For the given conditions in Figure 6.16(a-c), system B appears to be the best layout with the lowest freshwater cost. This is expected since system B is integrated with energy recovery system. This outcome is consistent with other performance metrics discussed earlier. However, it can also be noticed that system C which has heat recovery option has the largest cost of freshwater production. This is contrary to our earlier findings with other performance metrics that portrayed system C to be superior to system A in terms of GOR, RR, SEEC and productivity. The reason for this is because of the selected MR. Operating the systems at higher MR will portray the advantage of energy recovery for system C, which will yield lower cost of freshwater in comparison with system A. This can clearly be seen in Figure 6.16(d & e), where the systems are operated at MR = 3.1. Therefore, the cost benefit of recovering energy from the rejected brine for system C can be attained if the system is operated at high mass flowrate ratio of saline water to air and low effectiveness. In fact, the performance of system C (both in terms of energy and cost) can be superior to system B if all the systems (A, B and C) are operated at high MR and low humidifier effectiveness.

Electricity cost is an important parameter when evaluating the cost of water production from a desalination plant. Figure 6.16(d) demonstrates the effects of electricity cost on the cost of freshwater production. It can be noticed that high cost of electricity yielded high cost of freshwater production for all the proposed desalination systems. Varying the electricity cost from 0.04$/kWh to 0.09$/kWh increases the freshwater cost from

14.33\$/m^3 to 34.27\$/m^3, 7.33\$/m^3 to 13.43\$/m^3 and 12.35\$/m^3 to 28.66\$/m^3 for systems A, B and C respectively. These values corresponds to percentage increment of about 139%, 83%, and 132% respectively. The findings suggested that cost of electricity is highly correlated with the price of freshwater. Therefore, it is advisable to locate the plants in regions/areas having low cost of electricity, since the cost of electricity varied from region to region.

Table 6. 1: Capital investment cost for the main components of plants [99,107,118,120]

Item Description	**Prices (US $)**		
	System A	**System B**	**System C**
Packed Bed Humidifier	133	133	133
Water Tanks	200	200	200
Flowmeters	230	230	230
Pumps	150	150	150
Blowers/fans	100	100	100
Pipes, Fittings	35	35	35
Accessories	33	33	33
Semi Hermetic Compressor	1200	1200	1200
Shell and Tube Condenser	600	600	600
Shell & Tube Evaporator	600	600	600
Expansion Valve	100	100	100
Brine heat exchanger	-	600	600

The variations of life span of the plants (plant life expectancy) with freshwater production cost is illustrated in Figure 6.16(e). The Figure suggested that a desalination plant that is designed to last for a longer life will provide the lowest cost of freshwater. For all the three systems (A, B, and C), increasing the plant life span from 15years to 30years reduces the product cost from 15.59\$/m^3 to 13.15\$/m^3, 11.29\$/m^3 to 9.43\$/m^3 and 13.50\$/m^3 to 11.27\$/m^3 and respectively. In other words, the percentages reduction in the freshwater cost when the plant life increases from 15years to 30years is about 18.56, 19.69% and

19.79% for systems A, B, and C respectively. Depending on the system operating conditions, the minimum and maximum price of freshwater production from the proposed desalination systems is 7.35$/m^3 and 34.27$/m^3 respectively.

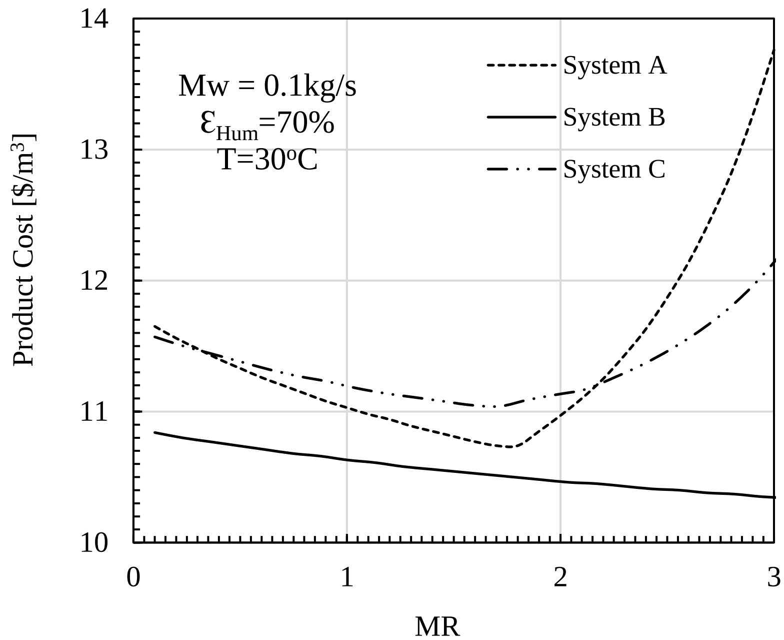

(a)

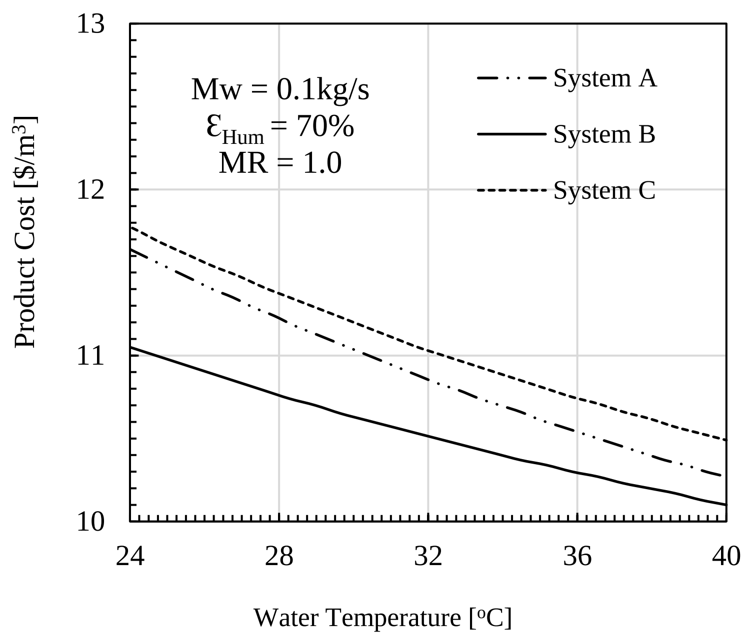

(b)

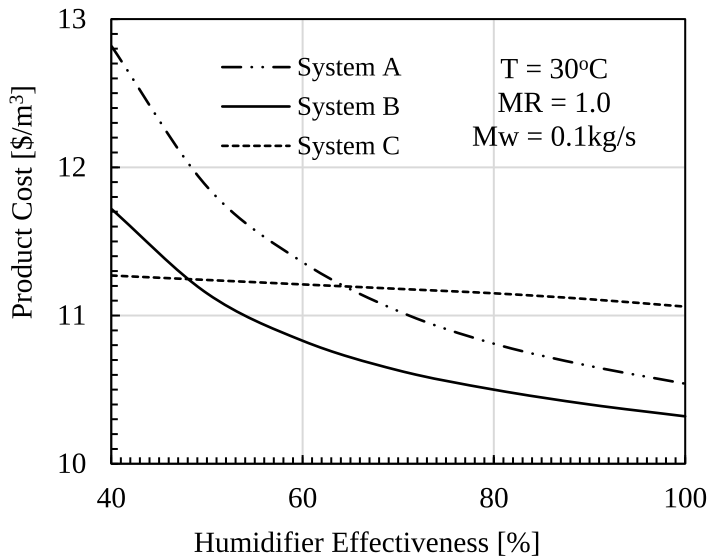
13
12
11
10
40
60
80
100
Product Cost [$/m3]
Humidifier Effectiveness [%]
System A
System B
System C
T = 30oC
MR = 1.0
Mw = 0.1kg/s

(c)

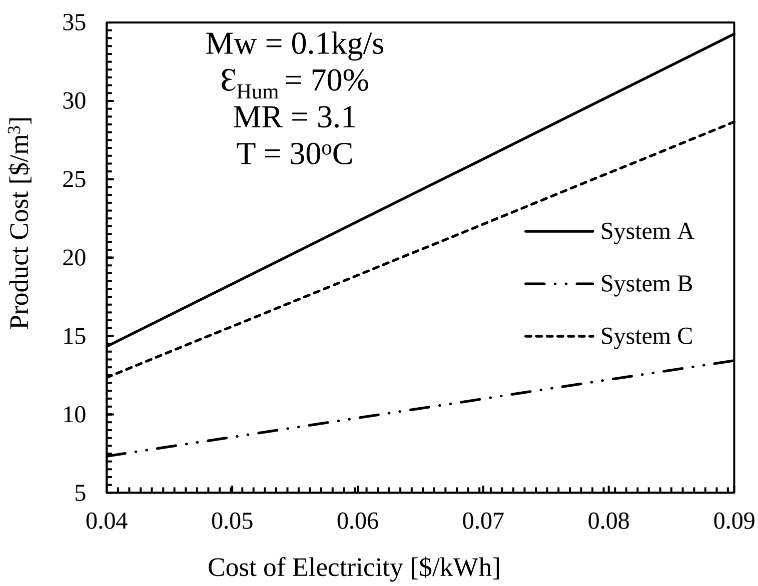
35
30
25
20
15
10
5
0.04
0.05
0.06
0.07
0.08
0.09
Product Cost [$/m3]
Cost of Electricity [$/kWh]
Mw = 0.1kg/s
εHum = 70%
MR = 3.1
T = 30oC
System A
System B
System C

(d)

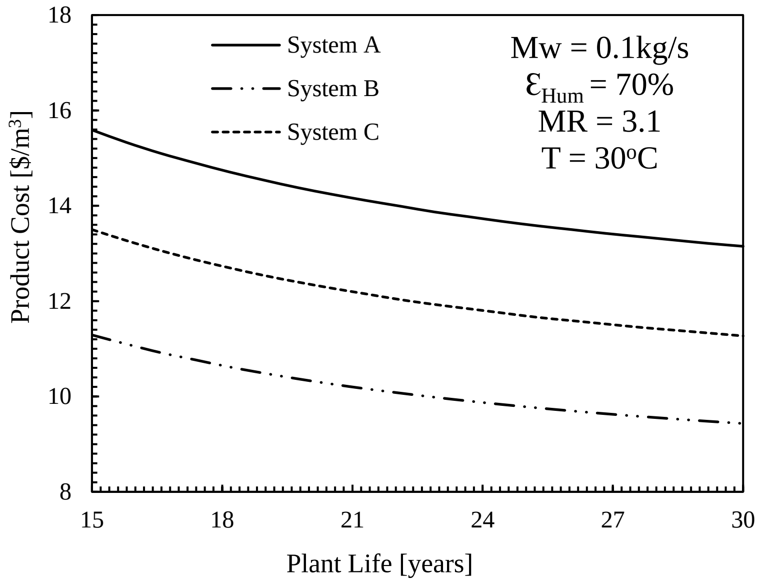

(e)

Figure 6. 16: Variation of product cost with (a) MR, (b) water temperature, (c) humidifier effectiveness, (d) cost of electricity and (e) Plant expectancy.

Models validation

To ensured that the results presented in the current work are correct and reliable, the equations for humidification dehumidification system is first validated against the work of Narayan et al. [14]. The considered HDH configuration is the water heated closed air open water HDH system. The validated results are demonstrated in Figure 6.17. The presented HDH models was found to be in good agreement with work of Narayan [14]. The HDH models is validated separately due to lack of data on the proposed novel integrated HDH-heat pump system. After ensuring the accuracy of HDH models, the mathematical models was then integrated with the heat pump model, and then validated against the work of Lawal et al. [106]. The integrated mathematical models was also found to be in excellent agreement with the work. Thereafter, the integrated mathematical models was modified to reflect various configurations (systems) presented in current work.

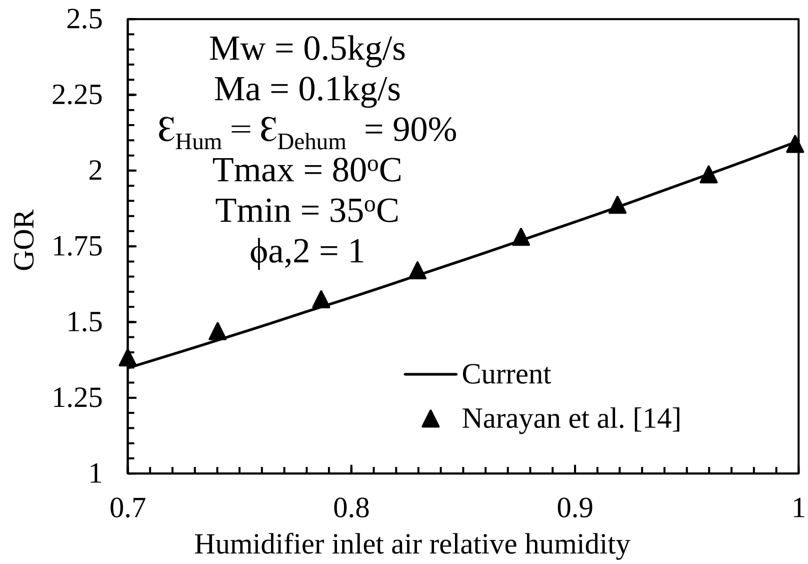

Figure 6. 17: Variation of gained output ratio against inlet air relative humidity and MR. A comparison between the current models and the existing data from Narayan et al. [14].

CHAPTER 7

7.0 Experimental Investigation of Water heated HDH System Integrated with heat Pump

In this section, an experimental investigation of the performance of humidification dehumidification (HDH) desalination system operated by heat pump (HP) is presented. The integrated unit produces freshwater as the primary output and cooling effect for space conditioning as the secondary benefit. The effect of feed water flowrate, feed water temperature and chilled water flowrate on the system general assessment metrics, such as gained output ratio (GOR), recovery ratio (RR), coefficient of performance (COP), energy utilization factor (EUF), Specific electrical energy consumption (SEEC) and productivity were evaluated and discussed. Furthermore, the cost of producing desalinated water from the desalination unit is estimated.

7.1 Experimental Setup and System Description

7.1.1 Process description

The schematic representation of the experimental set-up and process for the proposed integrated HDH desalination unit and heat pump is presented in Fig. 7.1. The desalination unit comprises two cycles namely: HDH cycle and heat pump cycle. The HDH cycle contained two main components (Humidifier and Dehumidifier), while the heat pump cycle entails condenser, evaporator, compressor and throttling valve. The hot saline water exiting the condenser of heat pump is sprayed in the humidifier over the packing materials. A portion of the hot saline water evaporates and carried by the incoming air, while un-evaporated saline water is rejected at the bottom of the humidifier as brine. A part of the discharged brine may be recycled through the condenser of heat pump depending on the desire water inlet temperature to the condenser of the heat pump. The saturated air leaving the humidifier is directed to the dehumidifier, where the vapor contained in the air is condensed (air is dehumidified) as a result of chilled water flowing through the heat exchangers of the dehumidifier. The condensed vapor is collected through the bottom of the dehumidifier as distillate (freshwater), while the low temperature dehumidified air exiting the dehumidifier may be used for space cooling. Effective dehumidification (vapor condensation) is achieved by pumping chilled water (water exiting the evaporation of heat pump) through the heat exchanger coil located in the dehumidifier. Hot saline water and chilled water are achieved by condensing and evaporating refrigerant in the condenser and evaporator of the heat pump respectively. Therefore heat pump system is used to simultaneously provide the cooling demand in the dehumidifier and heating demand in the humidifier. Chilled water is attained when the supply water (usually at room temperature) transfer heat to the refrigerant in the evaporator, while hot saline water is achieved when refrigerant in the condenser transfers heat to the saline feed water at various degree of temperatures. The HDH unit is operated at atmospheric condition (pressure is assumed to be 101.325 kPa). The plant performance is evaluated at the following conditions: Feed water inlet temperature of 30°C, 35°C, and 40°C with maximum variation of ±3°C. Feed saline water flowrate changes at 2.5 L/min, 4.0 L/min, 5.5 L/min, 7.0 L/min, 10.0 L/min, 13.0 L/min and 16.0 L/min, while the selected chilled water flowrates are 2.0 L/min, 4.0 L/min and 6.0L/min. The used feed saline water has salinity of 2440 parts per million (PPM). The heat pump evaporator water inlet temperature was kept constant at 27.5°C ± 0.5°C, while the air mass flowrate, temperature and its relative humidity fluctuates around 0.05497 kg/s, 26.5 ^{o}C ± 0.3°C and 48.7% respectively.

7.1.2 Experimental setup

The lab scale desalination unit was designed, built and tested at KFUPM-ME desalination lab. While the heat pump system was initially designed at KFUPM-ME for the specification of inlet and outlet values to the system. The system was re-designed for components sizing and later built by Zamil Air conditioners Jubail KSA. A photograph of the actual integrated desalination unit is depicted in Fig. 7.2(a). The humidifier and the dehumidifier are vertical rectangular towers depicted in Fig 7.2(b). The humidifier is equipped with packing material for direct contact heat exchange between hot water and cold air, while the dehumidifier is equipped with heat exchangers for effective condensation of water vapor contained in the air. Both humidifier and dehumidifier are fabricated with plexiglass acrylic sheet of 8mm thickness. The dimensions of the humidifier and the dehumidifier are 0.3m x 0.37m x 1.1m and 0.3m x 0.39m x 1.1m, respectively. Humidifier is equipped with three packing materials of 10cm height, 25cm width and 27cm length. The packing materials are made of cellulose pads, and are separated from each other by a gap of 3cm. Four pieces of fin tube heat exchangers whose tubes and fins are made from copper and aluminum materials respectively are installed inside the dehumidifier. Each exchangers is separated from others by a gap of 8cm.

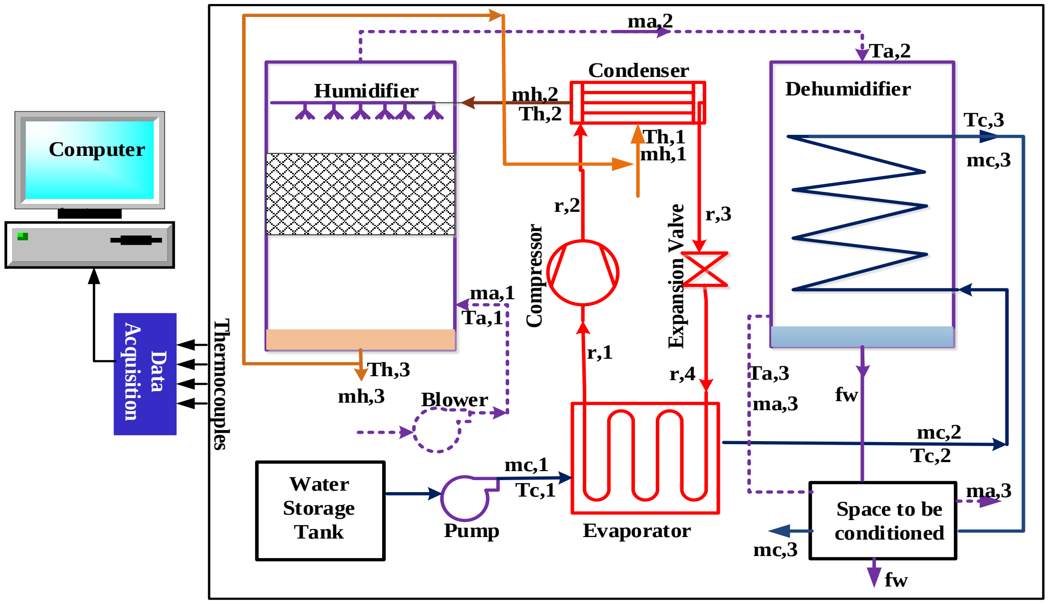

Figure 7. 1: Schematic Line diagram of the Experimental Set-Up

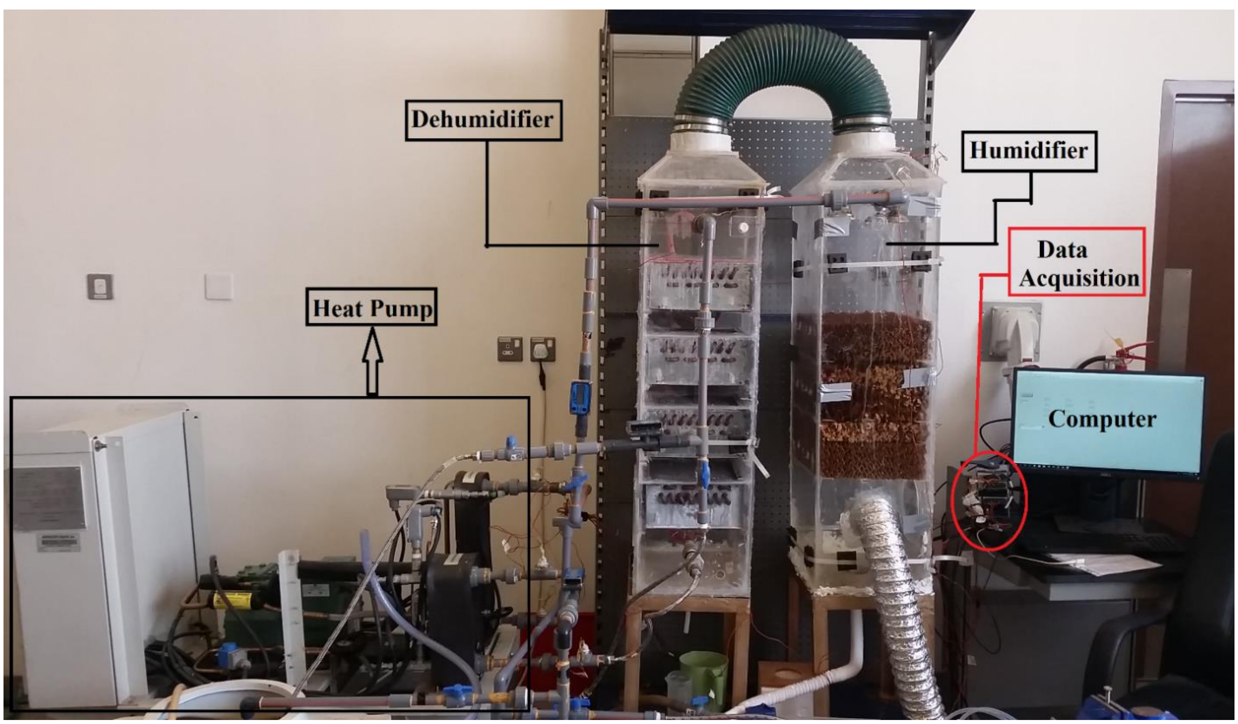

Figure 7. 2(a): A photograph of the actual laboratory unit.

The tubes of the heat exchanger has internal diameter of 8mm and the total length of each exchanger is 6.48m.The overall dimension of each exchanger is 13cm x 27cm x 30cm.

Two water tanks were used in the set-up (Figure 7.2(c)); the cold and hot water tank. The cold and hot water tanks have volume of 130 and 50 Liter respectively. Both the humidifier and dehumidifier are placed on a 40 cm steel stand. Two circulation pumps with 0.37kW each are used for circulating hot saline water and cooling water (Figure7.2(c)). An electric blower with 400 watts of power is used to supply the required air flowrate. The air flowrate is measured using an orifice meter connected to manometer. The orifice meter was originally designed and constructed by Hafiz [140]. The photograph of the blower and orifice meter are presented in Figure 7.2(d). Both the condenser and evaporator of the heat pump are made from Copper brazed plate heat exchangers.

The heat pump system is displayed in Fig. 7.2(e). The material specification of the exchangers are: the plate heat exchangers is made with stainless steel thickness 0.0138" (316L type), the connections is with stainless steel (304L type), and the brazing material is copper. The evaporator has a total number of 28 plates, length of 76mm and surface area of $0.86m^2$. While the condenser has a total number of 14 plates, length of 44mm and surface area of $0.43m^2$. The compressor type is semi-hermetic motor reciprocating compressors, and eco-friendly refrigerant R-134a is used for the heat pump, while the expansion device is thermostatic.

7.1.3 Instrumentation and uncertainty analysis

The integrated HDH-HP system is equipped with instrumentation for measuring air flowrate, water flow rate, air and water temperatures and air relative humidity. The air flowrate is measured with an orifice meter connected to a manometer which measure the pressure drop across the orifice plate as depicted in Figure 7.2(d), while the chilled water and hot water flowrate are monitored using electronic water meter (FTB695A). The air relative humidity was measured using handheld hygro thermometer data logger (RH318). K-type thermocouples were adopted to measure the chilled water temperature, hot water temperature, and air dry-bulb/wet-bulb temperatures at the inlet and outlet of the main components. Freshwater/distillate rate is measured using volume of the collected distillate and the time taken for the collection. All the measuring instruments are connected to the National Instrument (NI cDAQ 9174) data acquisition which host three temperature modules (NI 9211). The data acquisition is connected to computer where the system operating conditions are monitored and stored using a LabVIEW code as shown in Fig. 7.2(f).

Figure 7.2(b): A photograph of Humidifier and Dehumidifier

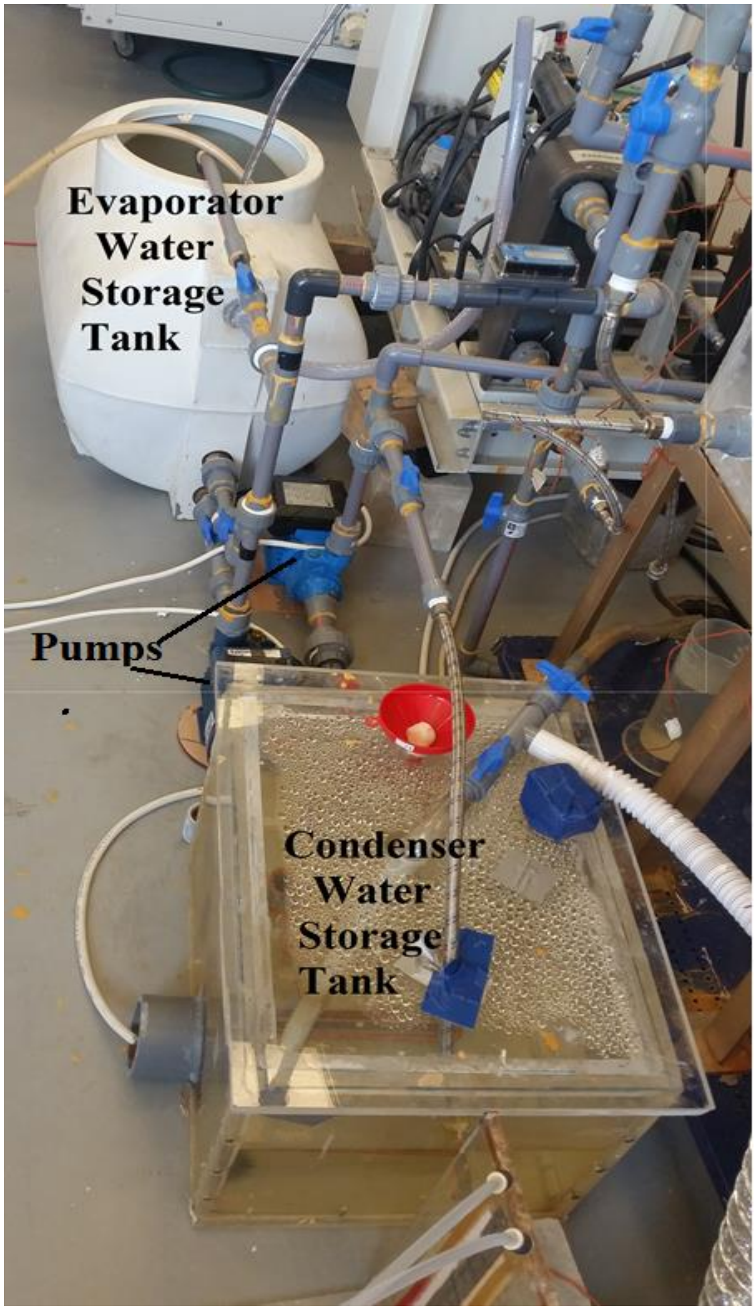

Figure 7.2(c): A photograph of two water storage tanks and circulating pumps

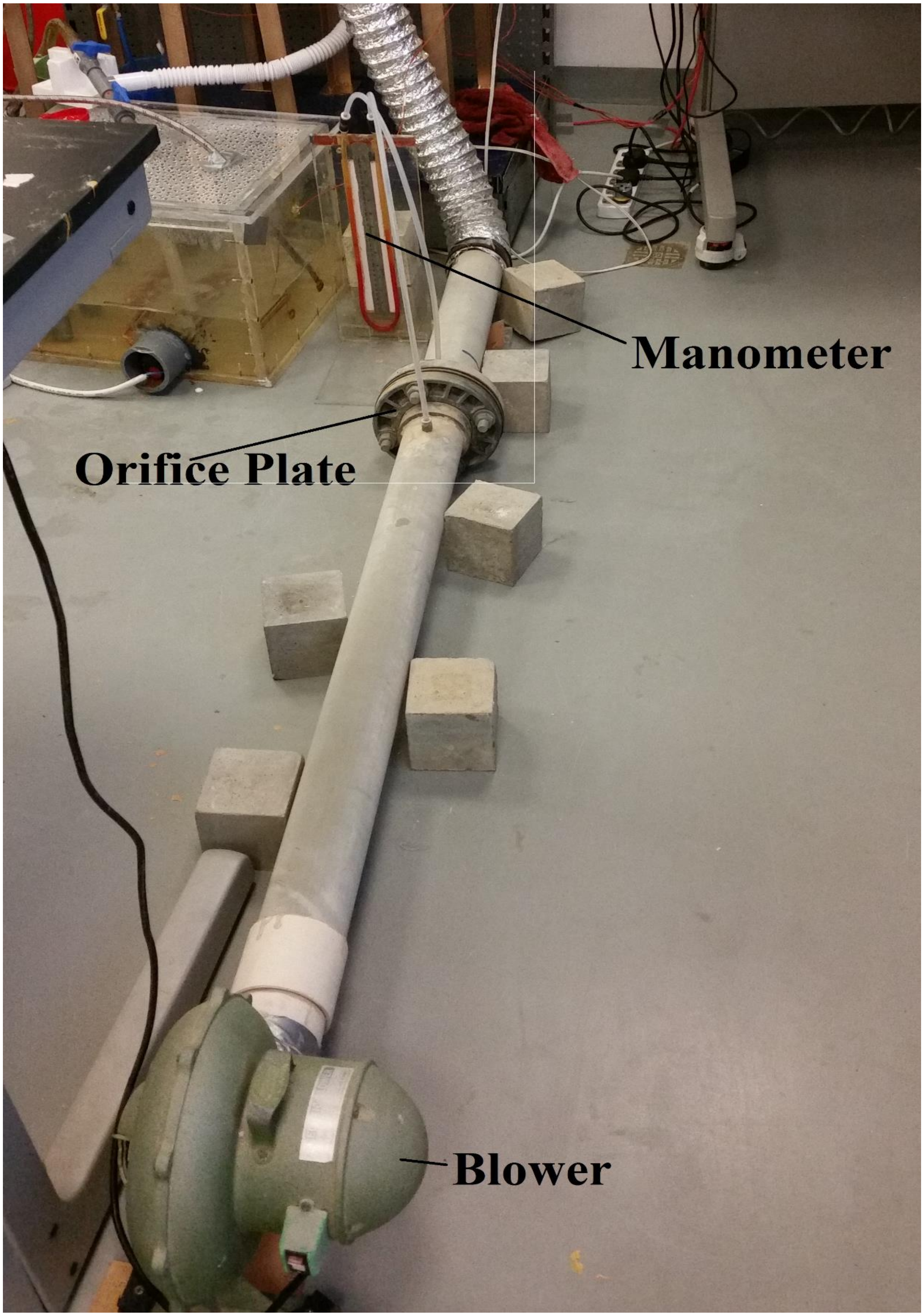

Figure 7.2(d): A photograph of blower and the orifice meter

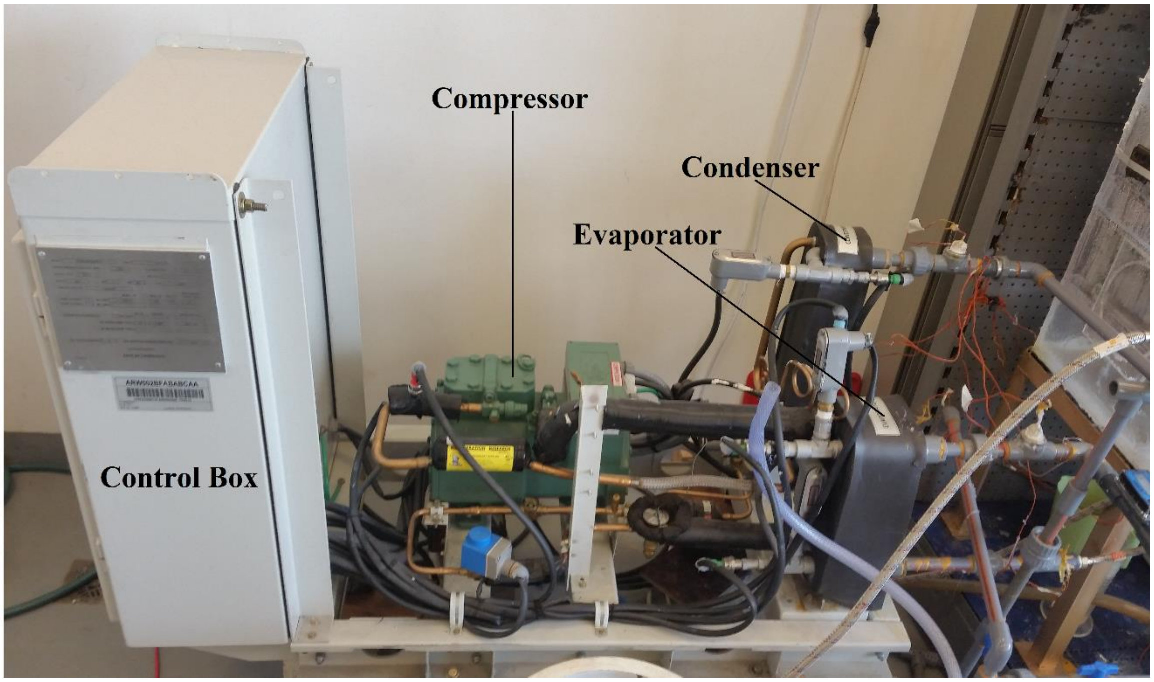

Figure 7.2(e): A photograph of Heat Pump system

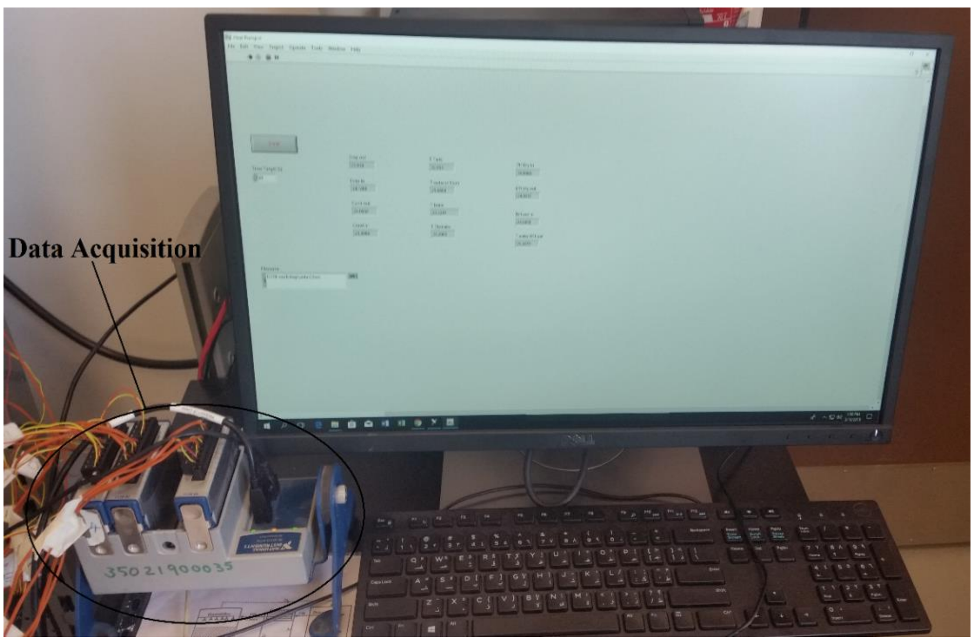

Figure 7.2(f): A photograph of DAQ and PC

The uncertainty present in the measuring instruments is calculated using the expression given in Eq. (1) [105,141], and uncertainty value estimated for each instrument is tabulated in Table 7.1. It is important to note that instrumental uncertainty depend on the accuracy of the instrument.

$$U = \frac{a}{\sqrt{3}} \tag{1}$$

Where (a) is the accuracy of each instrument and (U) is the uncertainty in the instrument.

The uncertainty in the calculated parameters (unit performance indicators) is evaluated based on the uncertainty of instrument. The expression for determining the uncertainty in the calculated parameters is given by Kline and McClintock [142], and can be expressed as:

$$\delta_R = \left[\left(\frac{\partial R}{\partial x_1}\delta_1\right)^2 + \left(\frac{\partial R}{\partial x_2}\delta_2\right)^2 + \ldots + \left(\frac{\partial R}{\partial x_n}\delta_n\right)^2\right]^{1/2} \tag{2}$$

Where (δ_R) is the uncertainty of result (R). The values of uncertainties for the evaluated results are given in Table 7.2.

Table 7. 1: Uncertainties associated with the measuring Instruments

Instrument	Measured parameter	Accuracy	Range	Uncertainty
Humidity Sensor	Relative Humidity	±2.0%	0 to 100% RH	±1.1547%
Thermocouple	Temperature	±0.5°C	-100 to1300 °C	±0.2887
Measuring beaker	Distillate volume	±10 mL	1 to 1000 mL	±5.774mL
Stopwatch	Timing	±0.01s	0-99 hrs	±0.005774s
Rotameter	Water flowrate	±3.0%	2 to 38 LPM	±1.7321%
Pressure	U-Tube manometer	± 1 mm	0.1 - 30 cm H_2O	± 0.5774 mm

Table 7. 2: Uncertainties associated with the calculated parameters

Calculated Parameter	Uncertainty
COP_{HP}	±0.04546
Humidifier effectiveness	±0.02156
Dehumidifier effectiveness	±0.004609
Cooling Effect	±0.1342
Productivity	±0.03464
RR	±0.01031
EUF	±0.05057
SEEC	±1.436
GOR_{HP}	±0.0377

7.1.4 System performance metrics

The cooling output from the desalination unit is calculated based on the energy associated with dehumidified air, distillate output, and discharged chilled water. The expression for evaluating the output cooling effect is as follows [105]:

$$\dot{Q}_{cooling} = \dot{Q}_{air} + \dot{Q}_{dist} + \dot{Q}_{water,deh,out} \tag{3}$$

Where;

$$\dot{Q}_{air} = \dot{m}_{air}\left(h_{air,ref} - h_{air,out}\right) \tag{4}$$

$$\dot{Q}_{dist} = \dot{m}_{dist}\left(h_{water,ref} - h_{dist}\right) \tag{5}$$

$$\dot{Q}_{water,deh,out} = \dot{m}_{water,deh,out}\left(h_{water,ref} - h_{water,deh,out}\right) \tag{6}$$

The performance of HDH system can be evaluated in terms of energy utilization factor (EUF). The energy utilization factor for the overall integrated unit (for freshwater and cooling load production) is calculated using the following [105,143]:

$$\mathrm{EUF}_{Combined} = \frac{\left(\dot{\mathrm{m}}_{\mathrm{dist}} \times \mathrm{h}_{\mathrm{fg}}\right) + \dot{\mathrm{Q}}_{\mathrm{cooling}}}{\dot{\mathrm{W}}_{\mathrm{comp}} + \dot{\mathrm{W}}_{\mathrm{P,hot,water}} + \dot{\mathrm{W}}_{\mathrm{P,cold,water}} + \dot{\mathrm{W}}_{\mathrm{Blower}}} \tag{7a}$$

Similarly, the energy utilization factor for desalination alone (for freshwater production only) is evaluated using the following expression:

$$\mathrm{EUF}_{\mathrm{Desalination}} = \frac{\left(\dot{\mathrm{m}}_{\mathrm{dist}} \times \mathrm{h}_{\mathrm{fg}}\right)}{\left(\dot{\mathrm{W}}_{\mathrm{comp}} + \dot{\mathrm{W}}_{\mathrm{P,hot,water}} + \dot{\mathrm{W}}_{\mathrm{P,cold,water}} + \dot{\mathrm{W}}_{\mathrm{Blower}}\right)} \tag{7b}$$

The gained output ratio (GOR) is an important parameter for the description of energy performance of the HDH desalination unit. For the current system, the GOR is calculated using the expression given in [106,107,109,111]:

$$\mathrm{GOR} = \frac{\dot{\mathrm{m}}_{\mathrm{dist}} \times \mathrm{h}_{\mathrm{fg}}}{\dot{\mathrm{W}}_{\mathrm{comp}}} \tag{8}$$

Since the current integrated system produces both freshwater and cooling effect, then the actual gained output ratio for the HDH desalination alone can be calculated by considering only the fraction of power consumed for freshwater production. Therefore, the expression for evaluating the actual GOR of HDH desalination system can be expressed as:

$$\mathrm{GOR}_{\mathrm{Desalination}} = \frac{\dot{\mathrm{m}}_{\mathrm{dist}} \times \mathrm{h}_{\mathrm{fg}}}{\dot{\mathrm{W}}_{\mathrm{comp}} \times \mathrm{F}_{\mathrm{c}}} \tag{9}$$

Where F_{c} is the fraction of compressor power consumed for desalination alone.

The GOR in both Eqs. (8 & 9) are based on the input power to the compressor of the heat pump system.

The specific electrical energy consumption (SEEC) indicates the amount of electrical energy consumed per meter cube of freshwater production. The SEEC of the integrated desalination plant can be expressed as [108,112]:

$$\mathrm{SEEC} = \frac{\dot{W}_{comp}}{\dot{m}_{dist}} \left({}^{kWh}\!/_{m^3} \right) \tag{10a}$$

Similarly, the actual electrical energy consumed to produce one cubic meter of freshwater can be estimated by considering only the fraction of electrical energy needed for desalination. Therefore, the following expression is used to calculate the actual SEEC of the desalination system:

$$\mathrm{SEEC}_{Desalination} = \frac{\dot{W}_{comp} \times F_c}{\dot{m}_{dist}} \left({}^{kWh}\!/_{m^3} \right) \tag{10b}$$

The coefficient of performance of the heat pump is evaluated based on the expression given in [108,109,144]:

$$\mathrm{COP}_{HP} = \frac{\text{Thermal energy rejected by condensers}}{\text{Energy input to compressor}} \tag{11}$$

$$\mathrm{COP}_{HP} = \frac{\dot{Q}_{Cond}}{W_{comp}} \tag{12}$$

The humidifier and dehumidifier effectiveness can be expressed as [11]:

$$\varepsilon_H = \max\left\{ \frac{h_{a,out} - h_{a,in}}{h_{a,out,ideal} - h_{a,in}}, \frac{h_{w,in} - h_{w,out}}{h_{w,in} - h_{w,out,ideal}} \right\} \tag{13}$$

$$\varepsilon_D = \max\left\{\frac{h_{a,in} - h_{a,out}}{h_{a,in} - h_{a,out,ideal}}, \frac{h_{w,out} - h_{w,in}}{h_{w,out,ideal} - h_{w,in}}\right\} \tag{14}$$

Where $h_{w,in}$ and $h_{w,out}$ are the enthalpy of water at the inlet and outlet of the components respectively, while $h_{a,in}$ and $h_{a,out}$ is the enthalpy of air at the inlet and outlet of the components respectively. The enthalpy of the ideal outlet air is evaluated at the water inlet temperature when the outlet air is fully saturated, and the ideal outlet water enthalpy is calculated at temperature of inlet air dry-bulb.

The desalination plant recovery ratio is calculated as:

$$RR = \frac{\dot{m}_{dist}}{\dot{m}_{hot,water}} \times 100\% \tag{15}$$

The expression for mass flowrate ratio is given as:

$$MR = \frac{\dot{m}_{hot,water}}{\dot{m}_{air}} \tag{16}$$

The cost of desalinated water from the current unit is evaluated using the expressions presented below. The cost analysis is based on the method presented by El-Dessouky and Ettouney [139]:

To evaluate the capital cost capital recovery factor (amortization factor) is required which can be calculated from:

Amortization factor (α):

$$\alpha = \frac{i(i+1)^n}{(i+1)^n - 1} \tag{17}$$

Annual capital cost:

$$\dot{Z}_f(\$/yr) = Z(\$) \times \alpha\ (1/yr) \tag{18}$$

The summary of capital cost of the main components of the plant is presented in Table 7.3. The plant components cost is based on the actual purchased prices from the vendors.

Annual electric power cost ($\dot{C}_{Elect}$):

$$\dot{C}_{Elect}(\$/yr) = COE \times \frac{SEEC_{Desalination}}{3600} \times Å \times \dot{V}_{fw}\ (m^3/day) \times 365 \tag{19}$$

The annual labor cost ($\dot{C}_L$):

$$\dot{C}_L(\$/yr) = \mathcal{L}(\$/m^3) \times Å \times \dot{V}_{fw}\ (m^3/day) \times 365 \tag{20}$$

The total annual cost ($\dot{C}_T$) [139]:

$$\dot{C}_T(\$/yr) = \dot{Z}_f(\$/yr) + \dot{C}_{Elect}\ (\$/yr) + \dot{C}_L(\$/yr) + \dot{C}_{mt}(\$/yr) + \dot{C}_{mg}(\$/yr) \tag{21}$$

Where $\dot{C}_{mt}$and $\dot{C}_{mg}$ is the annual maintenance and management costs, respectively.

Therefore, unit product cost (C_P):

$$C_P(\$/m^3) = \left(\frac{\dot{C}_T(\$/yr)}{Å \times V_{fw}\ (m^3/day) \times 365\ (day/yr)}\right) \tag{22}$$

7.2 Results and Discussion

An experimental study has been conducted to investigate the performance of heat pump driven humidification dehumidification desalination system for primary purpose of water desalination and secondary function of space conditioning. The influences of operating parameters on performance metrics are presented in this sections. The system operating variables and their corresponding ranges are previously presented in section 7.1.1. The findings from the study is presented in graphical representation as shown in Figures 7.3 to 7.18. The effect of MR, hot feed temperature and chilled water flowrate on the COP of the heat pump is depicted in Figure 7.3. The COP is noticed to be varying with mass flow rate ratio because of change in the cooling/heating loads. The increase in feed water to air mass flow rate ratio results to higher heat removal from condenser by the water, and leads to sub cool refrigerant, which contributes to rise in the COP of refrigerator. In this way, the heat pump demands more input with increased cooling load, thus the increase in COP. In other words, increasing the feed water flow rate results to higher heat removal from condenser, thereby increasing the heating demand from the condenser and consequently the increase in the COP of the heat pump. The COP of the heat pump is also observed to decrease with increase in condenser water temperature. This behavior may be attributed to the fact that the refrigeration effect decreases as condenser water temperature increases. These trends can easily be explained from the P-h diagram[115], which shows that the higher the condenser temperature, the lower the refrigeration effect, and consequently the lower the COP of the heat pump. The chilled water flowrate through the evaporator shows marginal effect on the COP of the heat pump, with higher water flowrate in the evaporator providing slightly higher COP. High chilled water flowrate leads to higher heat removal from the water by the refrigerant flowing through the evaporator, and consequently increases the heating load at the condenser, thereby increasing the COP of the system. Increasing feed water flowrate from 2.5L/min to 16L/min lead to about 21% increment in COP of the system on average, while mean percentage increment in COP is about 20% when the hot feed water temperature is decrease from 40ºC to 30 ºC.

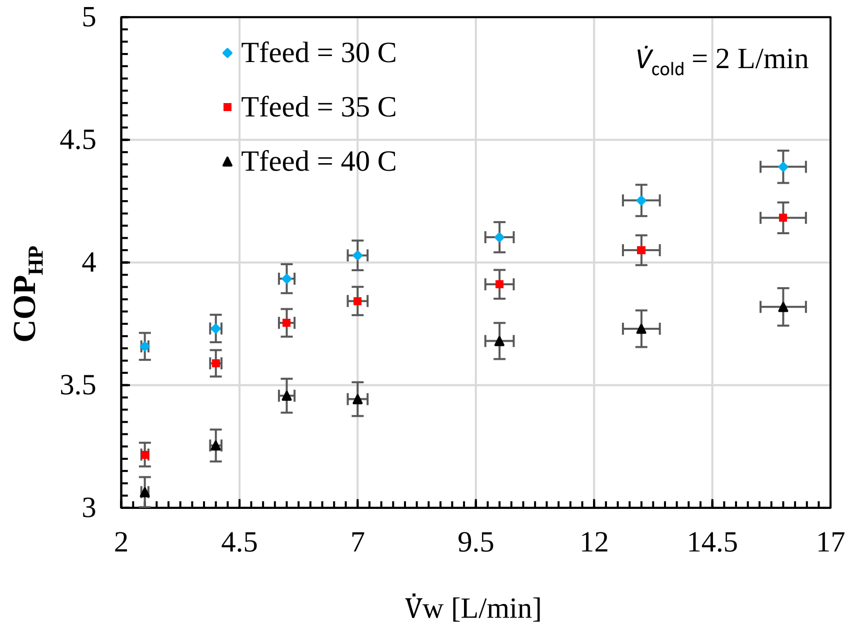

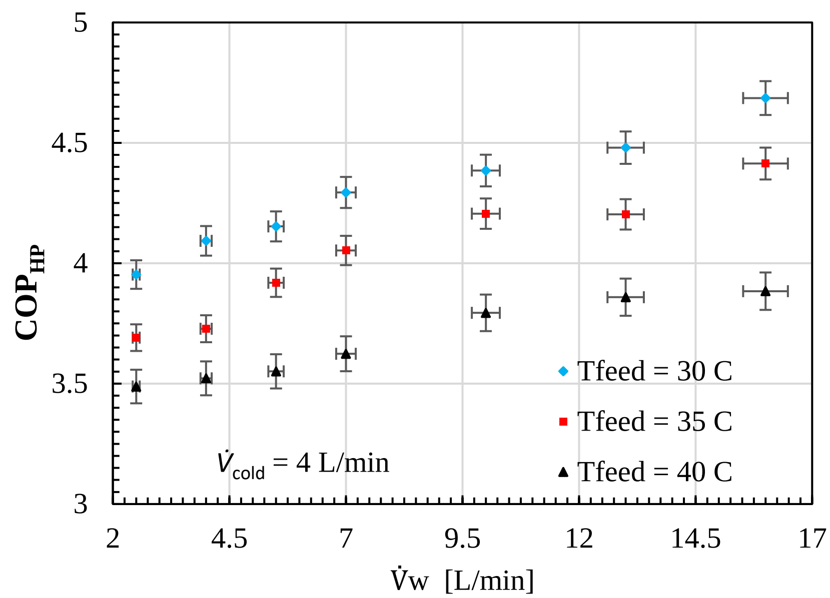

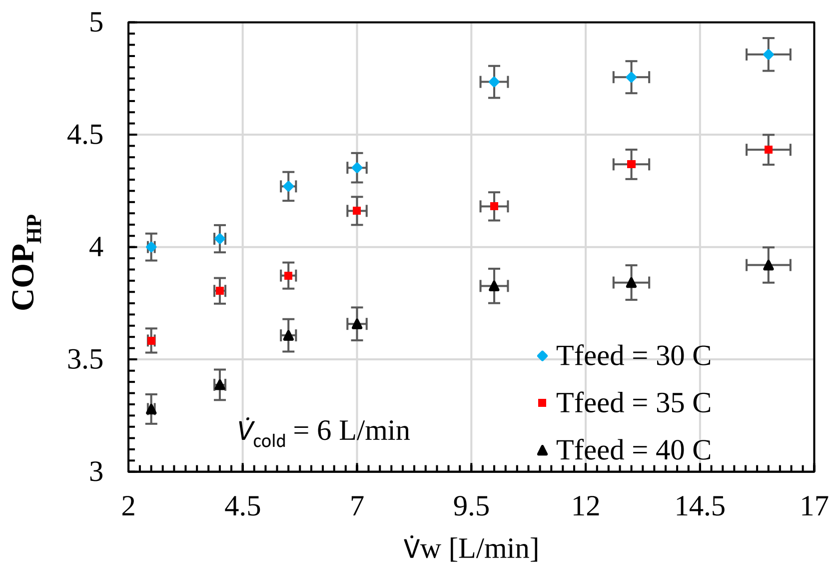

Figure 7. 3: Variation of COP with feed water flowrate, Hot Feed temperature and Chilled water flowrate

Figure 7.4 displayed the variation of water temperature differences in condenser and evaporator with MR, hot feed temperature and chilled water flowrate. From Figure 7.4, $\Delta T_{Cond} = T_{w,out} - T_{w,in}$, which is the temperature difference between outlet water and inlet water, while $\Delta T_{Evap} = T_{w,in} - T_{w,out}$ (inlet water temperature minus the outlet water temperature). The expression for mass flowrate ratio (MR) is given in Eq. (16), where mass flowrate of air is kept constant in the present study. Therefore, variation in MR is a direct effect of variation in feed saline water mass flow rate. As noticed from Fig. 7.4, decreasing MR leads to increase in ΔT_{Cond} as a result of increase in $T_{w,out}$. At low MR, there is high residence time of water flowing through the condenser. This allows the water to gain more heat from the refrigerant, therefore, the increase in ΔT of hot water. At high feed MR, the outlet temperature of the water leaving the condenser decreases and hence the decrease in ΔT of hot water. In another observation (for ΔT_{Evap}), a high flowrate of feed water (MR) results in high Reynolds number and so high heat transfer coefficient due to better mixing in the thermal boundary layer. Thus, at high condenser water flow rate, maximum heat it absorbed from the refrigerant, leading to a lower temperature of the liquid refrigerant exiting the condenser. Consequently, refrigerant of low quality saturated mixture enter the evaporator at lower temperature after throttling, which resulted in higher energy absorption from the evaporator water (higher cooling load), and hence lower water temperature exiting the evaporator, and thus, the increase in ΔT_{Evap}.

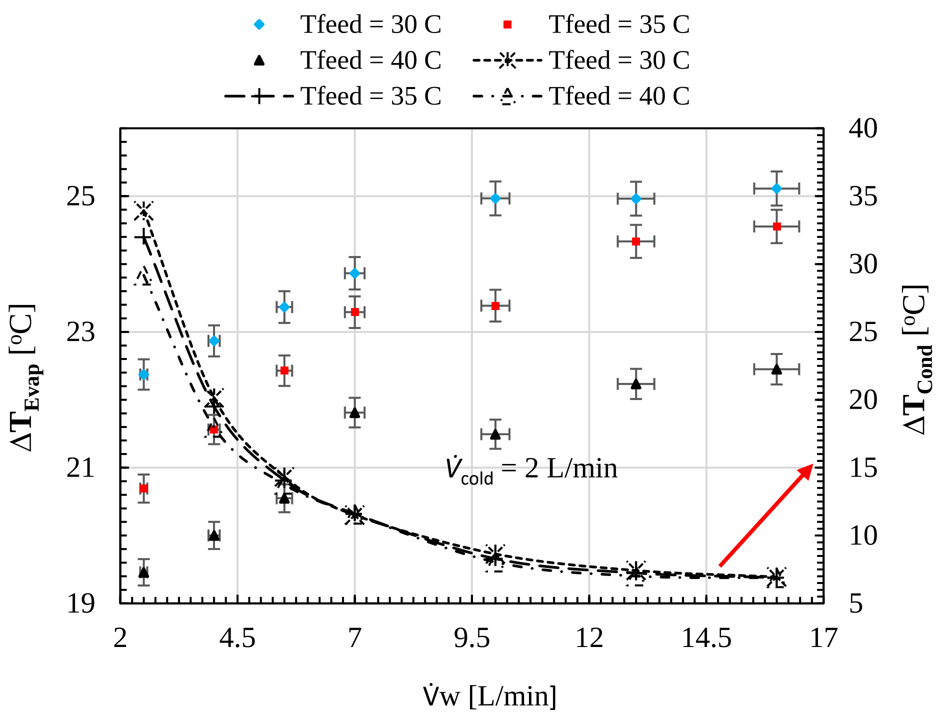

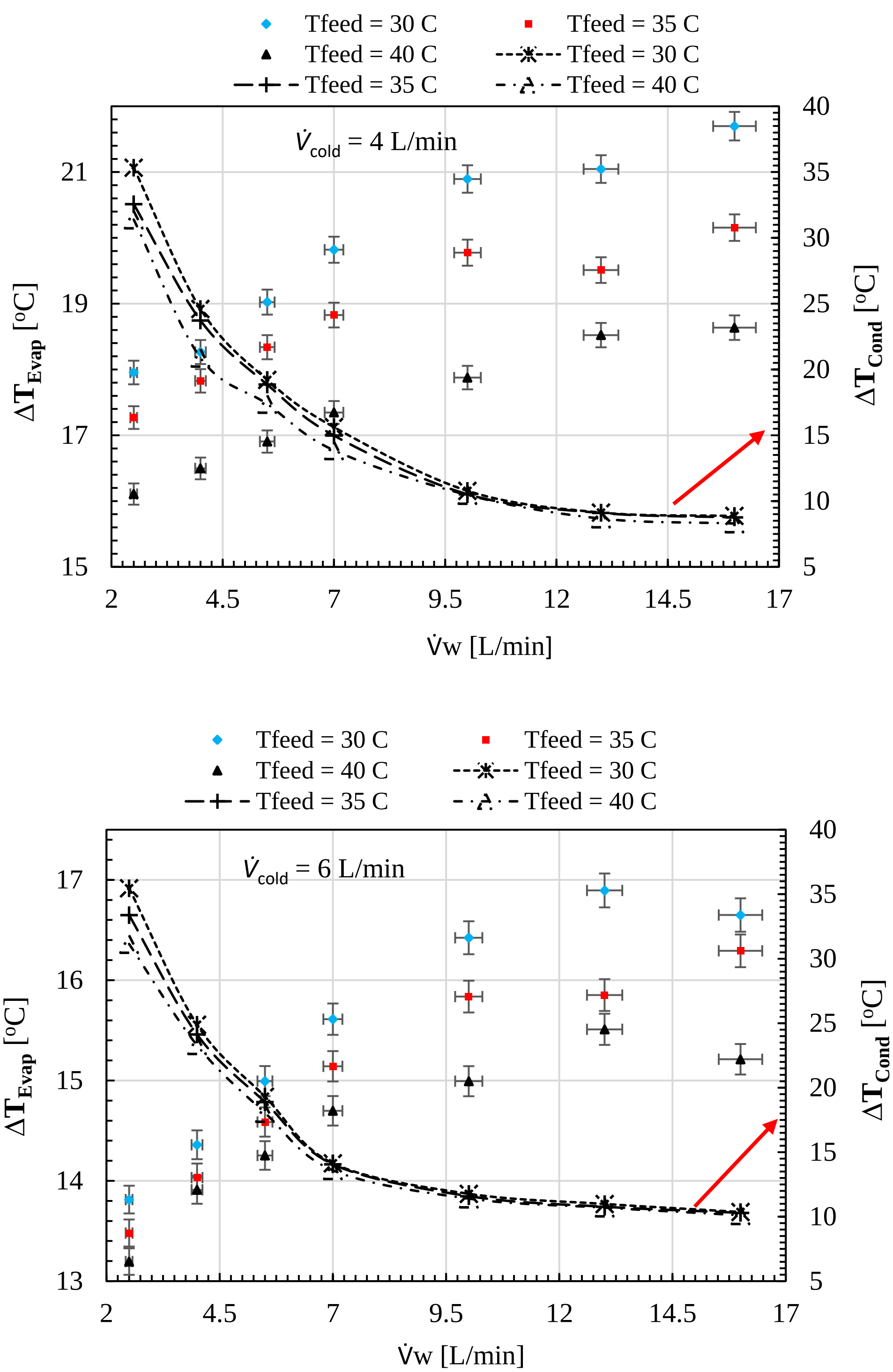

Figure 7. 4: Effect of MR, Hot Feed temperature and Chilled water flowrate on Condenser and Evaporator Temperature Difference

It can also be noticed that low feed inlet water temperature gives higher temperature difference for both the condenser and evaporator. The reason for this trend can best be explained using the P-h diagram [115], where lower evaporator and condenser temperatures leads to higher refrigeration effect, and consequently higher temperature differences. The maximum temperature difference between the inlet and outlet of condenser is 35.5 ^{o}C, obtained at hot water flowrate, feed inlet temperature and chilled flowrate of 2.5L/min, 30 ^{o}C and 6 L/min respectively, and that for evaporator is 25.1 ^{o}C, attained at hot water flowrate, feed inlet temperature and chilled flowrate of 16L/min, 30 ^{o}C and 2 L/min respectively.

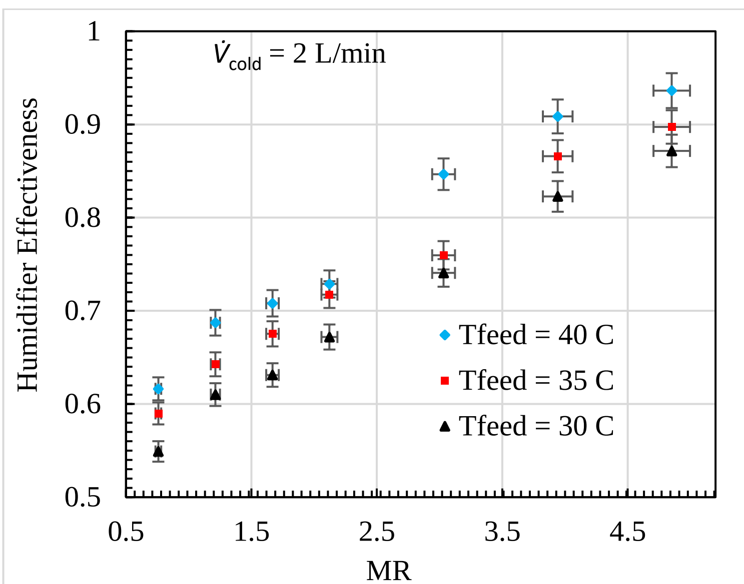

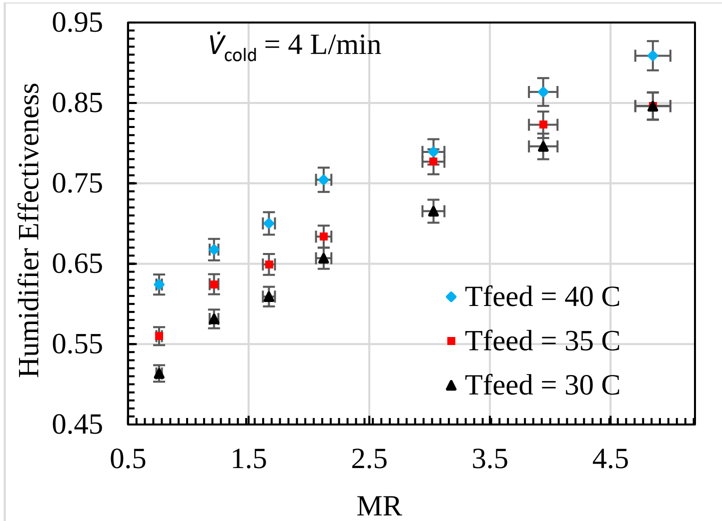

$\dot{V}_{cold}$ = 4 L/min
Humidifier Effectiveness
0.95
0.85
0.75
0.65
0.55
0.45
0.5
1.5
2.5
3.5
4.5
MR
Tfeed = 40 C
Tfeed = 35 C
Tfeed = 30 C

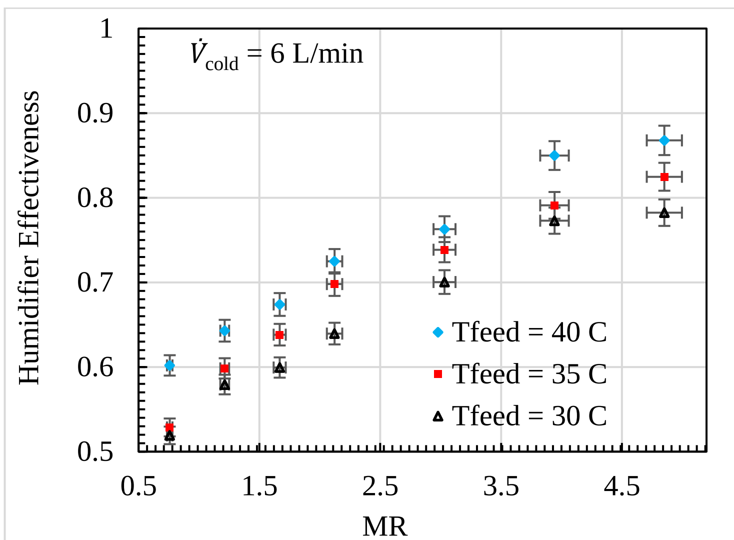

$\dot{V}_{cold}$ = 6 L/min
Humidifier Effectiveness
1
0.9
0.8
0.7
0.6
0.5
0.5
1.5
2.5
3.5
4.5
MR
Tfeed = 40 C
Tfeed = 35 C
Tfeed = 30 C

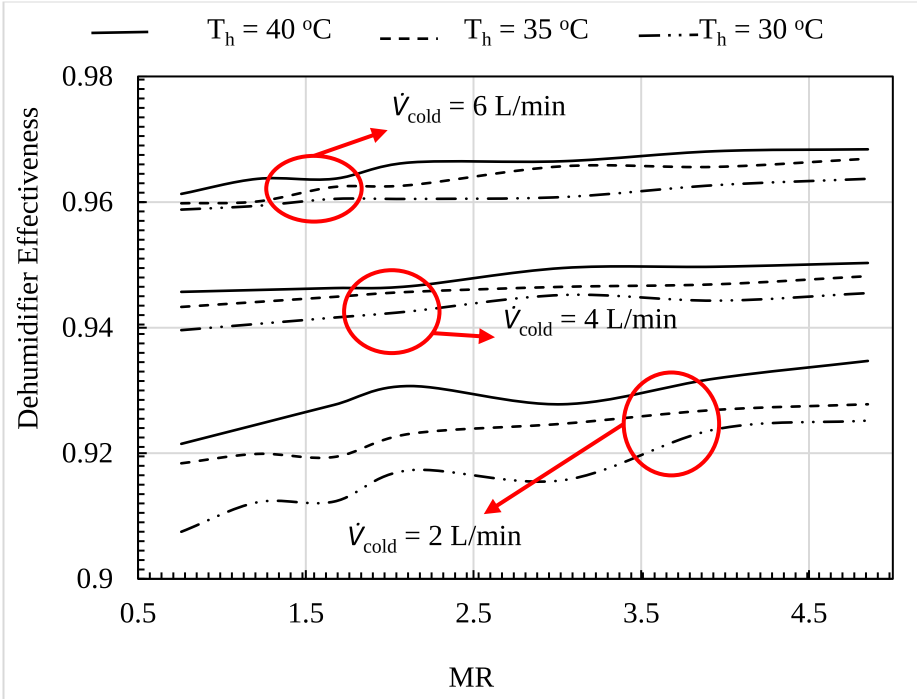

Figure 7. 5: Influence of MR, Hot Feed temperature and Chilled water flowrate on Humidifier and Dehumidifier Effectiveness

It can be observed from Figure 7.5 that the feed water temperature has direct correlation with the effectiveness of both humidifier and dehumidifier. Higher inlet feed water temperature enhances the humidifier and dehumidifier effectiveness. High humidifier effectiveness corresponds to efficient humidification process and more cooling of feed water to a low temperature of the discharged brine. At high feed water temperature, the difference in temperatures between the discharged brine and the feed stream increases, which elevates the enthalpy/energy difference, and hence the increase in the humidifier effectiveness. The increase in the humidifier effectiveness with increase in feed water temperature can also be attributed to the fact that air in the humidifier gained more heat from the hot feed water (efficient cooling of brine), and improve its moisture carrying capacity. The humidified air exit the humidifier at an elevated temperature, leading to a better heat and mass transfer which gives efficient operation of the humidifier and hence the improvement in effectiveness of humidifier. Similarly, high feed temperature leads to high dehumidifier effectiveness because of high temperature of saturated air entering the dehumidifier. The humidified air can better be condensed at an elevated temperature because of high temperature difference between the cooling water in evaporator and the hot humidified air (better heat exchange), which gives to higher temperature of cooling water exiting the dehumidifier, and consequently high dehumidifier effectiveness. In other words, low dehumidifier effectiveness means that the dehumidifier cannot adequately cool and dehumidify the circulated saturated air.

Another important findings from the presented results is the fact that higher MR leads to higher the effectiveness of both humidifier and dehumidifier. This shows that both humidifier and dehumidifier effectiveness are also influenced by the mass flowrate ratio of the working fluids of HDH cycle (water to air ratio). This behavior may be attributed to adequate wetting of the packing material with higher flow rates, which leads high vapor generation (in humidifier) and high vapor condensation (in dehumidifier). This enhances heat mass transfer coefficient and improves the humidification process (higher degree of air saturation with water vapor) and elevates the temperature of humidified air exiting the humidifier, and consequently better condensation and high dehumidifier effectiveness.

Cooling water flowrate is noticed to marginally influenced the humidifier effectiveness and significantly affect the dehumidifier effectiveness. This is expected because the functionality of humidifier component is independent of cooling water flowrate, while dehumidifier component greatly depend on cooling water flowrate. High cooling water flowrate increases the degree of vapor condensation process, since the rate of vapor condensation is increase with increase in cooling water flowrate. Increasing cooling water flowrate increases cooling water temperature leaving the evaporator of heat pump, which leads to high temperature of cooling water exiting the dehumidifier, and hence the increase in dehumidifier effectiveness. On average, the percentage rise in humidifier effectiveness when the feed water flowrate is increase from 2.5 to 16 L/min is about 53%, and when the feed temperature is increase from 30 ^{o}C to 40 ^{o}C is about 12%. Whereas the average percentage increment in dehumidifier effectiveness is 0.89% and 0.78% for the same range of feed flowrate and feed temperature respectively.

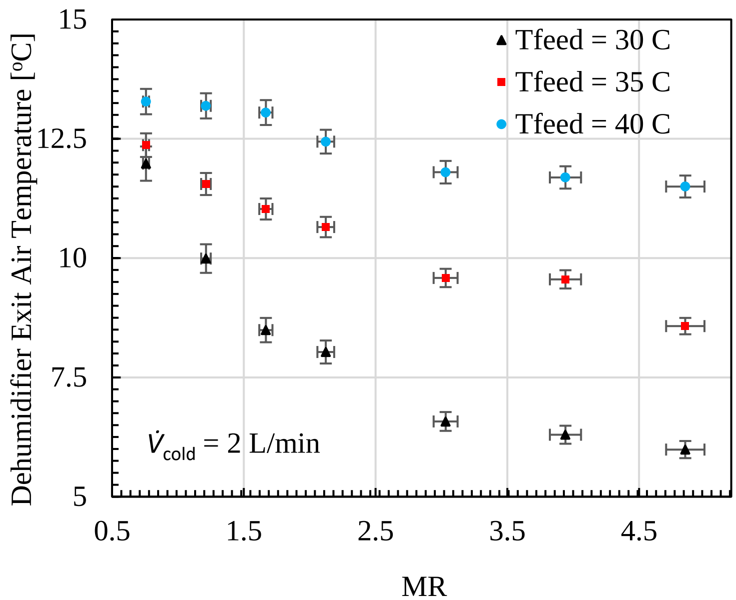

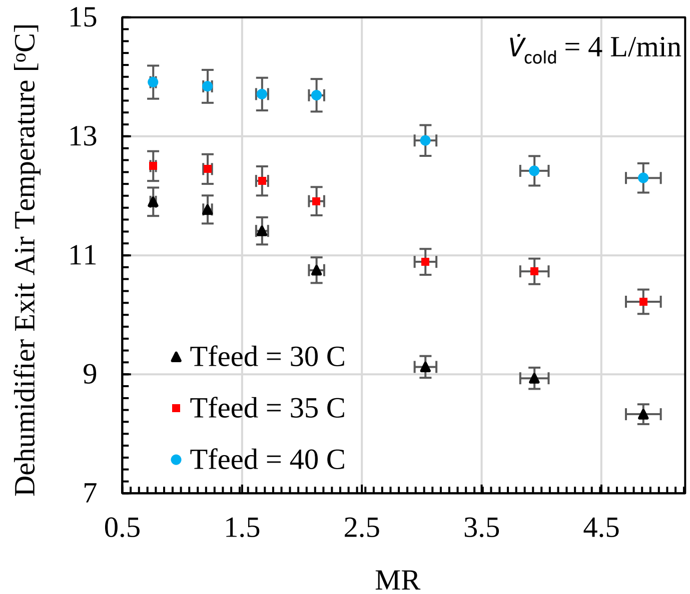

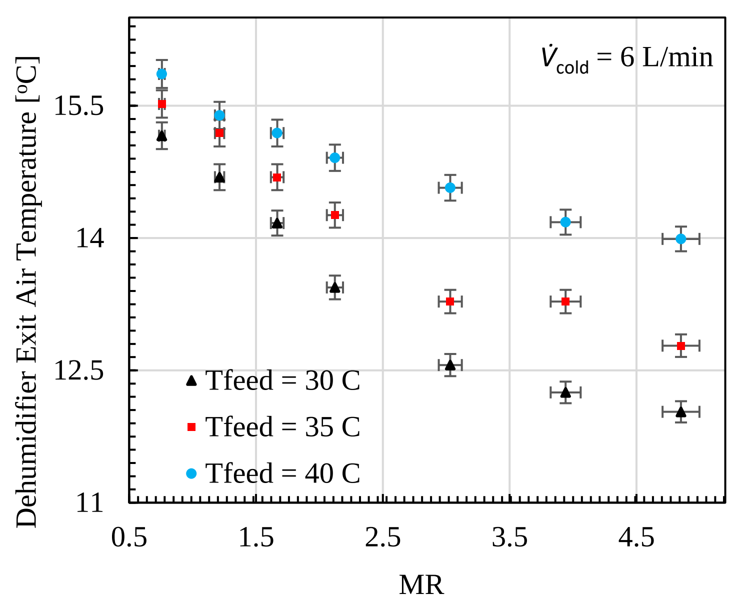

Figure 7. 6: Impact of MR, Hot Feed temperature and Chilled water flowrate on Dehumidifier Exit air temperature

The influence of hot feed temperature, feed water flowrate and chilled water flowrate on dehumidifier exit air is presented in Figure 7.6. It can be noticed that the temperature of the air exiting the dehumidifier increases with increase in the inlet feed water temperature, because of high saturated air temperature leaving the humidifier to the dehumidifier. Increasing MR decreases the air temperature exiting the dehumidifier. This may be attributed to the fact that as MR increases, the temperature of feed water leaving the condenser decreases because of less residence time of feed water in the condenser. Lower hot feed water heats up the air in the humidifier to a relatively low temperature, and consequently lower air temperature exiting the dehumidifier. Cooling water flowrate is seen to slightly influence the temperature of dehumidified air exiting the dehumidifier. High cooling water flowrate yields high chilled water temperature due to less residence time, thereby leading to higher air temperature exiting the dehumidifier. The dehumidifier exit air temperature is noticed to drop by about 32.45% on average when the feed water flowrate is increase from 2.5 to 16 L/min, and rises by about 33.1% when the feed temperature is increase from 30 ^oC to 40 ^oC.

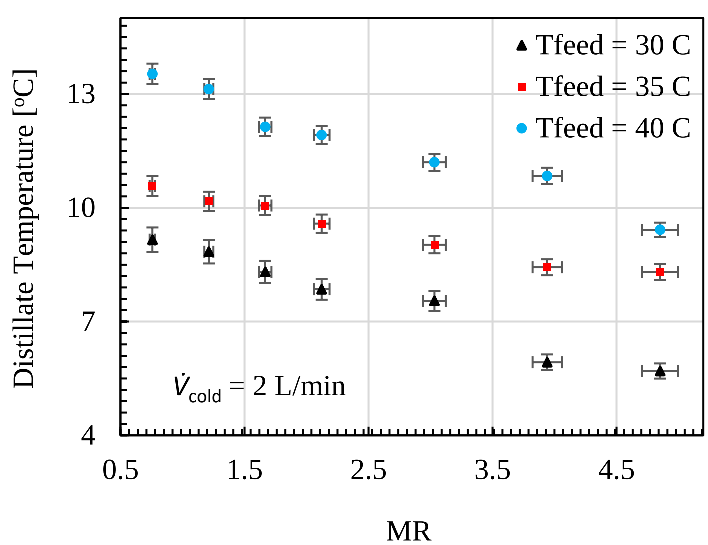

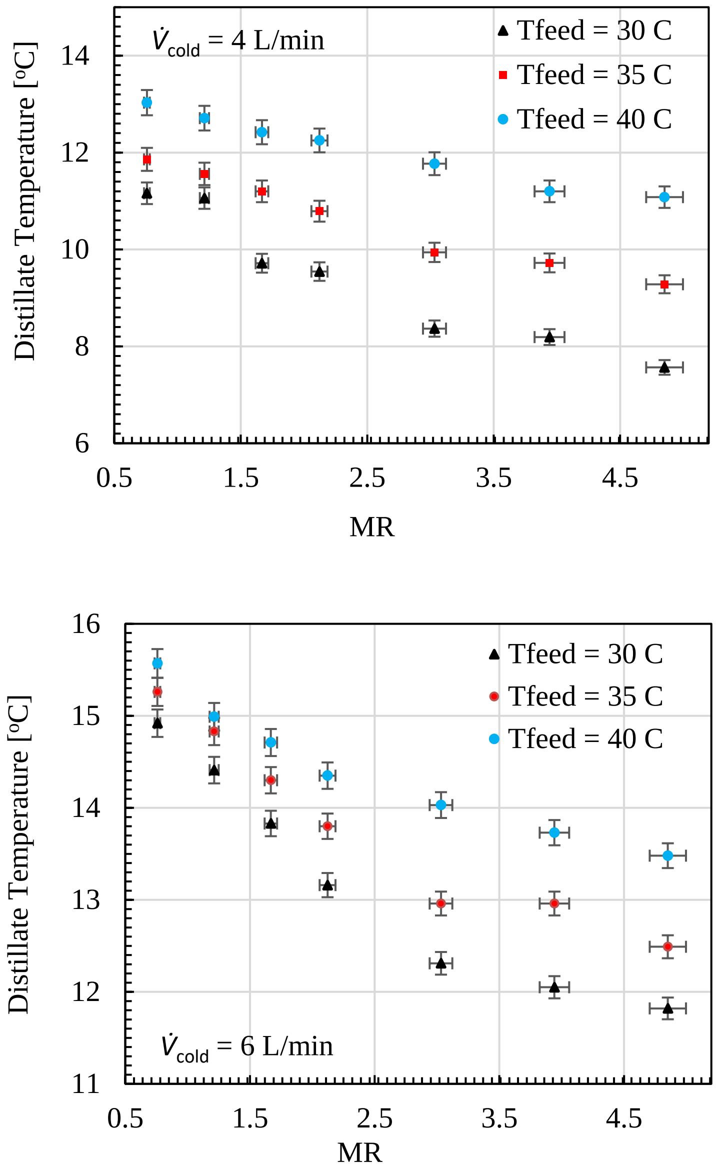

Figure 7. 7: Variation of Distillate Temperature with MR, Hot Feed temperature and Chilled water flowrate

The impact of hot feed temperature, chilled water flowrate and MR on the distillate temperature is illustrated in Figure 7.7. The temperature of the condensate (the produced freshwater) has been found to be influenced by MR, feed water temperature, and the cooling water flowrate. The distillate temperature was found to decrease with increase in MR as a results of decrease in feed water temperature with increase in MR, which leads to low temperature of hot air entering and exiting the dehumidifier, and consequently the decrease in the temperature of the condensate. The distillate temperature was also found to increase with increase in feed water inlet temperature, because of hot and high vapor generation in the humidifier, which increases the temperature of the saturated air exiting the humidifier. Higher cooling water flowrate has also been observed to increase the distillate temperature, due to higher temperature of cooling water entering and leaving the dehumidifier. The mean percentage decrement in condensate temperature when the feed water flowrate is increase from 2.5 to 16 L/min is about 32.06%. While the mean percentage increment in condensate temperature is about 31.81% when the feed temperature is increase from 30 ^{0}C to 40 ^{0}C, and condensate temperature increases by about 55.89% on average when the chilled water flowrate increases from 2 to 6 L/min.

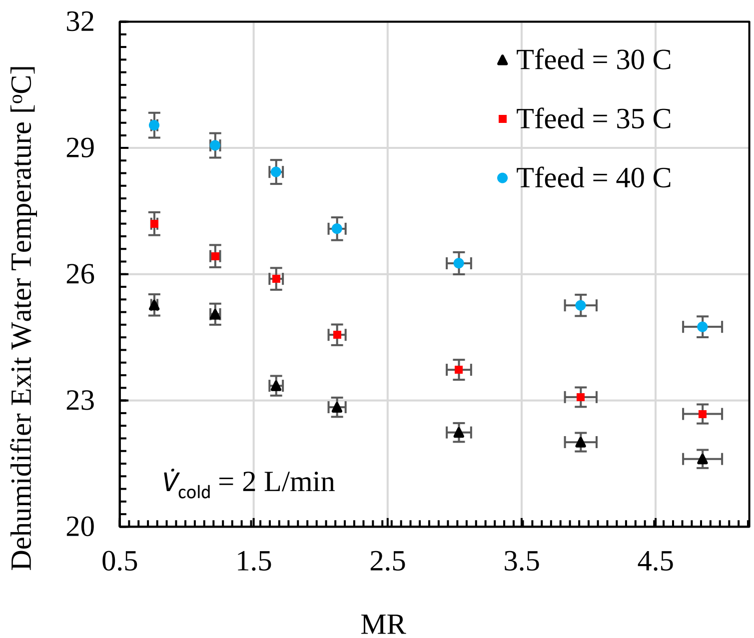

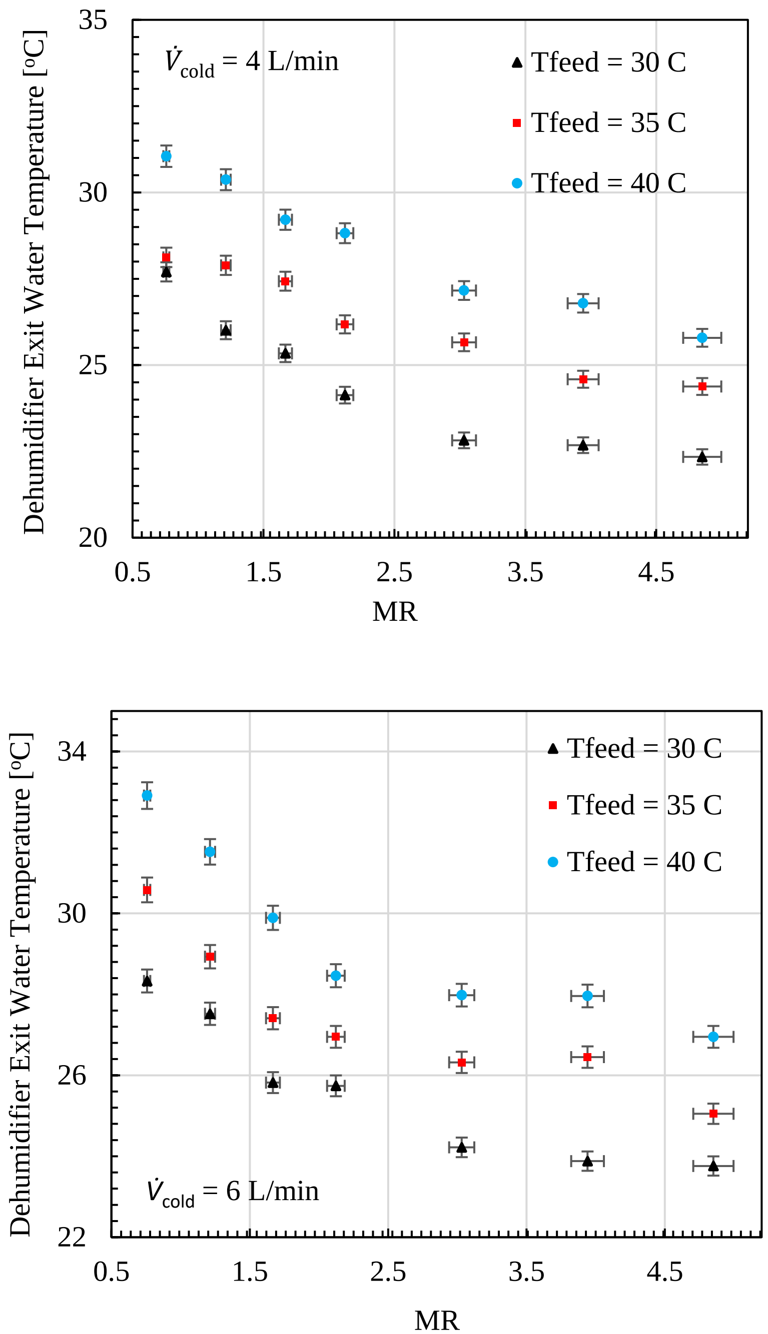

Figure 7. 8: Effect of MR, Hot Feed temperature and Chilled water flowrate on Dehumidifier Exit water temperature.

The variation of exit water temperature from the dehumidifier with the MR, hot feed temperature and chilled water flowrate is demonstrated in Figure 7.8. The cooling/chilled water temperature leaving the dehumidifier is observed to decrease with increasing MR, and increases with increasing feed water temperature and cooling water flowrate. The reasons for these behavior may be attributed to temperature of saturated air and the temperature of chilled water entering the dehumidifier. In other words, high temperature of chilled water as a result of high cooling water flowrate is responsible for the increase in the dehumidifier exit water temperature. The dehumidifier exit water temperature is observed to drop by about 19.93% on average when the feed water flowrate is increase from 2.5 to 16 L/min, and rises by about 16.18% when the feed temperature is increase from 30 ^{o}C to 40 ^{o}C. While increasing the chilled water flowrate from 2 to 6 L/min increases the mean dehumidifier exit water temperature by about 22.34%.

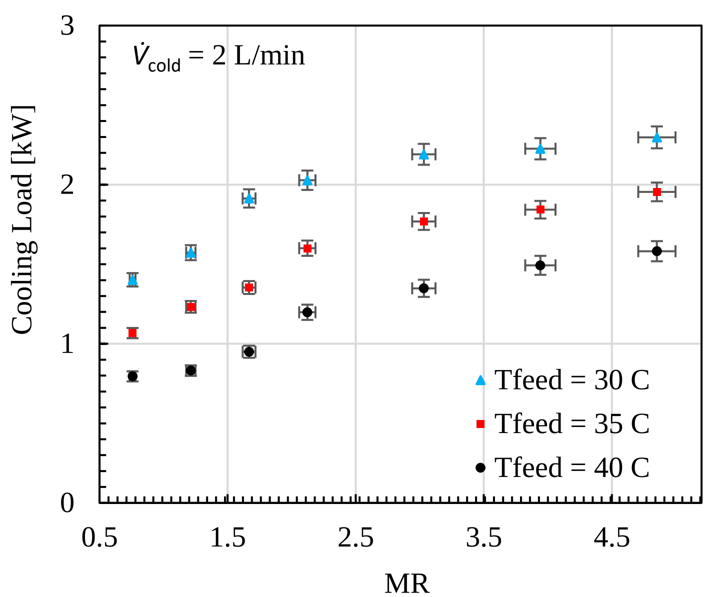

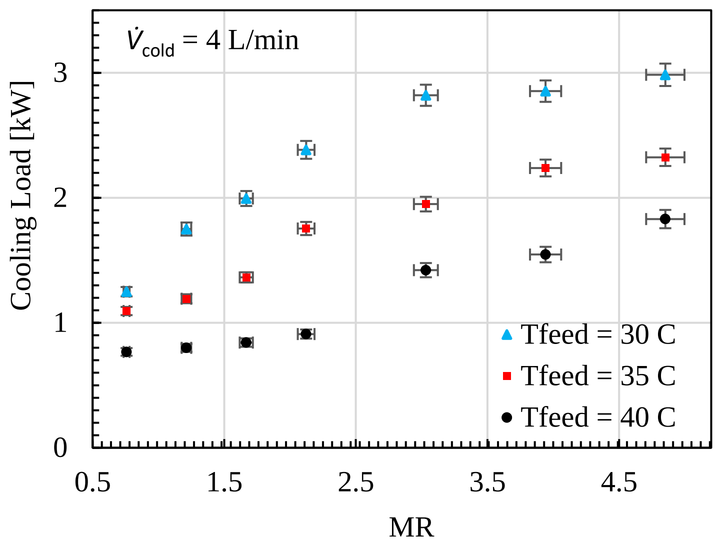

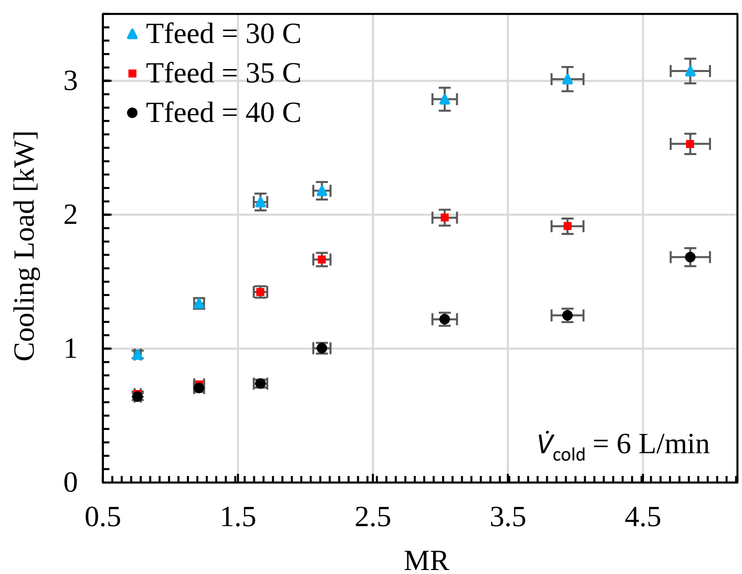

Figure 7. 9: Influence of MR, Hot Feed temperature and Chilled water flowrate on Cooling Load

Presented in Figure 7.9 is the effect of MR, hot feed temperature and chilled water flowrate on the estimated cooling effect given in Eq. (3). The total available cooling effect is estimated by summing up the cooling loads associated with distillate water, dehumidifier exit air and dehumidifier exit water. These variables are accompany with cooling load as they exit the dehumidifier, because their respective exit temperatures are well below room/reference temperature. It can be noticed that the available cooling energy for space conditioning changes with MR, feed water inlet temperature and cooling water flow rate. The cooling effect is noticed to increase with increasing MR and cooling/chilled water flowrate, and decreases with increasing hot feed water temperature. Decreasing feed inlet water temperature is noticed to increase the cooling effect. At high feed inlet water temperature, air carry more moisture content to the dehumidifier. Therefore, the heat/moisture rejected by the air will be more, resulting in more energy absorption by the chilled water flowing through the dehumidifier, and hence less cooling load/effect available for space cooling. It can also be observed that increasing the MR leads to increase in cooling energy available for space cooling. The reason for this trend can be attributed to the fact that increasing MR lowers the feed water temperature. Low feed water temperature decreases the moisture carrying capacity of air and demand less humidified air cooling in the dehumidifier, leading to more cooling load available for other uses. The available cooling effect is also seen to slightly increase with increase in cooling/chilled water flowrate. Increasing the chilled water flowrate elevates its temperature as it exit the evaporator. This in turn leads to high chilled water leaving the dehumidifier, and less available cooling effect. The mean percentage rise in cooling effect when the feed water flowrate is increase from 2.5 to 16 L/min is about 144%, whereas the mean percentage reduction in cooling effect is about 96% when the feed temperature is increase from 30 ^{o}C to 40 ^{o}C. The current unit is capable of producing a maximum cooling load of 3.07kW as the secondary benefit. This cooling effect is good enough to condition a space having an area between 40 to 50 square meters.

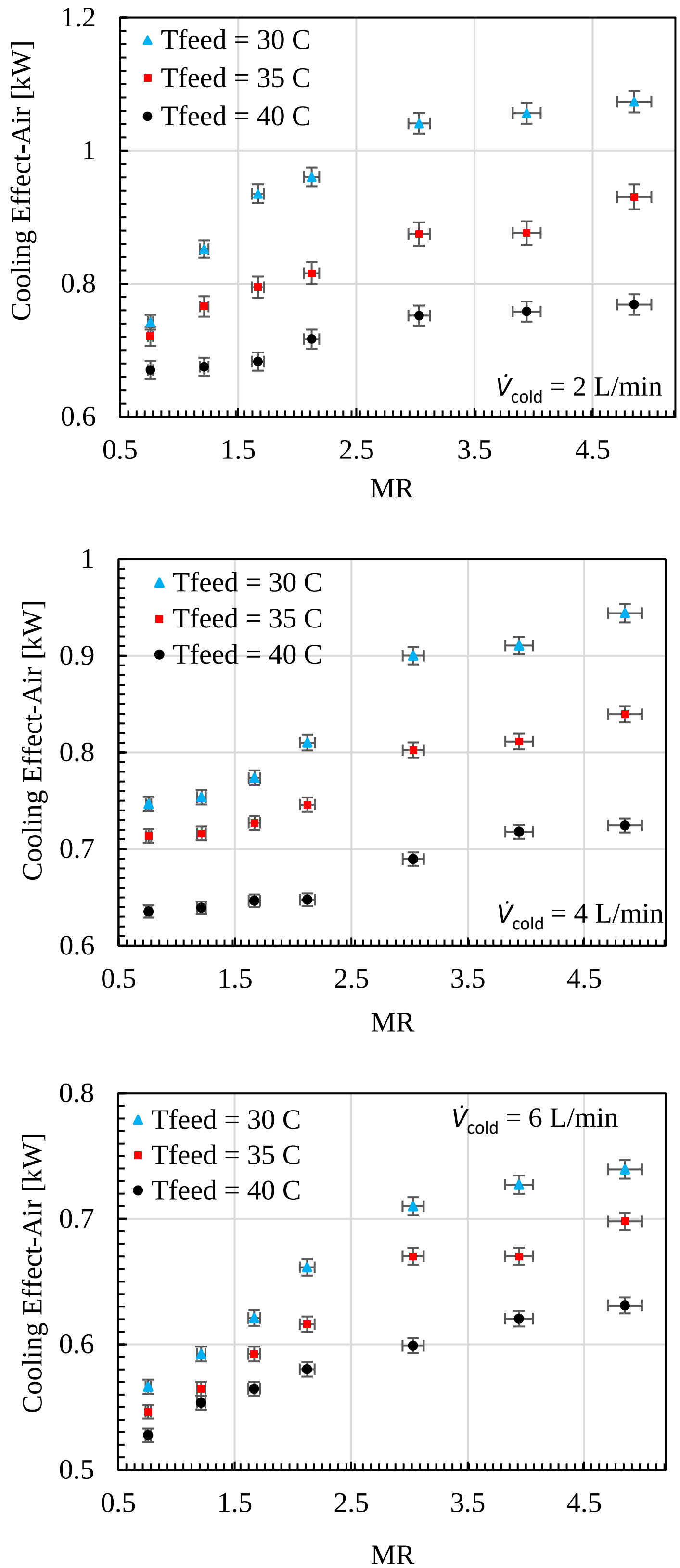

Figure 7. 10: Effect of MR, Hot Feed temperature and Chilled water flowrate on Exit Air Cooling Load

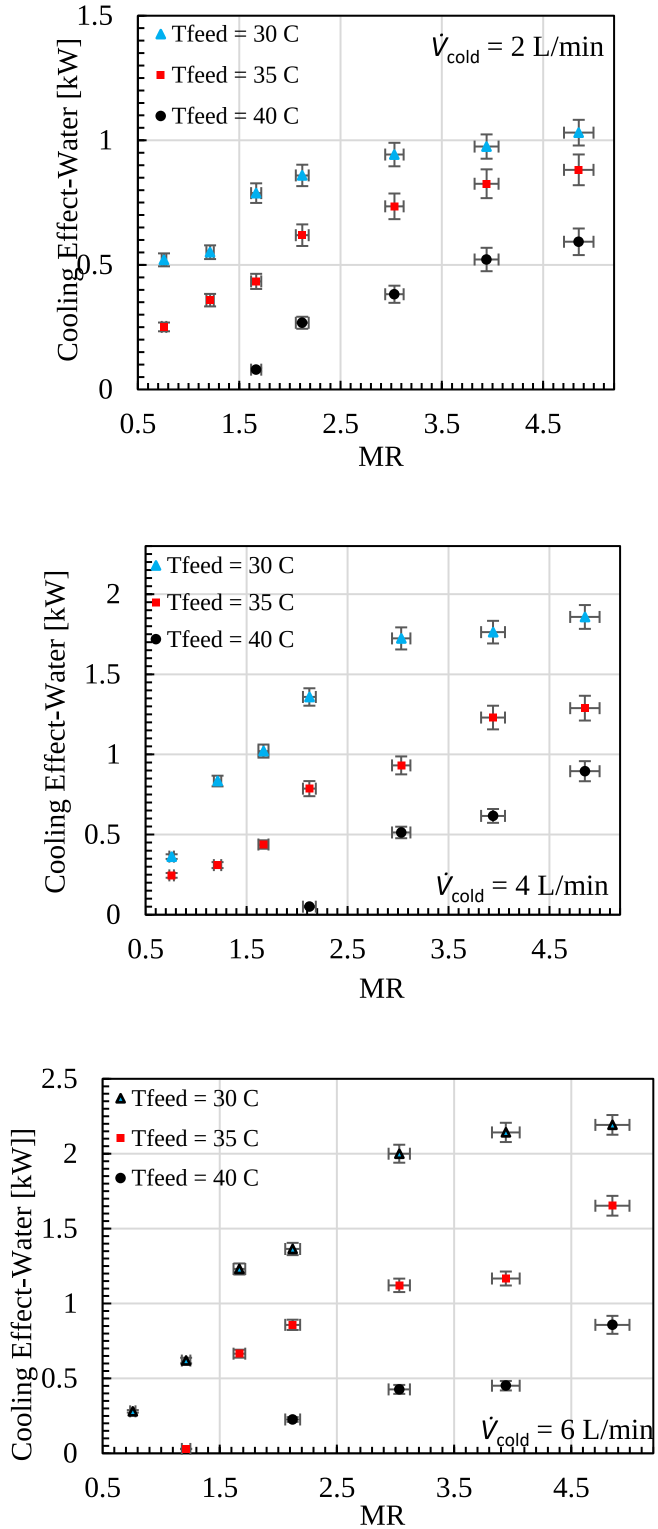

Figure 7. 11: Impact of MR, Hot Feed temperature and Chilled water flowrate on Exit Water Cooling Load

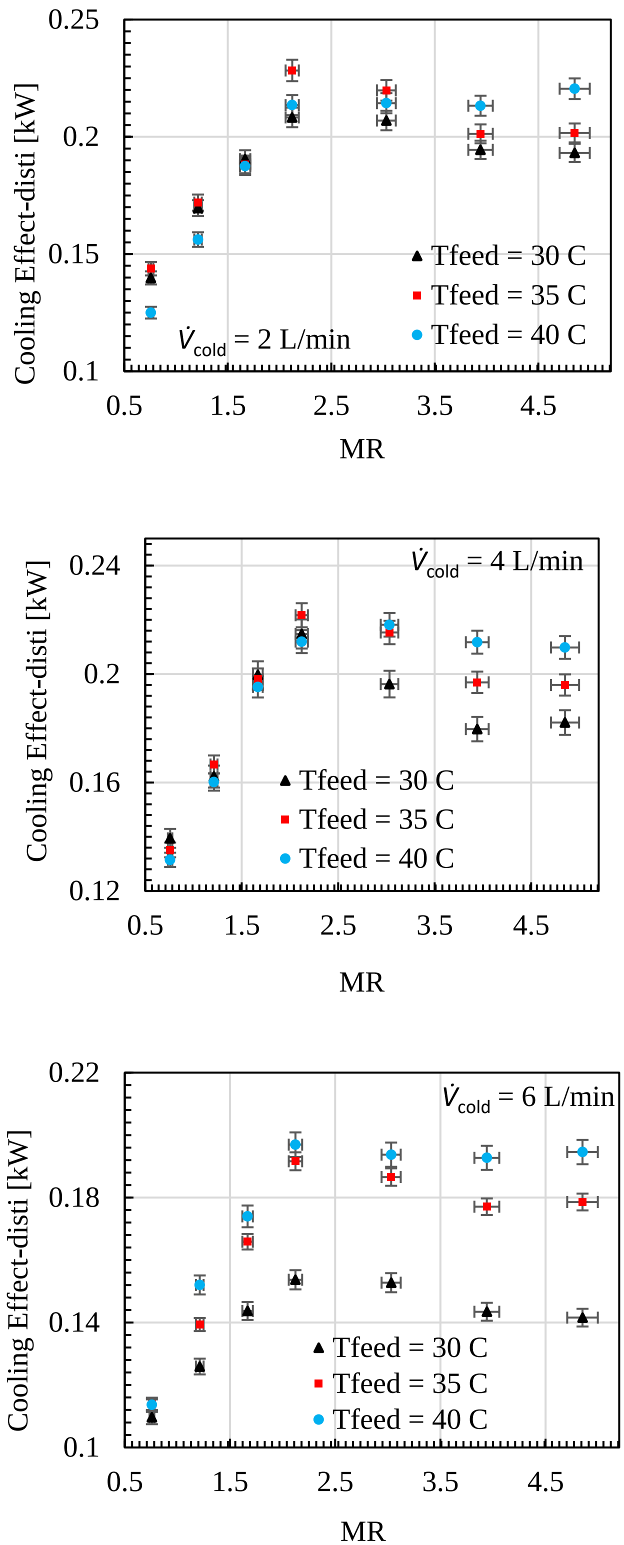

Figure 7. 12: Impact of MR, Hot Feed temperature and Chilled water flowrate on distillate Cooling Load

The individual contribution of dehumidifier exit air, dehumidifier exit water and distillate to the total/overall cooling effect is demonstrated in Figs. 7.10 – 7.12. Figure 7.10 portrayed the cooling effect for dehumidifier exit air and Figure 7.11 showed cooling load for dehumidifier exit water, while Figure 7.12 represents the cooling load associated with distillate. It is worth mentioning that dehumidifier exit air and chilled water exiting the dehumidifier provides the highest contribution to the cooling effect. On average, the percentage contribution of dehumidifier exit air and that of exit water are 54.92% and 34.58% respectively for chilled water flow rate of 2L/min. For chilled water flowrate of 4L/min, dehumidifier exit air and dehumidifier exit water contributes 50.05% and 41.99% respectively, while for the chilled water flowrate of 6L/min, the percentage contribution of dehumidifier exit air and dehumidifier exit water to the total cooling effect are 47.75% and 47.22% respectively.

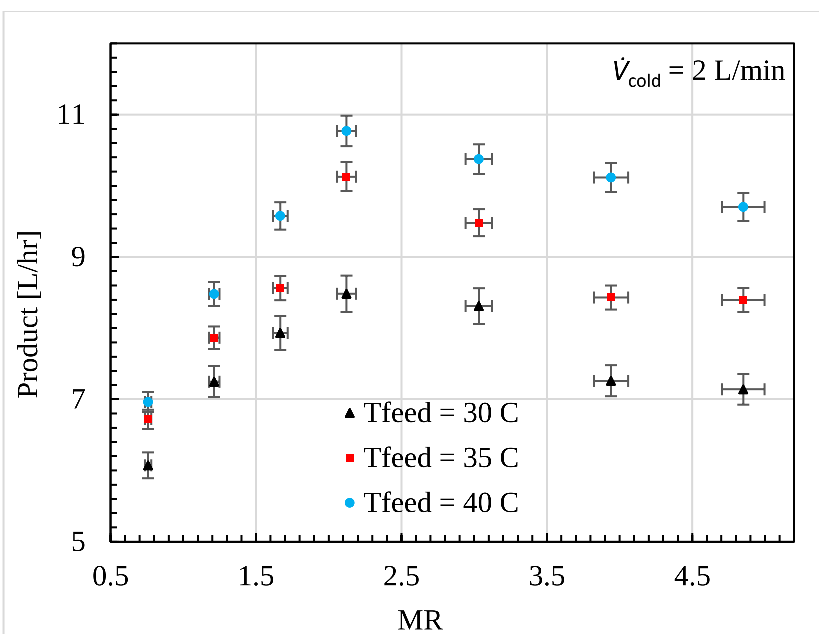

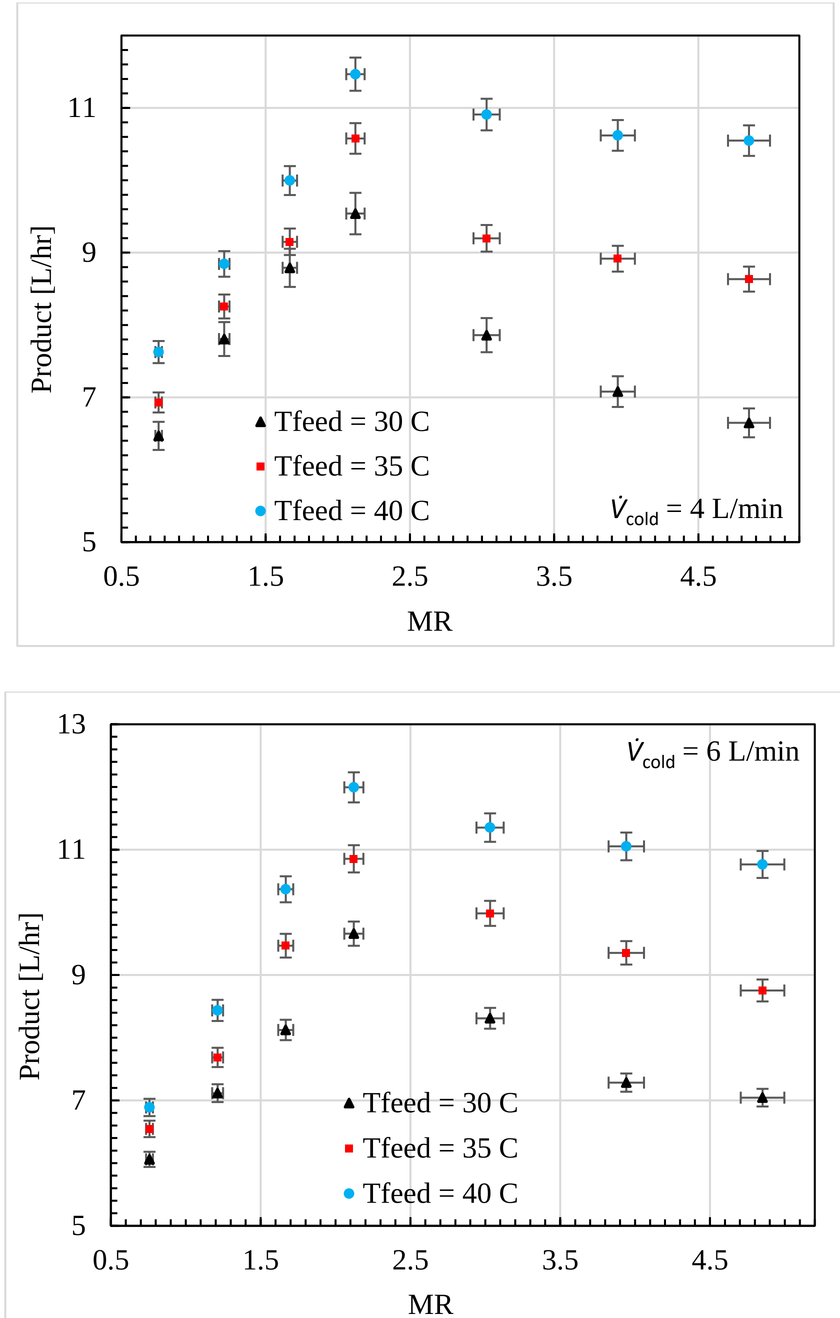

Figure 7. 13: Impact of MR, Hot Feed temperature and Chilled water flowrate on System productivity

The variation of system produced distillate with system operating parameters is depicted in Figure 7.13. Optimum MR occur for the effect of MR on the system productivity. The distillate was found to initially increase with increase in MR up to an optimum MR, due to increase in vapor generation from the feed water and absorption by the air. The declines in productivity after the optimum MR may be attributed to the flooding of the system because of much water sprayed in the humidifier as compared to the flowrate of the circulating air. Increasing the hot feed water enhances the system productivity because of increase in air capacity to absorb more moisture content, thereby increase in desalinated water. Obviously, there is little or no improvement in the system productivity with increase in cooling/chilled water flowrate, since the minimum system chilled water flowrate is enough to provide the necessary cooling surface for vapor condensation. Increasing the chilled water flowrate encourage high vapor condensation. However, this effect is cancelled out by the increase in chilled water temperature as a result of high flowrate of chilled water. The highest and least freshwater production from the proposed desalination system is about 11.99 L/hr and 6.06 L/hr respectively, corresponding to 288.8 and 145.4 liters of freshwater per day respectively. These values are obtained when the system is operating at mass flowrate of 7 kg/min (corresponding to MR of 2.12), feed temperature of 40 ^{o}C and chilled water flowrate of 6 L/min for maximum system productivity, and at feed flowrate of 2.5 kg/min (corresponding to MR of 0.758), feed temperature of 30 ^{o}C and chilled water flowrate of 2 L/min for minimum system productivity.

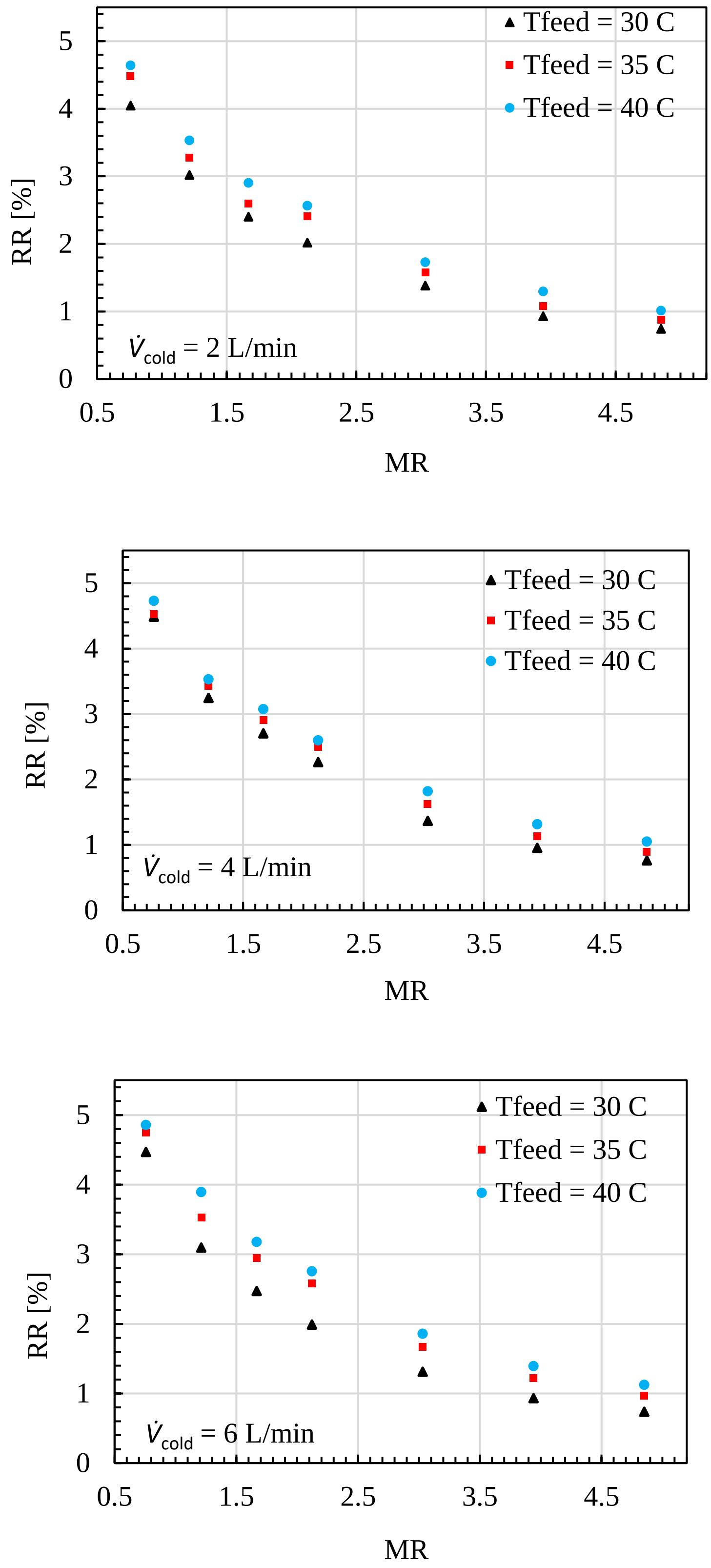

Figure 7. 14: Variation of RR with MR, Hot Feed temperature and Chilled water flowrate

Demonstrated in Figure 7.14 is the influence of chilled water flowrate, MR and hot feed temperature on the system recovery ratio. Recovery ratio (RR) is the ratio of desalinated water flowrate to the hot feed water flowrate. RR is the water conversion capacity of the plant. It can be noticed that RR decreases with increase in MR, and increase with increase in feed water temperature. This is an indication that the amount of freshwater recovered from the saline water at lower mass flowrate ratio is higher than that obtained at higher mass flowrate ratio. Therefore, less amount of fresh water is obtained per feed water flowrate. Chilled water flowrate plays no significant influence on the RR as observed from Figure 7.13 (system productivity). Since the minimum supply chilled water flowrate is enough for condensation. The feed water temperature is seen to affect the RR. Higher feed water temperature gives higher RR due to higher vapor generation/moisture content and consequently higher productivity. The recovery ratio of the water desalination plant is found to decrease by about 410% on average when the mass flowrate ratio, MR is increase from 0.758 to 4.851 (from 2.5 to 16 L/min), and the mean increment on the system recovery ratio is about 28% when the feed temperature is increase from 30 ^{o}C to 40 ^{o}C.

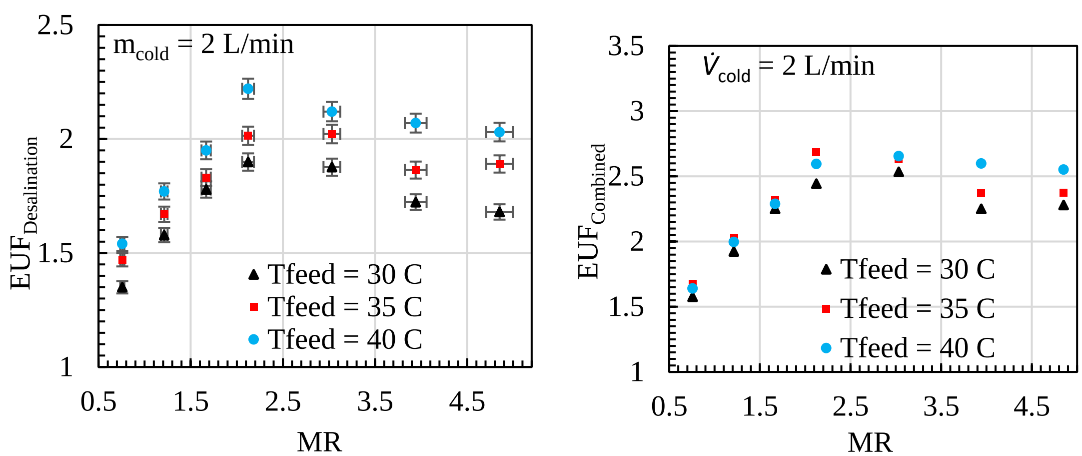

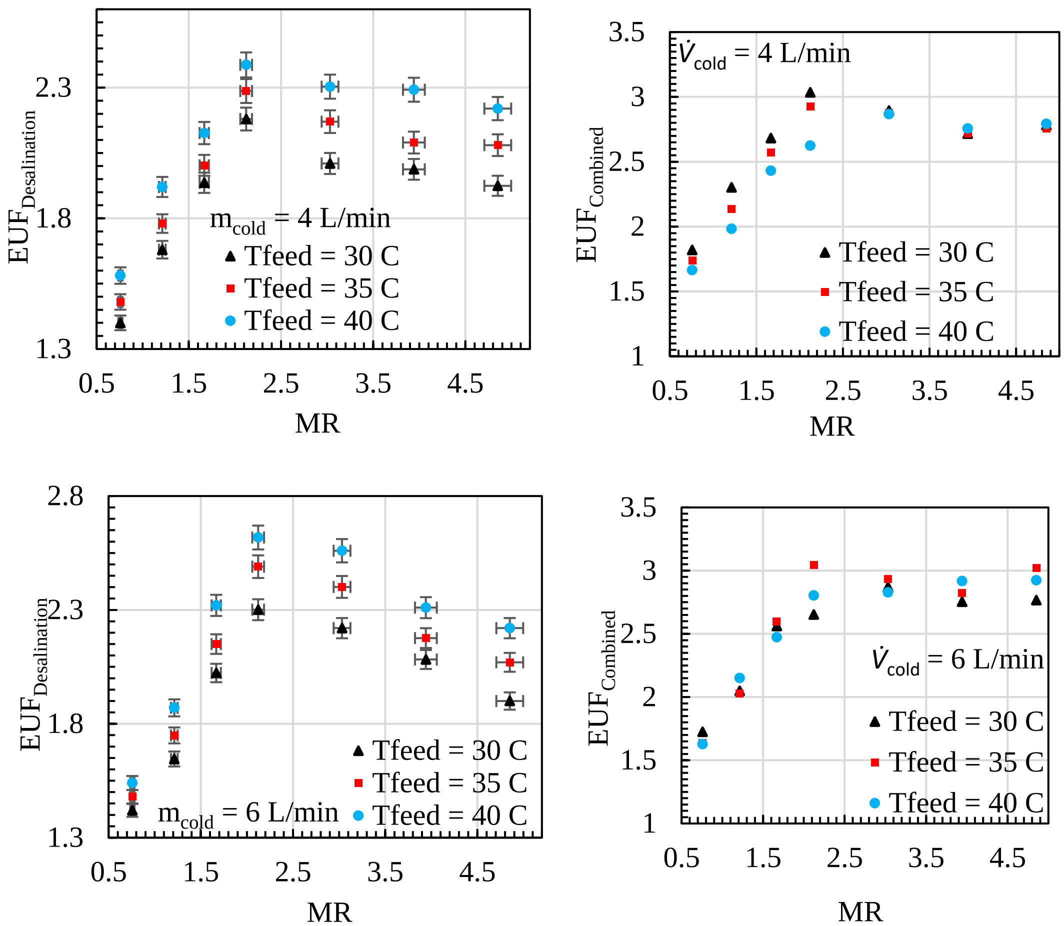

Figure 7. 15: Effect of MR, Hot Feed temperature and Chilled water flowrate on EUF

The variation of system EUF with the MR, hot feed temperature and chilled water flowrate is demonstrated in Figure 7.15. The combined Energy utilization factor ($EUF_{Combined}$) is evaluated based on the useful energies obtainable from the integrated system and the total input energy (electrical energy consumed by the compressor, water pumps and air blower). The useful energies consist of energy for space cooling and desalinated water. The $EUF_{Desalination}$ considered only the useful energy of water desalination. For both $EUF_{Desalination}$ and $EUF_{Combined}$, EUF is noticed to improve with increase in MR to the peak EUF where optimum MR occur, and then decline with further increase in MR. This is the same trends seen in system productivity, which show that EUF is greatly dominated by the system distillation rate. The effects of both feed water temperature and chilled water flowrate are marginal on the system EUF, because of the conflicting effect of productivity and available cooling effect. In other words, high feed water temperature promote system productivity and decreases the available cooling effect, which is responsible for the marginal influence of feed water temperature on the system EUF. The maximum and minimum energy utilization factor for the combined system are found to be 3.05 and 1.58 respectively, while that for the desalination alone are 2.59 and 1.22 respectively. These values were attained at the feed MR of 2.12, feed temperature of 35 ^{o}C and chilled water flowrate of 6 L/min for maximum EUF productivity, and at feed flowrate of 2.5 L/min (MR = 0.758), feed temperature of 30 ^{o}C and chilled water flowrate of 2 L/min for minimum system EUF. Both $EUF_{Desalination}$ and $EUF_{Combined}$ portrayed the advantage of integrating heat pump with HDH system for multiple productions (co-generation system). Obviously from Figure 7.15, the combined system production (freshwater and cooling effect) achieved higher energy utilization when compared to that for water desalination production alone. Respectively, a minimum and maximum of 12.22% and 46.89% improvement in energy utilization is recorded when the integrated HP-HDH unit produces multiple outputs as compared to when it is stand alone for freshwater production.

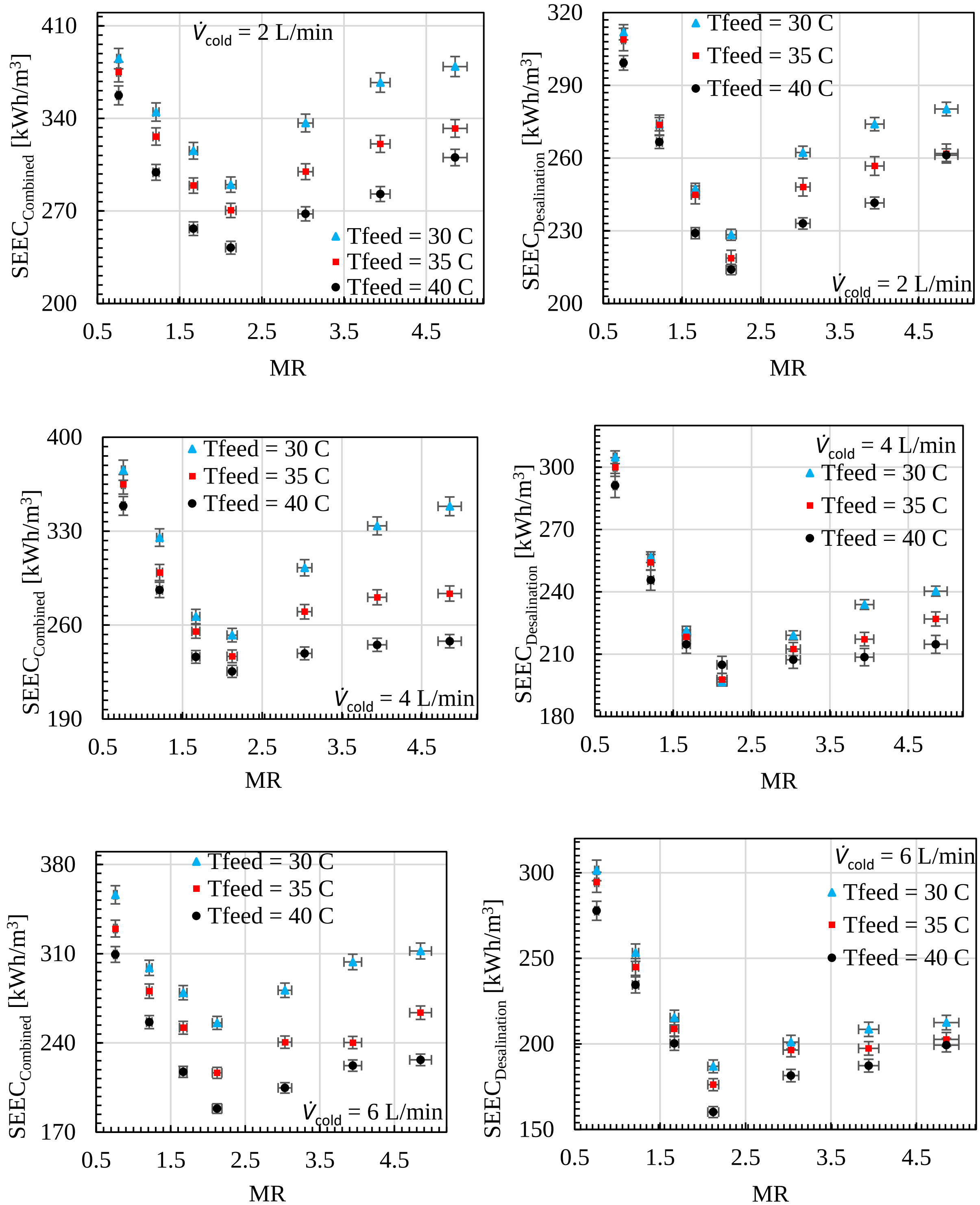

Figure 7. 16: Impact of MR, Hot Feed temperature and Chilled water flowrate on SEEC

The Specific electrical energy consumed to produce one cubic meter of desalinated water changes with chilled water flowrate, hot feed temperature and MR as illustrated in Figure 7.16. The Specific electrical energy consumption is evaluated based on the ratio of compressor power (kW), water pump power (kW) and air blower power (kW) used to desalinate water (meter cube per hour). Both the $SEEC_{Combined}$ and $SEEC_{Desalination}$ are observed to decrease with increase in MR and then increase after optimum MR. The decrease in specific energy consumption with increase in MR is an indication of less electrical energy consumed by the compressor, water pump and air blower, and the improvement in the rate of freshwater production. The specific energy consumption is also seen to decrease with increase in chilled water flowrate, due to higher system productivity at high chilled water flowrate. Increasing the feed water temperature leads to decrease in specific electrical energy consumption of the system, because the system productivity is high at high feed water temperature, and consequently the decrease in specific energy consumption. The minimum and the maximum $SEEC_{Combined}$ for the total system product is found to be about 188.5 kWhr/m^3 and 385 kWhr/m^3 of freshwater respectively, while the lowest and the highest $SEEC_{Desaliantion}$ for freshwater production is found to be about 160.16 kWhr/m^3 and 311.89 kilo-Watt hour per cubic meter of freshwater respectively. Mass flowrate ratio, MR of 2.12, feed temperature of 40 ^oC and chilled water flowrate of 6 L/min are the optimum operating condition at which SEEC is minimized.

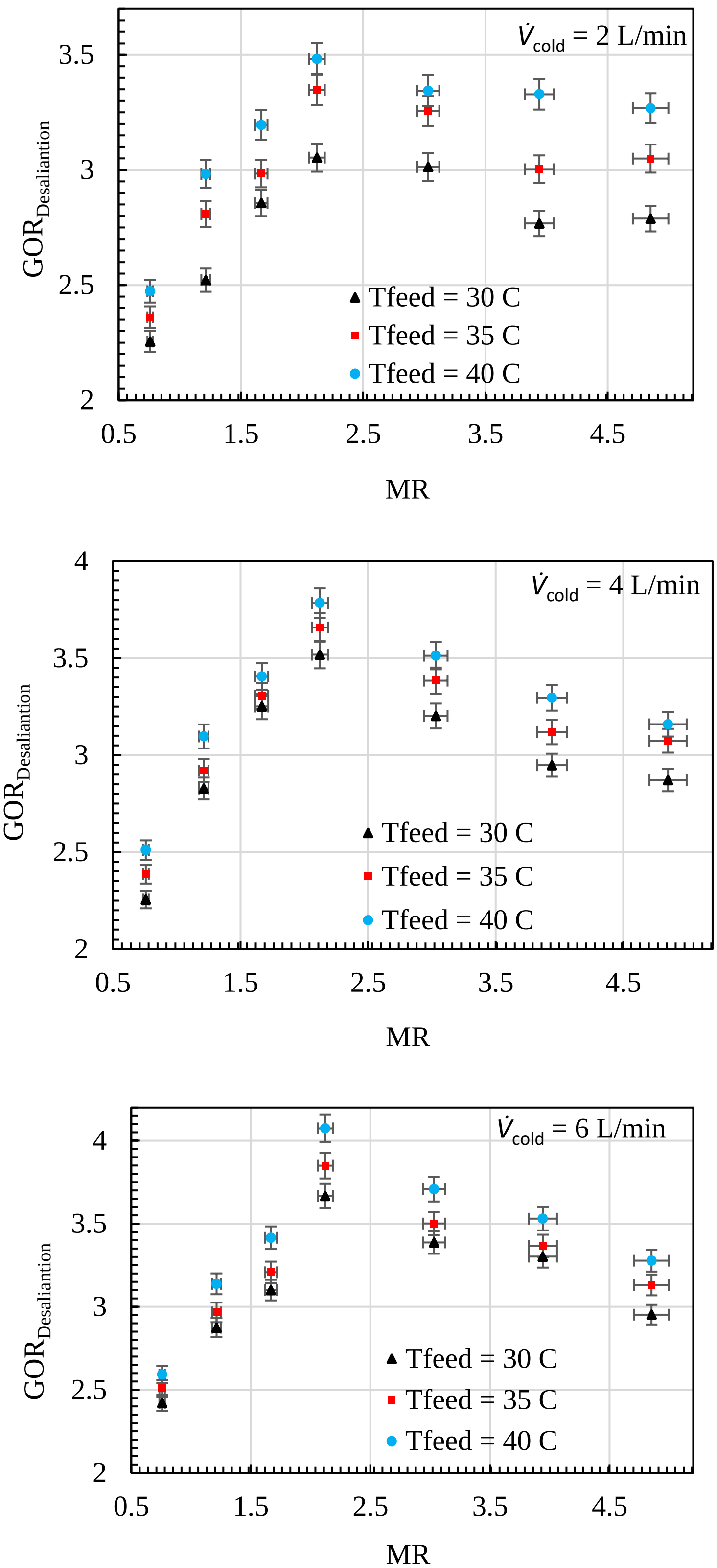

Figure 7. 17: Influence of MR, Hot Feed temperature and Chilled water flowrate on GOR

The system GOR is noticed to vary with MR, hot feed temperature and chilled water flowrate as presented in Figure 7.17. The gained output ratio GOR is evaluated based on the rate of desalinated water produce and the electrical energy consumed by the compressor. GOR is noticed to increase with MR to optimum value, and then decline with further increase in MR. The enhancement in GOR may be attributed to the increase in moisture content as MR increases, which resulted in an improve productivity. The GOR decrease with further increase in MR after the optimum MR because, the moisture content of air exiting the humidifier does not increase which may lead to unnecessary energy demand/consumption for the excess water supplied. Therefore, increasing the feed water flowrate beyond the optimum MR does not guarantee improvement in GOR of the system. In fact, it lead to poor energy performance of the system. Higher feed water temperature is observed to improve the GOR of the system. The system productivity is high at high feed water temperature, and this contribute majorly for the enhancement in the system GOR, even though there is high energy demand at high feed water temperature. The system GOR is also seen to be slightly influence by the chilled water flowrate. High chilled water flowrate lead to slightly higher system productivity and lower energy demand by the compressor (inverse of COP), and resulted in higher GOR of the system. The maximum attainable GOR from the proposed desalination plant based on the compressor input power is 4.07, obtained at the optimum MR of 2.12, feed temperature of 40 ^{o}C and chilled water flowrate of 6 L/min.

Also illustrated in Figure 7.17 is the GOR of the system evaluated based on the energy rejected at the condenser (heat input). Similar trends were noticed for the between the two evaluated GOR. However, the GOR evaluated based on compressor power is far greater than that obtained from the condenser rejected heat. This is because heat pump is a thermal system with high performance of energy conservation due to its high coefficient of performance (COP) [145]. The maximum system GOR evaluated based on the heat rejected from the condenser is found to be about 1.75, attained at the optimum MR of 2.12, chilled water flowrate of 2 L/min and feed temperature of 40 ^{o}C.

Table 7. 3: Capital investment cost for the main components of plant

Item Description	Prices (US $)
Packed Bed Humidifier	60
Dehumidifier	185
Water Tank	150
Flowmeters	230
Pumps	82
Blowers/fans	22
Pipes, Fittings	35
Accessories	20
Heat Pump System	7466

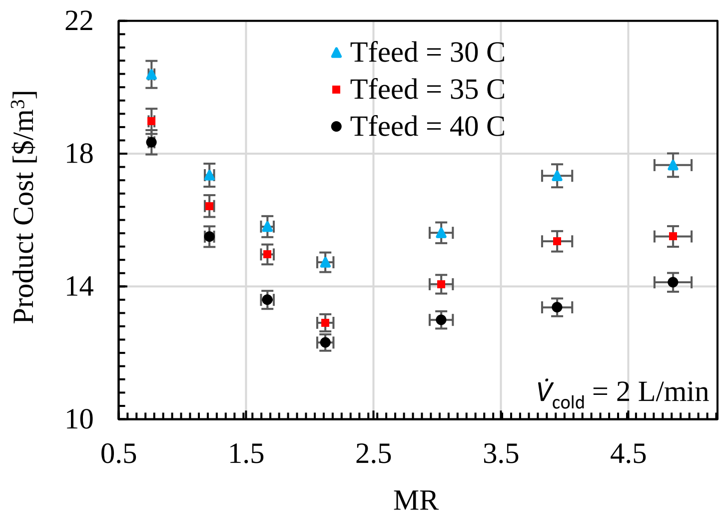

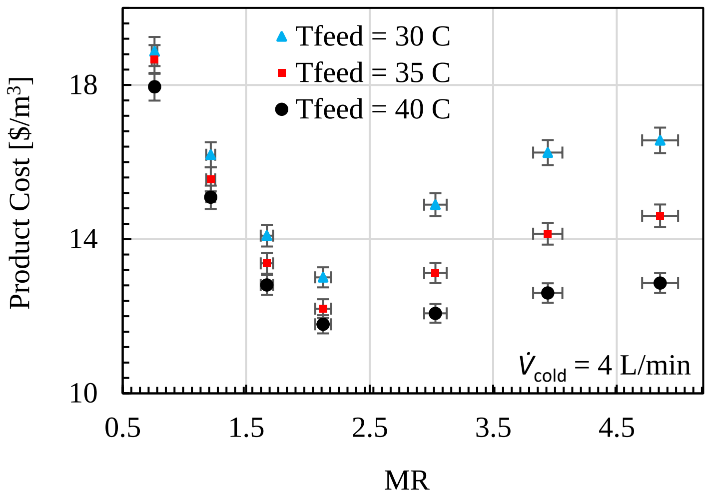

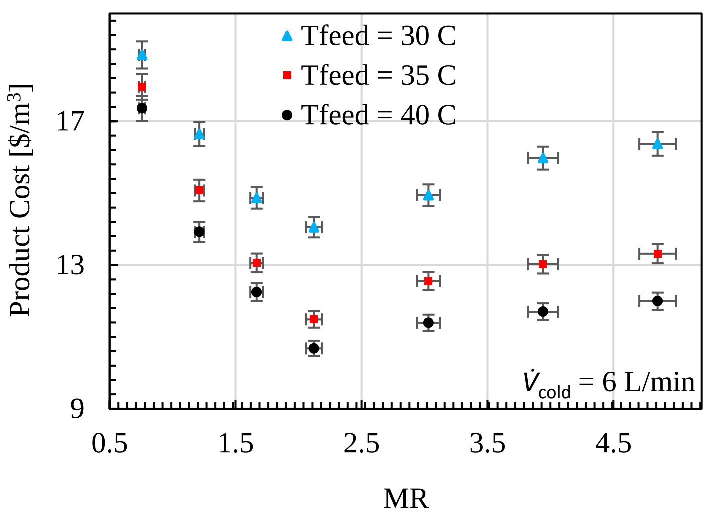

Figure 7. 18: Variation of Freshwater Cost with MR, Hot Feed temperature and Chilled water flowrate

Figure 7.18 displayed the influence of feed temperature, feed flowrate (MR), and chilled water flowrate of the cost of desalinated water. It can be seen that the product cost decreases with MR and then increase with MR after the optimum balanced mass flowrate ratio. The reduction and the increment in the cost of freshwater production may be due to increase and decrease in system productivity, as well as decrease and increase in specific electrical energy consumption of the system. System operating at feed temperature of 30 ^{o}C is noticed to provide higher cost of freshwater production as compared to the case operating at higher feed water temperature. The reason for the lower cost of desalinated water at higher feed temperature may be attributed to higher system productivity due to high vapor generation and increase in moisture carrying capacity of air. The influence of chilled water flowrate on the cost of freshwater production is not significant and thus considered marginal. The cost of saline water desalination from the current system ranges from 10.68 $\$/m^3$ to 20.39 $\$/m^3$ of desalinated water. If the annual labor cost, management cost and maintenance cost are neglected, the cost of desalinated water from the present system will be in the range of 7.21$\$/m^3$ to 14.04$\$/m^3$. The minimum cost of freshwater production from the present system is competitive with other HDH systems. For the purpose of comparison, we present the following cost of desalinated water from some of the HDH systems, including a bubble column HDH, solar still desalination and hybrid solar still-HDH desalination systems. For packed bed HDH systems (41.2$\$/m^3$ [146], 98.1$\$/m^3$ [147] and 32$\$/m^3$ [99]), for bubble column HDH system (19$\$/m^3$ [95]), solar still (13.5$\$/m^3$ [148]), and hybrid HDH-solar still system (34$\$/m^3$ [149]). It is worth noting that the price of desalinated water from the current system can be lower if the system is into mass production. The performance of some of HDH system with the present integrated HDH-HP desalination unit is presented in Table 7.4. The table of comparison showed a superior performance of the current integrated unit over other HDH desalination systems in terms of productivity, gained output ratio, energy utilization factor, as well as freshwater production cost.

Table 7. 4: Performance comparison of the proposed HDH system with other HDH desalination systems.

Energy Source	Productivity	GOR	EUF	Cost ($/m^3$)	Ref.
Solar Energy	1200 L/day				[93]
Solar Energy	60 L/day				[150]
Solar Energy	22 L/day	2.2		57.8	[151]
Solar Energy	3.4 L/h	2.1			[152]
Solar Energy	1.1173L/h	1		98.1	[147]
Heat Pump (vapor compression)	60 L/day				[103]
Heat Pump (vapor compression)	2.23 m^3/day			13.5	[153]
Heat Pump (vapor compression)	2.79 L/h	2.08		11.4	[154]
Solar Energy and vapor absorption refrigeration	1.5 L/h		0.45		[143]
Solar Energy and vapor absorption refrigeration	2.5 L/h		0.4		[155]
Heat Pump (vapor compression)	42.55 L/h	2.532		41.2	[146]
Heat Pump (vapor compression)	288 L/day	4.07	3.04	10.68	Present study

7.3 Mathematical Model for Validation

The mass and energy balance equations for the main components of the system are presented in the following section

Humidifier:

$$\dot{m}_a\left(h_{a,1} - h_{a,2}\right) = \dot{m}_{wh,3}h_{wh,3} - \dot{m}_{wh}h_{wh,2} \quad (1)$$

$$\dot{m}_{wh,1} = \dot{m}_{wh,2} = \dot{m}_{wh} \quad (2)$$

$$\dot{m}_{wh,3} = \dot{m}_{wh} - \dot{m}_{fw} \quad (3)$$

Dehumidifier:

$$\dot{m}_{fw} = \dot{m}_a\left(\omega_{a,2} - \omega_{a,3}\right) \quad (4)$$

$$\dot{m}_{wc}\left(h_{wc,2}-h_{wc,3}\right)=\dot{m}_{fw}h_{fw}+\dot{m}_{a}\left(h_{a,3}-h_{a,2}\right) \tag{5}$$

$$\dot{m}_{wc,1}=\dot{m}_{wc,2}=\dot{m}_{wc,3}=\dot{m}_{wc} \tag{6}$$

Condenser:

$$\dot{m}_{r}=\dot{m}_{r,1}=\dot{m}_{r,2}=\dot{m}_{r,3}=\dot{m}_{r,4} \tag{7}$$

$$\dot{Q}_{cond}=\dot{m}_{r}\left(h_{r,2}-h_{r,3}\right) \tag{8}$$

$$\dot{Q}_{cond}=\dot{m}_{wh}\left(h_{wh,2}-h_{wh,1}\right) \tag{9}$$

Evaporator:

$$\dot{Q}_{evap}=\dot{m}_{r}\left(h_{r,1}-h_{r,4}\right) \tag{10}$$

$$\dot{Q}_{evap}=\dot{m}_{wc}\left(h_{wc,1}-h_{wc,2}\right) \tag{11}$$

Compressor, and Expansion valve:

$$\dot{W}_{comp}=\dot{m}_{r}\left(h_{r,2}-h_{r,1}\right) \tag{12}$$

$$h_{r,3}=h_{r,4} \tag{13}$$

The following expressions are used for evaluating the components effectiveness.

Humidifier effectiveness:

$$\varepsilon_{H}=\max\left\{\frac{h_{a,2}-h_{a,1}}{h_{a,out,ideal}-h_{a,1}},\frac{h_{wh,2}-h_{wh,3}}{h_{wh,2}-h_{w,out,ideal}}\right\} \tag{14}$$

Dehumidifier effectiveness:

$$\varepsilon_D = \max\left\{\frac{h_{a,2} - h_{a,3}}{h_{a,2} - h_{a,out,ideal}}, \frac{h_{wc,3} - h_{wc,2}}{h_{wc,out,ideal} - h_{wc,2}}\right\} \tag{15}$$

The ideal air outlet enthalpy ($h_{a,out,ideal}$) is evaluated when the outlet air is fully saturated at the water inlet temperature, and the ideal water outlet enthalpy ($h_{w,out,ideal}$) is estimated when its temperature is equal to the temperature of the inlet air dry-bulb. The system performance and the price of desalted water are estimated using the expressions given in section 7.1.4 "System performance metrics". Some of the model prediction results are presented below.

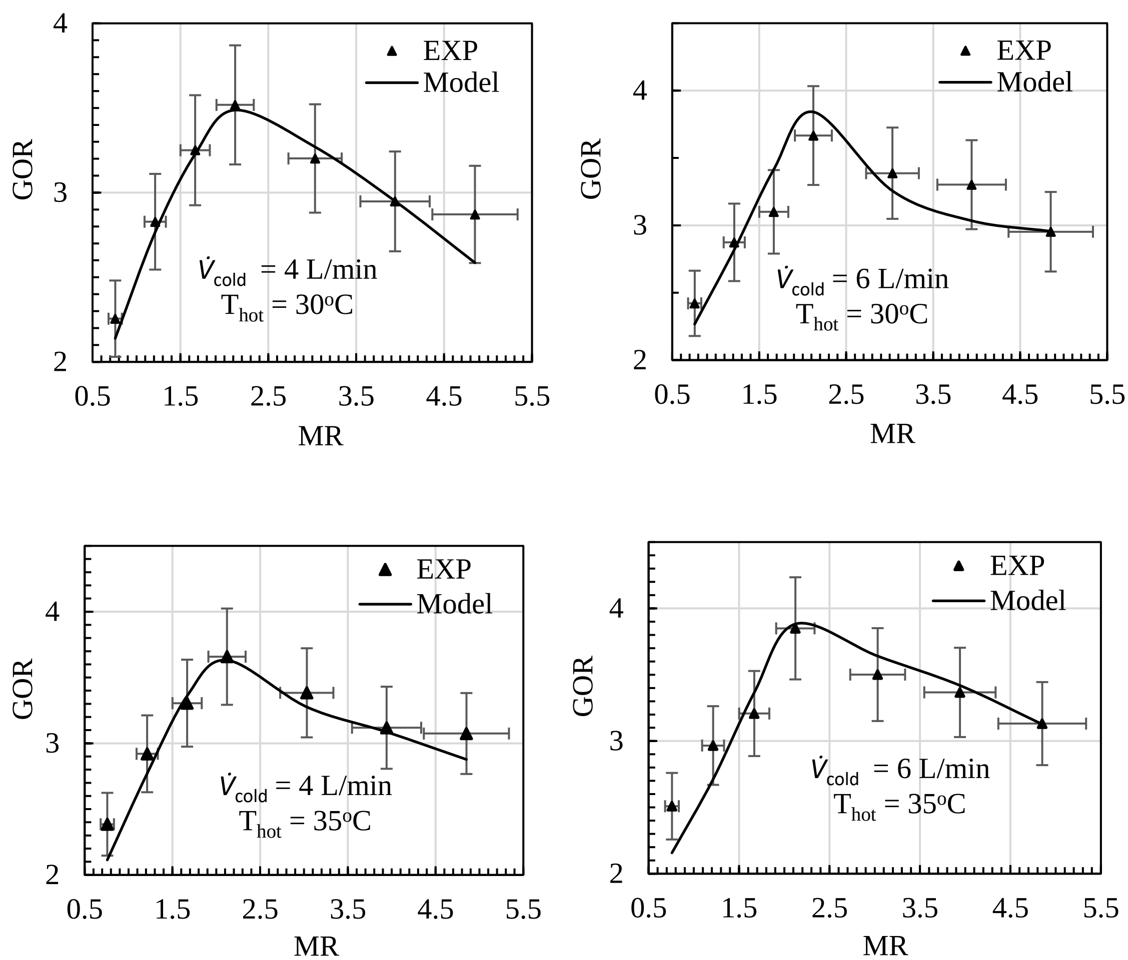

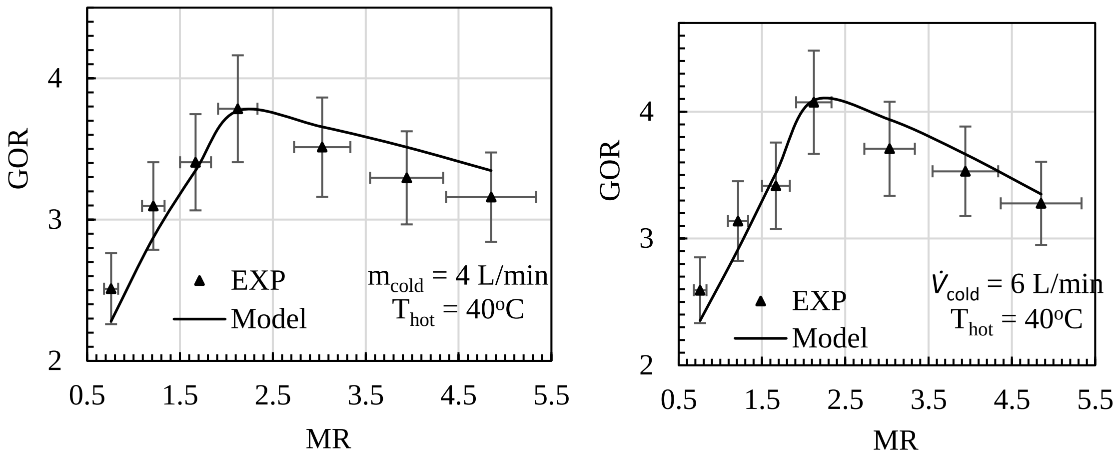

Figure 7. 19: Effect of MR, Hot Feed temperature and Chilled water flowrate on GOR

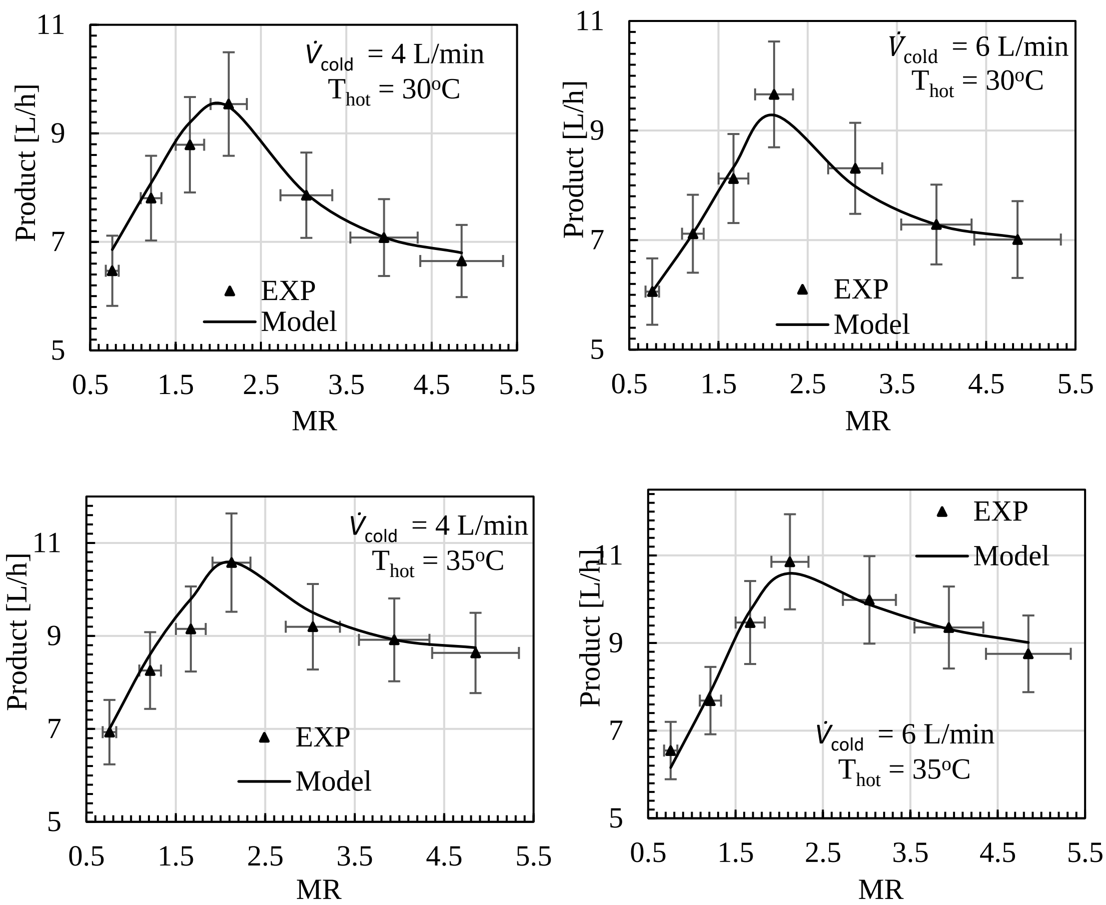

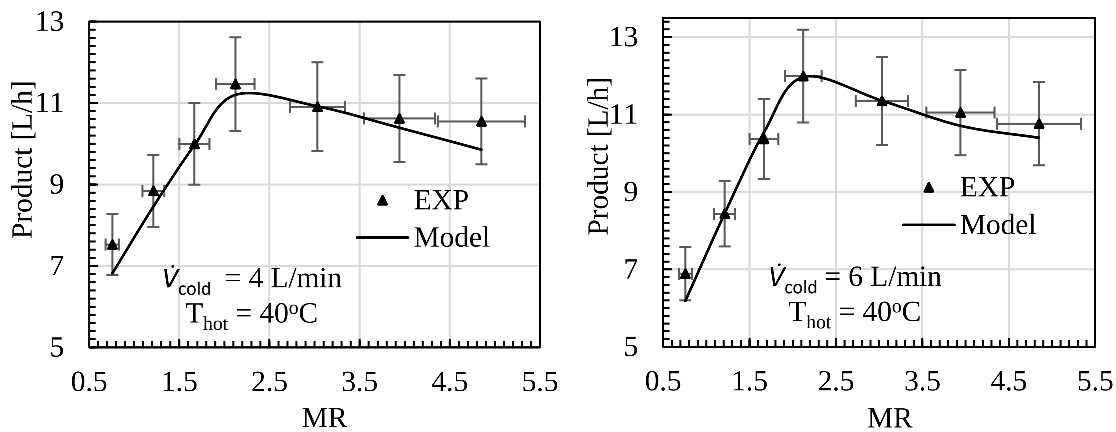

Figure 7. 20: Variation productivity with MR, Hot Feed temperature and Chilled water flowrate

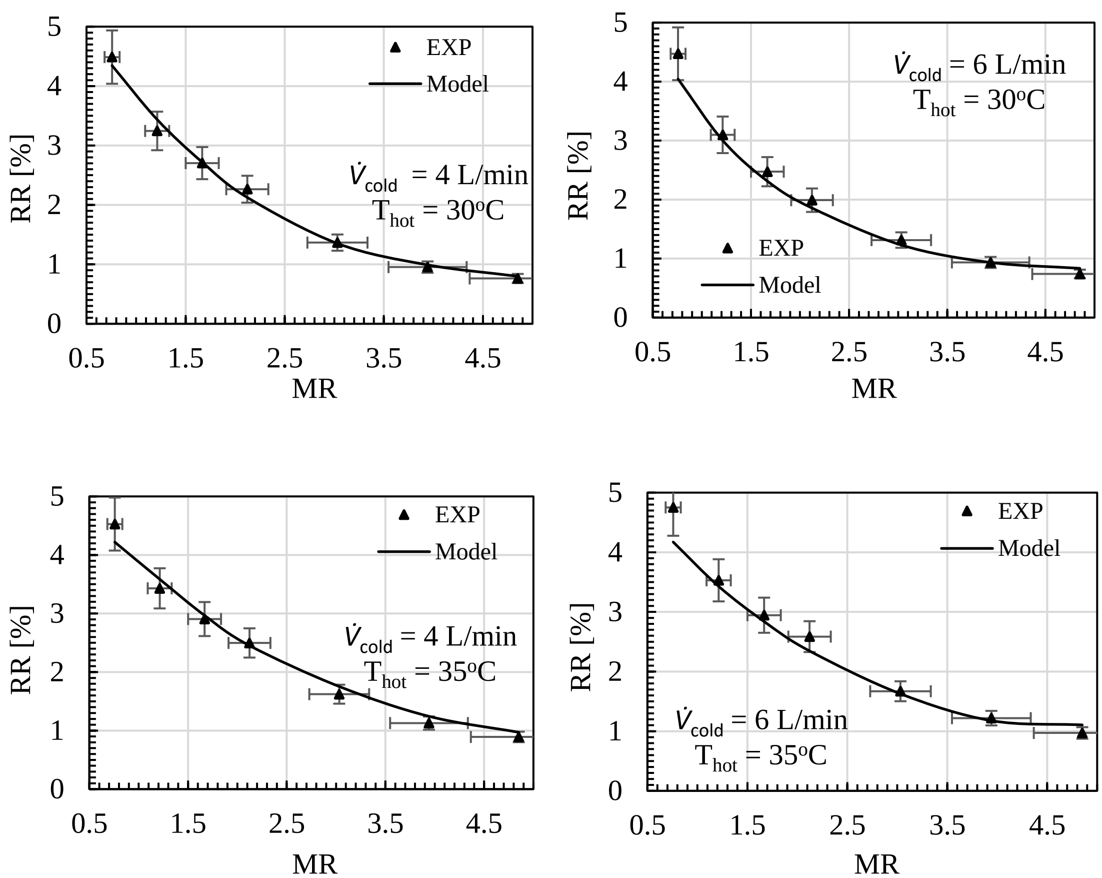

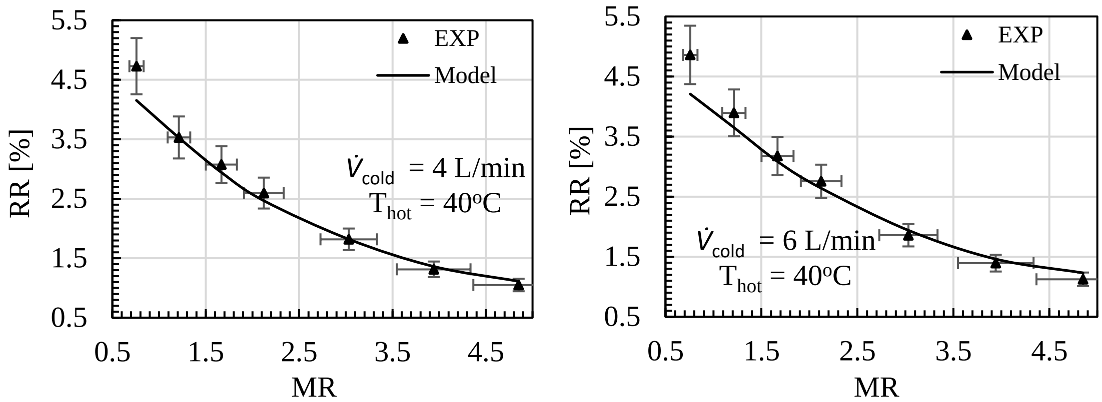

Figure 7. 21: Effect of MR, Hot Feed temperature and Chilled water flowrate on RR

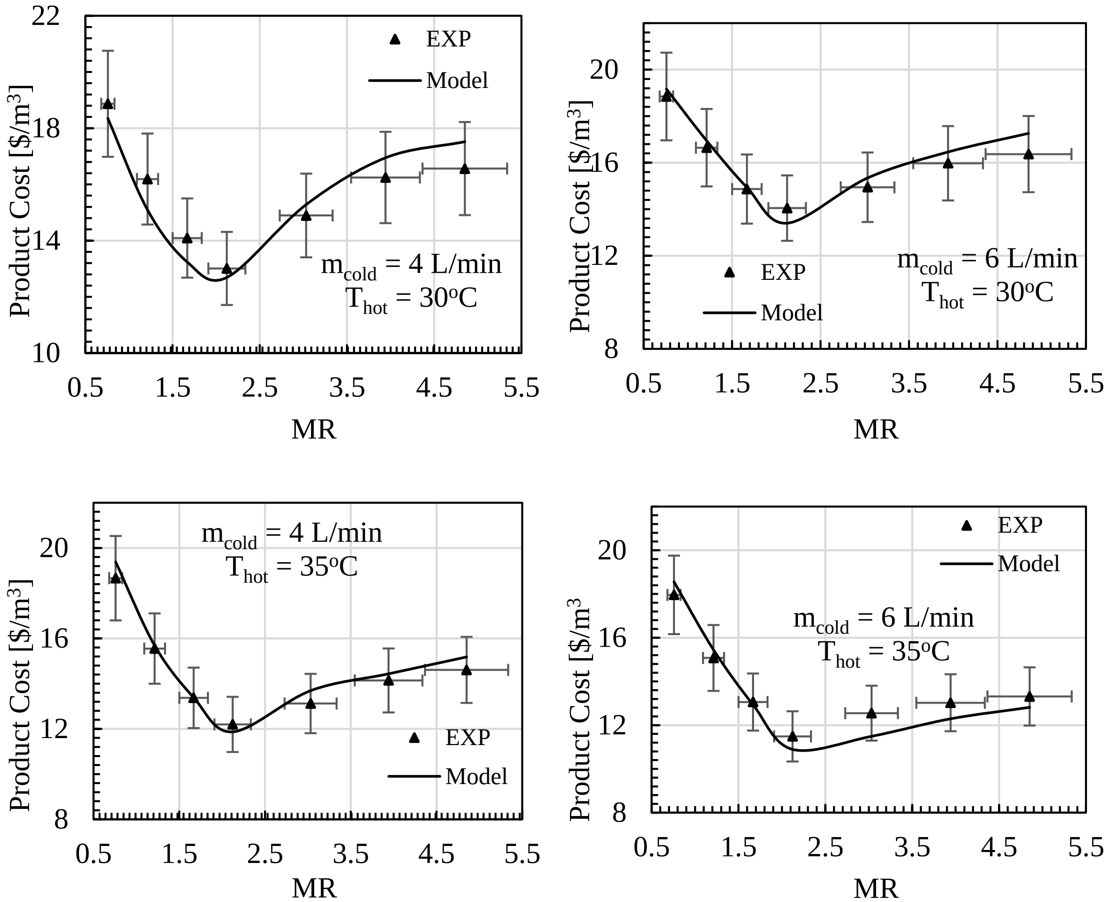

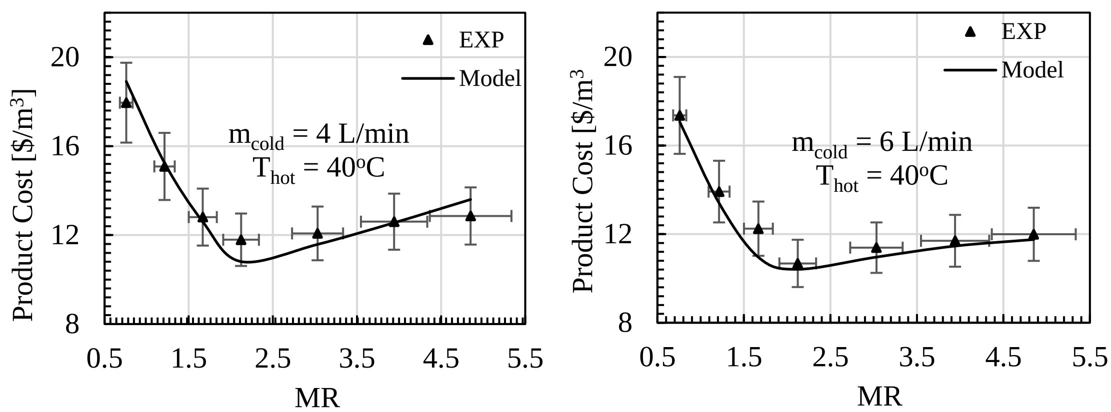

Figure 7. 22: Effect of MR, Hot Feed temperature and Chilled water flowrate on cost of freshwater

The results obtained from the theoretical model are plotted against the experimental data and presented in Figures 7.19 – 7.22. The estimated system performance metrics presented in this section includes the gained output ratio, system productivity, recovery ratio and the cost of desalinated water. It is clear from the presented results that the estimations given by the theoretical model is in good agreement with the theoretical model. The model is observed to be well fitted within the error bar, which is created at 10% deviation. Therefore, the presented model percentage deviation is within 10% of the experimental data, since all the model predictions are within 10% for all the presented performance metrics. The prediction for other system performance indicators against the experimental results are tabulated in Tables A1 – A6 and B1 – B6 in the appendix section.

CHAPTER 8

8.1 GENERAL CONCLUSION

This thesis has assessed the performance of humidification dehumidification desalination system coupled with heat pump (HP). Several layouts of integration of HDH and HP has been analysed theoretically. For all cases, increasing the mass flowrate ratio (MR), feed water temperature, humidifier effectiveness and dehumidifier effectiveness:

- Increases Gained output ratio
- Increases Recovery Ratio
- Increases Freshwater Productivity and
- Decreases Specific Electrical Energy Consumption.

However, optimum mass flowrate ratios exist where the system performance is maximized, except SEEC which is minimized at optimum MR. The optimum MR depends on system operating conditions and system configurations.

- Energy analysis suggested that the modified air heated integrated system gives superior performance when compared to water heated configuration, due to the low air specific heat capacity, better heat exchange in dehumidifier and the fact that moist air require less energy to reach system top temperature. The modified air heated layout recorded a maximum GOR of 8.88, RR of 6.4 and a minimum SEEC of 90 kWh/m^3.

- Exegy analysis revealed that the exergy destruction in all the components of the system are of the same order of magnitude, with evaporator producing the highest irreversibilities, which may be attributed to the temperature differences between the streams, friction, heat exchanged with the surroundings and higher entropy generation associated with the energy needed for vapor condensation process.
- The Exego-economic analysis also suggested that the modified air heat configuration provides the best performance with a maximum exergy efficiency of 1.1% and a minimum freshwater production cost of 2.42 $\$/m^3$, when compared to the water heated layout.
- The performance of water heated system has been improved by more than 200% through heat recovery from the discharged brine. However, the thermal recovery from the brine lost its significance after the high components effectiveness. Therefore, a limiting components effectiveness at which energy from the brine cannot be recovered are defined. Exceeding these limitations adversely decreases the system performance. The values for the components limitation are given in the specific conclusion.
- Experimental integrated unit produces multiple products (freshwater and cooling effect). The unit can simultaneously produces 288 Litres of freshwater per day and cooling load of 3070 Watts. The least SEEC and cost of freshwater production from the experimental unit are 160.16kWh/m^3 and 10.68$\$/m^3$ respectively, while the GOR and EUF of the unit are 4.07 and 3.05 respectively.

8.2 SPECIFIC CONCLUSION

8.2.1 Water and Modified Air Heated HDH Systems Coupled With Heat Pump

Theoretical investigation on the performance of HDH systems operated by heat pump has been presented. Water heated CAOW HDH system and the modified air-heated CAOW HDH system are considered. The main conclusions drawn from the study can be summarized as follows:

- Increasing both the humidifier and dehumidifier effectiveness increases gain output ratio. Increasing the dehumidifier effectiveness from 55 – 100% increases the GOR of the system from 3.7 to 10.4 (representing more than 180% increment) for 100% humidifier effectiveness for water-heated cycle.

- Increasing the MR increases the GOR of the system up to optimum GOR. However, further increase in MR leads to reduction in GOR due to surplus water flowrate or insufficient air supply, leading to over flooding of the system.

- Increasing the feed seawater temperature influence the RR and GOR of the system. A maximum GOR values of 10.6 and 6.3 were be obtained at feed seawater temperature of 56 ^{o}C and 29.2 ^{o}C for air heated and water heated cycles respectively. In addition, a recovery ratios of about 3.8% and 6.4% were reached for both water heated and modified air-heated system at the feed seawater temperature of 30.8 ^{o}C and 55 ^{o}C respectively.

- Increasing the refrigerant flow rate increases the GOR and decreases the specific work consumption of the system. About 25 % and 14% reduction in GOR were observed when refrigerant flow rate was increase from 0.02 to 0.1 kg/s for water heated and modified air heated system. For the air heated cycle, the system can reached a maximum gain output ratio of 13.5 using R-22 refrigerant at 80% components effectiveness and mass flow rate ratio of 0.56.

- Although the modified air-heated CAOW-HDH system slightly showed superior performance over the water heated CAOW-HDH system if operated at the same conditions. For instance, the water heated cycle attained a GOR of 7.63 at optimum MR of 1.3, whereas a GOR of 8.88 at the optimum MR of 0.63 was achieved for the modified air heated cycle. However, practical barriers such as ability to loss gained heat easily by modified air heated system makes the water heated CAOW HDH favorable despite its inferior performance to modified air heated cycle. The system GOR could even go beyond 12 if we run the system at certain conditions

- Based on our investigations, the best operating conditions (ranges) of practical interest are; mass flow rate ratio [1.2 – 1.5], feed seawater flow rate [1.2 – 1.3 kg/s], and feed seawater temperature [$\leq$ 30 ^{o}C] for water heated system. For modified air heated system, we have mass flow rate ratio [0.6 – 0.7], feed seawater flow rate [0.6 – 0.7 kg/s], and feed seawater temperature [$\geq$ 25 ^{o}C]. Refrigerant mass flow rate [$\leq$ 0.02 kg/s], effectiveness of humidifier and dehumidifier [$\geq$ 75%], and Tetrafluoroethane (Freon 134a) are recommended for both water heated and modified air heated systems.

8.2.2 Exergo-economic Analysis of Water and Modified Air Heated HDH Systems Coupled with Heat Pump

Second-law analysis and Exergo-economic analysis of the two layouts of HDH desalination plants (HP-HDH-AH and HP-HDH-WH) has been conducted. For the purpose of comparison, the same analysis was extended to a convectional electrically driven water heated HDH system (E-HDH-WH). The main conclusions drawn from the study are as follows:

- HP-HDH-AH desalination plant attained the highest gained output ratio and lowest Specific Electrical Energy Consumption, and E-HDH-WH system achieved the lowest GOR and highest SEEC.
- The highest irreversibility generated within the system occurs in the evaporator heat exchanger. The exergy destroyed in the compressor can be higher than other components for low values of compressor isentropic efficiency. The exergy destruction in all components is in the same order of magnitude. Therefore, careful design and selection of these components for such desalination systems is most essential, since components of inferior performance can considerably reduce the overall performance of the system.
- Irreversibilities within the evaporator, expansion valve, compressor and heater are insensitive to the variation in dehumidifier effectiveness and mass flowrate ratio. While exergy destroyed in the expansion-valve and compressor are not affected by changes in the feed water temperature.

- The exergy efficiency values for the HP-HDH-AH unit, HP-HDH-WH cycle, and E-HDH-WH plant is found to be 1.097%, 0.06965% and 0.05795%, respectively.
- The cost of desalinated water evaluated by current analysis for HP-HDH-AH system, HP- HP-HDH-WH plant, and E-HDH-WH unit varies from 4.61$/m^3 to 5.49$/m^3, 6.00$/m^3 to 7.14$/m^3, and 4.44$/m^3 to 14.95$/m^3, respectively. The cost of freshwater production can be as low as 2.42$/m^3, 5.29$/m^3 and 11.61$/m^3 for HP-HDH-AH, HP-HDH-WH, and E-HDH-WH systems, respectively, if the systems are operated at the dehumidifier effectiveness and humidifier effectiveness of 95% and 90% respectively.
- The product cost was found to be highly influenced by the variation in the cost of electricity, and less sensitive to the variations in the plant lifetime expectancy.
- HP-HDH-AH cycle shows better performance in terms of first-law analysis (GOR and SEEC), Second-Law analysis (exergetic efficiency), and the economic point of view, when compared to E-HDH-WH cycle, HP-HDH-WH system.
- It is expected that the present study will help engineers in the design, operation and simulation of HP-HDH air-heated, HP-HDH water-heated, and E-HDH water-heated systems in terms of both exergetic and thermo-economic evaluations.

8.2.3 Water heated HDH System Augmented with heat pump with Energy Recovery Option

The performance analysis of heat pump driven HDH desalination systems equipped with energy recovery system has been presented. Water heated HDH system presented in chapter three was modified to recover thermal energy associated with the discharged brine. According to our findings, the major conclusions can be summarized as follows:

- There is a need to recover thermal energy associated with the discharged brine for humidification dehumidification desalination plant coupled with a heat pump when they have poor component effectiveness, such as ineffective humidifier, especially for system A. The energy recovery could be achieved either through brine heat exchanger or via brine recirculation.

- The limits of components effectiveness at which energy recovery become a necessity is defined on the basis of water heated system presented by (Lawal et al. 2018). For system A, it becomes necessary to adopt energy recovery when the humidifier and dehumidifier effectiveness are below 59.16% and 63.6% respectively. Whereas for system B, energy recovery is needed when the humidifier effectiveness is lower than 91.25%. However, no limitation was placed on dehumidifier effectiveness of system B.

- The gained output ratio, recovery ratio and rate of desalted water production increases with increasing mass flowrate ratio, seawater temperature and component effectiveness. However, Specific Electrical Energy Consumption decrease with increasing mass flowrate ratio, seawater temperature and humidifier effectiveness. The optimum MR for the GOR, Product, RR and SEEC were found to be around 1.1 for the two systems, varies with feed water flowrate (system A and B) and temperature for system B.

- The cost of freshwater production is about 11.29 US$ and 8.16 US$ per cubic meter of desalted water for system A and system B respectively. Depending on the unit cost of electricity demanded by the proposed desalination plants, the price of desalinated water could be as low as 7.17$/$m^3$ and as high as 24.99$/$m^3$.

- In terms of thermo-economic evaluation and under the selected range of system operating parameters and conditions, the two proposed modifications to the water heated system presented in chapter three shows superior performances.

8.2.4 Heat Pump Driven Water heated HDH System with Different Layouts

Theoretical investigation of three different configurations of humidification dehumidification desalination systems integrated with vapor compression heat pump are presented. System A is without heat recovery, while system B and system C are equipped with energy recovery system to recover thermal energy from the rejected brine. The effects of different system operating conditions including MR, humidifier effectiveness, water flowrate and water temperature on the performance of the proposed desalination systems such as GOR, distillation rate, RR, SEEC and cost of freshwater production are investigated. The following are the major conclusion from the study:

Increasing the seawater temperature improves the system GOR, RR, and productivity. However, the specific electrical energy consumption decreases with raising saline water temperature.

- Increasing the saline water flowrate leads to poor performance of the proposed system. The GOR, RR, and productivity decreases, while the SEEC of the system increases.

- Higher effectiveness of the humidifier enhances the system productivity, RR, and GOR of the system, while the SEEC of the system decreases.

- Optimum mass flowrate ratio of saline water to air exist where the best performance of the systems are attained. The optimum values of MR tends to change with variations in various operating conditions.

- The prices of freshwater is highly influence by the cost of electricity, with higher cost of electricity yielding higher cost of freshwater. The plant life span is also noticed to influence the cost of freshwater. However, plant life influence on the product cost is about 5-7 folds inferior to that of electricity cost.

- Due to energy recovery option, system B and system C yielded superior performance compared to system A with no option of energy recovery.

- According to the considered range of the operating parameters, the best gained output ratio, productivity, recovery ratio, and the specific electrical energy consumption of the proposed desalination systems are 3.9, 8.5L/h, 3.1%, and 263kWh/m^3 of fresh water respectively.

- The price of freshwater obtained from the proposed plants varies from 7.35$/$m^3$ and 34.27$/$m^3$ of freshwater.

8.2.5 Experimental Investigation of Water heated HDH System Integrated with heat Pump

Experimental investigation of HDH desalination system integrated with heat pump is presented. The influence of several system operating parameters on the thermodynamic and cost performance of the system are presented and discussed. The following are the major conclusions drawn from the investigation:

- The integrated water desalination system can simultaneously provide freshwater as the primary objective and cooling energy as secondary benefit.
- Both feed water flowrate (MR) and feed water temperature significantly affect the integrated system, while chilled water flow has little or no influence on the integrated desalination unit.
- The plant can produce desalinated water between 145 to 288 Liters of freshwater per day, and cooling load between 641 to 3070 Watts available at the exit of the integrated unit. These values correspond to the feed temperature of 30ºC and MR of 0.758 and 4.851 respectively.
- A gained output ratio as high as 4.07 and recovery ratio of 4.9% are achievable from the proposed desalination system.
- The EUF and SEEC of the proposed integrated unit vary from 1.22 to 3.05 and 160.16 kWhr/m^3 to 311.89 kwhr/m^3 of freshwater respectively.
- The COP of the heat pump system ranges between 3.06 and 4.86, while the cost of freshwater production form the proposed desalination plant vary from 10.68 \$/m^3 to

20.39 $\$/m^3$ of freshwater. The presented product cost is evaluated based on the actual purchased price of its parts as available in the market.

8.3 RECOMMENDATIONS

- The mass flowrate ratio used in the current experimental study varies with water flowrate at fixed air flowrate. To fully understand the influence of MR on the system performance of the tested experimental unit, it is recommended to vary the MR by varying the air flowrate while keeping the water flowrate constant.
- The cooling load from the experimental unit has not been utilized for any application in this work. Therefore, it is recommended for future work to design application where the cooling effect can be used.
- The HDH performance can be improve by creating extractions and injections points on the humidifier and dehumidifier respectively
- Multi-stage HDH system can also be used for higher system productivity
- Theoretical analysis shows that recovering thermal energy from the rejected brine to pre-heat the air before injecting it into the humidifier can significantly enhance the overall system performance. Therefore, for the current experimental unit, a heat exchanger should be used to recover thermal energy of brine.
- The energy recovery analysis was performed for water heated layout. Therefore, it is recommended to perform the same analysis on the other configurations of HDH system.
- In the current experimental set-up, freshwater production consumed over 80% of useful energy and the remaining for cooling effect. The experimental layout should be modify to be flexible, such that it can provides more cooling load or more freshwater production depending on the demand.

References

[1] Coping with water scarcity-Challenge of the twenty-first century, World water day, 22nd March 2007.

[2] Mekonnen M.M.; Hoekstra A.Y.; "Four billion people facing severe water scarcity," *Science Advances*, vol. 2, no. 2, pp. e1500323, 2016.

[3] Narayan G.P.; Sharqawy M.H.; Summers E.K.; Lienhard J.H; Zubair S.M.; Antar M.A.; "The potential of solar-driven humidification-dehumidification desalination for small-scale decentralized water production," *Renewable and Sustainable Energy Reviews,* vol. 14, no. 4, pp. 1187-1201, 2010.

[4] Kabeel A.E.; Hamed M.H.; Omara Z.M.; Sharshir S.W.; "Water Desalination Using a Humidification-Dehumidification Technique-A Detailed Review," *Natural Resources,* vol. 4, pp. 286-305, 2013.

[5] El-Dessouky H.T.; Ettouney H.M.; "Fundamentals of salt water desalination," *Elsevier,* pp. 1-670, 1st Edition,2002.

[6] Lawand T.A.; "Systems for Solar Distillation," *Technical Report, Brace Research Institute*, Report no. R 115, September 1975.

[7] Fath H.E.S; "Solar distillation: A promising alternative for water provision with free energy, simple technology and a clean Environment," *Desalination, vol. 116, no. 1, pp.* 45-56.

[8] Tiwari G.N.; Singh H.N.; Tripathi R.;, "Present status of solar distillation," *Solar Energy*, vol. 75, no. 5, pp. 367-373, 2003.

[9] John H. L.; Antar M.A.; Amy B.; Julian B.; Zaragoza G.; "Solar Desalination," *Begell House Digital Library,* vol. 15, p. 277-347, 2012.

[10] Abdelmoez W.; Mahmoud M.S.; Farrag T.E.; "Water desalination using humidification/dehumidification (HDH) technique powered by solar energy: A detailed review," *Desalination and Water Treatment*, vol. 52, no. 25-27, pp. 4622-4640, 2014.

[11] Sharqawy M.H.; Antar M.A.; Zubair S.M.; Elbashir A.M.; "Optimum thermal design of humidification dehumidification desalination systems," *Desalination*, vol. 349, no. 14, pp. 10-21, 2014.

[12] Bourouni K.; Chaibi M.T.; Tadrist L.; "Water desalination by humidification and dehumidification of air: State of the art," *Desalination*, vol. 137:pp. 167-176. 2001.

[13] Giwa A.; Akther N.; Al Housani A.; Haris S.; Hasan S.W.; "Recent advances in humidification dehumidification (HDH) desalination processes: Improved designs and productivity," *Renewable and Sustainable Energy Reviews,* vol. 57, pp. 929-944, 2016.

[14] Narayan G.P.; Sharqawy M.H.; Lienhard V. JH.; Zubair S.M.; "Thermodynamic analysis of humidification dehumidification desalination cycles," *Desalination and Water Treatment,* vol. 16, pp. 339-353, 2010.

[15] Nawayseh N.K.; Farid M.M.; Al-Hallaj S.; Al-Timimi A.R.; "Solar desalination based on humidification process - I. Evaluating the heat and mass transfer coefficients," *Energy Conversion Management,* vol. 40, pp. 1423-1439, 1999.

[16] Müller-Holst H.; " Solar Desalination for the 21st Century," *Springer*, pp. 215-225 2007.

[17] Hepbasli A.; Kalinci Y.; "A review of heat pump water heating systems," *Renewable and Sustainable Energy Reviews*, vol. 13, pp. 1211–1229, 2009.

[18] Chua K.J.; Chou S.K.,; Yang W.M.; "Advances in heat pump systems: A review," *Applied Energy*, vol. 87, pp. 3611–2364, 2010.

[19] Laue H.J.; Heinloth K. (ed); "Renewable Energy. 9 Heat pumps," *Springer Materials*, vol. 3C, pp. 605-626, 2006.

[20] https://www.carrier.com/residential/en/us/products/heat-pumps/how-does-a-heat-pump-work/ (Accessed in 2019).

[21] Bahrami M.; "Refrigeration Cycle," pp. 1-8. http://www.sfu.ca/~mbahrami/ENSC%20461/Notes/Refrigeration%20Cycle.pdf

[22] Handbook A. HVAC Applications. *ASHRAE Inc*.; 2015.

[23] Sharqawy M.H.; Al-Shalawi I.; Antar M.A.; Zubair S.M.; "Experimental investigation of packed-bed cross-flow humidifier," *Applied Thermal Engineering*, vol. 117, pp. 584-590, 2017.

[24] Wang S.K.; "Air Systems: Components - Fans, Coils, Filters, and Humidifiers, In: Handbook of Air Conditioning and Refrigeration," *McGraw-Hill Education*, 2000.

[25] Treybal R.E.; "Mass Transfer Operations," *McGraw-Hill, New York, NY, third ed.*, 1980.

[26] Liu H.; Sharqawy M.H.; "Experimental performance of bubble column humidifier and dehumidifier under varying pressure," *International Journal of Heat and Mass Transfer*, vol. 93, pp. 934-44, 2016.

[27] Kreith F B.R.; "Direct contact heat transfer," *Washington: Hemisphere Corporation*, 1988.

[28] Xu Z.; Xiao Y.; Wang Y.; "Experimental and theoretical studies on air humidification by a water spray at elevated pressure," *Applied Thermal Engineering*, vol. 27, pp. 2549-258, 2007.

[29] Bonilla C.F.; Mottes J.R.; Wolf M.; "Air Humidification Coefficients in Spray Towers. Gas-Film Mass Transfer Coefficient at Low Air Velocities for Use in Scrubber Design," *Industrial and Engineering Chemistry*, vol. 42, pp. 2521-2525, 2005.

[30] Javed K.H.; Mahmud T.; Purba E.; "Enhancement of Mass Transfer Using Swirling Gas Flow," *C hemical Engineering Research and Design*, vol. 84, pp. 465-477, 2006.

[31] Amara M.B.; Houcine I.; Guizani A.; Maalej M.; "Experimental study of a multiple-effect humidification solar desalination technique," *Desalination*, vol. 170, pp. 209-221, 2004.

[32] Younis M.A.; Darwish M.A.; Juwayhel F.; "Experimental and theoretical study of a humidification-dehumidification desalting system," *Desalination*, vol. 94, pp. 11-24, 1993.

[33] Orfi J.; Laplante M.; Marmouch H.; Galanis N.; Benhamou B.; Nasrallah S. B.; Nguyen C.T.; "Experimental and theoretical study of a humidification-dehumidification water desalination system using solar energy," *Desalination*, vol. 168, pp. 151-159, 2004.

[34] Aburub A.; Aliyu M.; Lawal D.U.; Antar M.; "Experimental Investigations Of A Cross-Flow Humidification Dehumidification Desalination System," *International Water*

Technology Journal, vol. 7, no. 3, pp. 198-208, 2017.

[35] Aburub A;. Aliyu M.; Lawal D.U.; Antar M.; "Experimental Investigations Of The Performance Of A Cross-Flow Humidification Dehumidification Desalination System," *Twentieth. International Water Technology Conference - IWTC20*, pp. 17–26, 2017.

[36] El-Agouz S.A.; Abugderah M.; "Experimental analysis of humidification process by air passing through seawater," *Energy Conversion and Management*, vol. 49, pp. 3698–703, 2008.

[37] Chafik E.; "A new type of seawater desalination plants using solar energy," *Desalination*, vol. 156, pp. 333–348, 2003.

[38] Nematollahi F.; Rahimi A.; Gheinani T.T.; "Experimental and theoretical energy and exergy analysis for a solar desalination system," *Desalination*, vol. 317, pp. 23–31, 2013.

[39] Miller J.A.; John H.L.V.; "Impact of extraction on a humidification–dehumidification desalination system," *Desalination*, vol. 313, pp. 87–96, 2013.

[40] Ahmed H.A.; Ismail I.M.; Saleh W.F.; Ahmed M.; "Experimental investigation Corrugated, of humidification-dehumidification desalination system with packing in the humidifier," *Desalination*, vol. 410, pp. 19–29, 2017.

[41] Muthusamy C.; Srithar K.; "Energy saving potential in humidification-dehumidification desalination system," *Energy*, vol. 118, pp. 729-741, 2017.

[42] Rajaseenivasan T.; Srithar K.; "Potential of a dual purpose solar collector on humidification dehumidification desalination system," *Desalination*, vol. 404, pp. 35-40, 2017.

[43] El-Shazly A.H.; El-Gohary M.M.; Ossman M.E.; "Performance characteristics of a solar humidification dehumidification unit using packed bed of screens as the humidifier," *Desalination and Water Treatment*, vol. 16, pp. 17–28, 2010.

[44] Wu G.; Zheng H.; Ma X.; Kutlu C.; Su Y.; "Experimental investigation of a multi-stage humidification-dehumidification desalination system heated directly by a cylindrical Fresnel lens solar concentrator," *Energy Conversion and Management*, vol. 143, pp. 241–51, 2017.

[45] Chiranjeevi C.; Srinivas T.; "Combined two stage desalination and cooling plant," *Desalination*, vol. 345, pp. 56–63, 2014.

[46] Al-Enezi G.; Ettouney H.; and Fawzy N.; "Low Tempera- ture Humidification Dehumidification Desalination Process," *Energy Conversion and Management*, vol. 47, pp. 470–84, 2006.

[47] Yamali C.; Solmus I.; "A solar desalination system using humidification-dehumidification process: experimental study and comparison with the theoretical results," *Desalination*, vol. 220, pp. 538–51, 2008.

[48] Ahmed H.A.; Ismail I.M.; Saleh W.F.; Ahmed M.; "Experimental investigation of humidification-dehumidification desalination system with corrugated packing in the humidifier," *Desalination*, vol. 410, pp. 19-29, 2017.

[49] Houcine I.; Amara M. B.; Guizani A.; Maâlej M.; "Pilot Plant Testing of a New Solar Desalination Process by a Multiple-Effect-Humidification Technique," *Desalination*, vol. 196, pp. 105-124, 2006.

[50] Kabeel A.E.; Abdelgaied M.; "Experimental evaluation of a two-stage indirect solar dryer with reheating coupled with HDH desalination system for remote areas," *Desalination*, vol. 425, pp. 22–29, 2018.

[51] Hermosillo J.J.; Arancibia-Bulnes C.A.; Estrada C.A.; "Water desalination by air humidification: mathematical model and experimental study," *Solar Energy,* vol. 86, pp. 1070-6, 2011.

[52] Al-Hallaj S.; Farid M.M.; Tamimi A.; "Solar desalination with humidification-dehumidification cycle: performance of the unit," *Desalination*, vol. 120, pp. 273-80, 1998.

[53] Amer E.H.; Kotb H.; Mostafa G.H.; El-Ghalban A.R.; "Theoretical and experimental investigation of humidification-dehumidification desalination unit," *Desalination,* vol. 249, pp. 949-59, 2009.

[54] Yuan G.; Zhang H.; "Mathematical modeling of a closed circulation solar desalination unit with humidification-dehumidification," *Desalination,* vol. 205, pp. 156-62, 2007.

[55] Dai Y.J.; Zhang H.F.; "Experimental investigation of a solar desalination unit with humidification and dehumidification," *Desalination,* vol. 130, pp. 169–75, 2000.

[56] Dai Y.J.; Wang R.Z.; Zhang H.F.; "Parametric Analysis to Improve the Performance of a Solar Desalina- tion Unit with Humidification and Dehumidification," *Desalination,* vol. 142, pp. 107–18, 2002.

[57] Khedr M.; "Techno-Economic Investigation of an Air Humidification-Dehumidification Desalination Process," *Chemical Engineering Technology*, vol. 16, pp. 270-4, 1993.

[58] Eslamimanesh A.; Hatamipour M.S.; "Mathematical modeling of a direct contact humidification-dehumidification desalination process," *Desalination*, vol. 237, pp. 296–304, 2009.

[59] Hou S.; Zhang H.; "A Hybrid Solar Desalina- tion Process of the Multi-Effect Humidification Dehu- midification and Basin-Type Unit," *Desalination,* vol. 220, vol. 552–7, 2008.

[60] Nawayseh N. Kh.; Farid M.M.; Al-Hallaj S.; Al-Timimi A.; "Solar desalination based on humidification process—I. Evaluating the heat and mass transfer coefficients," *Energy Conversion and Management*, vol. 40, pp. 1423–39, 1999.

[61] Farsad S.; Behzadmehr A.; "Analysis of a solar desalination unit with humidification-dehumidification cycle using DoE method," *Desalination,* vol. 278, pp. 70–6, 2011.

[62] Nafey A.S.; Fath H.E.S.; El-Helaby S.O.; Soliman A.; "Solar desalination using humidification- dehumidification processes. Part II. An experimental investigation," *Energy Conversion and Management*, vol. 45, pp. 1263–77, 2004.

[63] Garg H.P.; Adhikari R.S.; Kumar R.; "Experimental design and computer simulation of multi-effect humidification (MEH) – dehumidification solar distillation," *Desalination*, vol. 153, pp. 81–6, 2002.

[64] Bacha B.H.; Damak T.; Bouzguenda B.; Maalej A.Y.; "Experimental Validation of the Distillation Module of a Desalination Station Using the SMCEC Principle," *Renewable Energ*y, vol. 28, pp. 2335–54, 2003.

[65] Klausner J.F.; Mei R.; Li Y.; Knight J.M.; "Innovative Fresh Water Production Process for

Fossil Fuel Plants," Annual Report, 2003.

[66] Muthusamy C.; Srithar K.; "Energy and exergy analysis for a humidification-dehumidification desalination system integrated with multiple inserts," *Desalination*, vol. 367, pp. 49-59, 2015.

[67] Zhani K.; Bacha H.B.; "Experimental investigation of a new solar desalination prototype using the humidification-dehumidification principle," *Renewable Energy*, vol. 35, pp. 2610–7, 2010.

[68] Farid M.M.; Al-Hajaj A.; "Solar desalination with a humidification-dehumidification cycle," *Desalination,* vol. 106, pp. 427–9, 1996.

[69] Bacha H.B.; Damak T.; Bouzguenda M.; Maalej A.Y.; "Experimental validation of the distillation module of a desalination station using the SMCEC principle," *Renewable Energy*, vol. 28, pp. 2335–54, 2003.

[70] Muller-Holst H, Engelhardt M.; Herve M.; Schölkopf W.; "Solar thermal seawater desalination systems for decentralized use," *Renewable Energy*, vol. 14, pp. 311–8, 1998.

[71] Sharqawy M.H.; Liu H.; "The effect of pressure on the performance of bubble column dehumidifier," *International Journal of Heat and Mass Transfer*, vol. 87, pp. 212–21, 2015.

[72] El-Agouz S.A., "Desalination based on humidification–dehumidification by air bubbles passing through brackish water," *Chemical Engineering Journal*, vol. 165, pp. 413–419, 2010.

[73] Narayan G.P.; Sharqawy M.H.; Lam S.; Das, S.K.; Lienhard J.H.; "Bubble columns for condensation at high concentrations of noncondensable gas: heat-transfer model and experiments," *AIChE Journa*l, vol. 59, pp. 1780–1790, 2013.

[74] Tow E.W.; Lienhard J.H.; "Experiments and modeling of bubble column dehumidifier performance," *International Journal of Thermal Sciences*, vol. 80, pp. 65–75, 2014.

[75] Abd-ur-Rehman H.M.; Al-Sulaiman F.A.; "A novel design of a multistage stepped bubble column humidifier for the humidification of air," *Applied Thermal Engineering*, vol. 120, pp. 530–6, 2017.

[76] Rajaseenivasan T.; Srithar K.; "An investigation into a laboratory scale bubble column humidification dehumidification desalination system powered by biomass energy," *Energy Conversion and Management*, vol. 139, pp. 232–44, 2017.

[77] Srithar K.; Rajaseenivasan T.; "Performance analysis on a solar bubble column humidification dehumidification desalination system," *Process Safety and Environmental Protection*, vol. 105, pp. 41–50, 2017.

[78] Chafik E.; "A new type of seawater desalination plants using solar energy," *Desalination*, vol. 156, pp. 333–48, 2003.

[79] Chafik E.; "Design of plants for solar desalination using the multi-stage heating/humidifying technique," *Desalination*, vol. 168, pp. 55–71, 2004.

[80] Klausner J.F.; Li Y.; Darwish M.; Mei R.; "Innovative Diffusion Driven Desalination Process," *Journal of Energy Resources Technology*, vol. 126, no. 3, pp. 219-225, 2004.

[81] Farid M.M.; Parekh S.; Selmanb J.R.; Al-hallaj S.; "Solar desalination with a humidification-dehumidification cycle: mathematical modeling of the unit," *Desalination*,

vol. 1, pp.153–64, 2002.

[82] Li Y.; Klausner J.F.; Mei R.; Knight J.; "Direct contact condensation in packed beds," *International Journal of Heat and Mass Transfer*, vol. 49, pp. 4751–61, 2006.

[83] Li Y.; Klausner J.F.; Mei R.; "Performance characteristics of the diffusion driven desalination process," *Desalination*, vol. 196, pp. 188–209, 2006.

[84] Threlkeld J.L.; "Thermal environmental engineering," *Prentice-Hall,* 1970.

[85] Yang K.T.; Pacheco-Vega A.; McClain R.L.; Sen M.; Díaz G.; "Heat Rate Predictions in Humid Air-Water Heat Exchangers Using Correlations and Neural Networks," *Journal of Heat Transfer,* vol. 123, no. 2, pp. 348-354, 2002.

[86] McQuiston .FC.; "Correlation of Heat, Mass and Momentum Transport Coefficients for Plate-Fin-Tube Heat Transfer Surfaces with Staggered Tubes," *ASHRAE Trans,* vol. 84, pp. 294–309, 1978.

[87] McQuiston F.C.; "Heat, mass and momentum transfer data for five plate-fin tube heat transfer surfaces," *ASHRAE Trans,* vol. 84, pp. 266–93, 1978.

[88] Amara M.B.; Houcine I.; Guizani A.A.; Maalej M.; "Efficiency investigation of a new-design air solar plate collector used in a humidification-dehumidification desalination process," *Renewable Energy,* vol. 30, pp. 1309–27, 2005.

[89] Nematollahi F.; Rahimi A.; Gheinani T.T.; "Experimental and theoretical energy and exergy analysis for a solar desalination system," *Desalination,* vol. 317, pp. 23–31, 2013.

[90] Yamali C.; Solmuş I.; "Theoretical investigation of a humidification-dehumidification desalination system configured by a double-pass flat plate solar air heater," *Desalination*, vol. 205,pp. 163–77, 2007.

[91] Gandhidasan P.; Antar M.A. Al-Sulaiman F.A.; Atif M.; Al-Dini S.A.; Zubair M.I.; "Humidification dehumidification desalination system using parabolic trough solar air collector," *Applied Thermal Engineering,* vol. 75, pp. 809–16, 2014.

[92] Antar M.A.; Sharqawy M.H.; "Experimental investigations on the performance of an air heated humidification–dehumidification desalination system," *Desalination and Water Treatment,* vol. 51, pp. 837–43, 2013.

[93] Li X.; Yuan G.; Wang Z.; Li H.; Xu Z.; "Experimental study on a humidification and dehumidification desalination system of solar air heater with evacuated tubes," *Desalination,* vol. 351, pp. 1–8, 2014.

[94] Summers E.K.; Antar M.A.; Lienhard J.H.; "Design and optimization of an air heating solar collector with integrated phase change material energy storage for use in humidification-dehumidification desalination," *Solar Energy,* vol. 86, pp. 3417–29, 2012.

[95] Rajaseenivasan T.; Shanmugam R.K.; Hareesh V.M.; Srithar K.; "Combined probation of bubble column humidification dehumidification desalination system using solar collectors," *Energy,* vol. 116, pp. 459–69, 2016.

[96] Elsafi A.M.; "Integration of humidification-dehumidification desalination and concentrated photovoltaic-thermal collectors: Energy and exergy-costing analysis," *Desalination,* vol. 424, pp. 17–26, 2017.

[97] Ho C.D.; Yeh H.M.; Wang R.C.; "Heat-transfer enhancement in double-pass flat-plate solar

air heaters with recycle," *Energy*, vol. 30, pp. 2796–817, 2005.

[98] Abdel Dayem A.M.; "Efficient Solar Desalination System Using Humidification/Dehumidification Process," *Journal of Solar Energy Engineering*, vol. 136, no. 4, pp. 041014, 2014.

[99] Zubair M.I.; Antar M.A.; Al-Dini S.A.; Ibrahim N.I.; Al-Sulaiman F.A.; "Performance and cost assessment of solar driven humidification dehumidification desalination system," *Energy Conversion and Management*, vol. 132, pp. 28–39, 2016.

[100] Zamen M;, Soufari, S. M.; Vahdat S.A.; Amidpour M.; Zeinali M. A.; Izanloo H.; Aghababaie H.; "Experimental investigation of a two-stage solar humidification–dehumidification desalination process," *Desalination*, vol. 332, pp. 1–6, 2014.

[101] Guofeng Y.; Zhifeng W.; Hongyong L.; Xing L.; "Experimental study of a solar desalination system based on humidification–dehumidification process," *Desalination*, vol. 277, pp. 92–8, 2011.

[102] Nada S.A.; Elattar H.F.; Fouda A.; "Experimental study for hybrid humidification–dehumidification water desalination and air conditioning system," *Desalination*, vol. 363, pp. 112–25, 2015.

[103] Gao P.; Zhang L.; Zhang H.; "Performance analysis of a new type desalination unit of heat pump with humidification and dehumidification," *Desalination*, vol. 220, pp. 531–7, 2008.

[104] Habeebullah B.A.; "Performance Analysis of a Combined Heat Pump- Dehumidifying System," *Journal of King Abdulaziz University*, vol. 21, pp. 97–114, 2010.

[105] Chiranjeevi C.; Srinivas T.; "Augmented desalination with cooling integration," *International Journal of Refrigeration*, vol. 80, pp. 106–19, 2017.

[106] Lawal D.U.; Antar M.A.; Khalifa A.K.; Zubair S.M.; Al-Sulaiman F.A.; "Humidification-dehumidification desalination system operated by a heat pump," *Energy Conversion and Management*, vol. 161, pp. 128–40, 2018.

[107] Lawal D.U.; Zubair S.M.; Antar M.A.; "Exergo-economic analysis of humidification-dehumidification (HDH) desalination systems driven by heat pump (HP)," *Desalination*, vol. 443, pp. 11–25, 2018.

[108] Dehghani S.; Date A.; Akbarzadeh A.; "Performance analysis of a heat pump driven humidification-dehumidification desalination system," *Desalination*, vol. 445, pp. 95–104, 2018.

[109] He W.F.; Han D.; Ji C.; "Investigation on humidification dehumidification desalination system coupled with heat pump," *Desalination*, vol. 436, pp. 152–60, 2018.

[110] Antar M.; "Water Desalination Using Solar Energy," *Advanced Materials Research*, vol. 1116, pp. 73–93, 2015.

[111] Siddiqui O.K.; Sharqawy M.H.; Antar M.A.; Zubair S.M.; "Performance evaluation of variable pressure humidification-dehumidification systems," *Desalination*, vol. 409, pp. 171–82, 2017.

[112] Narayan G.P.; McGovern R.K.; Thiel G.P.; Miller J.A.; Lienhard V. J.H.; Sharqawy M.H.; "Status of humidification dehumidification desalination technology," *IDA World Congress on Desalination and Water Reuse*, September 2011.

[113] Narayan G.P.; "Thermal Design of Humidification Dehumidification Systems for Affordable and Small-scale Desalination," *Massachusetts Institute of Technology*, PhD Thesis, 2012.

[114] Mistry K.H.; "Second law analysis and optimization of humidification dehumidification desalination cycles," *Massachusetts Institute of Technology,* Master Thesis, 2010.

[115] Cengel Y.; Boles M.; "Thermodynamics: An Engineering Approach," *McGraw-Hill, New York NY*; 7th edition.

[116] Wang Y.; Lior N.; "Thermoeconomic analysis of a low-temperature multi-effect thermal desalination system coupled with an absorption heat pump," *Energy,* vol. 36, pp. 3878–87, 2011.

[117] Nafey A.S.; Fath H.E.S.; Mabrouk A.A.; "Thermoeconomic design of a multi-effect evaporation mechanical vapor compression (MEE–MVC) desalination proces," *Desalination,* vol. 230. pp. 1–15, 2008.

[118] Kabeel A.E.; Elmaaty T.A.; El-Said E.M.S.; "Economic analysis of a small-scale hybrid air HDH–SSF (humidification and dehumidification–water flashing evaporation) desalination plant," *Energy*, vol. 53, pp. 306–11, 2013.

[119] Jamil M.A.; Zubair S.M.; "On thermoeconomic analysis of a single-effect mechanical vapor compression desalination system," *Desalination,* vol. 420, pp. 292–307, 2017.

[120] Jamil M.A.; Elmutasim S.M.; Zubair S.M.; "Exergo-economic analysis of a hybrid humidification dehumidification reverse osmosis (HDH-RO) system operating under different retrofits," *Energy Conversion and Management*, vol. 158, pp. 286–97, 2018.

[121] Sharqawy M.H.; Lienhard V.J.H.; Zubair S.M.; "Thermophysical properties of seawater: a review of existing correlations and data," *Desalinion and Water Treatment,* vol. 16, pp. 354–380, 2010.

[122] Mehrpooya M.; Ansarinasab H.; Sharifzadeh M.M.M.; Rosen M.A.; "Process development and exergy cost sensitivity analysis of a hybrid molten carbonate fuel cell power plant and carbon dioxide capturing process," *Journal of Power Sources,* vol. 364, pp. 299–315, 2017. doi:10.1016/J.JPOWSOUR.2017.08.024.

[123] Mehrpooya M.; Sharifzadeh M.M.M.; Zonouz M.J.; Rosen M.A.; "Cost and economic potential analysis of a cascading power cycle with liquefied natural gas regasification," *Energy Conversion and Management*, vol. 156, pp. 68–83, 2018.

[124] Mehrpooya M.; Sharifzadeh M.M.M.; Rosen M.A.; "Energy and exergy analyses of a novel power cycle using the cold of LNG (liquefied natural gas) and low-temperature solar energy," *Energy*, vol. 95, pp. 324–45, 2016.

[125] Bejan A.; Tsatsaronis G.; Moran M.; "Thermal design and optimization," *Wiley*, 1996.

[126] Mistry K.H.; McGovern R.K.; Thiel G.P.; Summers E.K.; Zubair S.M.; Lienhard V.J.H.; "Entropy generation analysis of desalination technologies," *Entropy*, vol. 13, pp. 1829–1864, 2011.

[127] Sharqawy M.H.; Lienhard V.J.H.; Zubair S.M.; "On exergy calculations of seawater with applications in desalination systems," *International Journal of Thermal Sciences,* vol. 50, pp. 187–96, 2011.

[128] Emad A.; Abdullah N.; Orfi J.; "Assessing the Thermal Efficiency of Brackish Water Desalination by Membrane Distillation Using Exergy Analysis," *Arabian Journal for Science and Engineering*, vol. 43, pp. 2413–2424, 2018.

[129] Al-Sulaiman F.A.; "Energy and Exergy Analyses of an Air Membrane Heat and Mass Exchanger for Air Conditioning Applications," *Journal of Energy Engineering*, vol. 143, pp. 04017028, 2017.

[130] Ozgur B.; Haydar A.; Arif H.; "Exergoeconomic analysis of a combined heat and power (CHP) system," *International Journal of Energy Research*, vol. 32, pp. 273–89, 2008.

[131] Gunerhan H.; Hepbasli A.; "Exergetic modeling and performance evaluation of solar water heating systems for building applications," *Energy and Buildings*, vol. 39, pp. 509–16, 2007.

[132] El-Sayed Y.M.; "Designing desalination systems for higher productivity," *Desalination*, vol. 134, pp. 129–58, 2001.

[133] Jamil M.A.; Qureshi B.A.; Zubair S.M.; "Exergo-economic analysis of a seawater reverse osmosis desalination plant with various retrofit options," *Desalination*, vol. 401, pp. 88–98, 2017.

[134] Zubair S.M.; Antar M.A.; Elmutasim S.M.; Lawal D.U.; "Performance evaluation of humidification-dehumidification (HDH) desalination systems with and without heat recovery options: An experimental and theoretical investigation," *Desalination*, vol. 436, pp. 161–75, 2018.

[135] Mistry K.H.; Lienhard J.H.; Zubair S.M.; "Effect of entropy generation on the performance of humidification-dehumidification desalination cycles," *International Journal of Thermal Sciences*, vol. 49, pp. 1837–47, 2010.

[136] Peñate B.; García-Rodríguez L.; "Energy optimisation of existing SWRO (seawater reverse osmosis) plants with ERT (energy recovery turbines): Technical and thermoeconomic assessment," *Energy*, vol. 36, pp. 613–26, 2011.

[137] Romero-Ternero V.; García-Rodríguez L.; Gómez-Camacho C.; "Thermoeconomic analysis of a seawater reverse osmosis plant," *Desalination*, vol. 181, pp. 43–59, 2005.

[138] Klein S.A.; "Engineering equation solver" *2018:EES Ver. 10.268: #1696)*.

[139] El-Dessouky H.T.; Ettouney H.M.; "Fundamentals of Salt Water Desalination," *Elsevier*, pp. 453–502, 2002.

[140] Abd-ur-Rehman H.M.; "Experimental investigation of solar driven multi-stage stepped bubble humidifier," *King Fahd University of Petroleum and Mineral, Dhahran Saudi Arabic*, Master Thesis, 2015.

[141] Elminshawy N.A.S.; Siddiqui F.R.; Addas M.F.; "Experimental and analytical study on productivity augmentation of a novel solar humidification–dehumidification (HDH) system," *Desalination*, vol. 365, pp. 36–45, 2015.

[142] Kline S.J.; McClintock F.A.; "Describing uncertainties in single-sample experiments," *Mechanical Engineering*, vol. 75, no. 1, pp. 75:3-8, 1953.

[143] Chiranjeevi C.; Srinivas T.; "Experimental and simulation studies on two stage humidification–dehumidification desalination and cooling plant," *Desalination*, vol. 376, pp. 9–16, 2015.

[144] Hawlader M.N.A.; Dey P.K.; Diab S.; Chung C.Y.; "Solar assisted heat pump desalination system," *Desalination*, vol. 168, pp. 49–54, 2004.

[145] Chen D.; Xie J.H.; "Handbook of Heat Pump," *Chemical and Industry Press, Beijing*; 2012.

[146] Zhang Y.; Zhang H.; Zheng W.; You S.; Wang Y.; "Numerical investigation of a humidification-dehumidification desalination system driven by heat pump," *Energy Conversion and Management*, vol. 180, pp. 641–53, 2019.

[147] Deniz E.; Çınar S.; "Energy, exergy, economic and environmental (4E) analysis of a solar desalination system with humidification-dehumidification," *Energy Conversion and Management*, vol. 126, pp. 12–9., 2016.

[148] Kabeel A.E.; Hamed A.M.; El-Agouz S.A.; "Cost analysis of different solar still configurations," *Energy*, vol. 35, pp. 2901–8, 2010.

[149] Sharshir S.W.; Peng G.; Yang N.; Eltawil M.A.; Ali M.K.A.; Kabeel A.E.; "A hybrid desalination system using humidification-dehumidification and solar stills integrated with evacuated solar water heater," *Energy Conversion and Managemen*t, vol. 124, pp. 287–96, 2016.

[150] Yamali C.; Solmus I.; "A solar desalination system using humidification-dehumidification process: experimental study and comparison with the theoretical results," *Desalination*, vol. 220, pp. 538–51, 2008.

[151] Hamed M.H.; Kabeel A.E.; Omara Z.M.; Sharshir S.W.; "Mathematical and experimental investigation of a solar humidification–dehumidification desalination unit," *Desalination*, vol. 358, pp. 9–17, 2015.

[152] Wu G.; Zheng H.; Ma X.; Kutlu C.; Su Y.; "Experimental investigation of a multi-stage humidification-dehumidification desalination system heated directly by a cylindrical Fresnel lens solar concentrator," *Energy Conversion and Management*, vol. 143, pp. 241–51, 2017.

[153] Habeebullah B.A.; "Performance Analysis of a Combined Heat Pump- Dehumidifying System," *Journal of King Abdulaziz University*, vol. 21, pp. 97–114, 2010.

[154] Shafii M.B.; Jafargholi H.; Faegh M.; "Experimental investigation of heat recovery in a humidification-dehumidification desalination system via a heat pump," *Desalination*, vol. 437, pp. 81–8, 2018.

[155] Chiranjeevi C.; Srinivas T.; "Experimental Analysis of Augmented Desalination by Cooling Integration," *Energy Procedia*, vol. 90, pp. 283–91, 2016.

Appendix A: Input Values for Numerical Confirmation of Experimental Data

The input data to the theoretical model used for the confirmation of the experimental results is provided in this appendix. These input values are the Feed water flow rate, Air inlet temperature, evaporator inlet water temperature and condenser water inlet temperature:

Table A. 1: Input data for evaporator flowrate of 6L/min and condenser Temperature of 30°C

	$\dot{V}_{cold}$ =6L/min, $T_{wh,in}$=30°C			
Feed flowrate [L/m]	**MR**	**Ta1**	**Tc1**	**Th1**
2.5	0.75799	26.8	27.5	32.9
4	1.21278	26.8	27.5	31.2
5.5	1.66758	26.8	27.5	30.5
7	2.12237	26.8	27.5	32.3
10	3.03196	26.8	27.5	31.8
13	3.94154	26.8	27.5	29.9
16	4.85113	26.8	27.5	29.8

Table A. 2: Input data for evaporator flowrate of 6L/min and condenser Temperature of 35°C

	$\dot{V}_{cold}$ =6L/min, $T_{wh,in}$=35°C			
Feed flowrate [L/m]	**MR**	**Ta1**	**Tc1**	**Th1**
2.5	0.75799	26.8	27.5	38.5
4	1.21278	26.8	27.5	36.7
5.5	1.66758	26.8	27.5	36.7
7	2.12237	26.8	27.5	38.1
10	3.03196	26.8	27.5	38.1
13	3.94154	26.8	27.5	36.9
16	4.85113	26.8	27.5	35.7

Table A. 3: Input data for evaporator flowrate of 6L/min and condenser Temperature of 40ºC

	$\dot{V}_{cold}$ =6L/min, $T_{wh,in}$=40ºC			
Feed flowrate [L/m]	**MR**	**Ta1**	**Tc1**	**Th1**
2.5	0.75799	26.8	27.5	42.9
4	1.21278	26.8	27.5	42.4
5.5	1.66758	26.8	27.5	42.6
7	2.12237	26.8	27.5	42.1
10	3.03196	26.8	27.5	39.9
13	3.94154	26.8	27.5	38.5
16	4.85113	26.8	27.5	38.5

Table A. 4: Input data for evaporator flowrate of 4L/min and condenser Temperature of 30ºC

	$\dot{V}_{cold}$ =4L/min, $T_{wh,in}$=30ºC			
Feed flowrate [L/m]	**MR**	**Ta1**	**Tc1**	**Th1**
2.5	0.75799	26.8	27.5	33.2
4	1.21278	26.8	27.5	32.8
5.5	1.66758	26.8	27.5	32
7	2.12237	26.8	27.5	31
10	3.03196	26.8	27.5	31.8
13	3.94154	26.8	27.5	30.5
16	4.85113	26.8	27.5	29

Table A. 5: Input data for evaporator flowrate of 4L/min and condenser Temperature of 35ºC

	$\dot{V}_{cold}$ =4L/min, $T_{wh,in}$=35ºC			
Feed flowrate [L/m]	**MR**	**Ta1**	**Tc1**	**Th1**
2.5	0.75799	26.8	27.5	38.4
4	1.21278	26.8	27.5	38.4
5.5	1.66758	26.8	27.5	34.4
7	2.12237	26.8	27.5	35.1
10	3.03196	26.8	27.5	35.1
13	3.94154	26.8	27.5	35.2
16	4.85113	26.8	27.5	34.5

Table A. 6: Input data for evaporator flowrate of 4L/min and condenser Temperature of 40°C

	$\dot{V}_{cold}$ =4L/min, $T_{wh,in}$=40°C			
Feed flowrate [L/m]	**MR**	**Ta1**	**Tc1**	**Th1**
2.5	0.75799	26.8	27.5	43.8
4	1.21278	26.8	27.5	43.9
5.5	1.66758	26.8	27.5	40.9
7	2.12237	26.8	27.5	40.5
10	3.03196	26.8	27.5	39.6
13	3.94154	26.8	27.5	39.2
16	4.85113	26.8	27.5	38.5

Appendix B: Results for Numerical Confirmation of Experimental Data

The results of the theoretical model against the experimental data is presented in this section. The presented results includes; Exit air temperature from humidifier and dehumidifier; exit water temperature from the evaporator, condenser, humidifier and dehumidifier; Cooling loads from the exit air at dehumidifier, exit water at dehumidifier and distillate; total cooling effects; and energy utilization factor.

Table B. 1: Results for evaporator flowrate of 6L/min and condenser Temperature of 30°C

	m_{cw}=6L/min, $T_{wh,in}$=30°C													
	Ta2		Ta3		Tc2		Tc3		Tc4		Th2		Th3	
MR	EXP	Model	EXP	Model	EXP	Model	EXP	Model	EXP	Model	EXP	Model	EXP	Model
0.75799	37.1892	37.92	15.1636	15.28	13.68	13.68	28.33	26.84	14.9221	14.48	68.4	68.4	42.8937	43.37
1.21278	39.7292	39.92	14.6915	14.91	13.13	13.13	27.52	28.54	14.4115	14.02	56.12	56.12	37.3127	37.27
1.66758	41.3385	41.35	14.1708	14.51	12.5	12.5	25.82	29.72	13.8305	13.5	49.84	49.84	34.2631	34.31
2.12237	41.5202	42.24	13.4431	13.93	11.88	11.88	25.74	30.48	13.1634	12.9	46.46	46.46	33.2287	33.27
3.03196	39.5018	40.18	12.5645	12.97	11.07	11.07	24.22	27.82	12.3136	12.02	43.6	43.6	35.5568	35.68
3.94154	38.2894	38.94	12.2511	12.34	10.6	10.6	23.88	26.38	12.0502	11.47	40.9	40.9	34.9834	35.34
4.85113	37.8546	38.46	12.0305	12.5	10.85	10.85	23.76	26.14	11.8231	11.67	40.18	40.18	35.8192	35.82

Table B. 2: Results for evaporator flowrate of 6L/min and condenser Temperature of 35°C

	m_{cw}=6L/min, $T_{wh,in}$=35°C													
	Ta2		Ta3		Tc2		Tc3		Tc4		Th2		Th3	
MR	EXP	Model	EXP	Model	EXP	Model	EXP	Model	EXP	Model	EXP	Model	EXP	Model
0.75799	36.7387	37.07	15.5244	15.54	14.01	14.01	30.58	26.19	15.2633	14.78	70.31	70.31	46.9717	47.17
1.21278	41.2543	41.43	15.1906	15.53	13.46	13.46	28.93	30.13	14.8343	14.49	61.76	61.76	39.8667	40.67
1.66758	43.5561	43.69	14.6925	15.21	12.91	12.91	27.41	35.55	14.315	14.06	55.21	55.21	37.0889	36.89
2.12237	45.1259	45.29	14.2633	14.93	12.35	12.35	26.95	34.21	13.803	13.64	50.19	50.19	34.1288	33.88
3.03196	42.9171	43.75	13.2813	13.94	11.66	11.66	26.32	32.05	12.9621	12.8	47.81	47.81	36.6953	37.53
3.94154	42.6803	42.73	13.2841	13.82	11.64	11.64	26.45	30.93	12.9632	12.73	45.79	45.79	39.1034	38.4
4.85113	41.2986	41.96	12.7844	13.26	11.2	11.2	25.05	29.83	12.4942	12.23	44.41	44.41	38.7289	38.73

Table B. 3: Results for evaporator flowrate of 6L/min and condenser Temperature of 40°C

				m_{cw}=6L/min, $T_{wh,in}$=40°C										
	Ta2		Ta3		Tc2		Tc3		Tc4		Th2		Th3	
MR	**EXP**	**Model**	**EXP**	**Model**	**EXP**	**Model**	**EXP**	**Model**	**EXP**	**Model**	**EXP**	**Model**	**EXP**	**Model**
0.75799	37.4037	37.97	15.8636	15.92	14.3	14.3	32.91	27.03	15.5735	15.11	74.06	74.06	48.9238	49.38
1.21278	42.5861	42.64	15.3932	15.8	13.58	13.58	31.52	31.32	14.9905	14.69	65.71	65.71	43.1321	43
1.66758	44.9563	45.52	15.1906	15.84	13.24	13.24	29.89	34.66	14.7138	14.54	60.66	60.66	40.1895	40.19
2.12237	47.2105	47.49	14.9115	15.77	12.79	12.79	28.46	37.18	14.3546	14.28	55.71	55.71	36.8922	37.22
3.03196	45.8413	46.48	14.5704	15.35	12.5	12.5	27.98	35.77	14.0303	13.93	51.32	51.32	39.1823	39.16
3.94154	44.8807	45.85	14.1835	14.69	11.98	11.98	27.96	34.75	13.7319	13.34	49.22	49.22	40.2389	40.22
4.85113	45.2438	45.96	13.9932	14.92	12.28	12.28	26.95	35.23	13.4816	13.6	49.23	49.23	42.0484	41.84

Table B. 4: Results for evaporator flowrate of 4L/min and condenser Temperature of 30°C

				m_{cw}=4L/min, $T_{wh,in}$=30°C										
	Ta2		Ta3		Tc2		Tc3		Tc4		Th2		Th3	
MR	**EXP**	**Model**	**EXP**	**Model**	**EXP**	**Model**	**EXP**	**Model**	**EXP**	**Model**	**EXP**	**Model**	**EXP**	**Model**
0.75799	37.9937	38.46	11.9	12.35	9.543	9.543	27.7	31.6	11.16	10.95	68.57	68.57	43.2157	42.51
1.21278	40.8563	41.05	11.77	12.53	9.233	9.233	26.01	35.35	11.06	10.88	57.43	57.43	37.1698	36.99
1.66758	41.5593	42.72	11.41	12.22	8.476	8.476	25.34	37.86	9.716	10.35	51.24	51.24	34.6589	34.13
2.12237	41.5701	42.84	10.75	11.6	7.682	7.682	24.13	37.96	9.544	9.642	46.54	46.54	33.3694	32.75
3.03196	38.8563	39.69	9.124	9.927	6.611	6.611	22.82	32.52	8.367	8.269	42.6	42.6	35.2686	34.99
3.94154	36.6685	37.97	8.933	9.504	6.46	6.46	22.68	30.07	8.192	7.982	39.65	39.65	34.1385	34.53
4.85113	36.0199	36.82	8.329	8.732	5.811	5.811	22.34	28.23	7.566	7.272	37.88	37.88	33.8952	34.1

Table B. 5: Results for evaporator flowrate of 4L/min and condenser Temperature of 35°C

				m_{cw}=4L/min, $T_{wh,in}$=35°C										
	Ta2		Ta3		Tc2		Tc3		Tc4		Th2		Th3	
MR	**EXP**	**Model**	**EXP**	**Model**	**EXP**	**Model**	**EXP**	**Model**	**EXP**	**Model**	**EXP**	**Model**	**EXP**	**Model**
0.75799	37.8859	38.1	12.5	12.96	10.23	10.23	28.12	31.19	11.86	11.59	70.98	70.98	45.8849	46.26
1.21278	42.1349	42.32	12.45	13.2	9.669	9.669	27.89	37.23	11.56	11.44	62.15	62.15	39.7286	40.08
1.66758	43.6859	44.05	12.25	13.1	9.16	9.16	27.43	40.13	11.2	11.13	55.28	55.28	37.1846	36.8
2.12237	44.8139	45.01	11.91	12.88	8.672	8.672	26.18	41.93	10.79	10.78	50.1	50.1	34.5798	34.32
3.03196	42.2596	42.55	10.89	11.55	7.727	7.727	25.66	37.23	9.94	9.64	45.64	45.64	36.7265	36.35
3.94154	41.1138	41.93	10.73	11.66	7.991	7.991	24.59	36.62	9.723	9.824	44.31	44.31	37.1269	37.42
4.85113	40.6798	41.22	10.22	10.92	7.347	7.347	24.38	35.3	9.282	9.132	43.27	43.27	38.2655	37.94

Table B. 6: Results for evaporator flowrate of 4L/min and condenser Temperature of 40°C

				m_{cw}=4L/min, $T_{wh,in}$=40°C										
	Ta2		Ta3		Tc2		Tc3		Tc4		Th2		Th3	
MR	**EXP**	**Model**	**EXP**	**Model**	**EXP**	**Model**	**EXP**	**Model**	**EXP**	**Model**	**EXP**	**Model**	**EXP**	**Model**
0.75799	37.7893	38.29	13.91	14.14	11.39	11.39	31.05	31.88	13.03	12.76	75.2	75.2	51.1235	50.37
1.21278	42.2856	42.44	13.84	14.52	11	11	30.37	37.92	12.71	12.76	64.8	64.8	42.8952	42.72
1.66758	44.5219	44.73	13.71	14.61	10.59	10.59	29.21	41.79	12.42	12.6	58.3	58.3	38.9946	39.11
2.12237	45.9856	46.64	13.69	16.28	10.15	10.15	28.82	44.55	12.25	13.22	53.38	53.38	35.8892	35.92
3.03196	45.2158	45.69	12.93	13.83	9.62	9.62	27.16	43.64	11.77	11.73	50.08	50.08	38.765	38.61
3.94154	44.5698	45.06	12.42	13.25	8.977	8.977	26.79	42.25	11.2	11.12	47.88	47.88	40.0236	39.39
4.85113	44.3168	44.99	12.3	13.09	8.863	8.863	25.79	42.3	11.08	10.97	47.01	47.01	40.5699	40.1

VITAE

Name	:	Dahiru Umar Lawal
Nationality	:	Nigerian
Date of Birth	:	08-Oct-1984
Email	:	Lawal.dahiru@gmail.com
Address	:	985 Sabuwar Gandu, Kano, Nigeria.
Academic background:		**Doctor of Philosophy (PhD)** in Mechanical Engineering, April, 2019. Mechanical Engineering Department, King Fahd University of Petroleum & Minerals, Dhahran, Saudi Arabia.
		Master of Science (MSc) in Mechanical Engineering, November, 2014. Mechanical Engineering Department, King Fahd University of Petroleum & Minerals, Dhahran, Saudi Arabia.
		Bachelors of Engineering (B.Eng.), June, 2010. Mechanical Engineering Department, Bayero University, Kano, Kano, Nigeria.

List of Publications

Filed Patent

Invention: Hybrid mechanically operated humidification dehumidification (HDH) desalination and climate control

Inventors: Mohamed A. Antar, **Dahiru Umar Lawal**, Atia E. Khalifa, Syed M. Zubair, and Fahad A. Al-Sulaiman

US patent office

Attorney Docket Number: 509724US.

Status: Filed

Journal Papers under Preparation from the Thesis

- Performance of Humidification Dehumidification Desalination System Coupled with Heat Pump

- Experımental Investıgatıon of Heat Pump Drıven Humıdıficatıon-Dehumıdıficatıon Desalınatıon System for Water Desalination and Space Conditioning

Submitted Journal Papers from the Thesis

- **D. U. Lawal**, , M. A. Antar, Performance Investigation of humidification dehumidification desalination system integrated with heat pump with energy recovery, International Journal of Green Energy, (ISI), Status: Under review. Impact factor: 1.171

Submitted Conference Papers from the Thesis

- Experimental Investigation of Heat Pump Driven Humidification-Dehumidification Desalination Unit, INTERNATIONAL DESALINATION ASSOCIATION, IDA's 2019 WORLD CONGRESS TECHNICAL PROGRAM, OCTOBER 20 – OCTOBER 24, 2019, Dubai, United Arab Emirates.

Published Journal Papers from the Thesis

- **D. Lawal,** S. Zubair, M. Antar, Exergo-economic analysis of humidification-dehumidification (HDH) desalination systems driven by heat pump (HP), Desalination (ISI), 443 (2018) 11–25. Impact factor: 6.603

- **D. Lawal,** M. Antar, A. Khalifa, S. Zubair, F. Al-Sulaiman, Humidification-dehumidification desalination system operated by a heat pump, Energy Conversion and Management (ISI), 161 (2018) 128–140. Impact factor: 6.377

Other Journal Publications

- Ismaila Kayode Aliyu, Muhammad Umar Azam, **Dahiru Umar Lawal**, Mohammed Abdul Samad, Optimization of SiC Concentration and Process Parameters for the Development of a Wear Resistant UHMWPE Nancocomposite using Taguchi Design, Polymers for Advanced Technologies, (ISI), Manuscript ID: PAT-18-752, Status: **Under review**. Impact factor: 2.137

- Binash Imteyaz, **D. U. Lawal,** Prospects of large-scale PV based power plants to replace the diesel power plants in the Kingdom of Saudi Arabia, International Journal of Green Energy, (ISI), Status: **Under review**. Impact factor: 1.171

- S. M. Zubair, M. A. Antar, S. M. Elmutasim, and **D. U. Lawal,** Performance evaluation of humidification-dehumidification (HDH) desalination systems with and without heat recovery options: an experimental and theoretical investigation, Desalination (ISI), 436 (2018) 161-175. Impact factor: 6.603

- **D. U. Lawal,** M. A. Antar, A. Aburub and M. Aliyu, Performance assessment of a cross-flow packed-bed humidification–dehumidification (HDH) desalination system – the effect of mass extraction, Desalination and Water Treatment (ISI), (2018) 1-10. doi: 10.5004/dwt.2018.21876. Impact factor: 1.631

- Aburub, M. Aliyu**, D. U. Lawal**, M. A. Antar, Experimental Investigations of A Cross-Flow Humidification Dehumidification Desalination System, International Water Technology Journal (IWTJ) (non ISI), 7(3) (2017) 198-208. Impact factor: 0.98

- Khalifa A., Imteyaz B**., Lawal D**, Abido M., Heuristic Optimization Techniques for Air Gap Membrane Distillation System, Arabian Journal for Science and Engineering, (ISI), 42(5) (2017) 1951–1965. Impact factor: 1.092

- **Dahiru Lawal,** Annas Bin Ali, Abdul Samad Mohammed, Tribological Investigations of carbon nanotube (CNTs) - reinforced Polymer (UHMWPE) nanocomposites Using Taguchi Methodology, Journal of Applied Polymer Science, (ISI), DOI: 10.1002/APP.44018 (2016). Impact factor: 1.092

- Atia E. Khalifa, **Dahiru U. Lawal** Application of Response Surface and Taguchi Optimization Techniques to Air Gap Membrane Distillation for Water Desalination- A Comparative Study, Desalination and water treatment, (ISI), 57 (59), pp. 28513-28530, (2016), DOI:10.1080/19443994.2016.1189850. Impact factor: 1.631

- Khalifa, **D. Lawal**, M. Antar, and M. Khayet, Experimental and theoretical investigation on water desalination using air gap membrane distillation, Desalination, (ISI), Vol. 376, pp. 94-108, (2015). DOI:10.1016/j.desal.2015.08.016. Impact factor: 6.603

- Atia E. Khalifa and **Dahiru U. Lawal**, Performance and Optimization of Air Gap Membrane Distillation System for Water Desalination, Arabian Journal for Science and Engineering, (ISI), pp. 1-13, (2015). DOI: 10.1007/s13369-015-1772-0. Impact factor: 1.092

- **Dahiru U. Lawal** and Atia E. Khalifa, Experimental investigation of an air gap membrane distillation unit with double-sided cooling channel, Desalination and Water Treatment, (ISI), 57 (24) pp. 11066-11080, (2016). DOI: 10.1080/19443994.2015.1042065. Impact factor: 1.631

- **Dahiru U. L.,** Abba A. A., Majed A. B., Rached B. M., A numerical study of steady and unsteady flow and heat transfer from a confined slot jet impinging on a constant heat flux wall, Journal of Mechanical Engineering and Technology (Scopus, non ISI), Vol. 6 (2), pp. 1-17, (2014). Metrics (SJR): 0.21

- **Dahiru U. L.,** Atia E. K., Flux Prediction in Direct Contact Membrane Distillation International Journal of Materials, Mechanics and Manufacturing (non ISI), vol. 2 (4), pp. 302-308, (2014). DOI: 10.7763/IJMMM.2014.V2.147. Impact factor: Not available

- **Dahiru U. L.,** Atia E. K., Theoretical and Statistical Models for Predicting Flux in Direct Contact Membrane Distillation, International Journal of Engineering Research and Applications (non ISI), vol. 4 (8), pp. 124-135, (2014).

- **Dahiru U. L**., Binash A. I., Antar A. M., Atia E. K., Performance of Spark Ignition Engine using Gasoline-91 and Gasoline-95, International Journal of Innovative Science, Engineering & Technology (non ISI), Vol. 1 (6), pp. 464-469, (2014).

Other Conference Papers

- Abdelrahman Aburub, Mansur Aliyu, **Dahiru U. Lawal** and Mohammed A. Antar, Experimental Investigations Of The Performance Of A Cross-Flow Humidification Dehumidification Desalination System, Twentieth International Water Technology Conference, IWTC20, Hurghada, 18-20 May 2017.

- Dauda Sh. Ibrahima, **U. D. Lawal**, A. A. Abubakar, & N.A. Muhammad, “Investigation and Development of Cascaded Vibration Based Energy Harvester with Complementary Coupled Magnets”, 2ND National Engineering Conference, ACICON (2016), Faculty of Engineering, Bayero University, Kano, Nigeria.

- Atia E Khalifa, **Dahiru U. Lawal**, and Mohammed A. Antar. “Performance of Air Gap Membrane Distillation Unit for Water Desalination”, ASME Proceedings, Energy, Paper No. IMECE2014-36031, pp. V06AT07A049, 6 page, November 14-20, (2014), Montreal, Canada. DOI:10.1115/IMECE2014-3603